Intragenic suppression of RNase-defective point mutation of the catalytic aspartate in the protein kinase domain of Ire1

AMNAH MAHMOUD OBIDAN

Abstract

In eukaryotic cells, proper folding of secretory and transmembrane proteins occurs within the endoplasmic reticulum (ER) before their exit the ER. The accumulation of unfolded proteins activates a response known as the unfolded protein response (UPR), mediated by Ire1. In *Saccharomyces cerevisiae*, Ire1 activation leads to the splicing of *HAC1* mRNA, which encodes a transcription factor involved in the UPR. In this study, we focused on specific mutations within the protein kinase domain of Ire1. Specifically, the protein kinase domain was subjected to mutations to alter the catalytic aspartate D797 and lysine K799, which interacts with the terminal phosphate group of ATP, to alanine. Also, point mutations in the Mg^{2+} coordinating loop converted asparagine N802 and aspartic acid D828 to alanine. To investigate the impact of these mutations, we performed several experiments. Northern blot analysis was employed to detect the splicing of *HAC1* mRNA, as it serves as an indicator of Ire1 activity and UPR induction. Additionally, β-galactosidase reporter assays were conducted to assess the expression of a UPRE-*lacZ* reporter gene, which is also regulated by the Ire1-Hac1 signalling pathway. The results demonstrated that single mutations in the catalytic domain and Mg^{2+} coordinating loop (K799A, D797A, N802A, and D828A) led to decreased levels of *HAC1* mRNA and reduced expression of the UPRE-*lacZ* reporter gene compared to the WT Ire1. Furthermore, the D797A mutant strain exhibited decreased survival under ER stress conditions when compared to other mutants within the Mg^{2+} coordinating loop and catalytic domain. Interestingly, the D797A mutation resulted in lower levels of *HAC1* mRNA species and β-galactosidase activity. However, introducing additional mutations such as D797A N802A or D797A K799A N802A led to significant increases in β-galactosidase activity, the percentage of *HAC1* mRNA, and restored growth compared to the single D797A Ire1 mutant. Notably, the expression levels of WT and protein kinase mutants were similar. In conclusion, the findings suggest that introducing specific additional mutations, such as K799A Ire1, D828A Ire1, or N802A Ire1, to the single D797A Ire1 mutant can restore the signalling activity of Ire1.

Intragenic suppression of RNase-defective point mutation of the catalytic aspartate in the protein kinase domain of Ire1

OBIDAN, AMNAH M.T.

This thesis is submitted as part of the requirements for the award of
Degree of Doctor of Philosophy

Department of Biosciences

Durham University

August 2023

TABLE OF CONTENTS

TABLE OF TABLES

TABLE OF FIGURES

DECLARATION

I confirm that this thesis is my own work and that it contains no material previously submitted for a degree in this or any other institute.

STATEMENT OF COPYRIGHT

LIST OF ABBREVIATIONS

ADP	Adenosine diphosphate
ATP	Adenosine triphosphate
(NH4)2SO4	Ammonium sulfate
aa	Amino acid
bp	Base pair
BSA	Bovine serum albumin
bZIP	Basic leucine zipper
C-terminus	Carboxyl-terminus
cAMP	cyclic adenosine monophosphate
$CHCl_3$	Chloroform
CYC1	Cytochrome c, isoform 1
d	Days
DEPC	Diethyl Pyrocarbonate
DNA	Deoxyribonucleic acid
dNTP	Deoxynucleotide triphosphates
DTT	Dithiothreitol
EDTA	Ethylenediaminetetraacetic acid
ER	Endoplasmic reticulum
ERAD	Endoplasmic reticulum-associated degradation
EtOH	Ethanol
g	Gram
GCN4	General Control Nonderepressible
h	Hour
$Hac1^i$	Hac1 protein
HAC1	Homologue of ATF/CREB1
IRE1	Inositol requiring enzyme 1
KAR2	Karyogamy
Kb	Kilobases
kDa	kilo Dalton (unit in mass)
l	Litre
LB	Lennox broth or lysogeny broth
M	Molar

Mg	Milligrams
Min	Minute
ml	Millilitre
mM	Millimolar
NBP	Nucleotide binding pocket
N-terminus	Amino terminus
ng	Nanogram
nt	Nucleotides
°C	Degree Celsius
PCR	Polymerase chain reaction
PKA	Protein kinase A
PSP2	Pre-sporulation medium
RLB	Reporter lysis buffer
RNA	Ribonucleic acid
RNase	Endoribonuclease
RT	Room temperature
SD	Synthetic dextrose medium
SDS	Sodium dodecyl sulphate
Sec	Second
SSC	Saline-sodium citrate
Tm	Tunicamycin
U	Units
UPR	Unfolded protein response
UPRE	Unfolded protein response element
UV	Ultraviolet
Vol	Volume
WT	Wilde type
YPD	Yeast extract peptone dextrose medium
β-gal	β-galactosidase
Δ	Deletion
λ	wavelength
µg	microgram
µM	micromolar

ACKNOWLEDGMENTS

I would like to take this opportunity to express my sincere gratitude to all those who have contributed to the successful completion of this thesis.

First and foremost, I want to express my deepest appreciation to my exceptional supervisor, Dr. Martin Schröder. His guidance, support, and encouragement have been the bedrock of this success of the project. From the inception of this research to its culmination, Dr. Schröder's expertise and dedication have been an inspiration that shaped the very direction of this work. His insightful feedback and constructive criticism have not only refined my ideas but also fostered a deeper understanding of the subject matter. Under his mentorship, I have grown both professionally and personally, and for that, I am forever grateful.

I must also acknowledge the invaluable contributions of Dr. Schröder's lab and the collaborative atmosphere they provided. Their expertise and camaraderie enriched the quality of this work and fostered a stimulating research environment. Special mention goes to Hanan Sagini, whose support and willingness to lend a helping hand when needed made a significant difference in this journey.

Moreover, I would like to express my gratitude to the members of my thesis committee, Dr. Akis Karakesisoglou and Professor Susan Pyner, for their time, attention, and constructive feedback throughout my academic journey as a PhD student at Durham University.

Furthermore, I want to acknowledge the pivotal role played by the University of Tabuk, supported by the Royal Embassy of Saudi Arabia Cultural Bureau, for believing in my potential and providing the unwavering support necessary to pursue my dreams of higher education. Without their initial support, this journey would not have been possible, and I am forever thankful for their trust and encouragement.

I extend my heartfelt gratitude to my family and friends for their encouragement and support, which have been a constant source of strength throughout the challenges and successes of this journey.

DEDICATION

I dedicate this work to those who have been my unwavering pillars of support and inspiration throughout this journey.

Commencing with my beloved parents, Mom and Dad, their constant love, steadfast encouragement, and heartfelt prayers have been the guiding light throughout this journey.

To my dearest Aleen and Ahmed, As I reflect on the journey we have shared, I cannot help but be overwhelmed with joy and pride at witnessing your growth and happiness. Amid the demanding lab work and numerous commitments, I often found myself grappling with feelings of guilt for not being there with you as much as I desired. However, your unwavering support, understanding, and encouragement throughout this time have been a constant source of strength for me, enabling me to persevere and achieve what I had set out to do. I am immensely grateful to my husband, whose unwavering love and dedication made it possible for me to pursue my dreams without compromising on being a present and caring parent. His support in taking care of Kids during my busy days allowed me the necessary space to focus on my goals.

To my family, who has been a steadfast pillar of support and understanding throughout this journey, empowering me to believe in myself, no matter the challenges I encountered. I want to express my deepest gratitude to Aisha, Mariam, Maram, and Sara for the immeasurable impact they have had on my life. Their unwavering presence has been a guiding light, illuminating my path and making the road less dauntin.

1 INTRODUCTION

In eukaryotic cells, the endoplasmic reticulum (ER) plays a crucial role in the folding of secretory and transmembrane proteins before they leave the ER. This folding process is facilitated by a variety of enzymes (Gething & Sambrook, 1992). Afterwards, these proteins are transported from the ER to the Golgi complex (Palade, 1975). Several diseases, including obesity, type II diabetes, and neurodegenerative disorders, have been linked to protein folding stress within the ER (Özcan et al., 2004). When unfolded or misfolded proteins accumulate and fail to exit the ER (Hebert & Molinari, 2007), it triggers the activation of specific sensor proteins residing in the ER: inositol requiring 1 (Ire1), double-stranded RNA-activated protein kinase (PKR)-like ER kinase (PERK), and activating transcriptional factor 6 (ATF6) (Schröder & Kaufman, 2005a). Ire1 is a protein kinase-endoribonuclease present across various species. Its RNase domain produces a signal that helps in cell survival, while its kinase activity stimulates cell death. The kinase activity of IRE1 is believed to control the activity of its RNase domain, but the mechanism by which it generates distinct signals that either promote survival or apoptosis is still unclear. In yeast cells *Saccharomyces cerevisiae*, Ire1, as a transmembrane protein located in the ER, plays a vital role in the unfolded protein response (UPR) pathway by promoting the splicing of *HAC1* pre-mRNA. This results in the production of mRNA for a transcription factor called *HAC1*^{i}, which contains a basic leucine-zipper (bZIP) domain. The active Hac1^{i} protein promotes the transcription of genes encoding ER-resident molecular chaperones and upregulates the process of ER-associated protein degradation (ERAD), which helps alleviate ER stress. In this introductory section, I will discuss the concept of ER stress and the UPR, which is a cellular signalling pathway activated in response to ER stress. The sensing of unfolded proteins by the luminal domain of Ire1 and the subsequent activation of the kinase domain of Ire1 during ER stress will be explained. Upon activation, the kinase domain of Ire1 undergoes autophosphorylation, leading to the activation of its RNase domain. The function of the kinase domain in activating the RNase domain and its role in the UPR response will be explored. Additionally, the investigation will focus on the role of Ire1 mutants and their potential for intragenic suppression.

1.1 The Endoplasmic Reticulum and the Unfolded Protein Response

1.1.1 The Endoplasmic Reticulum

The endoplasmic reticulum is a vital organelle responsible for the synthesis, modification, and delivery of most secreted proteins to their target destinations in eukaryotic cells. Proper protein folding is essential for the normal functioning of cells and organisms. The accumulation of misfolded or unfolded proteins in the ER, causing ER stress, can disrupt this process. Resident molecular chaperones and protein foldases in the ER prevent the aggregation and accumulation of unfolded and misfolded proteins (Credle et al., 2005; Gething & Sambrook, 1992; Stevens & Argon, 1999).

ER stress occurs due to various factors, including nutrient deprivation, oxidative stress, and mutations in genes that encode proteins involved in protein folding and quality control in the ER (Fig 1.1) (Ron & Walter, 2007). Molecular chaperones, such as BiP/Kar2/Grp78 and Grp94, play a critical role in preventing protein aggregation and facilitating proper folding of nascent proteins.

They are associated with sensors that detect ER stress, dissociating from them when ER stress occurs and leading to the activation of stress response pathways (Christianson & Ye, 2014). Lectin-like chaperones, including calnexin (Cnx) and calreticulin (Crt), are essential for folding and quality control of glycoproteins in the ER lumen (Ellgaard & Helenius, 2003; Hartl, 1996; Molinari et al., 2003). In yeast, several ER resident proteins, including Cnx, chaperones from the Hsp70 and Hsp90 families (e.g., BiP/Kar2/Grp78, Grp94), protein disulphide isomerases (Pdi), and peptidyl-prolyl isomerases, are involved in protein folding and quality control. These proteins assist in the formation of disulphide bonds and ensure proper protein folding, thus preventing ER stress (Gething & Sambrook, 1992).

The ER also plays a crucial role in post-translational modifications, including N-glycosylation and disulphide bond formation (Kukuruzinska & Lennon, 1998; Walsh, 2010) . N-glycosylation enhances protein solubility, reduces aggregation, and serves as a binding site for CNX. Additionally, it facilitates interactions with protein disulphide isomerases (PDI) and potentially marks proteins for ERAD (Aebi et al., 2010). Disulphide bond formation is catalysed by members of the PDI family, abundant in the ER lumen. These PDIs, including PDI, P5, and ERp57, play a role beyond disulphide bond formation, aiding in proper folding and preventing misfolded proteins from leaving the ER, thus contributing to protein

maturation (Bulleid & Ellgaard, 2011; Riemer et al., 2009). Peptidyl-prolyl isomerases (PPiases), a type of enzyme, catalyse the isomerisation of proline residues in nascent polypeptides, which is necessary for their proper folding (Fischer et al., 1984). Furthermore, the ER not only folds its resident proteins but also processes all other proteins entering the secretory pathway (Walter & Ron, 2011). BiP binds to nascent polypeptides, facilitating their folding through an ATP-dependent cyclic process of release and binding (Normington et al., 1989). Properly folded proteins and processed glycoproteins are released into transport vesicles, which then travel to the Golgi network for further processing and sorting (Bonifacino & Glick, 2004; Brodsky & Skach, 2011). Maintaining ER homeostasis is critical for cellular function, and disruptions in ER protein folding can lead to ER stress (Kaufman, 2002; Ron & Walter, 2007). To counteract ER stress, cells activate the UPR, a cellular stress response mechanism that aims to restore ER homeostasis by increasing the folding capacity of the ER and reducing protein synthesis (Walter & Ron, 2011).

1.1.2 The Unfolded Protein Response

The UPR aims to alleviate this stress by increasing protein folding capacity, reducing protein synthesis, degrading misfolded proteins and expanding the size of the ER (Ron & Walter, 2007; Xu et al., 2005). The UPR achieves this by upregulating the expression of molecular chaperones and protein foldases, increasing phospholipid production to expand the ER, attenuating general translation and transcription of secretory protein genes, and initiating ERAD to degrade unfolded proteins by the proteasome (Malhotra & Kaufman, 2007).

In the mid-1970s, researchers made a significant observation regarding the composition of cell membrane proteins in fibroblastic cells transformed by various oncogenic viruses (Isaka et al., 1975; Stone et al., 1974). These studies led to the discovery of two novel plasma membrane proteins, BiP (also known as GRP78) and GRP94, induced by viral infection in chick embryo fibroblasts. At that time, it was believed that the increased levels of BiP and GRP94 were a direct result of the viral infection itself.

Subsequent investigations have revealed a more intricate and nuanced understanding of the subject matter. It was found that the induction of BiP and GRP94 was not solely caused by the viral infection, but rather by a different factor. Specifically, the synthesis of these glucose-regulated proteins was triggered by the glucose depletion of the culture medium, leading to the accumulation of unfolded proteins within the cells. The cells responded to this

stress by increasing the expression of BiP and GRP94 as part of a protective mechanism to manage the accumulation of unfolded proteins (Shiu et al., 1977).

Initially, it was believed that GRP78 played a key role in UPR by binding to all three ER stress transducers and keeping them inactive (Bertolotti et al., 2000). However, it was later found that BiP, a protein essential for protein folding and translocation in the ER, could not be the sole factor determining the activity of the UPR regulator Ire1 (Bertolotti et al., 2000; Kimata et al., 2004).

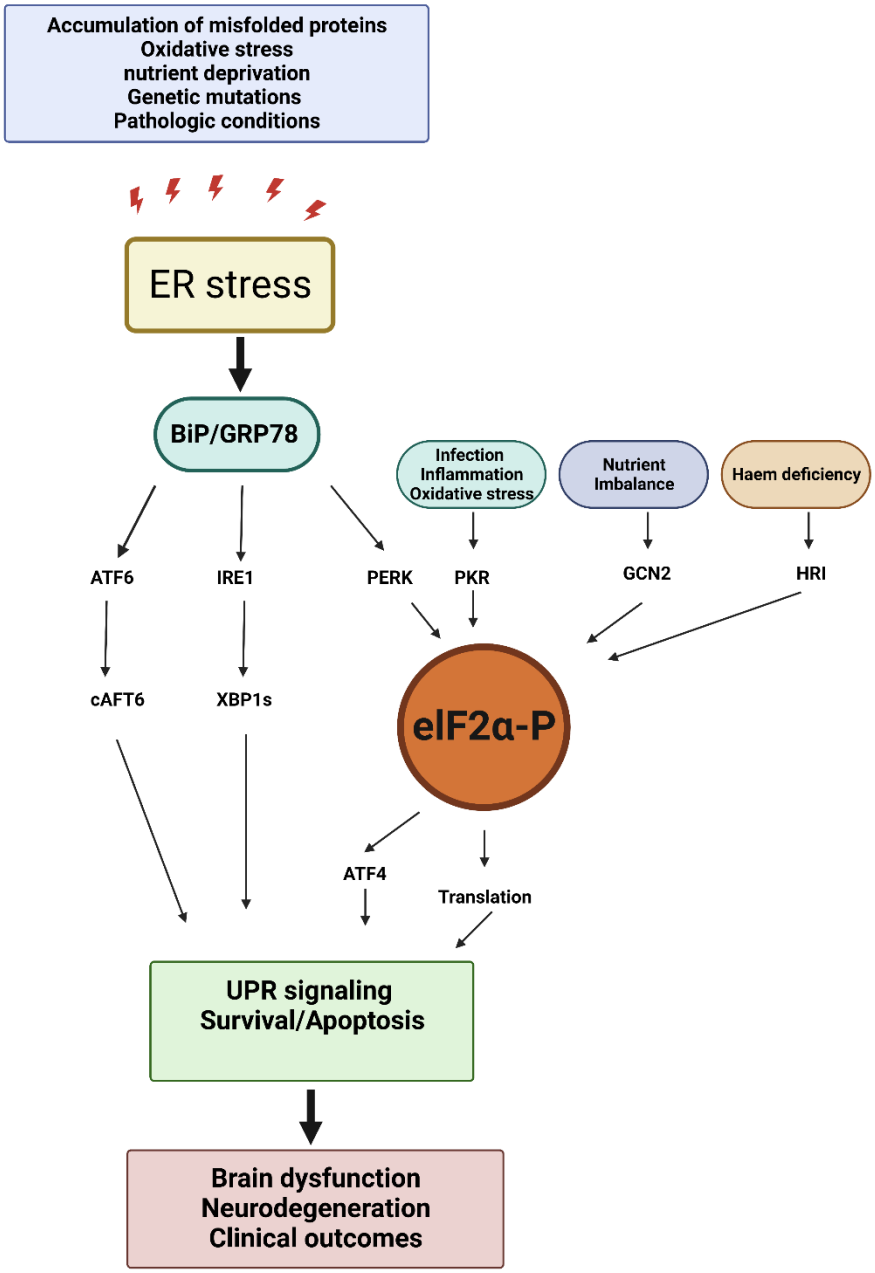

Figure 1.1. An early model of ER stress.
This model proposes that BiP (also known as GRP78) is the key protein that triggers UPR signalling. The UPR can be activated by abnormal ER stress in certain diseases, leading to the activation of three signalling pathways - ATF6, IRE1α/XBP1s, and PERK/eIF2α-P, "P" refers to phosphorylation. In addition, other factors such as infection, inflammation, nutrient deprivation, oxidative stress, and haem deficiency can activate eIF2α kinases, including PKR, GCN2, and HRI which can lead to increased levels of eIF2α-P and impaired protein synthesis. Excessive UPR activity and eIF2α-P signalling, along with their downstream effects, can impair cell function and lead to brain dysfunction and neurodegeneration. This occurs through the dysregulation of protein synthesis and the accumulation of misfolded proteins, leading to cellular damage and cell death. Created with BioRender.com

1.1.2.1 The UPR signal

The UPR is activated by three receptors present in the membrane of ER, known as inositol-requiring 1 (IRE1), protein kinase RNA-like endoplasmic reticulum kinase (PERK), and activating transcription factor 6 (ATF6) (Mori, 2009; Ron & Walter, 2007; Walter & Ron, 2011). These receptors sense the accumulation of unfolded proteins in the ER and initiate a cascade of signalling events that coordinate a range of processes, including protein folding, ERAD, and lipid metabolism, to alleviate ER stress and restore ER function (Mori, 2009; Zhang & Kaufman, 2004). IRE1 is the sole identified ER stress sensor in yeast, responsible for initiating the UPR in animals and plants (Chen & Brandizzi, 2013; Hetz & Glimcher, 2009; Nagashima et al., 2011). The other two proteins, PERK and ATF6, serve as distinct ER stress sensors in mammals, playing a crucial role in handling intricate UPR situations in higher organisms (Hetz, 2012; Moore & Hollien, 2012). When misfolded or unfolded proteins accumulate in the ER, ER stress is induced, and cells must respond to tolerate this stress and maintain cell survival (Walter & Ron, 2011).

1.1.2.1.1 ATF6 signalling

ATF6 is a transcription factor (Glembotski, 2014; Wang et al., 2000) (Fig. 1.2 A). ATF6 is a transmembrane protein characterized by an ER stress-sensing luminal domain and a cytosolic region that encodes a bZIP transcription factor. When there is no ER stress, ATF6 remains sequestered within the ER, a process facilitated by the interaction of BiP with its luminal domain and the presence of intra- and intermolecular disulfide bonds that maintain ATF6 within the ER (Hetz et al., 2020; Preissler & Ron, 2019). When unfolded proteins accumulate, ATF6 is enclosed in transport vesicles that bud off from the ER and transport it to the Golgi apparatus (Schindler & Schekman, 2009). Inside the Golgi, two proteases, S1P and S2P (site-1 and site-2 protease), sequentially remove the luminal domain and the transmembrane anchor, respectively (Haze et al., 1999; Shoulders et al., 2013; Ye et al., 2000). This processing results in the release of the N-terminal cytosolic fragment, ATF6(N), which translocates into the nucleus to activate specific UPR target genes including XBP1 and ER chaperones.

ATF6 target genes encompass crucial ER-resident proteins involved in protein folding, such as BiP (a chaperone of the heat shock protein HSP70 family), protein disulfide isomerase, and glucose-regulated protein 94 (GRP94; a chaperone of the Hsp90 family). ATF6 processing shares similarities with the regulation of sterol response element binding protein

(SREBP), a transcription factor controlling sterol biosynthesis in mammalian cells, as both utilize the same proteases (Brown & Goldstein, 1999). The regulation mechanism of SREBP at the ER exit level is well understood, but there is limited knowledge about how ATF6 responds to ER stress. ATF6 ER-luminal domain lacks sequence homology to other proteins. It interacts with BiP, and its release during ER stress might play a role in ATF6 activation. The ATF6 luminal domain also includes intra- and intermolecular disulphide bonds, potentially acting as redox sensors to monitor the ER environment (Walter & Ron, 2011).

Recent studies have explored the role of ATF6 in pancreatic diseases. One study in a mouse model examined ATF6's impact on chronic pancreatitis (CP), indicating that ATF6 contributes to CP development by influencing acinar cell apoptosis, elevating inflammatory factors, and upregulating p53 expression (Zhou et al., 2019). This study proposes that targeting ATF6-related ER stress mechanisms holds promise as a potential diagnostic and therapeutic strategy for CP. Another study investigated the role of ATF6 in severe acute pancreatitis (SAP). Elevated ATF6 expression was associated with pancreatic tissue damage and increased apoptosis in both SAP patients and a mouse model (Tan et al., 2020). ATF6 was found to regulate the gene AIFM2 through p53, contributing to SAP development. Inhibition of ATF6 or p53 displayed protective effects, suggesting potential targets for SAP treatment. Collectively, these studies underscore the significance of ATF6 in pancreatic diseases, highlighting its potential as a diagnostic and therapeutic target for conditions such as severe acute pancreatitis (SAP) and chronic pancreatitis (CP).

1.1.2.1.2 PERK signalling

The PERK signalling pathway represents the second branch of the UPR and is mediated by PERK, a transmembrane kinase residing in the endoplasmic reticulum (ER) (Fig. 1.2 B). Although yeast lacks the PERK pathway, interestingly, the luminal domain of PERK shows some homology to the luminal domain of IRE1, to the extent that they can function interchangeably in yeast (Liu et al., 2000; Schröder & Kaufman, 2005b).

PERK and IRE1 share similarities in their activation process, relying on the molecular chaperone BiP to be released for activation. Once activated upon sensing ER stress, PERK forms oligomers and auto-phosphorylates itself and eIF2α, a ubiquitous translation initiation factor. This autophosphorylation indirectly inhibits eIF2, resulting in reduced mRNA translation and alleviating ER stress (Harding et al., 1999; Liu et al., 2000). In this approach, PERK aids in the reduction of protein flow into the ER, so alleviating ER stress. However, a

distinct feature of the PERK pathway is its selective translation of specific mRNAs, particularly those containing short open reading frames in their 5'-untranslated regions. One of these mRNAs encodes the transcription factor ATF4, which induces the expression of target genes like CHOP and GADD34. CHOP is involved in apoptosis regulation, while GADD34 acts as a PERK-inducible regulatory subunit of the protein phosphatase PP1C, counteracting PERK by dephosphorylating eIF2α (Vattem & Wek, 2004). This balanced regulation of eIF2α dephosphorylation is crucial, as it influences the response of cell to ER stress and can play a role in either cell protection or cell death pathways.

The dualistic nature of the PERK branch in the UPR, with its protective and signalling roles, highlights the complexity of cellular responses to ER stress and the importance of finely tuned mechanisms to maintain cellular homeostasis (Marciniak et al., 2004; Tsaytler et al., 2011). The dynamic interplay among PERK, ATF4, and downstream effectors like CHOP and GADD34 significantly influences the overall cellular response to ER stress conditions. ATF4, a transcription factor, becomes preferentially translated when eIF2α is phosphorylated. It then regulates genes involved in redox homeostasis and amino acid metabolism (Ron & Walter, 2007).

1.1.2.1.3 IRE1α signalling

Ire1, the third branch of the UPR (Fig. 1.2 C), is a type-1 transmembrane ER-resident protein with bifunctional cytosolic kinase and RNase domains. The activation of its RNase function is triggered by conformational changes following lateral IRE1 oligomerisation in the ER membrane.

Once activated, IRE1α cleaves the mRNA encoding the UPR-specific transcription factor XBP1, removing an intron at two specific positions. The resulting spliced mRNA, known as XBP1s, serves as the active transcription factor (Cox et al., 1993; Mori et al., 1993; Walter & Ron, 2011). While IRE1 activity governs the entire UPR gene expression program in yeast, metazoans exhibit considerable redundancy among UPR-induced transcription factors. Nevertheless, XBP1s plays a distinct role in regulating lipid biosynthetic enzymes, components of ERAD, and promoting the development of a well-developed ER, characteristic of active secretory cells (Reimold et al., 2001).

Under normal conditions, IRE1α associates with the ER chaperone BiP (or GRP78) (Bertolotti et al., 2000). When the ER detects misfolded proteins, IRE1α dissociates from

BiP, and its kinase domain undergoes dimer-/oligomerisation and *trans*-autophosphorylation, leading to the activation of its RNase activity toward Xbp1 mRNA (He et al., 2010).

The activation of IRE1α of XBP1s results in the regulation of various ER chaperones, lipogenic genes, and ERAD components. Genetic studies have identified XBP1 as a risk factor for inflammatory bowel disease (IBD) (Kaser et al., 2008). In mice with intestinal epithelium-specific Xbp1 deficiency, IRE1α protein becomes hyperactivated, contributing to the development of IBD, partly through JNK activation (Adolph et al., 2013; Kaser et al., 2008).

IRE1α activation also has implications for c-Jun N-terminal kinase (JNK) signalling and regulated IRE1-dependent decay (RIDD). Upon activation, IRE1α can recruit TNF receptor-associated factor 2 (TRAF2), which, in turn, recruits apoptosis signal-regulating kinase 1 (ASK1). This activation pathway ultimately leads to the activation of JNK and p38 signalling (Nishitoh et al., 2002; Urano et al., 2000). JNK plays a pivotal role in determining cell fate under conditions of severe ER stress and may contribute to apoptosis when the cellular protein-folding machinery is overwhelmed. This apoptotic pathway underscores the ability of IRE1α to control the fate of the cell during ER stress. JNK activation occurs in response to various stressors like UV exposure, heat shock, ionizing radiation, and ER stress (Kyriakis et al., 1994). Once activated, JNK phosphorylates a Thr-Pro-Tyr motif and can lead to the activation of the transcription factor AP-1, which translocates to the nucleus and initiates the transcription of genes, including proinflammatory ones such as TNF, GM-CSF, IL-8, and cytokine receptors (Angel et al., 2001).

Additionally, IRE1α is associated with RIDD, a mechanism for degrading mRNAs localised to the ER (Hollien et al., 2009). IRE1α cleaves these mRNAs, resembling the cleavage sequence of *XBP1*, and cellular exoribonucleases further degrade the resulting mRNA fragments (Maurel et al., 2014). This process helps reduce the burden on the protein-folding of ER machinery, contributing to ER homeostasis (Kimmig et al., 2012).

RIDD is particularly important in maintaining ER protein homeostasis, especially in organisms like *Schizosaccharomyces pombe*, where *HAC1* splicing does not occur (Kimmig et al., 2012). Even in the absence of stress, basal levels of RIDD are essential for sustaining ER homeostasis (Lipson et al., 2006). IRE1α, through mechanisms like RIDD, helps balance ER homeostasis, ensuring cell survival during normal conditions and adapting to ER stress when unfolded proteins accumulate. If both splicing and RIDD mechanisms fail to alleviate

ER stress, RIDD can continue increasing and lead to the degradation of various mRNAs, potentially resulting in cell apoptosis, termed prodeath RIDD (Maurel et al., 2014).

Section 1.1.3 of this introduction will provide a more detailed discussion on the structure and function of IRE1.

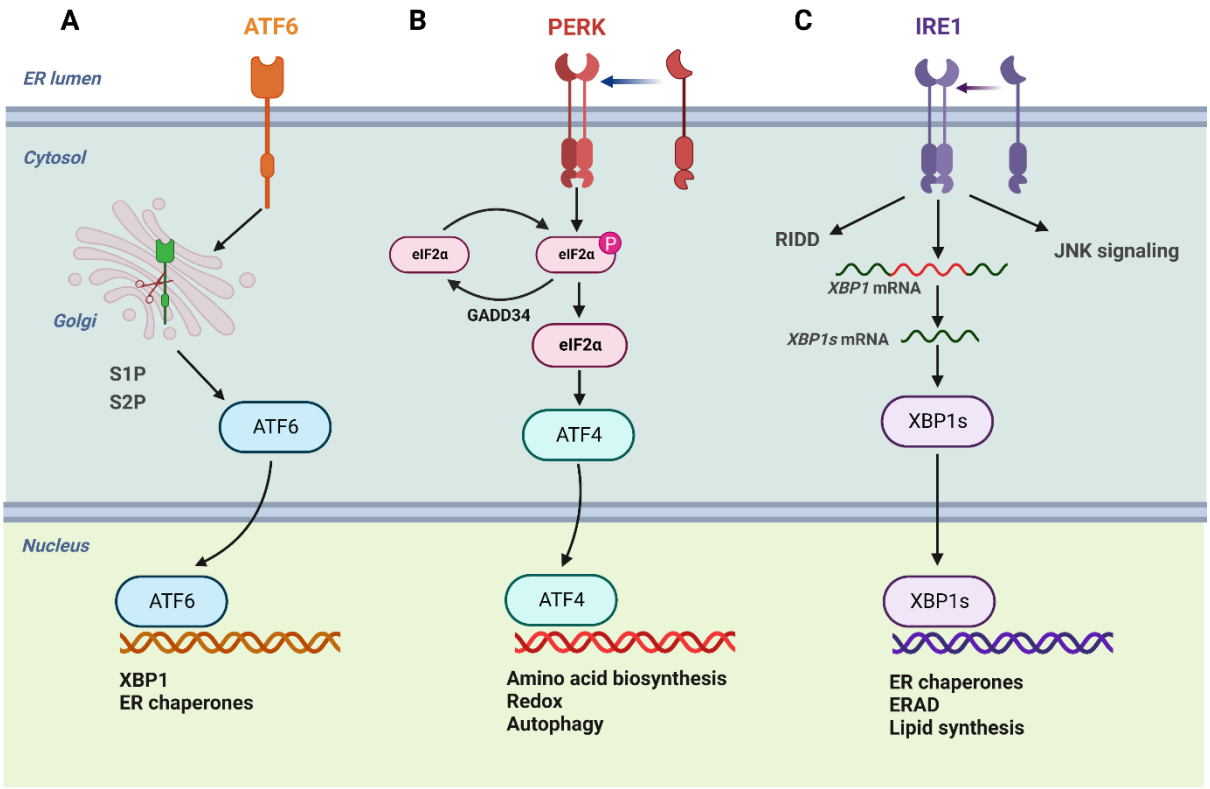

Figure 1.2. Branches of the UPR and signal transduction mechanisms.
(A to C) The UPR comprises three branches (ATF6, PERK, and IRE1), each represented by distinct families of signal transducers. Created with BioRender.com

1.1.3 IRE1: Structural and Functional Overview

1.1.3.1 Background

IRE1, the primary ER stress sensor in the UPR, is highly conserved across eukaryotes, from yeasts to plants and mammals. It was initially discovered during the cloning and sequencing of yeast genes to complement a mutant with a myo-inositol deficiency (Nikawa & Yamashita, 1992). While initially thought to be involved in inositol prototrophy, its role in detecting and responding to ER stress was revealed later (Mori et al., 1993). The importance of IRE1 became evident when yeast mutants lacking IRE1 failed to activate genes encoding essential ER chaperones and displayed reduced viability under ER stress conditions (Cox et al., 1993).

By screening a human fetal liver cDNA library with specific oligonucleotide primers, human IRE1α was identified as a type 1 transmembrane serine/threonine protein kinase. It exhibits autophosphorylation activity and contains a domain similar to RNase L. Notably, although the cytoplasmic domain of human IRE1α closely resembles its yeast counterpart and retains the ability to cleave *HAC1* mRNA, the luminal domain has undergone significant divergence (Tirasophon et al., 1998). IRE1 plays an essential role in the unfolded protein response by detecting ER stress induced by unfolded proteins and transmitting this information to the nucleus in a manner dependent on its kinase activity. This is achieved through the cleavage of an intron from the mRNA encoding the Hac1p protein, leading to increased Hac1p levels. Hac1p acts as a transcription factor by binding to the UPRE elements in the promoters of genes involved in ER resident proteins. Impairment of the unfolded protein response occurs when there is a loss of kinase activity in both yeast and human IRE1. However, the loss of endoribonuclease activity does not necessarily affect kinase activity (Tirasophon et al., 1998).

1.1.3.2 Structure and Function of IRE1

IRE1 consists of five functional domains, including a cytosolic kinase/RNase domain and an ER-luminal domain (Fig 1.2). The ER-luminal domain senses misfolded proteins, leading to its oligomerisation and subsequent activation of the cytosolic kinase and ribonuclease domains of IRE1 (Walter & Ron, 2011). This activation process has been studied in yeast, where IRE1 is involved in adaptive responses to ER stress (Lin et al., 2007; Walter et al., 2015).

Upon sensing unfolded proteins, the luminal domain of IRE1 undergoes oligomerisation, resulting in the activation of the cytoplasmic kinase and ribonuclease domain of IRE1. IRE1 uses a special method to transduce the UPR signals (Walter & Ron, 2011). One proposed explanation is that the luminal domain of Ire1 detects unfolded proteins within the ER and directly interacts with them, leading to the assembly of larger protein complexes (Credle et al., 2005; Pincus et al., 2010). Another possibility is that regulatory proteins, such as Kar2 (BiP), compete with unfolded proteins by binding to the receptor site of the luminal domain of Ire1 (Kimata et al., 2007; Zhou et al., 2006). IRE1 undergoes oligomerisation followed by trans-autophosphorylation, which activates its RNase domain (Gardner & Walter, 2011). Upon activation, the RNase domain of Ire1 cleaves the mRNA that encodes a UPR-specific transcription factor. In the yeast *S. cerevisiae*, the mRNA target of RNase activity is Hac1. The spliced *HAC1* mRNA is then translated into Hac1 protein, which stimulates the

transcription of genes, such as the essential chaperone protein Bip, that is localised in the lumen of the ER and is encoded by the *KAR2* gene of *S. cerevisiae* (Mori et al., 1992). Synthesis of BiP is induced by the accumulation of unfolded proteins in the ER (Kohno et al., 1993). The short promoter element, described as the UPRE, is found in numerous Hac1 target genes (Mori et al., 1998). Previous studies have shown that Hac1 activity is modulated by the interaction with the transcription factor Gcn4p, which helps alleviate ER stress (Patil et al., 2004).

IRE1 is also involved in several other cellular processes, including inflammation, apoptosis, and lipid metabolism (Martinon & Glimcher, 2011). Studies have shown that dysregulation of IRE1 activity can lead to a variety of diseases, including cancer, neurodegenerative disorders, and metabolic diseases (Volmer et al., 2013). For example, in neurodegenerative diseases, such as Alzheimer's and Parkinson's disease, IRE1 activation leads to neuronal cell death (Das et al., 2015; Hoozemans et al., 2009). Inhibition of IRE1 has been shown to reduce neuronal cell death and improve cognitive function in animal models of neurodegenerative diseases (Das et al., 2015; Hoozemans et al., 2009).

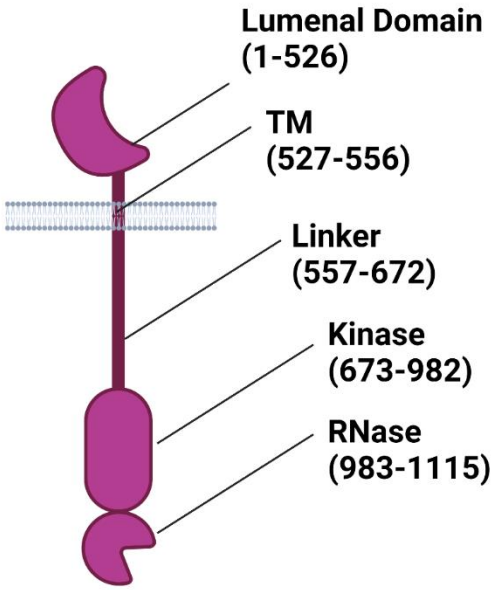

Figure 1.3. Schematic illustrates the structure of yeast Ire1.
This schematic highlighting five functional domains and indicating the specific amino acid sequence boundaries of each domain. Created with BioRender.com

1.1.3.3 Activation Mechanism and Cellular Localisation of IRE1

IRE1 is a key component of the UPR pathway, which is responsible for detecting ER stress and initiating a cellular response to restore ER homeostasis. The luminal domain of IRE1 serves as a sensor for ER stress and is involved in downstream signalling pathways (Gardner & Walter, 2011; Liu et al., 2000).

1.1.3.3.1 Clustering of Ire1

The clustering of Ire1 is a critical step in the activation of the UPR pathway. Studies have shown that point mutations that prevent or deform interfaces between Ire1 molecules in the luminal domain, involved in dimerisation or oligomerisation, reduce Ire1 activity, indicating that the formation of interfaces is critical in both the luminal and cytosolic domains of Ire1 (Credle et al., 2005). Moreover, it has been suggested that the oligomerisation of Ire1 is a critical step in its activation, as it induces the *trans*-autophosphorylation of the kinase domain of Ire1, leading to RNase domain activation and UPR induction (Kimata et al., 2007).

During ER stress with unfolded proteins, yeast IRE1 forms visible puncta as observed by immunofluorescence microscopy. These puncta rapidly associate and disassociate in wild-type IRE1, a phenomenon beyond simple dimerisation (Kimata et al., 2007)

These findings suggest that the clustering of Ire1 is a complex and highly regulated process that involves interactions between multiple domains of Ire1 and is necessary for the proper activation of the UPR pathway. It occurs either before or during autophosphorylation, shortly after the initial ER stress detection (Kimata et al., 2007).The clustering process is crucial for UPR activation, and inhibiting clustering, for instance, by modifying the IRE1 dimerisation interface, results in reduced splicing and disrupts foci clustering after ER stress induction (Li et al., 2010). Moreover, inhibiting clustering hinders UPR signalling at the cluster centres, preventing Hac1 recruitment to Ire1(Aragón et al., 2009).

IRE1 clustering in yeast involves the formation of a helical rod structure composed of multiple IRE1 molecules per helical turn, enabling outward-facing RNase domains that interact with *HAC1* mRNA (Korennykh et al., 2009). On the other hand, crystal structures of human IRE1 suggest an intermediate multimeric state, where proximity of the activation loops of kinase domains allows autophosphorylation. Nucleotide binding strengthens the interaction between IRE1 monomers, enabling phosphorylation and conformational changes necessary for splicing (Ali et al., 2011)

Microscopy studies have shown that the distribution of Ire1 varies in different cellular environments. Under normal conditions, when Ire1 is fused with mCherry (a red fluorescent protein), it exhibits a characteristic pattern consistent with an ER protein, with areas of fluorescence observed around the nucleus and the cell surface. This fluorescence is concentrated around the perinuclear and cortical ER regions, indicating the presence of Ire1 in these areas. Additionally, the localisation pattern of Ire1-mCherry overlaps with that of a green fluorescent protein (GFP) fused to the C-terminus of the Sec63 subunit, a component of the ER protein translocation channel (Prinz et al., 2000). Under stressed condition, Ire1 oligomerises and concentrates in clusters at ER membrane (Kimata et al., 2007).

1.1.3.3.2 Activation and Deactivation of Ire1

Activation of IRE1 differs between yeast and mammalian cells. In yeast, IRE1 is primarily activated by the presence of unfolded proteins or ligands, while in mammalian cells, its activation is mainly dependent on its interaction with BiP (Liu et al., 2000). Yeast IRE1

exhibits a MHC-like peptide binding groove, suggesting a direct activation mechanism by unfolded proteins. Studies using the ER luminal domain of yeast IRE1 support this, demonstrating preferential binding to specific residue-containing peptides, leading to activation upon peptide binding (Gardner & Walter, 2011).

Despite variations in the activation mechanisms between yeast and mammalian systems, downstream activation processes appear to be conserved across eukaryotes. In response to ER stress, IRE1 undergoes oligomerisation, mediated by the luminal domain of the peptide-binding structures in yeast, positioning it in the ER membrane plane. This allows for *trans*-autophosphorylation and initiation of RNase activity (Li et al., 2010; Lin et al., 2007).

However, under prolonged stress in HEK293 cells, IRE1 seems to become incapacitated, possibly to prevent activation of apoptotic cascades even in the absence of stress relief. This incapacitation is characterised by dissociation of clusters over 6-8 hours after stress induction, accompanied by dephosphorylation starting at four hours and decreasing at six hours, leading to reduced XBP-1 splicing (Li et al., 2010).

The deactivation process can be considered a natural consequence of the formation of multimers. Once free IRE1 molecules become trapped within higher-order structures, their steric freedom to activate and deactivate diminishes. As the structures grow in size, more IRE1 monomers are sequestered within higher-order structures, resulting in their reduced availability in the free cytoplasmic reservoir (Pincus et al., 2010). The fully functioning kinase domain is likely involved in the deactivation mechanism. In yeast, a kinase-defective IRE1 mutant failed to properly deactivate in a reporter assay, causing continuous ER stress and impairing cell survival (Rubio et al., 2011). Phosphorylation and de-phosphorylation processes are likely necessary for both the assembly and disassembly of the IRE1 multimer, contributing to the homeostatic adaptation to ER stress.

1.1.4 *HAC1* mRNA Splicing Process by the Ire1 RNase Domain

In the process of Hac1 splicing, it is important to note that $HAC1^u$ mRNA ("u" for uninduced) is continuously transcribed, but it is not translated in the cytosol (Rüegsegger et al., 2001) . When the cytosolic RNase domain of Ire1 is activated, it cleaves the intron from $HAC1^u$ mRNA at the 5' and 3' splice junctions, resulting in the splicing of *HAC1* mRNA and the removal of a 252-nucleotide sequence from near the 3' end of $HAC1^u$ mRNA (Rüegsegger et al., 2001; Sidrauski & Walter, 1997). This splicing produces $HAC1^i$ mRNA ("i" for induced),

which can be translated into Hac1 transcription factor (Cox & Walter, 1996), leading to activation of the UPR. The two resulting exons are then joined together by tRNA ligase, producing a new mRNA called *HAC1*^{i} ("i" for induced) (Gardner et al., 2013; Sidrauski et al., 1996). *HAC1*^{i} mRNA encodes a different protein with an 18 amino acid tail containing the transactivation domain (Sidrauski et al., 1996). Without the removal of the intron, *HAC1* mRNA remains untranslated due to an interaction between the intron and the 5' untranslated region (5' UTR) of HAC1 (Rüegsegger et al., 2001). The newly generated *HAC1*^{i} mRNA can be efficiently translated to produce a functional transcription activator, Hac1^{i} (Cox & Walter, 1996). The process of splicing out the intron is essential for *HAC1* mRNA to produce functioning protein. This is because the intron contains a transcriptional attenuator that inhibits *HAC1* mRNA translation (Rüegsegger et al., 2001) (Fig 1.3). Hac1$_{i}$ is a transcription factor that contains a potent bZIP domain, which is required for the expression of UPR genes such as *KAR2* and *PDI1* that code for molecular chaperones, aiding in the tolerance and recovery from ER stress (Mori et al., 1992).On the other hand, *HAC1*^{u} mRNA is continuously transcribed but remains untranslated due to the presence of a transcriptional attenuator that inhibits *HAC1* mRNA translation (Rüegsegger et al., 2001). However, experimental manipulation such as mutating the nucleotides involved in base-pairing can allow for the translation of *HAC1*^{u}, although its encoded protein is unable to activate transcription as efficiently as Hac1^{i} (Chapman & Walter, 1997; Cox et al., 1997). To activate UPR-associated genes, the bZIP transcription factor of Hac1^{i} associates with a conserved promoter sequence known as the UPRE (Kimata et al., 2003; Kohno et al., 1993). The UPRE is responsible for the specificity of the UPR in gene expression response.

1.1.5 Activation of UPR by Hac1^{i}

Once Hac1^{i} is produced through the splicing of *HAC1*^{u} mRNA, it plays a pivotal role in triggering the UPR. Hac1^{i} is transported into the nucleus via its nuclear localisation sequence (29-RKRAKTK-35), which is present in both forms of Hac1(Gardner et al., 2013). Once inside the nucleus, Hac1^{i} functions as a transcription factor by binding to specific conserved sequences called unfolded protein response elements (UPREs) (Kimata et al., 2003; Kohno et al., 1993).. UPREs are found in the promoters of several UPR target genes, including ER resident chaperones like *KAR2*, *PDI1*, *EUG1*, *FKB2*, and *LHS1*, as well as components of the protein secretory pathway and genes involved in ER-associated degradation (Mori et al., 1998; Travers et al., 2000).

Transcription of these UPR target genes is further facilitated by the co-activator complex SAGA histone acetyltransferase, composed of Gcn5, Hfi1, Ada2, Ngg1, Ada5, Spt3, and Spt7 (Welihinda et al., 1999).The Gcn5/Ada5 complex subunits enhance histone acetylation at the chromatin encoding UPR-related genes UPR-related genes, promoting transcription by reducing positive charge interactions between lysine residues in histones and the negatively charged DNA wrapped around them (Brownell et al., 1996; Welihinda et al., 2000).

The UPR, triggered by the activation of $Hac1^{i}$, goes beyond regulating ER protein folding and homeostasis. It also plays a crucial role in sensing and mediating nitrogen-regulating effects and influencing cellular development and environmental adaptation (Kaufman, 2002; Schröder et al., 2000).The transcriptional activation of nitrogen-sensitive genes is modulated by the UPR-sensitive bZIP transcription factor $Hac1^{i}$, providing further complexity to the response (Schröder et al., 2004).

1.1.6 Regulation of Hac1 Half-life and the UPR

Both $Hac1^{u}$ and $Hac1^{i}$, which are two different transcripts originating from the same transcription start site, have a relatively short half-life of approximately 1.5-2.0 minutes, leading to their rapid degradation through the ubiquitination pathway. The degradation of Hac1 is facilitated by its PEST degron, which interacts with the SCF^{Cdc4} ubiquitin-ligase complex (Chapman & Walter, 1997). Additionally, $Hac1^{u}$ has a slightly shorter half-life compared to $Hac1^{i}$ due to post-transcriptional silencing mediated by a 10 amino acid intron-encoded C-terminal tail (Di Santo et al., 2016).

The rapid turnover of Hac1 is essential to ensure a continuous supply of Hac1, which is vital for sustaining the UPR. To achieve this, the *HAC1* gene undergoes autoregulation through its own UPRE promoter region (Ogawa & Mori, 2004).This autoregulatory mechanism creates a positive feedback loop, where elevated levels of Hac1 lead to enhanced transcription of *HAC1*, ultimately resulting in the production of more Hac1.This feedback loop ensures a robust UPR activation to cope with ER stress

As a consequence, the splicing of $HAC1^{u}$ by Ire1 is reduced (Welihinda et al., 1998), leading to the rapid degradation of the remaining Hac1 protein. This regulatory mechanism helps to fine-tune the UPR and prevent excessive activation once ER stress is resolved.

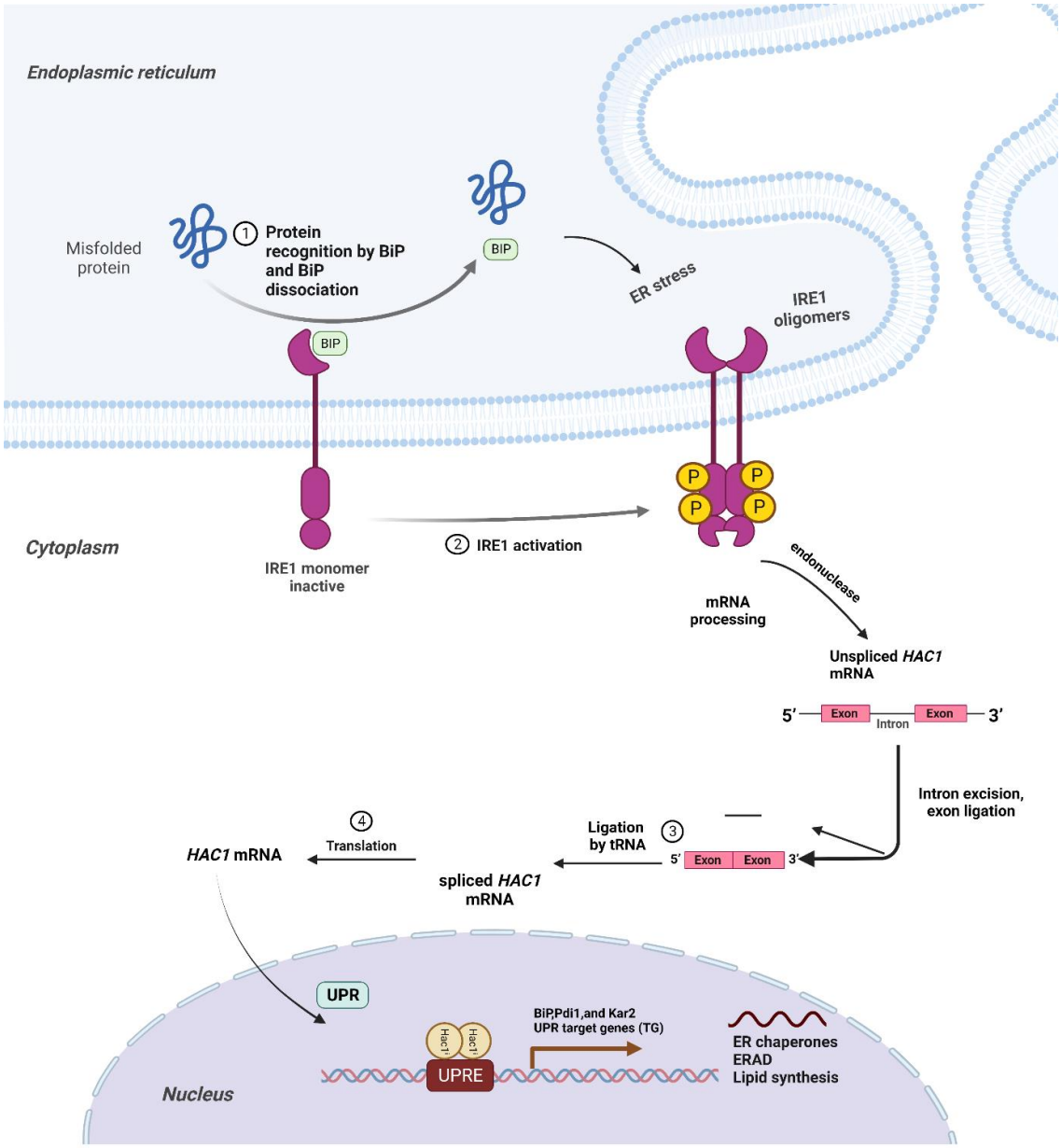

Figure 1.4. A schematic representation of UPR signalling pathway.
1) Under normal conditions in the ER, inactive Ire1 monomers, which are purple transmembrane proteins, are bound to BiP, a light green labelled protein. 2) When there is ER stress and unfolded proteins accumulate, BiP dissociates from Ire1 and binds to the unfolded proteins. This leads to Ire1 monomers undergoing *trans*-autophosphorylation, a process that activates the endoribonuclease domain by phosphorylation shown with orange circles on the cytosolic side of the membrane. 3) Once activated, the endoribonuclease cleaves the *HAC1* mRNA, and the spliced mRNA is ligated by tRNA ligase. 4) The newly spliced mRNA is referred to as *HAC1*^{i} mRNA, which is labelled light orange. The *HAC1*^{i} mRNA is then translated to the functional transcription factor Hac1^{i} which enters the nucleus and binds the UPRE promoter region which is labelled dark brown, and it is a regulatory element in the promoter region of certain genes. This binding initiates the transcription of genes involved in the unfolded protein response.

1.2 Understanding the Functional Interplay between the Kinase and Endonuclease Domains of Ire1

The cooperative nature of the activity of Ire1 is crucial for achieving full RNase activity, which is only attained when multiple Ire1 molecules come together in an oligomeric form (Korennykh et al., 2009). Analysis of the crystal structure reveals a symmetrical arrangement of the kinase domains, attached to an RNase dimer that possesses two distinct active sites (Fig. 1.5) (Lee et al., 2008). Notably, the crystal structures of human IRE1α indicate that the RNase activity is limited when the kinase domains are in an inactive conformation, whereas active endonuclease domains correlate with active kinase conformations (Joshi et al., 2015). The formation of higher order oligomers is facilitated by the active conformation of the kinase domain, which is bound to nucleotide (Lee et al., 2008). Initially, it was believed that phosphorylation by the kinase domain was essential for activating the RNase domain of IRE1 (Korennykh et al., 2009; Shamu & Walter, 1996). However, in the presence of the ATP-competitive kinase inhibitor 1NM-PP1, the UPR remained intact, indicating that a conformational change, rather than phosphorylation, is pivotal for the function of Ire1 (Papa et al., 2003). This discovery led to the proposition that 1NM-PP1 enforces a closed conformation, promoting dimerisation and activation of the RNase domain (Lee et al., 2008). It is also postulated that the binding of 1NM-PP1 may differ significantly from ADP binding, rendering Ire1 unresponsive to its phosphorylation status or exerting a strong enough binding force to shift the inhibitory conformation of the activation segment. Furthermore, the UPR mediated by IRE1 may not necessarily require phosphorylation, as treatment with the ATP-competitive kinase inhibitor did not disrupt UPR function (Papa et al., 2003). This suggests that a conformational change in IRE1 is potentially more important for its activity than the phosphorylation of specific residues. Other studies have also investigated the role of conformational changes in regulating IRE1 activity. For instance, the decay of endoplasmic reticulum-localised mRNAs involves both RNase-dependent cleavage events and destabilisation due to altered mRNA structure or interactions with other proteins (Hollien & Weissman, 2006). Collectively, these studies suggest that while post-translational modifications, such as phosphorylation, can play a role in regulating IRE1 function under specific conditions, they are likely just one component of a broader network involving dynamic structural rearrangements driven by ligand binding or other stimuli.

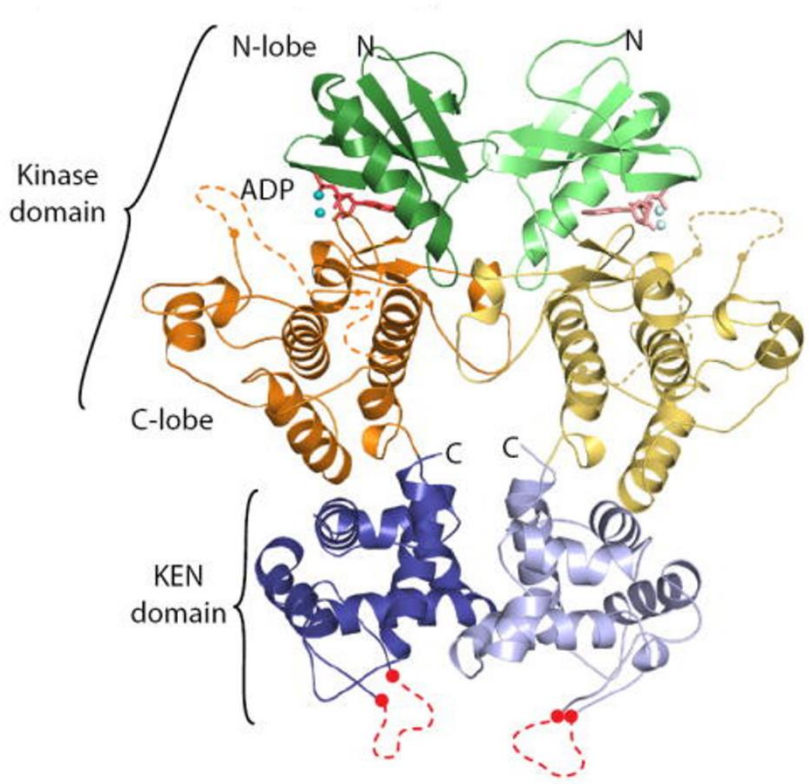

Figure 1.5. An illustration of the crystal structure of the kinase domain of Ire1.
This figure, as documented by Lee et al. (2008), illustrates the crystal structure of the kinase domain of Ire1. In the figure, the N-lobe, C-lobe, and KEN domain are depicted in green, orange, and blue, respectively. The blue region corresponds to the kinase-extension nuclease (KEN) domain, housing the RNase domain responsible for splicing *HAC1* mRNA. ADP, along with coordinating metal ions, can be observed within the catalytic cleft of the kinase domain. The figure specifically emphasises the binding of ADP to the nucleotide-binding pocket (NBP).

1.3 Gaining Insight into the Ire1 Protein Kinase Activity through Examination of Evolutionary Conservation in Kinases mutants

Protein kinases, such as Ire1, catalyse the transfer of the γ-phosphate group of ATP onto serine, threonine, or tyrosine residues of substrate proteins (Hodgson & Schröder, 2011). These kinases operate through a bi-substrate kinetic mechanism, requiring both ATP and substrate protein for the reaction (Adams, 2001). The catalytic functions of kinases rely on the presence of numerous conserved residues near the phosphoryl transfer site, as supported by X-ray, biochemical, and biophysical data (Adams, 2001).

Phosphorylation is vital for various cellular processes, including protein regulation and signal transduction. One common regulatory mechanism for protein kinases involves phosphorylating the activation loop (Nolen et al. 2004). Activation of numerous kinases involves the phosphorylation of a specific region called the activation segment. This segment has garnered significant attention in studying the correlation between the structure and function of protein kinases. The initial crystal structure of the PKA catalytic subunit was determined while it was in an active state, and it exhibited phosphorylation within the activation segment. This structure provided valuable insights into how the phospho-residue within the activation segment interacts with a cluster of positively charged residues on the surface of the kinase (Knighton et al., 1991). Early studies on inactive protein kinase structures demonstrated that the unphosphorylated activation loop could assume diverse conformations, which were notably different from those observed in PKA. In some instances, these unphosphorylated activation loops even displayed disorder in the crystal structures (Goldberg et al., 1996; Hubbard et al., 1994; Zhang et al., 1994). The activation segment in kinases possesses distinct structural characteristics and components that play a crucial role in their function. It is positioned between the conserved DFG and APE tripeptide motifs and generally spans a length of 20-35 residues. Of particular importance is the DFG motif, which serves as a binding site for Mg^{2+} ions. The activation segment also encompasses secondary structural elements, including a short β sheet known as β9, the activation loop, and the P+1 loop. These components collectively contribute to the overall structure and regulation of kinases (Nolen et al., 2004). Several well-studied mutations in the core cytosolic area affecting Ire1 activity have shed light on its functional mechanisms. For instance, K702 in the catalytic region is predicted to facilitate nucleophile attack by interacting with the α- and β-phosphates of ATP and neutralising the negative charges on the β-phosphate. It has been reported as essential for Ire1 activity (Mori et al., 1993). Mutations of D828 to alanine

(D828A) have been proposed to bind ATP but fail to undergo autophosphorylation (Chawla et al., 2011). Consequently, the assumption that nucleotide binding mimics an active RNase conformation necessary for mRNA splicing may be questionable. Alternative residues, specifically D797 and K799, have been proposed to serve as catalytic elements, participating in the coordination of the terminal ATP phosphate and promoting the transfer of phosphate (Rubio et al., 2011). Mutations in conserved residues within the endonuclease domain disrupt RNase activity but do not hinder autophosphorylation, indicating that RNase activity is not necessary for kinase activity (Tirasophon et al., 2000). For instance, studies on the activation loop of Ire1 have found that the D836 residue can partially bypass phosphorylation, but its effectiveness depends on the phosphorylation of S837, T844, or S850 residues for maximum UPR activation. This suggests a hierarchical relationship among phosphorylation sites, with S841 and S840 acting as primary phosphorylation sites (Armstrong et al., 2017). The investigation of protein kinase mutants holds immense significance in unraveling the intricate relationship between kinase and RNase activities in Ire1. These mutants serve as valuable tools to investigate specific mutations that exhibit RNase activity despite lacking kinase activity. Understanding the functional interplay between these domains is crucial for elucidating the underlying mechanisms of Ire1 activation and its role in UPR. By studying these mutants, I propose to gain insight into the complex regulatory networks governing the activity of Ire1 and its implications for cellular stress responses. Furthermore, identifying mutations that decouple kinase and RNase activities can shed light on alternative pathways and mechanisms that contribute to UPR signalling.

The molecular mechanisms of oligomerisation and activation of the RNase domain are not entirely clear. There are various theories concerning the deactivation of the kinase domain. According to one study, the process involves *trans*-autophosphorylation within the hyperphosphorylation loop, which is a 28-amino acid loop highly phosphorylated between residues 864 and 892. This phosphorylation event is essential for disassembly and functions as a reset mechanism (Rubio et al., 2011). In contrast, another publication argues that dephosphorylation, rather than phosphorylation, serves as the switch for attenuating the UPR (Chawla et al., 2011). These findings, as depicted in Figure 1.6, highlight the significance of these specific amino acid mutations and their potential implications for the Ire1 function.

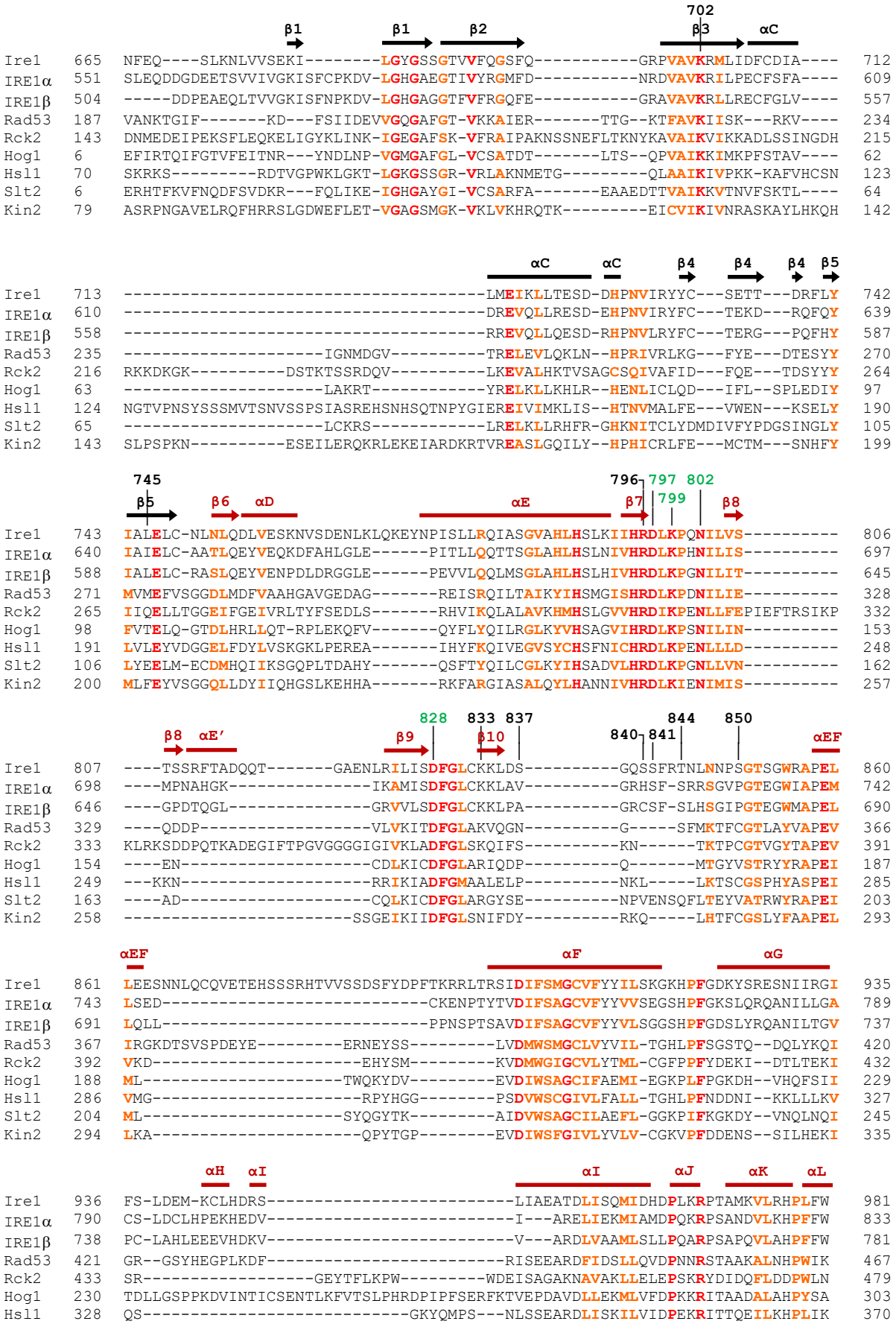
β1 β1 β2 702 β3 αC
Ire1 665 NFEQ----SLKNLVVSEKI--------LGYGSSGTVVFQGSFQ----------GRPVAVKRMLIDFCDIA---- 712
IRE1α 551 SLEQDDGDEETSVVIVGKISFCPKDV-LGHGAEGTIVYRGMFD----------NRDVAVKRILPECFSFA---- 609
IRE1β 504 -----DDPEAEQLTVVGKISFNPKDV-LGHGAGGTFVFRGQFE----------GRAVAVKRLLRECFGLV---- 557
Rad53 187 VANKTGIF-------KD---FSIIDEVVGQGAFGT-VKKAIER-------TTG--KTFAVKIISK---RKV---- 234
Rck2 143 DNMEDEIPEKSFLEQKELIGYKLINK-IGEGAFSK-VFRAIPAKNSSNEFLTKNYKAVAIKVIKKADLSSINGDH 215
Hog1 6 EFIRTQIFGTVFEITNR---YNDLNP-VGMGAFGL-VCSATDT-------LTS--QPVAIKKIMKPFSTAV---- 62
Hsl1 70 SKRKS---------RDTVGPWKLGKT-LGKGSSGR-VRLAKNMETG---------QLAAIKIVPKK-KAFVHCSN 123
Slt2 6 ERHTFKVFNQDFSVDKR---FQLIKE-IGHGAYGI-VCSARFA-------EAAEDTTVAIKKVTNVFSKTL---- 64
Kin2 79 ASRPNGAVELRQFHRRSLGDWEFLET-VGAGSMGK-VKLVKHRQTK---------EICVIKIVNRASKAYLHKQH 142
αC αC β4 β4 β4 β5
Ire1 713 -----LMEIKLLTESD-DHPNVIRYYC---SETT---DRFLY 742
IRE1α 610 -----DREVQLLRESD-EHPNVIRYFC---TEKD---RQFQY 639
IRE1β 558 -----RREVQLLQESD-RHPNVLRYFC---TERG---PQFHY 587
Rad53 235 ----------IGNMDGV----------TRELEVLQKLN--HPRIVRLKG---FYE---DTESYY 270
Rck2 216 RKKDKGK----------DSTKTSSRDQV----------LKEVALHKTVSAGCSQIVAFID---FQE---TDSYYY 264
Hog1 63 ----------LAKRT----------YRELKLLKHLR--HENLICLQD---IFL--SPLEDIY 97
Hsl1 124 NGTVPNSYSSSMVTSNVSSPSIASREHSNHSQTNPYGIEREIVIMKLIS--HTNVMALFE---VWEN---KSELY 190
Slt2 65 ----------LCKRS----------LRELKLLRHFR-GHKNITCLYDMDIVFYPDGSINGLY 105
Kin2 143 SLPSPKN----------ESEILERQKRLEKEIARDKRTVREASLGQILY--HPHICRLFE---MCTM---SNHFY 199
745 796 797 802
β5 β6 αD αE β7 799 β8
Ire1 743 IALELC-NLNLQDLVESKNVSDENLKLQKEYNPISLLRQIASGVAHLHSLKIIHRDLKPQNILVS---------- 806
IRE1α 640 IAIELC-AATLQEYVEQKDFAHLGLE------PITLLQQTTSGLAHLHSLNIVHRDLKPHNILIS---------- 697
IRE1β 588 IALELC-RASLQEYVENPDLDRGGLE------PEVVLQQLMSGLAHLHSLHIVHRDLKPGNILIT---------- 645
Rad53 271 MVMEFVSGGDLMDFVAAHGAVGEDAG-------REISRQILTAIKYIHSMGISHRDLKPDNILIE---------- 328
Rck2 265 IIQELLTGGEIFGEIVRLTYFSEDLS-------RHVIKQLALAVKHMHSLGVVHRDIKPENLLFEPIEFTRSIKP 332
Hog1 98 FVTELQ-GTDLHRLLQT-RPLEKQFV-------QYFLYQILRGLKYVHSAGVIHRDLKPSNILIN---------- 153
Hsl1 191 LVLEYVDGGELFDYLVSKGKLPEREA-------IHYFKQIVEGVSYCHSFNICHRDLKPENLLLD---------- 248
Slt2 106 LYEELM-ECDMHQIIKSGQPLTDAHY-------QSFTYQILCGLKYIHSADVLHRDLKPGNLLVN---------- 162
Kin2 200 MLFEYVSGGQLLDYIIQHGSLKEHHA-------RKFARGIASALQYLHANNIVHRDLKIENIMIS---------- 257
828 833 837 844 850
β8 αE′ β9 β10 840 841 αEF
Ire1 807 ----TSSRFTADQQT-------GAENLRILISDFGLCKKLDS----------GQSSFRTNLNNPSGTSGWRAPEL 860
IRE1α 698 ----MPNAHGK----------IKAMISDFGLCKKLAV----------GRHSF-SRRSGVPGTEGWIAPEM 742
IRE1β 646 ----GPDTQGL----------GRVVLSDFGLCKKLPA----------GRCSF-SLHSGIPGTEGWMAPEL 690
Rad53 329 ----QDDP----------VLVKITDFGLAKVQGN----------G-----SFMKTFCGTLAYVAPEV 366
Rck2 333 KLRKSDDPQTKADEGIFTPGVGGGGIGIVKLADFGLSKQIFS----------KN------TKTPCGTVGYTAPEV 391
Hog1 154 ----EN----------CDLKICDFGLARIQDP----------Q-------MTGYVSTRYYRAPEI 187
Hsl1 249 ---KKN----------RRIKIADFGMAALELP----------NKL-----LKTSCGSPHYASPEI 285
Slt2 163 ----AD----------CQLKICDFGLARGYSE----------NPVENSQFLTEYVATRWYRAPEI 203
Kin2 258 ----------SSGEIKIIDFGLSNIFDY----------RKQ-----LHTFCGSLYFAAPEL 293
αEF αF αG
Ire1 861 LEESNNLQCQVETEHSSSRHTVVSSDSFYDPFTKRRLTRSIDIFSMGCVFYYILSKGKHPFGDKYSRESNIIRGI 935
IRE1α 743 LSED----------CKENPTYTVDIFSAGCVFYYVVSEGSHPFGKSLQRQANILLGA 789
IRE1β 691 LQLL----------PPNSPTSAVDIFSAGCVFYYVLSGGSHPFGDSLYRQANILTGV 737
Rad53 367 IRGKDTSVSPDEYE---------ERNEYSS---------LVDMWSMGCLVYVIL-TGHLPFSGSTQ--DQLYKQI 420
Rck2 392 VKD----------EHYSM---------KVDMWGIGCVLYTML-CGFPPFYDEKI--DTLTEKI 432
Hog1 188 ML----------TWQKYDV---------EVDIWSAGCIFAEMI-EGKPLFPGKDH--VHQFSII 229
Hsl1 286 VMG----------RPYHGG---------PSDVWSCGIVLFALL-TGHLPFNDDNI--KKLLLKV 327
Slt2 204 ML----------SYQGYTK---------AIDVWSAGCILAEFL-GGKPIFKGKDY--VNQLNQI 245
Kin2 294 LKA----------QPYTGP---------EVDIWSFGIVLYVLV-CGKVPFDDENS--SILHEKI 335
αH αI αI αJ αK αL
Ire1 936 FS-LDEM-KCLHDRS----------LIAEATDLISQMIDHDPLKRPTAMKVLRHPLFW 981
IRE1α 790 CS-LDCLHPEKHEDV----------I---ARELIEKMIAMDPQKRPSANDVLKHPFFW 833
IRE1β 738 PC-LAHLEEEVHDKV----------V---ARDLVAAMLSLLPQARPSAPQVLAHPFFW 781
Rad53 421 GR--GSYHEGPLKDF----------RISEEARDFIDSLLQVDPNNRSTAAKALNHPWIK 467
Rck2 433 SR----------GEYTFLKPW---------WDEISAGAKNAVAKLLELEPSKRYDIDQFLDDPWLN 479
Hog1 230 TDLLGSPPKDVINTICSENTLKFVTSLPHRDPIPFSERFKTVEPDAVDLLEKMLVFDPKKRITAADALAHPYSA 303
Hsl1 328 QS----------GKYQMPS---NLSSEARDLISKILVIDPEKRITTQEILKHPLIK 370

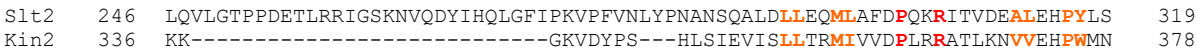

Figure 1.6. Amino acid sequence alignment of protein serine/threonine kinase domains.
The amino acid sequence alignment includes the protein serine/threonine kinase domains of several organisms: *S. cerevisiae* 1 Ire1 (NP_011946.1), human IRE1α (NP_001424.1), human IRE1β (NP_150296.1), Rad53 (NP_015172.1), Rck2 (NP_013349.1), Hog1 (NP_013214.1), Hsl1 (NP_012821.1), Slt2 (NP_011895.1), and Kin2 (NP_013197.1). Additionally, the α helices and β strands in the N (black) and C (red) lobes of Ire1, as described by (Lee et al., 2008), are indicated by lines or arrows, respectively. Conserved residues are shown in red, and point mutations used in the study are depicted in green, while similar residues are displayed in orange. This sequence alignment was created by Dr. Martin Schroeder.

1.4 A Model for Investigating intrageneic Suppression in Ire1 Mutants

In this study, I present a novel model for examining intrageneic suppression in Ire1, a critical protein involved in cellular stress response pathways. By using alanine mutants, I aim to elucidate the intricate mechanisms underlying this phenomenon. The strategic use of alanine mutants enables precise observation of the effects resulting from targeted amino acid substitutions, providing specific and detailed information about the structural and functional implications of intragenic suppression in Ire1. D797A is a mutant in the protein kinase domain and this mutant has no detectable protein kinase or RNase activity (Lee et al., 2008). In previous research, specific residues, namely D797 and K799, within the nucleotide-binding pocket of Ire1 kinase were altered by substituting them with asparagine. These mutations disrupted the transfer of protons and completely inhibited phosphorylation, while preserving the overall structure of the kinase. Mass spectrometry analysis demonstrated that the mutant variant, D797N K799N Ire1, was unable to undergo phosphorylation. However, despite this lack of phosphorylation, the mutant retained its endoribonuclease activity and remained capable of cleaving RNA substrates similar to the WT Ire1 (Rubio et al., 2011). Through a series of experiments, this research efforts to advance our comprehension of this captivating regulatory mechanism and its impact on the function of Ire1 within cellular stress response pathways.

1.4.1 Mutational analysis

In-depth understanding of the protein function within signalling cascades can be achieved through the use of point mutations, which allow assessment of the contributions of individual motifs. Such mutations can provide information regarding the specific members of these pathways that are influenced by the protein.

In this study, point mutants were employed to target the kinase domain of IRE1. However,

comprehending the effects of these mutations requires an understanding of how these domains function in the WT Ire1.

The kinase domains, which are present in approximately 2% of eukaryotic genes, consist of highly conserved motifs within a core region of 200-250 amino acids. These motifs enable protein kinases to catalyse the transfer of the γ-phosphate of ATP to specific tyrosine or serine/threonine residues on the target protein. This process is facilitated by the presence of a divalent metal ion, such as $Mg^{2+,}$ and protein kinases usually exhibit specificity towards either tyrosine or serine/threonine residues. Consequently, the mechanisms by which kinases catalyse the transfer of the γ-phosphate of ATP to target proteins are well understood, allowing manipulation through point mutations (Fig. 1.6).

These point mutations induce conformational changes, causing the activation loop to fold and interact with positively charged residues within the ribonuclease activity and dimerisation pocket. By altering amino acids within the core region of 200-250 amino acids in the kinase domain, a series of mutants lacking kinase activity have been created (Fig. 1.7). These mutant variants are outlined below.

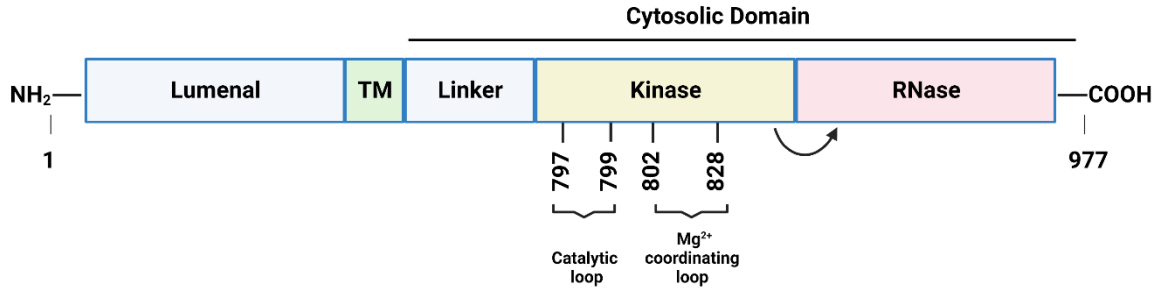

Figure 1.7. Simplified structure of yeast Ire1: kinase and RNase domains.

The diagram shows a simplified structure of yeast Ire1, consisting of two interconnected domains, namely the kinase domain and the RNase domain. The kinase domain controls the RNase domain, as represented by the arrow in the diagram. Under the graph, there are indications of mutations that occur in the Ire1 structure. Created with BioRender.com

1.4.1.1 D797A

In yeast, the D797A mutation in the protein kinase domain of Ire1 has been studied to unravel the molecular mechanisms underlying protein kinase activity and RNase activity. This mutation disrupts the catalytic aspartate residue, D797, which plays a crucial role in

positioning the nucleophile for attack and abstracting a proton during the late stage of the phosphoryl transfer reaction (Fig. 1.8). As a result of the D797A mutation, both protein kinase activity and RNase activity are lost (Lee et al., 2008). To further explore the interplay between the D797A mutation and other mutations, as well as the potential for intragenic suppression by other mutants, previous studies have revealed the rescue of RNase activity in the D797N K799N mutant, indicating the presence of compensatory mechanisms or interactions among different mutations that impact Ire1 activity (Rubio et al., 2011).This analysis could shed light on potential compensatory mechanisms or interactions between different mutations in the context of Ire1 activity.

1.4.1.2 K799A

In this study, I aim to explore the functional significance of the amino acid residue K799 (lysine) in the context of the kinase domain. K799 plays a crucial role in stabilising the interaction between the phosphate and the γ phosphate of ATP, thereby facilitating the transfer of phosphoryl groups and ensuring proper kinase domain function (Fig. 1.8) (Adams, 2001). To investigate the specific impact of the K799A mutation, where lysine is replaced with alanine, I will compare the behaviour of the mutant to that of the WT protein. By examining how the mutation affects the activity of protein, I can gain insights into the functional contributions of K799 and deepen understanding of the molecular mechanisms underlying the function of kinase domain. Additionally, I will explore the interactions between the K799A mutant and other mutants, such as D797A. The D797A mutation disrupts the catalytic aspartate residue, which is involved in positioning the nucleophile during the phosphoryl transfer reaction. By combining the K799A and D797A mutants, I can investigate how these mutations collectively impact the overall activity and behaviour of the Ire1. This combinatorial approach allows to unravel the intricate interplay between different residues within the kinase domain and their influence on Ire1 function. Through these investigations, I seek to uncover the functional consequences of these mutations and shed light on the underlying mechanisms that govern the kinase domain of the Ire1.

1.4.1.3 D828A

The D828A mutation refers to a substitution of the amino acid aspartic acid (D) with alanine (A) at position 828 in the kinase domain of Ire1. This mutation disrupts the DFG motif, which is a conserved motif involved in stabilising the active conformation of many protein

kinases. Aspartic acid (D828) interacts with the essential Mg^{+2} and it has very important role in catalytic function (Fig. 1.8) (Adams, 2001). In the context of ER stress, the D828A mutation prevents proper attenuation of the RNase activity of Ire1 when ER function is recovered. This lack of attenuation leads to cell death under ER stress conditions. The inability of cells expressing D828A Ire1 to grow under ER stress highlights the importance and necessity of proper attenuation mechanisms during the activation and recovery processes of the UPR (Chawla et al., 2011). By combining the D828A and D797A mutants, I aim to examine the combined effects of these mutations on the overall activity and behaviour of Ire1. This aims to investigate the precise molecular interactions between these residues within the kinase domain of Ire1. By studying the specific roles and interplay among these residues, I can gain a better understanding of their collective contributions to the catalytic function and activity of Ire1.

1.4.1.4 N802A

The N802A mutation in the kinase domain of Ire1 involves substituting the amino acid asparagine (N) with alanine (A) at position 802. This mutation affects the coordination of the second Mg^{2+} ($Mg_2{}^{2+}$) ion, which is facilitated by the amido group of N802 and the carboxylate of D828. This coordination is crucial for stabilising the negative charges that arise during the cleavage of the bond between the oxygen atom bridging the β and γ phosphates. Both the N802A and D828A residues play critical roles in coordinating the magnesium ions and neutralising charges on the phosphate groups of ATP/ADP. Given the importance of these residues, it is hypothesised that mutations affecting N802 and D828 would have significant effects on the function and activity of the kinase domain. Through the combination of the N802A and D797A mutants, I will examine the cumulative effects of these mutations on the overall activity and behaviour of Ire1. To understand the combined effects of these mutations, the N802A and D797A mutants will be studied together. This approach will allow for an investigation into the additive impact of these mutations on the overall activity and behaviour of Ire1. By examining the interplay between the N802A and D797A mutations, a detailed understanding can be obtained regarding the intricate interactions and their consequences within the kinase domain.

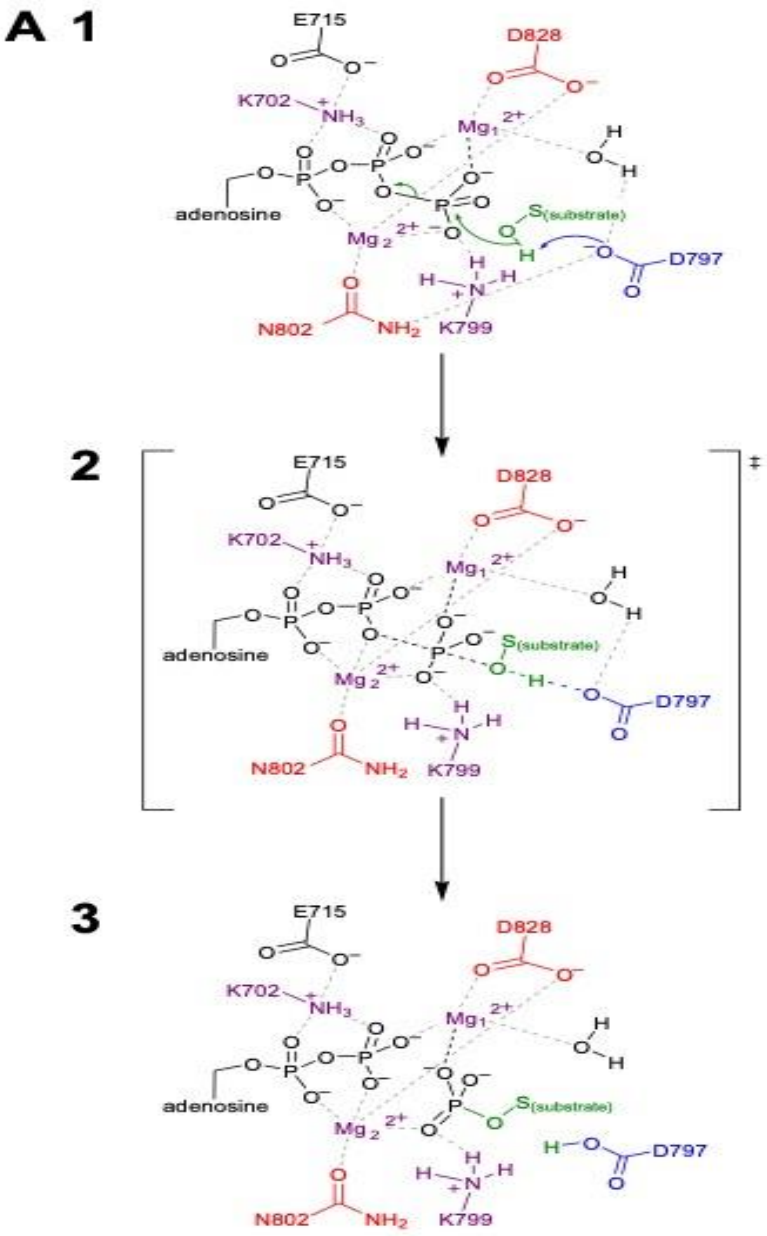

Figure 1.8. Protein kinase catalytic mechanism.
(A 1) schematic shows the location of each functional domain and the orientation of substrate binding to various domain in Ire1. D797 (catalytic aspartate) in Ire1, positions the nucleophile for attack and abstracts a proton from the nucleophile late in the phosphoryl transfer reaction. Blue colour indicates catalytic residues, red colour indicates the residues engaged in correctly positioning the triphosphate group of ATPs for γ-phosphoryl transfer reaction, and in purple, residues have both functions. (A 2) γ-phosphoryl transfer is started by nucleophilic attack of the hydroxyl group of a serine or threonine. (A 3) after completion of the γ-phosphoryl transfer reaction, products bound to catalytic site.

1.5 Aims and objectives

1.5.1 Aim

Previous studies have reported that certain protein kinase mutants, such as K702A and D797A (Mori et al., 1993; Lee et al., 2008), exhibit minimal or no RNase activity. Conversely, other mutants, including D828A and D797N K799N (Chawla et al., 2011; Rubio et al., 2011), demonstrate significantly higher levels of RNase activity. Consequently, the primary objective of this thesis is to investigate whether the rescue of RNase activity observed in the D797N K799N mutant can also be observed in alanine mutants (D797A K799A). Previous research suggests that the RNase activity in the D797N K799N mutant is attributed to the minimal disruption of the hydrogen bonding network, a characteristic that should not be present in the D797A K799A mutant. Additionally, we aim to address concerns regarding the catalytic role of the aspartate residue in protein kinase reactions, as substituting it with an amide residue is expected to result in reduced catalytic capacity.

In addition to the previously stated objectives, an exploration of the shared functional characteristics of K799, N802, and D828 can provide compelling evidence supporting their crucial roles in the RNase activity of Ire1. These residues exhibit direct interaction with the γ-phosphate of ATP, which is a fundamental component in protein kinase reactions. This direct contact strongly suggests their involvement in critical processes such as ATP binding and subsequent phosphorylation events.

Moreover, their interactions with Mg^{2+} ions, facilitating the interaction with the triphosphoryl group of ATP, add another layer of importance. Mg^{2+} ions act as indispensable cofactors in numerous enzymatic reactions, including ATP hydrolysis, which is vital for the catalytic function of Ire1. The interactions of K799, N802, and D828 with Mg^{2+} ions likely contribute to stabilising the ATP-bound state and facilitating the necessary conformational changes crucial for efficient catalysis.

To further elucidate the specific roles of K799, N802, and D828 in the RNase activity of Ire1, we intend to conduct a detailed analysis of the phenotypes exhibited by single point mutants targeting these residues. By carefully studying the phenotypes of mutants generated by substituting these specific amino acids, such as K799A, N802A, and D828A, we aim to uncover the functional consequences of these substitutions.

Specifically, we will investigate the impact of mutations such as K799A, N802A, D828A on the RNase activity of Ire1. By comparing the phenotypes of these mutants to WT Ire1, we can discern the specific functional characteristics conferred by these residues. Furthermore, investigating whether introducing the K799A, N802A, or D828A mutations into the D797A Ire1 can restore RNase activity would provide insights into the functional similarities and shared mechanisms among these residues.

By conducting a thorough examination of the structural and biochemical data obtained from these experiments, we can robustly confirm and enhance the proposed functional similarities among D797A, K799A, N802A, and D828A Ire1. This comprehensive analysis will greatly contribute to our understanding of the complex molecular mechanisms underlying intragenic suppression in Ire1, specifically regarding the restoration of RNase activity in D797A Ire1. These accomplishments directly meet the objectives outlined in sections 1.5.2.1 - 1.5.2.5, specifically concerning the suppression phenomenon in Ire1 and the restoration of RNase activity in D797A Ire1.

1.5.2 Objectives

1.5.2.1 Direct in vivo detection of HAC1 mRNA processing through Northern Blot analysis

The direct in *vivo* detection of *HAC1* mRNA processing through Northern Blot analysis was a crucial component of this study, aimed at investigating the process of *HAC1* mRNA processing and its translation into $Hac1^{i}$ protein.

The primary objective of this study was to examine the impact of specific mutations, namely K799A, N802A, and D828A, on the RNase activity of Ire1. By comparing the gene expression levels, specifically the percentage of $HAC1^{i}$ mRNA, *KAR2* mRNA, and *PDI1* mRNA levels, exhibited by these mutants with WT Ire1, the distinct functional characteristics conferred by these residues could be determined. Additionally, by comparing the phenotypes among the mutants themselves, potential additive effects resulting from each mutation could be explored.

Furthermore, the study sought to evaluate whether introducing these mutations into the D797A Ire1 mutant could restore RNase activity. By assessing the percentage of $HAC1^{i}$ mRNA in these mutants and comparing it with the levels observed in WT Ire1 and D797A

Ire1, the study aimed to investigate the functional similarities and shared mechanisms among these residues.

1.5.2.2 Quantifying UPR activation through the β-Galactosidase reporter assay

The translation of $Hac1^{i}$ protein subsequently triggers the expression of UPR-associated genes by interacting with the UPRE region (Mori et al., 1996), which can be detected using a reporter assay. The β-galactosidase reporter assay provides a direct measurement of protein expression levels, allowing for the detection and characterisation of discrepancies between mRNA levels and protein abundance. Evaluating systems like the UPR requires assessing protein activity in addition to mRNA expression profiles, as post-transcriptional regulation and mRNA modifications can impact protein abundance levels (Ghaemmaghami et al., 2003). The UPRE-associated β-galactosidase reporter assay quantifies the reporter protein (β-galactosidase) in the lysate extract, enabling the precise measurement of subtle differences in the ER stress signal transduced by Ire1 in the mutants. This assay serves as a tool to observe, quantify, and compare the activation of UPR-associated gene expression in response to ER stress.

1.5.2.3 Expression of the Ire1 protein in mutants

By conducting Western blot analysis using HA-tagged Ire1, it is possible to evaluate the steady-state expression levels of Ire1 in the mutant strains. This analysis allows for the assessment of whether the mutants exhibit a complete absence of Ire1 or demonstrate significant changes in Ire1 levels. To facilitate comparison between the mutants, the levels of Ire1 protein are normalised against a highly abundant non-UPR-associated protein, such as β-actin. This normalisation approach enables the evaluation of any variations in Ire1 expression and aids in the interpretation of the observed phenotypic differences in response to ER stress.

1.5.2.4 Evaluating ER stress tolerance in vivo through spotting assays

In *vivo* spotting assays provide a means to assess the impact of reduced ER stress tolerance resulting from mutations in Ire1. Deficiencies in ER stress tolerance can be observed through reduced colony growth, indicating impaired survival under ER stress conditions. By varying the concentrations of ER stressors such as DTT, Tm, and 2DDG across multiple agar plates, the ability of the UPR to respond to different levels of ER stress can be examined. This approach is crucial as in vitro UPRE-associated reporter protein assays only provide a

snapshot of the UPR response at a specific time point. Spotting assays, on the other hand, enable the investigation of the effect of Ire1 mutations on cell fate in a live organism.

1.5.2.5 Microscopic visualisation of Ire1 clustering during ER stress

Activation of the luminal domain of Ire1 leads to the formation of clusters in *vivo* (Aragón et al., 2009; Kimata et al., 2007). Fluorescence microscopy techniques can be utilised to visualise and study the clustering phenomenon of activated luminal domain of the Ire1. By using the mCherry fluorescent protein as a label on Ire1, the clustering of Ire1 can be observed at various time points, enabling the examination of clustering dynamics over time. Moreover, through the utilisation of GFP labelling on the Sec63 protein, the localisation of Ire1 clusters to the ER membrane can be tracked throughout the duration of the experiment. Real-time in *vivo* imaging provides valuable insights into the dynamic nature of Ire1 clustering under ER stress conditions.

2 MATERIALS AND METHODS

2.1 Materials

2.1.1 Reagents

2.1.1.1 Yeast media reagents

The following list displays the reagents that were used to prepare the liquid and solid growth media used for cells.

Table 2.1. All components that used to prepare media.

Name	Supplier	Catalogue Number
Acetic acid, potassium salt 99+%, pure anhydrous (KOAc)	Acros Organics, Leicestershire, UK	220150010
Adenine Sulphate	ForMedium, Norfolk, UK	DOC0229
Agar	ForMedium	AGA03
Ampicillin	Apollo Scientific, Cheshire, UK	BIA0104
D-Glucose	Fisher Scientific, Leicestershire, UK	10385940
L-Arginine	Sigma-Aldrich, Dorset, UK	W381918
L-Aspartic acid	ForMedium	DOC0121
LB-Broth (Lennox)	ForMedium	LBX0102
LB-Agar Lennox	ForMedium	LBX0202
L-Histidine	ForMedium	DOC0144
L-Isoleucine	ForMedium	DOC0152
L-Glutamic acid	ForMedium	DOC0132
L-Leucine	ForMedium	DOC0157
L-Lysine	ForMedium	DOC0161
L-Methionine	ForMedium	DOC168
L-Phenylalanine	ForMedium	DOC0173
L-Serine	ForMedium	DOC0181
L-Threonine	ForMedium	DOC0185
L-Tryptophan	ForMedium	DOC0188
L-Tyrosine	ForMedium	DOC0192

L-Valine	ForMedium	DOC0197
Peptone	ForMedium	PEP03
Potassium hydrogen phthalate (K-phthalate)	VWR Chemicals (BDH), Leicestershire, UK	26948.260
Yeast Extract Powder	ForMedium	YEA02
Yeast Nitrogen base without amino acid	ForMedium	CYN0410
YPD Agar	ForMedium	CCM0105
YPD Broth	ForMedium	CCM0210

2.1.1.2 Chemical reagents

The following table displays the reagents that were used in the various experiments conducted in this thesis.

Table 2.2. Chemical reagents

Name	Company	Catalogue number
Acetic acid (HOAc)	11463473	Fisher Scientific
4-(2-Aminoethyl) benzenesulphonyl fluoride hydrochloride (AEBSF)	BIMB2003	Apollo Scientific
Agarose	BP 1356-500	Fisher Scientific
Ammonium persulphate	A3678	Sigma Aldrich
Acrylamide	164855000	Fisher Scientific
β-Mercaptoethanol	A15890	Alfa Aesar, Leicestershire, UK
Bovine serum albumin (BSA)	BP 1600-100	Fisher Scientific
Benzamidine hydrochloride hydrate	OR11123	Apollo Scientific
Butanol	100616J	VWR Chemicals (BDH
Dithiothreitol (DTT)	BIMB1015	Apollo Scientific
Dowex® MR-3 LCNG hydrogen and hydroxide	13684-U	Sigma-Aldrich
Dimethyl sulphoxide	D8418	Sigma-Aldrich
DNA gel loading dye (6 x)	11541575	Fisher Scientific
Ethanol	12807182	Fisher Scientific
EDTA	BPE119-500	Fisher Scientific
Ethidium bromide	E1510-10ML	Sigma-Aldrich
Formamide	181090025	Fisher Scientific

Ficoll® PM 400	17-0300-10	Amersham, Dorset, UK
Glycerol	G/0600/17	Thermo Fisher Scientific
Glyoxal	G5754	Sigma-Aldrich
Hydrochloric acid	10458980	Fisher Scientific
Iodoacetamide	I-6125	Sigma-Aldrich
Methanol (MeOH)	11976961	Fisher Scientific
Potassium hydroxide	10509390	Fisher Scientific
Potassium acetate	P3760153	Fisher Scientific
Phenol/chloroform/isoamyl Alcohol (25:24:1 Mixture)	BPE1752P-400	Fisher Scientific
Reporter lysis 5 x buffer	E397A	Promega, Hampshire, UK
Salmon sperm DNA solution (10 mg/ ml)	15632011	Fisher Scientific
SDS	BPE116-500	Fisher Scientific
Tween 20	10485733	Fisher Scientific

2.1.2 Buffers and solutions

The protocols for the buffers and solutions are described in Tables 2.3 and 2.4. All solutions are made in type I laboratory water produced by the NANO pure Diamond UV/UF TOC water purification (resistivity 18 MΩ cm, total organic carbon < 1 ppb, microorganisms < 1 cfu/ml, particles < 0.05 μm diameter) and autoclaved (121°C, 20–30 min) to ensure sterilisation. If this is not practicable, solutions are made in type I laboratory autoclaved water and then filtered through a 0.22 m filter to sterilise them.

Table 2.3. Protocol for commonly used buffers and solutions

Solution	Quantity	Protocol
Ethylenediaminetetraacetic acid (EDTA), 0.5 M	500 ml	1. Dissolve 93.1 g $Na_2EDTA{\cdot}2H_2O$ in ~350 ml H_2O. 2. Adjust pH to 8.0 with 10 M NaOH (~25 ml) 3. Add H_2O to 500 ml. 4. Autoclave.
Magnesium chloride ($MgCl_2$), 1 M	100 ml	1. Dissolve 20.33 g in ~ 80 ml H_2O. 2. Add H_2O to 100 ml. 3. Autoclave
Na_2CO_3, 1 M	500 ml	1. Dissolve 53.0 g in ~ 400 ml H_2O. 2. Add H_2O to 500 ml.
NaH_2PO_4, 0.4 M	500 ml	1. Dissolve 24 g NaH_2PO_4 in ~400 ml H_2O.

		2. Add H_2O to 500 ml. 3. Autoclave.
Na_2HPO_4, 0.4 M	500 ml	1. Dissolve 28.4 g Na_2HPO_4 in ~400 ml H_2O. 2. Add H_2O to 500 ml. 3. Autoclave
10 % (w/v) Sodium dodecyl sulphate (SDS)	500 ml	1. Dissolve 50 g SDS in ~450 ml H_2O. 2. Add H_2O to 500 ml.
1 x Tris(hydroxymethyl)aminomethane (Tris)-acetate-EDTA (TAE)	1 l	20 ml 50 x TAE Add H_2O to 1 l
50 x TAE	1 l	1. Dissolve 242 g Tris, 57.1 ml HOAc and 37.2 g $Na_2EDTA{\cdot}2H_2O$ in ~800 ml H_2O. 2. Add H_2O to 1 l.
10 X TBST	1 l	1. Dissolve 24.2 g Tris, 80 g NaCl, and 10.6 g Tween 20 in ~900 ml H_2O. 2. Adjust pH 7.6 to 7.6 with conc. HCl and add H_2O to 1 l. **Note:** This was diluted with deionised H_2O to 1 x for use in blocking solution and washing of PVDF membranes.
10 x TE (PH 8.0)	4 l	1. 400 ml 1 M Tris·HCl (pH 8.0) 2. 80 ml 0.5 M EDTA 3. Add H_2O to 4 l. 4. Autoclave
Tris(hydroxymethyl)aminomethane (Tris)·HCl (pH 8.0), 1 M	1 l	1. Dissolve 121.14 g Tris in ~800 ml H_2O. 2. Adjust pH to 8.0 with conc. HCl (~ 42 ml). 3. Add H_2O to 1 l. 4. Autoclave.
Tris·HCl (pH 6.8), 1 M	1 l	1. Dissolve 121.14 g Tris in ~800 ml H_2O. 2. Adjust pH to 6.8 with conc. HCl (~ 42 ml). 3. Add H_2O to 1 l. 4. Autoclave.
Tris·HCl (pH 8.9), 1 M	1 l	1. Dissolve 121.14 g Tris in ~800 ml H_2O. 2. Adjust pH to 8.9 with conc. HCl. 3. Add H_2O to 1 l. 4. Autoclave.
10 %(v/v) Tween 20	500 ml	1. Dissolve 55.5 g Tween 20 in ~ 400 ml autoclaved

		H_2O. 2. Add H_2O to 500 ml. 3. Filter sterilise.

Table 2.4. Specialist solutions and buffers and their protocol

Solution	Quantity	Protocol
30 % (w/v) Acrylamide, 0.8 % (w/v) *N*,*N*'-methylenebisacrylamide	500 ml	Dissolve 150 g of acrylamide, 4 g of N,N'-methylenebisacrylamide in ~ 400 ml of H_2O. Then, add H_2O to 500 ml. Add 25 g of Dowex MR-3 mixed bed ion ex-changer and stir the mixture for 1 h at RT. Filter the solution over a 0.22 µm filter and store in the dark at 4 ºC.
50 mg/ml Ampicillin	50 ml	Dissolve 2.5 g of ampicillin, sodium salt in ~ 40 ml of H_2O. Add H_2O to 50 ml and filter sterilise. Store the solution in 1.0 ml aliquots at -20 °C.
2 x Assay buffer	400 ml	Dissolve 177 ml 0.4 M Na_2HPO_4, 23 ml 0.4 M NaH_2PO_4, 0.8 ml 1 M $MgCl_2$, 2.8 ml β-mercaptoethanol, 532 mg 2-nitrophenyl-β-D-galactopyranoside in 400 ml H_2O and mix well. Store the solution in 50 ml aliquots at -20 °C.
Bicinchoninic acid protein assay working solution (BCA)	15 ml	Reagent A: 10 g/l bicinchoninic acid disodium salt, 20 g/l $Na_2CO_3 \cdot H_2O$, 1.6 g/l disodium tartrate, 4.0 g/l NaOH, 9.5 g/l $NaHCO_3$. Adjusted to pH 11.25 with 10 M NaOH. Reagent B: 40 g/l $CuSO_4 \cdot 5H_2O$. Mix 50 parts of reagent A with 1 part of reagent B. Note: When mixing reagents A and B a white precipitate may form [$Cu(OH)_2$]. This will dissolve upon further mixing of the reagents.
Chemiluminescence detection with luminol	15 ml	15 ml 100 mM Tris·HCl (pH 8.5) + 0.1 % (v/v) Tween 20, 75 µl 250 mM luminol, 33.3 µl 90 mM *p*-coumaric acid, 4.35 µl 30 % (w/w) H_2O_2. Mix well and keep protected from light.
1 M Dithiothreitol (DTT)	10 ml	Dissolve 1.54 g of dithiothreitol in ~ 9 ml of H_2O, then add H_2O to 10 ml. Filter sterilise and store at -20 °C. To inhibit protein folding in the yeast ER, use the solution at a concentration of 2 mM.
10 mg/ml Ethidium bromide	25 ml	Dissolve 250 mg ethidium bromide in ~ 20 ml sterile H_2O. Add sterile H_2O to 25 ml and store at 4 °C, protected from light.
30 % (v/v) Glycerol	250 ml	Dissolve 94.5 g glycerol in ~200 ml and mix well by stirring. Add H_2O to 250 ml and autoclave.
Glycine·HCl (pH 2.5), 1 M	500 ml	Dissolve 37.535 g glycine in 400 ml H_2O. Adjust the pH to 2.5 with

		HCl. Add H_2O to 500 ml and then autoclave.
10 mU/ µl β-galactosidase	100 µl	Add 1 µl 1 U/µl β-galactosidase to 99 µl ice-cold 1 x Reporter Lysis Buffer (RLB) and mix well, place on ice. **Note:** Prepare fresh daily.
0.1 mU/ µl β-galactosidase	1 ml	Add 10 µl of 10 mU/ µl β- galactosidase to 990 µl ice-cold 1 x RLB and mix well, and place on ice.
0.1 M Iodoacetamide + 0.1 M Tris·HCl (pH 8.0)	10 ml	Add 184.96 mg iodoacetamide to 1 ml 1 M Tris·HCl (pH 8.0), then add H_2O to 9 ml and mix. Add H_2O to 10 ml and store at -20 °C.
1 M Lithium acetate (LiOAc)	250 ml	Dissolve 25.50 g LiOAc·$2H_2O$ in ~200 ml H_2O. Add H_2O to 250 ml. Filter sterilise.
One- step buffer (0.2 M LiOAc + 40 % (w/v) PEG 4000)	10 ml	Add 2 ml of 1 M LiOAc to 8 ml 50 % (w/v) PEG 4000 and then mix solution well.
50% (w/v) PEG 4000	500 ml	250 g PEG 4000 and add ~200 ml H_2O. Stir for a few minutes, add H_2O to ~ 450 ml, stir until PEG4000 is nearly completely dissolved, add H_2O to 500 ml and mix. Filter sterilise.
1 x RLB	50 ml	Add 10 ml of 5 x RLB to 40 ml ice-cold autoclave H_2O.
10 x SDS-PAGE running buffer	1 l	144.13 g glycine, 30.03 g Tris, 10.00 g SDS. Add H_2O to ~ 900 ml, stir until completely dissolved, then add H_2O to 1 l.
6 x SDS-PAGE + β-mercaptoethanol sample buffer.	10 ml	3.50 ml 1 M Tris·HCl, pH 6.8, 3.78 g glycerol, 1.00 g SDS, 1.25 ml 4.0 g/l bromophenol blue, 200 µl β-mercaptoethanol. Add H_2O to ~ 9 ml, dissolve overnight if necessary. Add H_2O to 10 ml. Store in 1.5 ml aliquots at -20 °C.
1 x Semi-Dry Transfer Buffer + 5 % Methanol	1 l	100 ml 10 x semi-Dry transfer buffer, 50 ml Methanol. Adjust with H_2O to 1 l.
10 X Semi-dry transfer buffer	1 l	Dissolve 12.11 g Tris, 14.41 g glycine in ~ 900 ml H_2O, stir until completely dissolved, then add H_2O to 1 l.
1 x TBST + 5 % (w/v) skimmed milk powder	100 ml	Dissolve 5 g of Milk powder in 90 ml of 1 x TBST. Then, adjust the volume to 100 ml with 1 x TBST.
10 mg/ml Tunicamycin	1 ml	Add 1 ml DMSO to 10 mg tunicamycin (content of one bottle). Mix to dissolve. Store in 50 or 100 µl aliquots at -20 °C. Use at 0.1 – 2.0 µg/ml to inhibit protein folding in the yeast ER.

2.1.3 RNA Buffers and solutions

The protocols for the buffers and solutions used for RNA experiments are described in Table 2.5. The preparation of all solutions involves type I laboratory H_2O that was treated with 0.1 % diethylpyrocarbonate (DEPC) for 30 min with vigorous stirring and then autoclaved. These were prepared using sterilised plastic ware, baked stir bars, baked glasses, and baked spatulas. If this is not practicable, solutions are made in type I laboratory autoclaved DEPC-H_2O**.**

Table 2.5. Buffers and solutions used for RNA work and their protocol

Solution	Quantity	Protocol
100 x Denhardt's solution	500 ml	10 g Ficoll 400 10 g Polyvinylpyrrolidone 10 g BSA (fraction V) Dissolve in 400 ml DEPC-H_2O. Adjust to 500 ml with DEPC-H_2O and filter sterilize. Aliquot into 50 ml tubes and store at 4 °C.
DEPC-H_2O	1 l	1 l H_2O 1 ml DEPC, stir for 30 min Autoclave.
EDTA (pH 8.0), 0.5 M	500 ml	1. Dissolve 93.1 g $Na_2EDTA{\cdot}2H_2O$ in ~350 ml in DEPC-H_2O. 2. Add DEPC-H_2O to 500 ml. 3. Add 0.5 mL DEPC, stir 30 min 4. Autoclave.
50 % (v/v) Formamide, 1 % (w/v) SDS, 0.1 x SSC.	500 ml	250 ml formamide, 2.5 ml 20 x saline-sodium citrate (SSC), 50 ml 10 % (w/v) SDS and then add DEPC-H_2O to 500 ml.
Hybridization	5 ml	Add 1.25 ml 20 x SSC,0.5 ml 10 % (w/v) SDS, 250 µl 100 x Denhardt's solution to a 15 ml tube and prewarm to 42 °C. Add 50 µl 10 mg/ml salmon sperm DNA to 450 µl DEPC-H_2O in a 1.5 ml microcentrifuge tube. Denature DNA by boiling for 5 min, then place in an ice-water bath. Add denatured salmon sperm DNA to the prewarmed mixture of 20 x SSC, SDS, Denhardt's solution and DEPC-H_2O. Mix, add labelled DNA

		probe and salmon sperm mix, then add 2.5 ml formamide prewarmed to 42 °C, and mix.
10 mM $Na_xH_{3-x}PO_4$, (pH 7.0)	1 l	Add 100 ml 100 mM $Na_xH_{3-x}PO_4$, (pH 7.0) Add DEPC- H_2O to 1 l.
100 mM $Na_xH_{3-x}PO_4$, (pH 7.0)	1 l	195 ml 200 mM NaH_2PO_4, 305 ml 200 mM Na_2HPO_4. Add DEPC-H_2O to 1 l. Add 1 ml DEPC, stir 30 min at RT and autoclave.
200 mM Na_2HPO_4	500 ml	1. Dissolve 14.21 g Na_2HPO_4 (35.83 g $Na_2HPO_4 \cdot 12 H_2O$) in ~450 ml DEPC-H_2O, add DEPC- H_2O to 500 ml. 2. Add 0.5 ml DEPC and stir for 30 min at RT. 3. Autoclave.
200 mM NaH_2PO_4	500 ml	1. Dissolve 12.21 g NaH_2PO_4 in ~450 ml DEPC-H_2O, add DEPC- H_2O to 500 ml. 2. Add 0.5 ml DEPC and stir for 30 min at RT. 3. Autoclave.
0.5 M NH_4OAc	500 ml	1.Dissolve 38.54 g $NaOAc \cdot 3 H_2O$ in ~ 400 H_2O. 2. Adjust to 500 ml then autoclave.
Phenol: $CHCl_3$: isoamyl alcohol (25:24:1 (v/v/v)), saturated with RNA buffer	50 ml	1. Add 25 ml Phenol: $CHCl_3$: isoamyl alcohol (25:24:1 (v/v/v)), buffered with 0.1 M Tris·HCl (pH 8.0) to a 50 ml tube and mix vigorously with 25 ml RNA buffer. 2. Centrifuge for 2 min at 3,000 rpm to separate phases and discard the upper phase. 3. Repeat steps 1 and 2 once, this time leave ~ 5 ml of upper phase solution to prevent oxidation on top of the phenol: $CHCl_3$: isoamyl alcohol (25:24:1 (v/v/v)) saturated with RNA buffer. 4. Store in 50 ml tube protected from light at 4°C.
RNA buffer	500 ml	1. Dissolve 14.61 NaCl in 390 ml DEPC-H_2O. 2. Add 390 µl DEPC and stir for 30 min at RT. 3. Autoclave. 4. Add 100 ml 1 M Tris·HCl (pH 7.5) and 10 ml 0.5 M EDTA (pH 8.0)
RNA denaturation solution	192.2 µl for 5 sample	42.2 µl glyoxal, 125 µl DMSO, 25 µl 100 mM $Na_xH_{3-x}PO_4$, (pH 7.0)
6 x RNA sample loading buffer	100 ml	1.To 63 g glycerol and 250 mg bromophenol blue add

		10 ml 100 mM $Na_xH_{3-x}PO_4$ (pH 7.0) and DEPC- H_2O to ~ 90 ml. 2. Stir until bromophenol blue is dissolved. 3. Add DEPC-H_2O to 100 ml. 4. Add 100 µl DEPC and stir for 30 min at RT. 5.Autoclave.
10 % SDS	500 ml	1. Dissolve 50 g SDS in ~450 ml DEPC-H_2O. 2. Add H_2O to 500 ml. 3. Add 0.5 ml DEPC and stir 30 min at RT. 4. Leave overnight in oven at 50-60 °C. **Note:** Do NOT autoclave.
2 x SSC	1 l	100 ml 20 x SSC Add DEPC-H_2O to 1 l.
20 x SSC	1 l	Dissolve 175.3 g NaCl, 88.2 g Na_2-citrate ~~dissolve~~ in ~ 800 ml DEPC-H_2O. Adjust to 1 l with DEPC-H_2O. Add 1 ml DEPC and stir at RT for 30 min and then autoclave.
0.2 x SSC + 0.1 % (w/v) SDS	1 l	10 ml 20 x SSC, 10 ml 10 % (w/v) SDS and then add DEPC-H_2O to 1 l.
2 x SSC + 0.1 % (w/v) SDS	1 l	100 ml 20 x SSC, 10 ml 10 % (w/v) SDS and then add DEPC-H_2O to 1 l.
1% (w/v) SDS, 0.1 x SSC.	500 ml	2.5 ml 20 x SSC, 50 ml 10 % (w/v) SDS and then add DEPC-H_2O to 500 ml.
Tris·HCl (pH 8.0), 1 M	500 ml	1. Dissolve 60.57 g Tris in ~ 400 ml DEPC-H_2O. 2. Adjust pH w/conc HCl. 3. Add DEPC-H_2O to 500 ml. 4. Autoclave.
20 mM Tris·HCl (pH 8.0)	500 ml	Add 10 ml 1 M Tris·HCl (pH 8.0). Add DEPC-H_2O to 500 ml.
6 M Glyoxal, deionized	50 µl	Mix 50 ml 6 M glyoxal with 5 g Dowex MR-3 mix bed ion exchanger for 1 h at RT. Remove ion exchanger by filtration and store 6 M glyoxal at −80 °C in single use 0.5 ml aliquots.

2.1.4 Yeast Strains

PWY 260 (W303 MATα *ire1*Δ::*TRP1 ade2-1 can1-100 his3-11,-15*::*HIS*$^{+}$-UPRE-*lacZ leu2-3,-112*::*LEU2*$^{+}$-UPRE-*lacZ trp1-1 ura3-1*) (Papa et al., 2003) was transformed with plasmid YCplac33 carrying different Ire1 mutants (Table 2.6). Yeast strains were transformed using lithium acetate (LiOAc) method (Chen et al., 1992). All CEN-ARS low copy yeast-shuttle vectors used to carry *IRE1* alternative genes were derivatives of YCplac33 (Gietz & Sugino, 1988). Mutants of Ire1 were generated using the QuikChange kit (Stratagene) by Dr. Sergej Šestak, a collaborator from the Slovak Academy of Sciences in Bratislava, Slovakia.

Table 2.6. Plasmids used in the experiments and their resources

PWY 260 was the strain used for β-galactosidase, Western blot, Northern blots, and spotting assay experiments.

Plasmid	Source
YCplac33	Martin Schröder group
YCplac33-IRE1-HA	Martin Schröder group
YCplac33-K799A-IRE1-HA	Martin Schröder group
YCplac33-N802A-IRE1-HA	Martin Schröder group
YCplac33-D828A-IRE1-HA	Martin Schröder group
YCplac33-K799A-N802A-IRE1-HA	Martin Schröder group
YCplac33-K799A-D828A-IRE1-HA	Martin Schröder group
YCplac33-D797A-IRE1-HA	Martin Schröder group
YCplac33-N802A-D828A-IRE1-HA	Martin Schröder group
YCplac33-K799A-N802A-D828A-IRE1-HA	Martin Schröder group

YCplac33-D797A-K799A-IRE1-HA	Martin Schröder group
YCplac33-D797A-N802A-IRE1-HA	Martin Schröder group
YCplac33-D797A-D828A-IRE1-HA	Martin Schröder group
YCplac33-D797A-K799A-N802A-IRE1-HA	Martin Schröder group
YCplac33-D797A-K799A-D828A-IRE1-HA	Martin Schröder group
YCplac33-D797A-N802A-D828A-IRE1-HA	Martin Schröder group
YCplac33-D797A-K799A-N802A-D828A-IRE1-HA	Martin Schröder group

2.1.5 List of restriction enzymes

A list of restriction enzymes is presented in Table 2.7.

Table 2.7. Restriction enzymes

Name	Product Number	Company
*Bam*HI	ER0502	Fisher Scientific
*Bss*HII	ER1091	Fisher Scientific
*Hin*dIII	R3104S	Fisher Scientific
*Sac*I	ER1131	Fisher Scientific

2.1.6 Plasmids

Plasmids expressing mCherry-tagged versions of mutant Ire1 were created by Dr. Martin Schröder and his group for use in confocal microscopy. In the Northern blot analysis, the ~2.3 kBp *Hin*dIII fragment of pC4/2 plasmid (Su & Mitchell, 1993) was used. Figure 2.1 displays the plasmids maps for pEvA97 (Aragón et al., 2009), YCplac33-IRE1mutant-HA (Papa et al., 2003) and pJK59 (Prinz et al., 2000), which were utilised in the confocal microscopy study, while the pC4/2 plasmid was used for the Northern blot analysis.

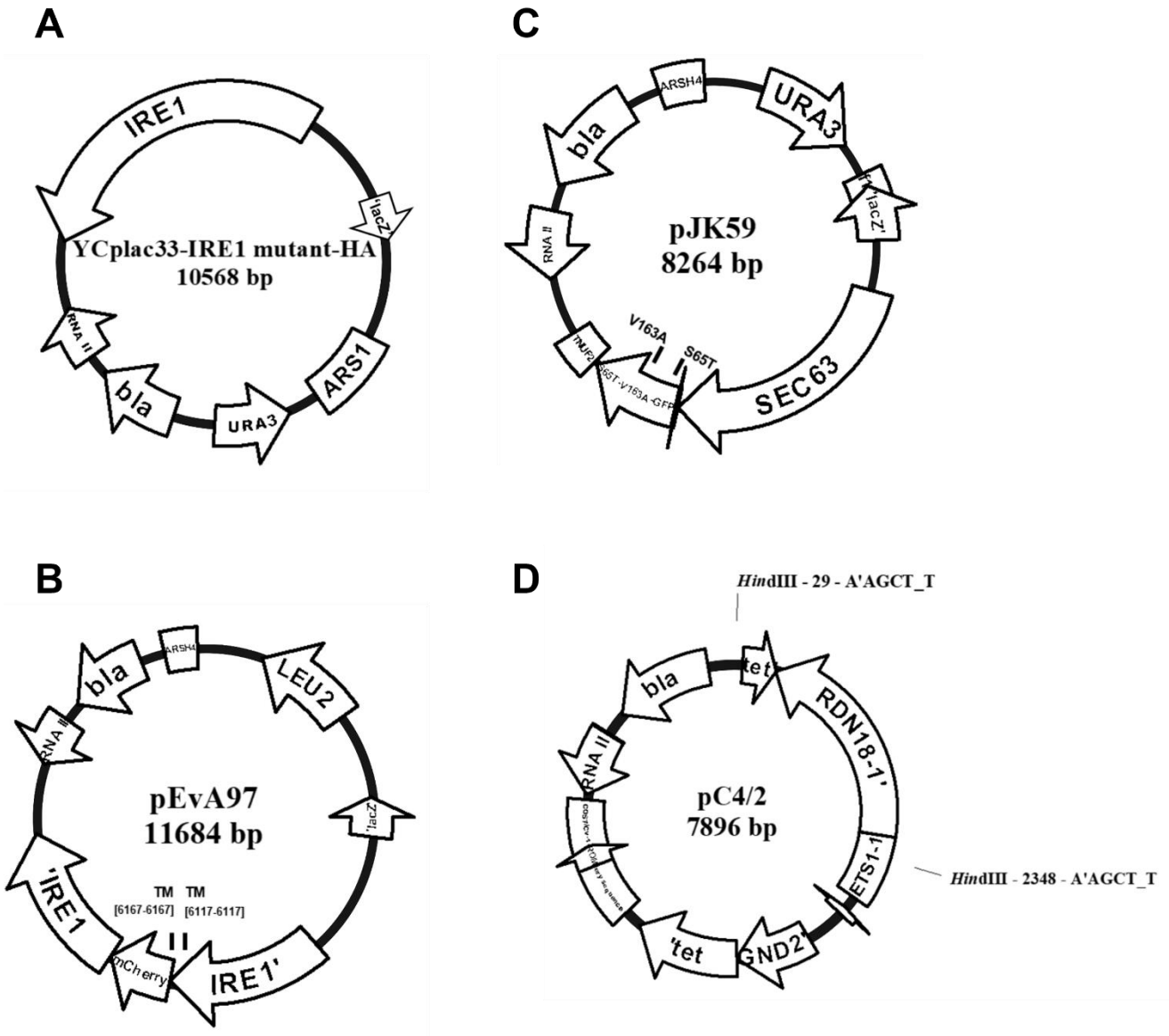

Figure 2.1. Plasmids maps

Plasmids maps that contain pEvA97, Sec63-GFP and IRE1-mCherry for microscopy analysis. A) YCplac33-IRE1-HA (Papa et al., 2003) includes URA3, CEN4-ARS1, and a HA-tag at the C-terminal end. The element "tet"' refers to the tetracycline resistance gene, "bla" denotes the ampicillin resistance gene, and "GND2"' signifies a specific promoter or regulatory region. The primed symbol ('), when attached to an element, typically denotes a modified or altered version of that element. B) The plasmid pJK59 (Prinz et al., 2000) include the URA3 gene and pEvA97. The arrows indicate TM refers to a transmembrane domain. The notation [6117- 6117] and [6167 - 6167] after the TM indicates the amino acid residues at which the transmembrane domain begins and ends. C) The plasmid pEvA97 (Aragón et al., 2009) contains the LEU2 gene and the arrows indicate V163A-S65T likely refers to a protein variant that has been mutated at two specific amino acid positions: valine (V) at position 163 has been changed to alanine (A), and serine (S) at position 65 has been changed to threonine (T). D) The ~2.3 kBp *Hin*dIII fragment of pC4/2 was used in the Northern blots (Su & Mitchell, 1993).

2.1.6.1 Antibodies

Table 2.8 displays the antibodies used in the experiments to detect Ire1 protein labeled with the HA epitope and the actin loading control. All antibodies listed in the table belong to the IgG type.

Table 2.8. Antibodies

Antibody	Species	Clonality	Supplier	Dilution Factor	Batch/lot no.	Catalogue Number
anti-HA	Rabbit	Polyclonal	Sigma-Aldrich	1000	0000097653	H6908
anti-rabbit IgG (H+L)-peroxidase	Goat	Polyclonal	Cell Signalling, Hitchin, UK	2000	30	7074S
anti-β-actin	Mouse	Monoclonal [8F10G10]	Abcam, Cambridge, UK	10000	GR3371939-8	ab170325
anti-mouse IgG (H+L)-peroxidase	Goat	Polyclonal	Fisher Scientific	10000	WC3216884	15393896

2.1.7 Commercial kits

The experiments involved the use of commercial kits for certain procedures like plasmid extraction or β-galactosidase assays. The information regarding these kits, including their supplier and catalogue number is provided in Table 2.9.

Table 2.9. Commercial kits

Name	Supplier	Catalogue Number
β-Galactosidase Enzyme Assay System with Reporter Lysis Buffer	Promega	E2000
DC™ Protein assay reagent A	ThermoFisher Scientific	500-0113
DC™ Protein assay reagent B	Bio-Rad, Watford, UK	500-0114
Gel filtration on a Microspin S-200 HR column	Cytiva, Buckinghamshire, UK	27-5120-01
GeneRuler 1 kb DNA ladder	Fisher Scientific	SM0311
Pierce™ ECL 2 Western Blotting Substrate.	Fisher Scientific	11517371
PureYield™ Plasmid Midiprep System	Promega	A2492
QIAGEN Plasmid Plus Midi Kit	QIAGEN, Manchester, UK	12943
Random primed labelling kit RediPrime II	Cytiva	RPN 1633
Wizard SV Gel and PCR Clean-Up System	Promega	A9282

2.2 Methods

2.2.1 Microbiology

2.2.1.1 Yeast media and growth maintenance

Rich dextrose YP (1 % (w/v) yeast extract, 2 % (w/v) peptone, supplemented with 2 % (w/v) glucose (YPD) (Esposito & Esposito, 1969), and 2 % (w/v) agar for solid media were used to revive, grow, and maintain *Saccharomyces cerevisiae* (Table 2.10).Plasmids were selected and maintained in yeast on synthetic media (0.67 % (w/v) yeast nitrogen base (without amino acids)) and supplemented with 2 % (w/v) glucose and 2 % (w/v) agar for solid selective media. Pre-cultures were generated using two types of selective liquid media: one lacking uracil (SD-Ura) and the other lacking both uracil and leucine (SD-Ura-Leu), as described in Table 2.10. I used rich acetate media YP (1 % (w/v) yeast extract, 2 % (w/v) peptone) supplemented with 2 % (w/v) KOAc to isolate cells and test for growth on non-fermentable carbon sources (YPAc). Alternatively, I used synthetic acetate media for plasmid selection, which contained 0.67 % (w/v) yeast nitrogen base (without amino acids) and the necessary supplements, including 0.1 % (w/v) yeast extract and 1 % (w/v) KOAc and 50 mM K-phthalate (adjusted with KOH to pH 5.0) (PSP2-Ura, PSP2 – Ura -Leu).

Table 2.10. Liquid media for yeast

All stock solutions were sterilised by autoclaving**.**

Medium	Composition	Quantity	Recipe
SD medium (Sherman, 1991; Wickersham, 1951)	0.67 % (w/v) yeast nitrogen base w/o amino acids 2 % (w/v) D-glucose 30 mg/l L-Tyr 20 mg/l uracil 20 mg/l L-Arg·HCl 20 mg/l L-His·HCl 20 mg/l L-Met 20 mg/l L-Trp 30 mg/l L-Ile 30 mg/l L-Lys·HCl 150 mg/l L-Val 375 mg/l L-Ser 20 mg/l adenine sulphate 50 mg/l L-Phe 100 mg/l L-Glu 100 mg/l L-Leu 100 mg/l L-Asp 200 mg/l L-Thr	600 ml	4 g yeast nitrogen base w/o amino acids 12 g D-glucose 18 mg L-Tyr 5 ml 2.4 g/l uracil 5 ml 2.4 g/l L-Arg·HCl 5 ml 2.4 g/l L-His·HCl 5 ml 2.4 g/l L-Met 5 ml 2.4 g/l L-Trp 5 ml 3.6 g/l L-Ile 5 ml 3.6 g/l L-Lys·HCl 5 ml 18 g/l L-Val 5 ml 45 g/l L-Ser 10 ml 1.2 g/l adenine sulphate 10 ml 3.0 g/l L-Phe 10 ml 6.0 g/l L-Glu 16.7 ml 3.6 g/l L-Leu 15 ml 4.0 g/l L-Asp 5 ml 24 g/l L-Thr H_2O was added to 540 ml, stirred until all solid dissolved, and the mixture was then dispensed into bottles and autoclaved.

Medium	Composition	Quantity	Recipe
PSP2 Medium (Roth, 1969)	0.67 % (w/v) yeast nitrogen base w/o amino acids 0.10 % (w/v) bacto-yeast extract 1 % (w/v) KOAc 30 mg/l L-Tyr 50 mM K-phthalate (pH 5.0) 20 mg/l uracil 20 mg/l L-Arg·HCl 20 mg/l L-His·HCl 20 mg/l L-Met 20 mg/l L-Trp 30 mg/l L-Ile 30 mg/l L-Lys·HCl 150 mgl/ L-Val 375 mg/l L-Ser 20 mg/l adenine sulphate 50 mg/l L-Phe 100 mg/l L-Glu 100 mg/l L-Leu 100 mg/l L-Asp 200 mg/l L-Thr	600 ml	4 g yeast nitrogen base w/o amino acids 0.6 g yeast extract 6 g KOAc 18 mg L-Tyr Dissolve 6.13 g K-phthalate in ~ 400 ml H_2O, adjust pH to 5.0 with KOH pellets 5 ml 2.4 g/l uracil 5 ml 2.4 g/l L-Arg·HCl 5 ml 2.4 g/l L-His·HCl 5 ml 2.4 g/l L-Met 5 ml 2.4 g/l L-Trp 5 ml 3.6 g/l L-Ile 5 ml 3.6 g/l L-Lys·HCl 5 ml 18 g/l L-Val 5 ml 45 g/l L-Ser 10 ml 1.2 g/l adenine sulphate 10 ml 3.0 g/l L-Phe 10 ml 6.0 g/l L-Glu 16.7 ml 3.6 g/l L-Leu 15 ml 4.0 g/l L-Asp 5 ml 24 g/l L-Thr H_2O was added to 540 ml, stirred until all solid dissolved, and the mixture was then dispensed into bottles and autoclaved.

The solidified media (SD or PSP2) was prepared by adding 2 % (w/v) of agar to the media solution, resulting in the production of 24 plates.

2.2.1.2 Yeast cell culture

From an agar plate, a single isolated *S. cerevisiae* colony was transferred to 2-4 ml of medium. The tubes were then incubated till saturation (usually 2-3 d) at 30 °C in an incubator shaker (preculture) with shaking at ~220 rpm. The optical density at 600 nm (OD_{600}) (Pringle, 1975) was measured in a 1:10 dilution in a cell density meter (WPA, Cambridge, UK. model no. CO8000). Sterile Erlenmeyer flasks were filled with the suitable medium at the designated volumes. The quantity of inoculum needed was determined based on achieving an OD_{600} reading of approximately 0.001. Then the flasks were incubated overnight at 30 °C in a shaker incubator with shaking at 225-250 rpm. After 12-24 h of incubation, the growth of the culture was monitored by measuring the OD at 600 nm. The yeast strains were grown until they reached mid-exponential phase, as indicated by an $OD_{600\ nm}$ reading of 0.4-0.8. Once within this range, samples of each culture were taken at 0 h, spun at 3,500 rpm for 2 min at 4 °C, the supernatant was discarded, and the pellet was flash frozen in liquid nitrogen and stored at – 80 °C. 10 ml were collected for β-galactosidase assays, 20 ml for Northern blots, and 50 ml for Western blot. For β-galactosidase reporter assays and Northern blot the remaining cultures were treated with 2 mM dithiothreitol (DTT) for 1 and 2 h. For western blots, cultures were treated with 2 mM dithiothreitol (DTT) for 2 h. For spotting assays cultures were treated with different concentrations of tunicamycin (Tm), DTT, or 2-deoxy-D-glucose (2DDG) (Back SH, 2005). Collected samples were processed as described above. For long-term storage, glycerol stocks of *S. cerevisiae* transformed using plasmids were prepared. Once the cultures reached late log-phase, glycerol was added to the culture, resulting in a final concentration of 1 ml culture to 1 ml of 30 % (v/v) glycerol. Cultures were then frozen in liquid nitrogen and stored at -80 °C (Sherman, 1991).

2.2.1.3 Growth of Escherichia coli (E. coli)

E. coli cells were grown in lysogeny broth (LB), which was supplemented with 100 µg/ml ampicillin. LB medium contains 1 % (w/v) tryptone, 0.5 % (w/v) yeast extract, and 1 % (w/v) sodium chloride. The broth was then inoculated with a single *E. coli* colony obtained from an LB-agar plate, providing a starting point for the growth of the bacterial culture. The inoculated cultures were placed in a shaking incubator set at 225 - 250 rpm and incubated at a temperature of 37 °C overnight.

To freeze *E. coli* stocks, the samples were processed using the same method as described previously for yeast cell stock (refer to section 2.2.1.2)

2.2.2 Spotting assays

2 ml fresh overnight yeast cultures were prepared, and their optical densities at 600 nm were adjusted to 3.0 (OD_{600} = 3) in a 100 µl volume of H_2O. Next, a 10-fold serial dilution of each strain was prepared from the adjusted cultures. Survival of ER stress was determined by spotting 3 µl of serial 10-fold dilutions of fresh overnight cultures onto freshly prepared synthetic medium agar plates lacking uracil and containing different concentrations of Tm, DTT, or 2DG. Then plates were dried before being moved to a 30 °C incubator and then the plates were photographed by using an ENDURO™ GDS Touch instrument (Labnet) after 2 and 3 d of growth.

2.2.2.1 Cell culture for fluorescence microscopy

Cells were grown in a 2 ml preculture in SD-Leu medium. The same medium was used to inoculate 20 ml with an initial OD_{600} of 0.001 and then grown overnight at 30 °C at 220 rpm. After overnight growth, cells were collected by centrifuging at 3000 x g for 3 min at 4 °C. After that, cell pellets were resuspended in 1 ml of SD-Leu medium (Table 2.10). The cell suspension was then transferred to a 1.5 ml microcentrifuge tube. The microscope pictures were captured at several times, including 0 min before and 5, 15, 30, and 60 min after the cells were stressed with DTT (2 mM concentration). The glass slide was prepared by spotting 3 µl of cell suspension and the cover slip was then attached and sealed with nail polish. The Zeiss LSM 880 with Airyscan confocal inverted light microscope was used to image the slides (Zeiss Ltd, Cambridge, UK). Table 2.11 contains information on the parameters of the system.

2.2.2.2 Microscopy analysis

The microscope used a two-channel setup to detect both the GFP signal and the mCherry signal. Sec63-GFP signal was detected using the Ch1-T1 (photomultiplier tube) channel with excitation at 488 nm, emission at 523 nm, detection wavelength of 523. The Ch2 GaAsP-T2 (gallium arsenide phosphide detector) channel with an excitation wavelength of 594 nm, an emission wavelength of 611 nm, and a detection wavelength of 611 nm was used for the

IRE1–mCherry signal. The IRE1-mCherry signal detection needed greater sensitivity, which the GaAsP channel possesses. The Plan-Apochromat 63x/1.4 Oil DIC M27 objective lens was used with the MDS 488/594 beam splitter. A 488 nm laser was employed. Image quality was optimised by using the 594 nm laser at a power of 28–40 % and the 488 nm laser at a power of 5–8 %. Gain levels between 650 and 900 were used to enhance image clarity and minimise background noise. Table 2.11 shows the microscope settings that were used for each image capture.

Table 2.11. The settings used for the Zeiss LSM 880 with Airyscan microscope

These settings were reused for each mutant.

Setting	Channel 1	Channel 2
Contrast Method	Fluorescence	Fluorescence
Laser Wavelength	488 nm: 0.96 %	594 nm: 0.43 %
Channel Name	ChA-T1	ChA-T2
Channel Description	Ch1-T1	Ch2 GaAsP-T2
Channel Color	Green	Red
Excitation Wavelength	488	594
Emission Wavelength	523	611
Detection Wavelength	523-523	611-611
Binning Mode	1x1	1x1
Detector	Airyscan	Airyscan
Detector Gain	880.0	880.0
Detector Offest	0.0	0.0
Detector Digital Gain	1.0	1.0
Airyscan Mode	Superresolution	Superresolution

2.2.2.3 Zen Blue lite image presentation

The Zen Blue Lite 2.1 software was used to modify the images taken with the Zeiss 880 Airyscan confocal laser scanning microscope for presentation and file format conversion (Zeiss Ltd, Cambridge, UK). Airyscan is a type of confocal microscopy that uses a special detection system to improve image resolution and signal-to-noise ratio. It works by collecting a series of small, overlapping images of a sample using a high numerical aperture objective lens. The system then uses computational algorithms to combine the individual images into a

final, high-resolution image with improved clarity and contrast. Scale bars were added to each channel, and the pseudo-color of each channel was adjusted according to the best linear fit recommended by the software. To ensure that all images were scaled to the same size using the 5 µm scale bar as a reference, this scale bar was used in figure preparation. The original data were kept, and the images were saved and exported as tif files of the various channels.

2.2.3 Molecular Biology

2.2.3.1 Plasmid extraction from E. coli

Depending on the desired concentration and the intended use of the plasmid, various commercially available kits were used to extract plasmids from *E. coli* (Table 2.9). Below is a methodology for each kit. Additionally, I used plasmid DNA miniprep from *E. coli* for plasmid diagnostic reasons.

2.2.3.2 QIAGEN Plasmid Plus Midi Kit

The procedure was done in accordance with the instructions provided by the manufacturer.

2.2.3.3 Promega PureYield Plasmid Midiprep System

The procedure was done in accordance with the instructions provided by the manufacturer.

2.2.3.4 Plasmid DNA miniprep from E. coli (Birnboim & Doly, 1979)

1.5 ml of an overnight *E. coli* culture were placed into a 1.5 ml microcentrifuge tube and the remaining culture were stored at 4 °C. Then the tubes were centrifuged for 1 min at 14,000 x g at RT, and the supernatant was aspirated. The cells were centrifuged again for 1 min at 14,000 x g at RT, and the supernatant was aspirated. The cells were resuspended in a solution of 50 mM D-Glucose, 25 mM Tris·HCl (pH 8.0), and 10 mM EDTA (100 µl) and mixed by vortexing or pipetting up and down. Then the tubes were incubated 5 min at RT. 200 µl of 0.2 N NaOH and 1 % (w/v) SDS were added, mixed by inverting the tubes 4-6 times, and incubated for 5 min on ice. 150 µl of ice-cold 5 M KOAc (pH 4.8) were added, mixed by inverting 4-6 times, and incubated for 5 min on ice. Then the tubes were centrifuged for 3 min at 14,000 x g at 4 °C and the supernatant was transferred into a new 1.5 ml microcentrifuge tube. This was followed by adding 0.8 ml of 100 % (v/v) ethanol and mixed

by flipping the tubes over 2-3 times. The tubes were then either stored at – 20 °C or incubated at RT for 2 min. The tubes were then centrifuged at 14,000 x g for 1 min at RT and the supernatant was discarded. 1 ml of 70 % (v/v) ethanol was added to the tubes, which were then centrifuged at 14,000 x g for 1 min at RT. The resulting supernatant was aspirated, and the remaining liquid at the bottom of the tube was collected after a second brief centrifugation. The residual ethanol was then removed by pipetting, and the collected pellets were air-dried for 15 min at RT. The pellets were resuspended in 30 µl 1 x TE (pH 8.0), 0.3 mg/ml RNase A, and incubated at 4 °C for ~ 0.5 to 1 h until the pellets were completely dissolved.

2.2.4 Plasmid quantification

Plasmid quantification is the process of determining the concentration and purity of plasmid DNA in a solution. Two absorbance techniques were used to calculate the concentration of plasmid DNA and RNA from extractions.

2.2.4.1 NanoDrop 1000 UV V3.8

Plasmid DNA in the amount of 1 µl was placed on the fiber optic cable of the NanoDrop 1000 UV Visible Spectrophotometer, and the spectrophotometer measured the wavelengths at 260, 280, and 320 nm. The fiber optic cable is lightly wiped before the required sample is measured, and 1 µl of water is measured to create a blank that the samples are then measured against.

2.2.4.2 Molecular Devices SpectraMAX 190 Plate Reader

Using sterile H_2O, plasmid DNA was diluted 1:10 to a final volume of 100 µl. The samples and a 100 µl blank (H_2O) were added onto a Greiner 96 well UV transparent plate (Sigma-Aldrich, # M3812-40EA), which was then read at 260, 280, and 320 nm using a Molecular Devices SpectraMAX 190plate reader (Molecular Devices, Sunnyvale, USA, model no. 190). I also measured RNA samples using this technique.

To convert the absorbance readings obtained from the plate reader into nucleic acid concentration, the following formulas were used:

Nucleic acid concentration [in mg/ml] = $-36.0 \times (OD_{280} - OD_{320}) + 62.9 \times (OD_{260} - OD_{320})$

Ratio = $(OD_{260} - OD_{320}) / (OD_{280} - OD_{320})$

In the above equations, OD_{260} represents the nucleic acid absorbance, OD_{280} represents the protein absorbance, and OD_{320} represents the background absorbance.

2.2.5 Restriction Endonuclease Digestion of Plasmid DNA

I have two methods available for digesting the DNA plasmid: preparative digest for obtaining specific DNA fragments, and analytical digest for analyzing the resulting fragments.

2.2.5.1 Preparative Digests

For the preparative digest, between 20 to 50 µg of the plasmid DNA were digested in 50 to 100 µl of reaction volume with 20-50 U of the desired restriction endonuclease in 1 X buffer. Then the digests were incubated overnight at the recommended temperature.

2.2.5.2 Analytical Digests

For analytical digests, between 200 ng to 1 µg of plasmid DNA were digested with 5 U of the desired restriction endonuclease for 1 hour according to the manufacturer's instructions. The resulting digested DNA fragments were analyzed by gel electrophoresis to confirm the expected sizes of the fragments.

2.2.6 DNA Templates for synthesis of labelled probe

The DNA templates that were amplified from 10 ng of genomic DNA (PWY 260) or 10 ng of plasmid DNA were used to identify the presence of complementary nucleic acid sequences (target sequences) by hybridisation in Northern blots. The PCR reaction had a final volume of 100 µl and included the following components: 5 x colorless GoTaq Flexi buffer, 25 mM $MgCl_2$, 200 µM dNTPs, 1 µM primers, 5 U/µl of GoTaq G2 flexi polymerase, and 0.1 ng/µl of template DNA. The PCR reactions followed the cycling parameters specified in Table 2.12.

Table 2.12 Cycling parameters used in PCR

Step	Cycles	Time	Temperature
Initial Denaturation	1	2 min	94 °C
Denaturation	30	30 s	94 °C
Annealing	30	30 s	51 °C
Extension	30	30 s	72 °C
Final Extension	1	10 min	72 °C
Refrigeration	Hold	∞	10 °C

After performing the PCR reaction, the resulting product was purified on the Wizard SV columns to remove any contaminants and unwanted DNA fragments. The purified PCR product was then tested for successful amplification by running it on an agarose gel. The purpose of this step was to confirm that the PCR reaction had produced the expected fragment size and to ensure that the amplification had occurred without any non-specific products. Following confirmation of successful amplification, the resulting PCR product was used as a target sequence in a Northern blot analysis. For this, a probe was generated separately by labelling a single-stranded DNA or RNA molecule that was complementary to the target sequence. The probe was then hybridized with the PCR product on the Northern blot, allowing for the detection and analysis of the target sequence.

2.2.7 Agarose gels

Plasmid DNA or fragments were analysed, diagnosed, and separated using a 1 % (w/v) agarose gel that was created by microwave-dissolving the required quantity of electrophoresis-grade agarose powder into the proper volume of 1 x TAE buffer in an Erlenmeyer flask. The agarose was melted for 1 to 5 min at the maximum power setting in a microwave, stirring every 30 to 60 s to achieve even mixing and to prevent the agarose solution from boiling over. After allowing the flask to cool to around 55 °C at RT, 0.5 µg/ml of ethidium bromide was added to the mixture and stirred. After melting, the agarose was poured into the casting platform and the gel comb was carefully inserted to ensure that no bubbles were trapped underneath. Any bubbles on the surface of the agarose were also eliminated before allowing the gel to set. Once the gel solidified, the gel comb was carefully removed to avoid damaging the sample wells. The casting platform was then removed to access the sealed ends after the gel set. The gel was submerged in a tank filled with 1x TAE buffer and 0.5 µg/ml ethidium bromide. The DNA samples were prepared in a 1.5 ml

microcentrifuge tube using DNA sample loading buffer, DNA sample, and water to reach the final volume. The Gene Ruler DNA ladder 1kb and samples were loaded. Electrophoresis was initiated by setting the voltage, typically ranging from 1 to 5 V/cm, based on the size of the gel and the desired running time. The power supply was then turned off when the blue dye had migrated a sufficient distance, typically reaching approximately two-thirds (2/3) of the gel length. The gel was then visualised by exposing to a UV light source (254 nm) to observe the DNA and take a picture, or the plasmid DNA fragments were excised.

2.2.8 DNA Gel Extraction

An agarose gel was used to separate the fragments of digested plasmid DNA according to size. The required fragments were then visualised and cut out with a clean scalpel using a UV transilluminator and UV light at a wavelength of 312 nm. The UV source was turned off during DNA fragment excising to prevent DNA damage. After that, the fragment was placed in a clean 15 ml tube. Each gel fragment inside each 15 ml tube was weighed after the empty tube. The weight of the gel slices was calculated by subtracting the weight of the empty 15 ml tube from the total weight (gel fragment + 15 ml tube).

2.2.8.1 Gel and PCR Clean-Up

For cleaning PCR and gels Wizard SV Gel and PCR Clean-Up System kit were used according to the manufacturer's instructions.

2.2.8.2 Ligation of DNA fragments

In the DNA ligation process, the vector is typically used at a consistent amount of 100 ng. The amount of insert DNA added is calculated based on a desired molar ratio, either 3:1 or 7:1 (insert to vector). To calculate the amount of insert DNA required, the following formula is used: ((100 ng of vector) x (kb size of insert))/ (kb size of vector)) x (molar ratio of (insert/vector)) = (ng of insert DNA). For each ligation reaction,1 U of T4 DNA ligase, and 1 µl of 10 x ligation buffer that was supplied with the enzyme (Promega) are included. The reactions were incubated overnight at 15 °C.

2.2.9 Transformation of *E. coli*

45 to 50 µl of competent *E. coli* cells (DH5α) were added to a cold 14 ml BD falcon polypropylene round-bottom tube after the cell suspension thawed on ice. To the competent cells, 5 µl of a solution containing the desired plasmid or ligation reaction product were added. Cells were incubated for 30 min on ice and then cells were placed in a water bath and heat-shocked for 90 s at 42 °C. The tubes were placed on ice for 2 min after removal from the water bath. 1 ml of LB medium was added. The cultures were shaken at ~250 rpm for 1 h at 37 °C. One LB agar plate with 100 µg/ml ampicillin was plated with 200 µl of cell suspension following incubation. The remaining 700 µl of liquid were centrifuged at 12,000 x g for 30 s at RT in a benchtop microcentrifuge to pellet the cells, and the supernatant was aspirated. The cell pellet was resuspended in 100 µl of the proper medium before plating onto a single LB agar plate that contained 100 µg/ml of ampicillin. Plates were incubated at 37 °C for 16 h. To ascertain whether contamination of the materials results in undesirable colonies during the chemical transformation, 5 µl 1 x TE (pH 8.0) was used as a negative control.

2.2.10 Transformation of yeast

The lithium acetate/single-stranded carrier DNA/PEG technique was used (Chen et al., 1992). A single colony was inoculated into 2 ml of YPD broth to grow the cells, which were then incubated until the culture reached saturation (OD_{600} > 3.0). 5 ml YPD broth was inoculated for each transformation (for example, 45 ml of media would be inoculated for 8 transformations), with an OD_{600} = 0.001 using the preculture and incubated at 30 °C with shaking at 250 rpm. The absorbance was measured the next day to check if the culture has reached an OD_{600} of ~ 0.8-1.2, indicating the desired growth phase. If the OD of the culture fell within this range, it confirmed that it had reached the desired growth phase. However, if the OD of the culture was found to be above the target range, it would be discarded. On the other hand, if the OD was below the target range, the culture would be returned to the incubation condition and checked every 30 min until it reached the log phase range. This allows for further growth until the desired OD range is achieved. Then the culture was transferred into a 50 ml tube, spun for 2 min at 3,500 rpm at 4 °C, the supernatant was discarded, and the cell pellet was placed on ice. One-step buffer (1 part 0.2 M LiOAc and 4 parts 40 % (w/v) PEG 4000) was used to resuspend the pellet in 8 ml. The cell suspension was centrifuged again at 3,500 rpm for 2 min at 4 °C, after which the supernatant was once more discarded. The pellet was placed back on ice and allowed for 1 to 2 min to allow one-

step buffer to settle at the bottom of the tube and be removed. For each required transformation, 88 µl of one-step buffer were added. A further 88 µl were added to make sure there was enough cell suspension. The pellet was vortexed until there were no clumps left. A sterile 1.5 ml tube with 10 µl of 10 mg/ml sheared salmon sperm DNA (Clontech/Takara # 630440) (boiled for 5 min in a heat block then placed on ice), 1 µg (for single plasmid transformation), or 200 ng and 1 µg (for two plasmid transformations), were added to each tube. The tubes were then vortexed for 15 s at top speed. The tubes were incubated at 42 °C in a water bath for 30 min and then placed on ice. The tubes were briefly spun at 13,000 x g for 10 s at RT to collect the cells, and the supernatant was aspirated. The cell pellet was resuspended in 200 µl of sterile water, and the entire suspension was plated onto an appropriate selective agar plate. The selection strategy for the plasmid was determined by the marker present in the plasmid, which could involve dropout of uracil or other required nutrients such as leucine. The specific nutrient dropout in the medium allowed for the selective growth of cells carrying the respective plasmid. The plate was incubated at 30 °C for 5-7 d until colonies had formed.

2.2.10.1 Replica plating and acetate testing

To determine which cells could grow on media containing only a non-fermentable carbon source and to avoid cells with a mutation that inhibits respiratory growth (known as petite cells), a technique called replica plating from SD-dropout plates to synthetic acetate plates (PSP2-dropout) was used. Plates were replica plated to PSP2 agar plates to isolate colonies that were able to grow on non-fermentable carbon sources. The PSP2-dropout plate was incubated at 30 °C for 2 d to allow for single colonies to grow. These colonies were then compared to the SD-dropout plates to identify the non-petite cells. These cells were streaked onto a fresh SD-dropout plate and incubated again at 30 °C for 3-5 d to allow single colonies to grow for future use. The colonies that were able to grow on the non-fermentable carbon source were selected, prepared for cryopreservation, and stored at -80 °C.

2.2.11 Protein Extraction for β-Galactosidase reporter assays

The frozen yeast culture samples were thawed on ice. The pellet was fully thawed before resuspending in 1 ml of ice-cold water. The cell culture was put into a 1.5 ml microcentrifuge tube, centrifuged for 1 min at RT at 12,000 x g, and the supernatant was aspirated. 100 µl of ice-cold RLB were added, and the pellets were then vortexed back into suspension. 150 mg

of glass beads were added, and the cells were then homogenised in the Precellys 24 device (Bertin Technologies, Montigny-le-Bretonneux, France) at 6500 rpm for 3 cycles of 10 s, with a 5 min break in between each cycle during which the samples were kept on ice. 100 µl of ice-cold 1 x RLB buffer were added to each sample after homogenisation, and each tube was briefly vortexed. After that lysates were centrifuged at 12,000 g and 4 °C for 3 min and then the supernatant was transferred into clean microcentrifuge tubes. Samples of protein lysate were flash frozen in liquid nitrogen and stored at -80 °C.

2.2.11.1 DC Protein assay

DC assay was used to measure the total amount of protein in the lysate. 5 µl was added to a U-bottomed well after a BSA protein standard was prepared in H_2O at concentrations of 62.5, 125, 250, 500, 1000, and 2000 µg/ml. 5 µl of lysate were added to each well after being diluted 1:10 (in H_2O or 1 x RLB). 25 µl reagent A and 200 µl reagent B were added into each well. The absorbance was measured at 750 nm with the Spectramax 190 plate reader after the plate was shaken at 50 rpm for 15 min at RT.

2.2.11.2 β-Galactosidase reporter assays (Miller, 1972; Schenborn, 1993)

β-Galactosidase reporter assays were performed as described in previous work. The β-galactosidase reporter assay kit (Promega) was used to measure the levels of β-galactosidase activity and, consequently, the expression of reporter genes. To 99 µl of ice cold 1 x RLB (Table 2.4), 1 µl of 1 U/µl of β-galactosidase was added to make a dilution of 1:100. The mixture was then put on ice. A 1:10,000 dilution was created by mixing 10 µl of this 1:100 dilution with 990 µl of ice-cold 1 x RLB. A standard range of β-galactosidase concentrations was prepared: 0, 1.0, 2.0, 3.0, 4.0 and 5.0 mU/50 µl. After that 50 µl of 2 x assay buffer were added to each well and the plate was covered with parafilm. The plate was incubated at 37 °C for 30 min and then the reaction was stopped by adding 150 µl of 1 M Na_2CO_3. The absorbance was read at 420 nm by using a microtiter plate reader.

2.2.12 Protein extraction for western blotting analyses (Papa et al., 2003)

The frozen pellets were resuspended in cold, sterile water after thawing, and then placed in a 1.5 ml microcentrifuge tube. The sample was centrifuged at 12,000 x g for 1 min at 4 °C to remove the supernatant. The pellet was then resuspended in 200 µl of lysis buffer containing

8 M urea, 2.5% (w/v) SDS, 50 mM Tris·HCl (pH 7.5 at 4 °C), 6 mM EDTA, 5 mM β-mercaptoethanol, 2 mM PMSF, and 6 mM AEBSF. The whole suspension was then transferred into a 2 ml flat-bottom screw-cap tube to which ~ 150-200 mg of acid-washed glass beads has already been added. The samples were homogenised in the Precellys 24 device for 4-6 cycles of 10 s at 6,500 rpm, with a 5 min break in between each cycle during which the samples were kept on ice. To isolate the supernatant, which contained the protein, samples were centrifuged at 12,000 x g for 2 min at 4 °C. A clean 1.5 ml microcentrifuge tube was used to collect the supernatant and then frozen in liquid nitrogen and stored at – 80 ˚C until required.

2.2.12.1 Bicinchoninic Acid (BCA) protein assay (Smith et al., 1985)

A bicinchonic acid (BCA) test was used to measure the amount of protein that was extracted in 8 M urea. The blank, standards, and protein lysates were prepared by diluting 1:10 with 0.1 M 2-iodacetamide in 0.1 M Tris-HCl (pH 8.0) and then incubated at 37°C for 15 min to destroy β-mercaptoethanol. After the incubation, 10 µl of BSA standard (0, 62.5, 125, 250, 500, 1000 and 2000 µg/ml), blank, and sample were added to the bottom of a U-bottom 96 well plate. Then 200 µl of working solution (Table 2.4) were added to each well. The plate was covered and incubated at 60 °C for 30 min. The Molecular Devices SpectraMAX 190 was used to read the absorbance at 562 nm.

2.2.12.2 SDS-PAGE (Laemmli, 1970)

Protein lysates were run on a 1 mm thick 10 % SDS-PAGE gel. The stacking gel is prepared by mixing 2.50 ml 30 % (w/v) acrylamide, 0.8 % (w/v) *N*,*N*'-methylenebisacrylamide, 1.875 ml 1 M Tris-HCl (pH 8.9), and 3.02 ml H_2O. The solution was then degassed for 5 min. 75 µl 10 % (w/v) SDS, 22.5 µl 10 % (w/v) ammonium persulfate, and 5 µl N,N,N',N'-tetramethyl ethylenediamine were added. The final mixture was poured into a casting stand and overlaid with water-saturated *n*-butanol. The gel casting mixture was left to polymerise for approximately 40 min at RT, after which it was washed with deionised H_2O. The separating gel was prepared by mixing 330 µl 30 % (w/v) acrylamide, 0.8 % (w/v) *N*,*N*'-methylenebisacrylamide, 625 µl 1 M Tris·HCl, pH 6.8, 1.50 ml H_2O. The solution was degassed for 5 min. Following that 25 µl 10 % SDS (w/v), 11.25 µl 10 % ammonium persulphate (APS) (w/v) and 3.75 µl *N*,*N*,*N*',*N*'-tetramethyl ethylenediamine (TEMED) were added. Then the solution was poured into the casting stand, and a comb was inserted. The gel

was left to solidify at RT for approximately 15 m. Following polymerisation, lysate samples were diluted to the appropriate concentration in water on ice. 6 x SDS-PAGE + β-Mercaptoethanol loading buffer was added to the sample. The sample was then heated at 40 °C for 10 min, left to cool to 3 min at RT and the sample was loaded into the well. The gel was run in a for 90 min at 120 V.

2.2.12.3 Western blotting (Towbin et al., 1979)

The stacking gel was carefully removed when the gel had been taken out of the electrophoresis unit. The separating gel was placed into a tray containing semi-dry buffer and incubated at 50 rpm for 5 min at RT. After cutting the PVDF membrane to the size of the gel, the membrane (Amersham HyBond^{TM}-P, pore size 0.45 µm, GE Healthcare, Little Chalfont, UK, cat. No. RPN303F) was soaked in methanol for 5 min before being transferred to a tray with semi-dry buffer. Eight pieces of Whatman 3 MM paper were cut to the size of the gel and soaked in semi-dry buffer. After preparation, each component was placed on the semi-dry horizon blot system (Atto, East Sussex, UK, Model #AE-6675L). Before stacking the parts, the area of the blot transfer apparatus where the stack was assembled was wetted with semi-dry buffer. Air bubbles were removed from between each of the four pieces of Whatman paper by gently rolling a glass tube over the stack. After that, the Whatman paper was covered with the prewetted PVDF membrane and subsequently the SDS-PAGE gel. As before, any air bubbles were removed. Air bubbles were removed before the last four pieces of Whatman paper were placed on top of the gel. The transfer was performed with a constant current of 2 mA/cm^2 of membrane for 75 min. After transfer, the membrane was stored overnight in 5 % milk-TBST at 4 °C (cold room) on a shaker at 35 rpm.

2.2.12.4 Antibody staining and detection

The membrane was incubated on a roller mixer at RT in 2 ml of 5 % milk in TBST containing anti-HA antibody dilution for 2 h. See Table 2.8 for additional information about the antibodies. Following incubation, the membrane was washed 4 times in 50 ml TBST at 50 rpm for 5 min each wash. Anti-rabbit IgG (H+L)-peroxidase HRP linked secondary antibody was used to incubate the membrane for 1 h at RT and then the membrane was washed in TBST as described above.

Proteins were visualised using two detection reagents. ECL2 was used to detect low protein amounts. A detecting agent of 5 ml Tris-HCl pH 8.5 + 0.1 % (v/v) Tween 20, 1.45 µl of 30 % (v/v) H_2O_2, 11.1 µl of 90 mM *p*-coumaric acid, 25 µl of 250 mM luminol was used for larger amounts of protein (Schneppenheim et al., 1991). 2 ml of the detection reagent were applied to the membrane which was then left to develop for 5 min at RT for ECL2. For the luminol/p-coumaric acid mixture, the membrane was left to develop for 1 min at RT. For the earlier blots, X-ray films (Thermo-Scientific CL-X-Posure X-ray film, Thermo Fisher Scientific, Cramlington, UK, cat. No. 34091) were exposed for exposure times ranging from 1 s to 10 min in a dark room, and the exposed films were developed using the Xograph Compact X4 (Xograph imaging systems, Stonehouse, UK). For the rest of blots, images were captured using the Invitrogen™ iBright™ CL1500 Imaging System (Invitrogen A44114 brand) at different exposure times.

2.2.12.5 Stripping of Western blots

The PVDF membrane was washed twice for 5 min in 50 ml of100 mM Tris-HCl (pH 8.5) + 0.1 % (v/v) Tween 20 at RT with shaking at 50-60 rpm. Following that, the membrane was incubated twice in 25 ml of 100 mM Tris-HCl, pH 8.5 + 200 mM β-mercaptoethanol + 0.1 % (v/v) Tween 20 for 15 min at RT with shaking at 50-60 rpm. The membrane was then twice washed in 50 ml of TBST for 5 min at room temperature. The membrane was then incubated twice in 100 mM glycine·HCl, pH 2.5 + 0.1 % (v/v) Tween 20 for 15 min each time, at 65 °C. The membrane was then twice washed in 50 ml of TBST for 5 min at RT. The membrane was then dipped in 5 % (v/v) milk with TBST and stored at 4 °C after this last wash.

2.2.13 RNA methods

2.2.13.1 RNA Isolation from yeast (Collart & Oliviero, 1993)

The frozen yeast culture samples (as described in the method above 2.2.1.2) were thawed on ice. The cell pellet was resuspended in 1 ml of ice-cold DEPC-H_2O and collected by centrifugation at 12,000 g, RT, for 10 s and then transferred to a 2 ml screw-cap tube (RNase free). In a 2 ml screw-cap microcentrifuge tube, cells were then resuspended in 300 µl of RNA buffer. The screw-cap tube had already received 200 mg (equal to ~200 µl) of acid-washed glass beads with a diameter of 0.45-0.55 mm that had been sterilised by baking at 200 °C for 4 h. Then 300 µl of phenol/$CHCl_3$/isoamylalcohol RNA buffered were added. The tube

was mixed by flipping. Cells were lysed using two cycles of 30 s each at 6,500 rpm, with a rest of 30 s in between in the Precellys instrument. The sample was centrifuged for 1 min at 12,000 g at 4 °C and then the upper phase was transferred into a new 1.5 microcentrifuge tube. 300 µl of phenol/$CHCl_3$/isoamylalcohol, RNA buffered was added to the 1.5 microcentrifuge tube, the tube briefly vortexed, and centrifuged for 1 min at 12,000 x g at 4 °C. The upper phase was transferred into a new 1.5 microcentrifuge tube. 900 µl of ice-cold ethanol were added, the tubes mixed, and then incubated at -80 °C overnight. The samples were centrifuged at 12,000 x g for 2 min at 4 °C repeated once for 10 s and then the supernatant was aspirated and removed from the sample. After washing the pellet in 70 % (v/v) EtOH, the pellet was centrifuged at 12,000 x g for 2 min at 4 °C repeated once for 10 s. The supernatant was aspirated, and the pellet was given 5-10 min to dry on air. The RNA pellet was dissolved in 50-100 µl of formamide over 1-2 h at RT with mixing (Chomczynski, 1992).The sample was centrifuged at RT for 5 min at 12,000 x g and then the supernatant was transferred to a clean 1.5 ml microcentrifuge tube. The RNA sample was then measured by diluting 1:200 with sterile H_2O to a final volume of 400 µl and added to a microtitre UV transparent plate, along with a blank consisting of H_2O. The plate was then read at 260 nm. Finally, the RNA sample was stored at -80 °C for further use.

2.2.13.2 Denaturating Agarose Gel Electrophoresis (Brown & Mackey, 1997)

The electrophoresis apparatus was carefully washed with 2 % (w/v) SDS. After that, the electrophoresis apparatus was carefully rinsed with ultrapure water to remove remaining SDS. To prepare a 1.4 % (w/v) gel, agarose was dissolved in 10 mM $Na_xH_{3-x}PO_4$ (pH 7.0) by heating and the solution was then allowed to cool to 55 °C. Once cooled, the gel was cast, a comb inserted and then allowed to solidify. The agarose gel was immersed in 10 mM $Na_xH_{3-x}PO_4$ (pH 7.0) running buffer and the buffer was recirculated during the electrophoresis run. 10 µg of RNA and the RNA denaturation solution (Table 2.5) were added in RNase-free 1.5 ml microcentrifuge tubes. After mixing the sample, the RNA was denatured by incubating the mixture in a heat block for 1 h at 50 °C. The sample was centrifuged at RT for 10 s at 12,000 x g and cooled to room temperature to collect the sample at the bottom of tube. 10 µl of 6 x RNA sample loading buffer was added and the sample was vortexed. The sample was loaded onto the gel after centrifugation at 12,000 x g for 10 s. One blank lane was left in between the lane holding the size marker and the sample, and 10 µg of denatured DNA size marker was added to the first lane. The gel was run at 3 V/cm of electrode distance with constant buffer recirculation until the bromophenol blue tracking dye

migrated around 80 % along the length of the gel. The size marker lane was cut off and stained overnight with 0.5 M NH_4OAc and 0.5 µg/ml ethidium bromide. The size marker lane gel was destained with water and then photographed under UV light with a wavelength of 254 nm.

2.2.13.3 Capillary transfer of RNA onto nylon membranes

The gel was cut out with a clean scalpel and a ruler to guide the cutting lines. A positively charged nylon membrane and eight Whatman 3 MM pieces were cut to the size of the agarose gel. A Whatman 3 MM paper was placed onto a ~10 cm high stack of paper towels. The sides were taped off. Three more pieces of Whatman 3 MM paper were wetted with 20 x SSC buffer and added to the stack, taking care to remove any air bubbles by rolling a pipette over each sheet. A Nylon membrane with a positive charge was soaked in DEPC-H_2O to wet it, and then placed into a solution of 20 x SSC. Following the previous step, the Nylon membrane was placed on the prepared stack of wetted Whatman 3 MM papers, and any air bubbles were carefully removed by rolling a pipette over the membrane. 20 x SSC was pipetted onto the membrane until liquid covered a significant portion of it. At that point, the gel was quickly placed to the membrane by aligning it with one of its two shorter sides. After that, the gel was gently and steadily released while being watched to make sure no air bubbles were getting caught in the liquid front between the gel and the membrane. The final four Whatman 3 MM papers were soaked in 20 x SSC and laid on the gel. Bubbles were removed by rolling the pipette over the surface of the paper. After being soaked in 20 x SSC, the large piece of Whatman 3 MM paper was soaked in 20 x SSC and set on top of the stack; the piece was long enough to connect both trays that were also filled with 20 x SSC. The stack of trays was covered with cling film, and a glass plate was placed on top of the stack. The arrangement was kept overnight at RT. The membrane was then placed on a piece of Whatman 3 MM paper with the nucleic acid side facing up, and UV irradiation (λ = 254 nm, 120 mJ/cm^2) was used to covalently crosslink the RNA to nylon membrane. The membrane was wrapped in Saran wrap and stored at 4 °C.

2.2.13.4 Hybridisation

Membranes were incubated in about 50 ml of 20 mM Tris-HCl (pH 8.0) for 15 min at 65 °C. This step strips covalently bound glyoxal from RNA and was only done once for every membrane. The membranes were prehybridised with 125 µl/cm^2 (20 ml/membrane)

prehybridisation solution at 42 °C for 3 h using the prehybridization solution described in Table 2.3. Formamide and denatured salmon sperm were added right before the solutions were added to the hybridization bottle. The concentration of the DNA probe used was 10 ng per 5 ml of the hybridisation solution. 10–25 ng of DNA template were diluted in 45.0 – 47.5 µl of 1 x TE buffer, pH 8.0. The DNA template was heated at 95 to 100 °C for 5 min to denature it. The sample was centrifuged for 10 s after chilling for 5 min in an ice-water bath. The denatured DNA was added to the reaction tube, which is part of a commercial kit (Table 2.9), contains a buffered solution of dATP, dGTP, and dTTP, along with exonuclease-free Klenow enzyme and random primers. The mixture was flicked to dissolve a blue pellet and then centrifuged for 10 s at RT to collect the entire solution at the bottom of the tube. 5 µl of 10 µCi/µl [α-^{32}P] dCTP were added and then the sample was incubated at 37 °C for 10 min. 5 µl of 0.2 M EDTA was added to stop the reaction. The gel filtration in a Microspin S-200 HR column was resuspended by vortexing, according to manufacturer's instructions. Following this, 0.5 ml of 1 mg/ml salmon sperm sample and the labelled DNA probe were denatured by heating to 95–100 °C for 5 min, then immediately put into an ice-water bath for 5 min. After a short centrifugation, the tubes were returned to the ice-water bath. Next, a labelled probe and denatured salmon sperm were added to the hybridisation solution. The membranes were hybridized overnight.

Membranes were placed in large trays and washed with a large amount of 2 x SSC, 0.1 % (w/v) SDS three times for 5 min at RT, as well as 0.2 x SSC, 0.1 % (w/v) SDS once for 5 min at RT. The trays used during the washing process were covered with a 1 cm thick Perspex sheet glass top and shaken continuously for thorough mixing. Membranes were transferred back to clean hybridisation bottles and incubated for 15 min at 42 °C with ~ 50 ml of prewarmed 0.2 x SSC, 0.1 % (w/v) SDS. The membranes were rinsed in 2 x SSC and blotted dry to remove any extra liquid. Damp membranes were wrapped in Saran wrap and placed inside storage phosphor imaging cassettes. Different time points were used to expose the wrapped blots to the Molecular Dynamics Storage Phosphor Screens. The image is captured from the PhosphorImager screen using a Typhoon 9400 system (GE Healthcare, Little Chalfont, UK). Bands were quantified with ImageQuant Version 5.2. Volumetric data were normalised to the loading control pC4/2.

2.2.13.5 Stripping and Rehybridisation

Membranes were incubated with 50 ml of 50 % (v/v) formamide, 1 % (w/v) SDS, and 0.1 x SSC at 65 °C for 30 min. After discarding the solution, the incubation process was repeated once more. The membranes were then incubated at 65 °C for 10 min with about 50 ml of 1 % (w/v) SDS and 0.1 x SSC. The membranes were either re-prehybridized as described above for additional hybridisations, or they were wrapped in Saran wrap and stored at 4 °C.

2.2.14 Statistical Analyses

Statistical analyses were conducted to assess the normality and determine significant differences among the data sets. Prior to analysis, the normality of the data was assessed using the Shapiro-Wilk test, a commonly used statistical test for this purpose. The data sets subjected to this test included the β-galactosidase assays, Northern blot, and Western blot data.

For the β-galactosidase assays, a specific approach was employed due to the nature of the data. The β-galactosidase reporter data was logarithmically transformed using a natural base (ln). The analysis of the β-galactosidase assays involved the utilisation of a non-parametric Scheirer-Ray-Hare test, followed by a Games-Howell post-hoc test. The decision to opt for the Scheirer-Ray-Hare test instead of an ordinary two-way ANOVA was driven by the persistence of unequal variances in the data, even after logarithmic transformation.

Regarding the Northern blot and Western blot data, ordinary 2-way ANOVA (Khuri, 2013) was performed with Tukey's correction for multiple comparisons (Tukey, 1949). The purpose of this analysis was to determine if there were statistically significant differences ($p < 0.05$) between the means of the data sets in both the Northern and Western blot experiments. The software used for this analysis was Prism 8 from GraphPad Software, Inc. (La Jolla, California).

To represent the levels of statistical significance in the results, stars (*) were used following the convention: *, $p \leq 0.05$; **, $p \leq 0.01$; ***, $p \leq 0.001$; ****, $p \leq 0.0001$. These stars were included to identify the groups or conditions that exhibited significant differences in their expression levels. It is important to note that the figures presented in both the Northern blot and β-galactosidase assays depict different representations of the same underlying data.

3 CHARACTERISATION OF PROTEIN KINASE MUTANTS TO INVESTIGATE DIFFERENT RNASE ACTIVITY PHENOTYPES

3.1 Rationale

Previous studies on Ire1 suggest that in *trans* autophosphorylation of the activation loop in the protein kinase domain precedes activation of RNase activity (Armstrong et al., 2017; Lee et al., 2008; Mannan et al., 2013b). As mentioned before in earlier research, D797A is a mutant in the protein kinase domain, and this mutant has no detectable protein kinase or RNase activity (Lee et al., 2008). The two mutations D797N K799N together resulted in the inactivation of Ire1 protein kinase activity but displayed significant RNase activity (Chawla et al., 2011; Rubio et al., 2011). This led me to investigate the effect of several amino acid mutations in the Ire1 protein kinase domain to elucidate how the kinase domain regulates RNase activity, trying to resolve why different point mutations in the protein kinase domain have different effects on RNase activity. These mutations included alanine mutations of the catalytic aspartate (D797), a lysine located in the catalytic loop, K799 and the Mg^{2+}-coordinating amino acids N802 and D828. I will utilise Northern blotting, a technique for direct detection and analysis of specific RNA molecules. This method enables the detection and characterisation of specific RNA species based on their size. By subjecting the RNA samples to electrophoresis and subsequent transfer onto a membrane, the *HAC1* mRNA and its spliced variants can be visualised and distinguished. The spliced *HAC1* mRNA results in a smaller size compared to the unspliced form, enabling their differentiation on the blot. This technique provides a direct measurement of the splicing efficiency and allows for the identification and quantification of different *HAC1* mRNA species. By analysing the intensities and sizes of the bands on the Northern blot, it is possible to understand the behaviour of *HAC1* mRNA in response to different mutations in Ire1. Thus, Northern blotting serves as a robust tool in elucidating the molecular mechanisms underlying the regulation of *HAC1* mRNA and its splicing patterns, complementing the findings obtained from other experimental approaches.

In this study, I will utilise Northern blot analysis to investigate the RNase activity of Ire1 mutants, including single point mutations D797A, K799A, N802A, and D828A. Additionally, double mutants will also be examined. Moreover, I performed a comprehensive mutational analysis of the protein kinase domain, especially regarding the rescue of RNase

activity of the D797A mutant when another point mutation in the protein kinase domain was introduced into this mutant.

3.2 Characterisation of RNase activity in single point mutations

3.2.1 Characterisation of RNase activity in single point mutations over time course

To investigate the temporal dynamics of the function of Ire1 alleles in response to ER stress, a time course analysis was conducted. The focus was on characterising the RNase activity of single point mutations, including D797A, K799A, D828A, and N802A Ire1. The analysis was conducted at three time points: 0 h, 1 h, and 2 h. These time points provide information about the temporal behaviour of Ire1 alleles and their response to ER stress. The experiment involved introducing different alleles into a strain that lacked for the *IRE1* and these alleles coded for WT Ire1. The strains were grown to mid-exponential growth phase, and then ER stress was induced by adding 2 mM DTT to the cultures. To evaluate RNase activity, 20 ml samples were collected at the initial time point 0 h and compared to 20 ml samples obtained at 1 h and 2 h after adding 2 mM DTT and RNA then was extracted from these samples.

DTT, a reducing agent, is selected because it directly disrupts protein folding by reducing disulfide bonds, closely mimicking the cellular response to protein misfolding. This aligns with the objective of the study of understanding the function of IRE1 alleles in the context of ER stress. DTT also offers a controlled and consistent means of inducing stress, and its mechanism is simpler, making it a better fit for this research compared to Tm which operates through a more complex pathway by inhibiting protein glycosylation.

Northern blotting was performed on the extracted RNA using probes specific to *HAC1*, *KAR2*, and *PDI1* mRNAs. The resulting blot was normalised to the loading control, pC4/2, which hybridises to 18 S rRNA (Schroeder, unpublished) (Fig 3.1).

For data analysis, a one-way analysis of variance (ANOVA) was employed. The factors considered in the analysis were the time points and the different Ire1 alleles. The one-way ANOVA allowed for the examination of the main effects of these factors and their interactions on RNase activity levels. This statistical approach enabled the assessment of the significance of observed differences between time points and alleles. The resulting p values in Figure 3.1 reflect the statistical significance of these differences. By applying this analytical method, I was able to rigorously evaluate the temporal dynamics of Ire1 allele function in response to ER stress.

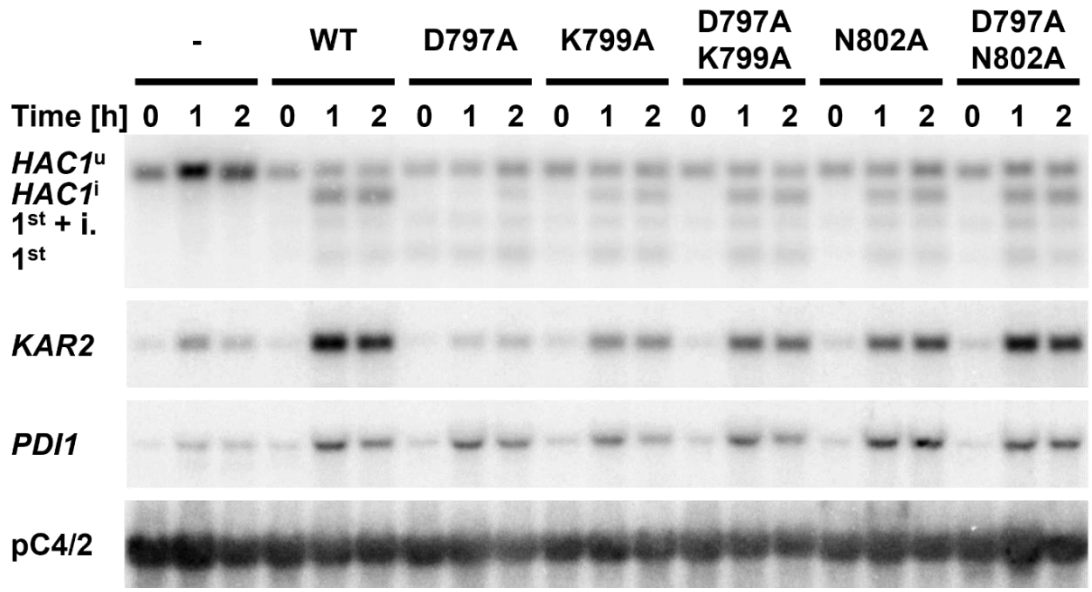

Figure 3.1. Northern blots of IRE1 mutants: analysis of gene expression for *HAC1*, *KAR2*, *PDI1*, and loading control pC4/2.
Northern blots for *HAC1*, *KAR2*, *PDI1*, and the loading control pC4/2 on RNA extracted from *ire1*Δ strains carrying and expressing the indicated *IRE1* mutants from YCplac33 or empty vector (-). Cells in the mid-exponential-growth-phase were treated with 2 mM DTT for the indicated times. Abbreviations: H*AC1*^{u}, unspliced *HAC1* mRNA; *HAC1*^{i}, spliced *HAC1* mRNA; 1st + i., 1st exon of *HAC1*^{u} mRNA + the intron; 1st, 1st exon of *HAC1*^{u} mRNA.

As anticipated, strains lacking Ire1 displayed minimal levels of the *HAC1* mRNA species, for example *HAC1*^{i} due to the absence of Ire1 (Fig 3.2 A). The WT cells exhibited the anticipated pattern, showing an increase in RNase activity over time, with the most significant difference observed between the 0 h sample and the 2 h sample (Fig 3.2 B). There was no statistical difference, calculated by one-way ANOVA, for D797A cells, indicating that their behaviour closely resembles that of strains lacking Ire1 (Fig 3.2 C). The mutants K799A, D828A, and N802A Ire1 exhibited an increase in RNase activity from 0 to 1 h, as well as from 0 to 2 h, although no significant differences were observed between the 1 to 2 h time points (Figs 3.2 D, 3.2 E, 3.2 F). These findings suggest that the absence of Ire1 leads to minimal RNase activation, while specific mutations in Ire1 can modulate the temporal dynamics of RNase activity in response to ER stress.

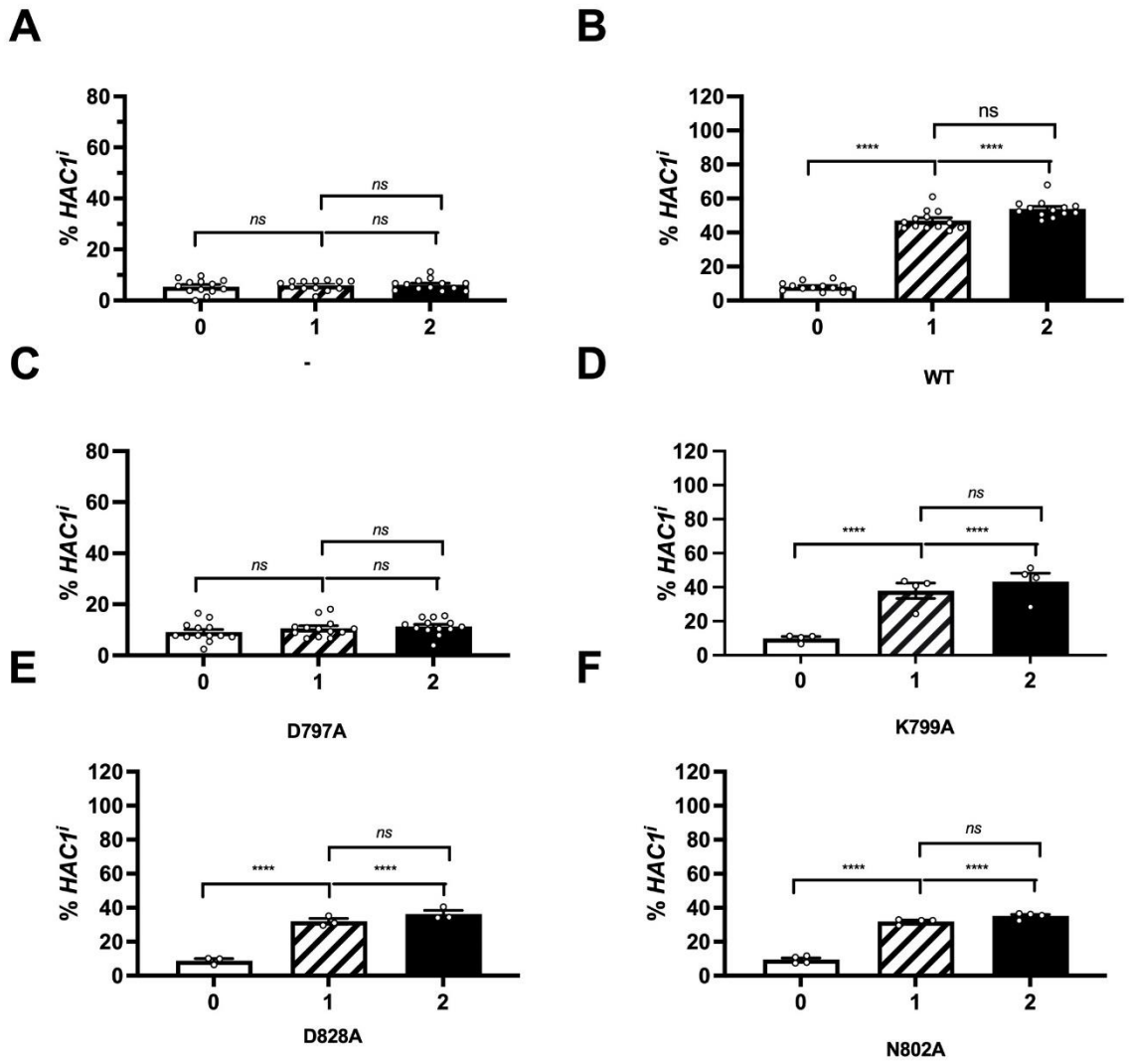

Figure 3.2. Percentage of *HAC1*^{i} mRNA in single point mutations and WT Ire1 over time.
The graph displays the percentage of *HAC1*^{i} mRNA (% *HAC1*^{i}) over time for (A) strain lacking Ire1 (-) (B) WT Ire1 (C) D797A Ire1 (D) K799A Ire1 (E) D828A Ire1 and (F) N802A Ire1. Bars represent the standard errors. The data presented in the graphs were obtained by calculating the average and standard error from three clones for each of the mutant strains (n=3). However, for the *IRE1* deletion strain, WT strain, and D797A strain, the data were obtained from four biological repeats of three clones, resulting in a total sample size of n=12 Statistical analyses were conducted using an ordinary one-way ANOVA with Tukey's correction for multiple comparisons. The stars indicate the ranges of p values that were calculated. *, $P \leq 0.05$; **, $P \leq 0.01$; ***, $P \leq 0.001$; ****, $P \leq 0.0001$.

3.2.2 Similar expression Levels of *HAC1*^{i} mRNA in K799A Ire1 and WT Ire1

The study investigated the RNase activity of the K799A mutation in Ire1 by comparing it to both WT Ire1 and the strain lacking Ire1. Additionally, the RNase activity of the K799A mutation was compared to other mutations, namely D797A, N802A, and D828A. The objective was to assess the differences in RNase activity among these mutations and determine if the K799A mutation had distinct functional consequences compared to other mutations in Ire1.

Furthermore, the gene expression levels of K799A Ire1 compared to WT Ire1 to elucidate the specific effects of this alteration on gene expression. By studying the K799A mutation individually, I can discern whether it has distinct functional consequences compared to other mutations or the WT Ire1.

The percentage of *HAC1*^{i} mRNA increased from 8.1 % ± 0.7 % to 47.1 % ± 1.6 % after a 1 h treatment with 2 mM DTT in cells expressing WT Ire1 and reached 53.9 % ± 1.4% after 2 h of exposure of WT cells to 2 mM DTT (Fig 3.3 A). A similar increase in the percentage of *HAC1*^{i} mRNA in cells expressing K799A Ire1 was not statistically significantly different from the increase seen in cells expressing WT Ire1.

Additionally, after 1 and 2 h of ER stress induction, a significant increase in *HAC1* splicing was noted between cells lacking Ire1 and those expressing K799A Ire1 (Fig 3.3 A). A significant decrease was observed between the D797A mutant and the other single mutants in relation to their percentage of *HAC1*^{i} mRNA, *KAR2* and *PDI1* mRNA levels at both the 1 h and 2 h time points (Figs. 3.3 A, 3.3 B and 3.3 C). However, when comparing the K799A to D828A, and N802A mutants, no significant differences were detected. These finding suggest that the K799A mutation in Ire1 acts similarly to WT, as there were no statistically significant differences observed in the percentage of *HAC1*^{i} mRNA.

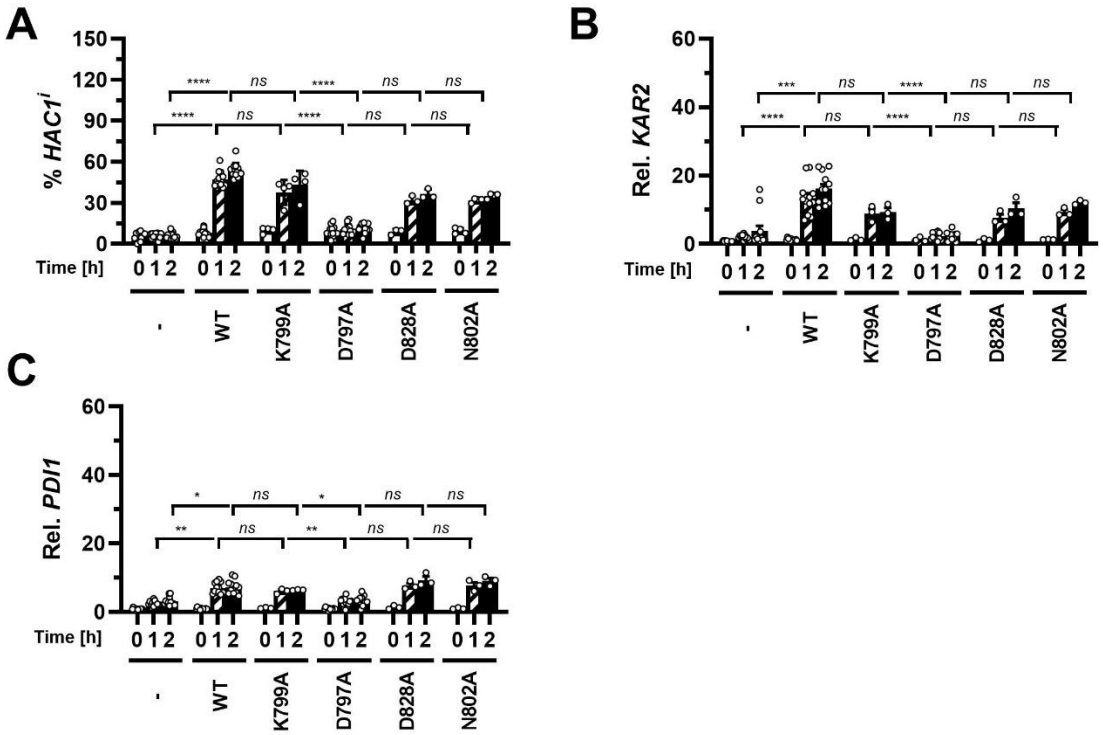

Figure 3.3. Comparison of percentage of *HAC1*^{i} mRNA, *KAR2* and *PDI1* mRNA levels in K799A and other single point mutations.

The graphs compare K799A Ire1 to WT Ire1, strains lacking Ire1 and to other single mutations. The percentage of *HAC1*^{i} mRNA (A), induction of *KAR2* mRNAs (B), and induction of *PDI1* mRNAs (C), are presented. The data presented in the graphs were obtained by calculating the average and standard error from three clones for each of the mutant strains (n=3). However, for the *IRE1* deletion strain, WT strain, and D797A strain, the data were obtained from four biological repeats of three clones, resulting in a total sample size of n = 12. Significance determined by 2-way ANOVA and the stars indicate the ranges of p values that were calculated.

3.2.3 The presence of D828A mutations in the catalytic residues within the kinase domain results in a reduction of *HAC1^{i}* mRNA compared to WT

The amino acid residue D828 is located near the active site of the kinase domain and plays a crucial role in catalysing the phosphoryl transfer reaction. It interacts with the substrate and the ATP molecule, and when mutated to alanine, this interaction is disrupted, resulting in a reduction in the catalytic activity of the kinase domain. Moreover, the coordination of two Mg^{+2} ions is the major role of D828 in the protein kinase catalytic core (Mannan et al., 2013b; Mori et al., 1993).

Given the proximity and potential similarity in behaviour between the D828A mutant and the K799A mutant due to their location, it is worth investigating the function of the D828A Ire1 mutant. This mutant has been extensively studied in previous research (Chawla et al., 2011; Mannan et al., 2013b; Mori et al., 1993). Northern blot was conducted to explore any similarities between these mutants and gain further insights into their effects on gene expression of Ire1.

Northern blot showed that D828A Ire1 retained partial RNase activity compared to cells expressing WT Ire1 and was statistically significant compared to cells lacking Ire1 (Fig 3.4 A). An increase in the percentage of *HAC1*^{i} mRNA from 8.8 % ± 1.2 % to 32.1 % ± 1.7 % after a 1 h treatment with 2 mM DTT in cells expressing D828A Ire1 and reached 36.3 % ± 2.1 % after 2 h of exposure of D828A cells to 2 mM DTT albeit lower than that observed in cells expressing the WT Ire1. Moreover, after 1 and 2 h of ER stress induction, a statistically significant increase in *HAC1* splicing was observed between cells lacking Ire1 and those expressing D828A Ire1 (Fig 3.4 A).

Comparing the D797A mutant to D828A Ire1, the induction of *KAR2* and *PDI1* mRNAs as well as *HAC1* splicing were both decreased (Figs. 3.4 A, 3.4 B and 3.4 C). However, when comparing D828A to other single mutations such as K799A and N802A mutants in terms of the percentage of *HAC1^{i}* mRNA, *KAR2* and *PDI1* mRNA levels, no significant differences were detected (Figs 3.4 A, 3.4 B, and 3.4 C). These data suggest that the inclusion of D828A mutations in the catalytic residues within the kinase domain leads to a decrease in *HAC1^{i}* mRNA expression compared to the WT Ire1.

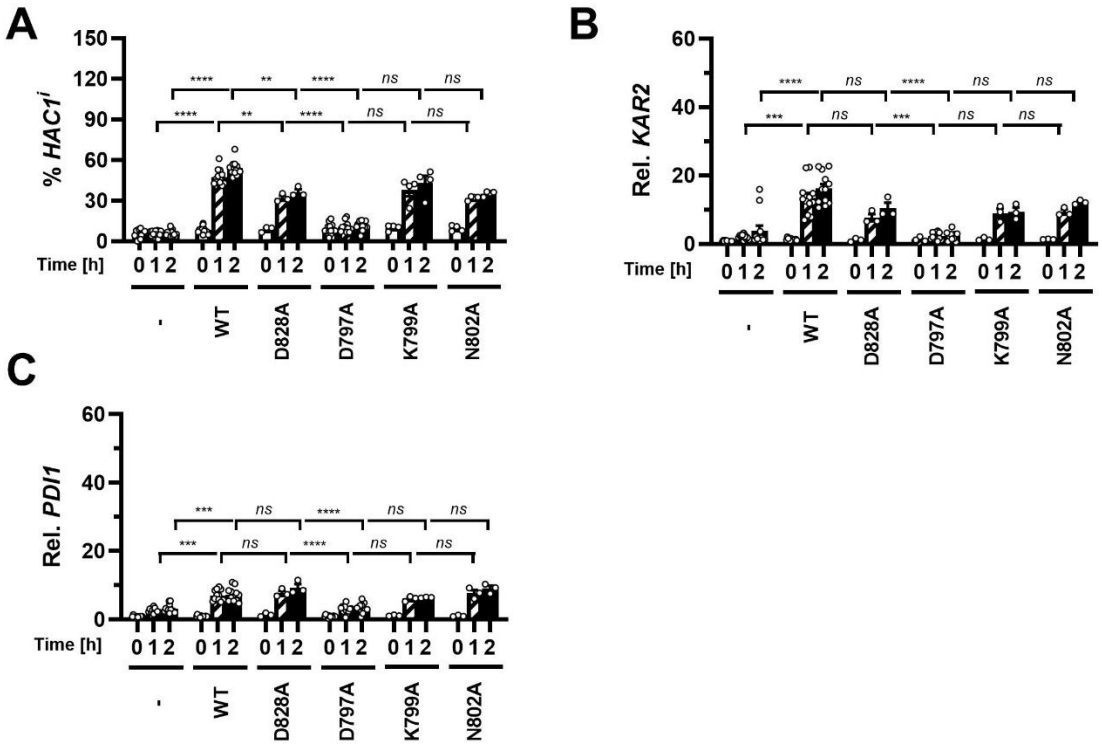

Figure 3.4. Comparison of percentage of *HAC1*^{i} mRNA, *KAR2* and *PDI1* mRNA levels in D828A and other single point mutations.

The graphs compare D828A Ire1 to WT Ire1, strains lacking Ire1 and to other single mutations. The percentage of *HAC1*^{i} mRNA (A), induction of *KAR2* mRNAs (B), and induction of *PDI1* mRNAs (C), are presented. The data presented in the graphs were obtained by calculating the average and standard error from three clones for each of the mutant strains (n=3). However, for the *IRE1* deletion strain, WT strain, and D797A strain, the data were obtained from four biological repeats of three clones, resulting in a total sample size of n=12. Significance determined by 2-way ANOVA and the stars indicate the ranges of p values that were calculated.

3.2.4 N802A mutations in kinase domain decrease *HAC1*^{i} mRNA expression compared to WT Ire1

The N802A mutation in Ire1 is characterised by the involvement of the amido group of N802 on the catalytic loop in coordinating the second Mg^{2+} ion. This observation suggests a potential similarity in behaviour between the N802A mutant and the K799A mutant, as both mutations interact with the phosphates of ATP/ADP through Mg^{2+} ions. To investigate the functional implications of the N802A Ire1 mutant and to determine if it behaves similarly to K799A, Northern blot analysis was conducted.

An increase in the percentage of *HAC1*^{i} mRNA from 9.5 % ± 1.1 % to 31.9 % ± 0.8 % after a 1 h treatment with 2 mM DTT in cells expressing N802A Ire1 and reached 35.2 % ± 0.9 % after 2 h of exposure of N802A cells to 2 mM DTT albeit lower than that observed in cells expressing the WT Ire1. Comparing the N802A Ire1 mutant to WT Ire1, reduced levels of *HAC1* splicing were observed (Figs. 3.5 A). Moreover, after 1 and 2 h of ER stress induction, a statistically significant increase in *HAC1* splicing, induction of *KAR2* and *PDI1* mRNA levels were observed between cells lacking Ire1 and those expressing N802A Ire1 (Figs. 3.5 A, 3.5 B and 3.5 C). A significant increase in the percentage of *HAC1*^{i} mRNA and *KAR2* and *PDI1* mRNA levels were observed when compared to D797A Ire1. While no significant were observed when compared to other single mutants K799A and D828A.

These findings indicate that the N802A mutation in Ire1 has implications for *HAC1* splicing during ER stress and does not exhibit similar patterns to the K799A mutants.

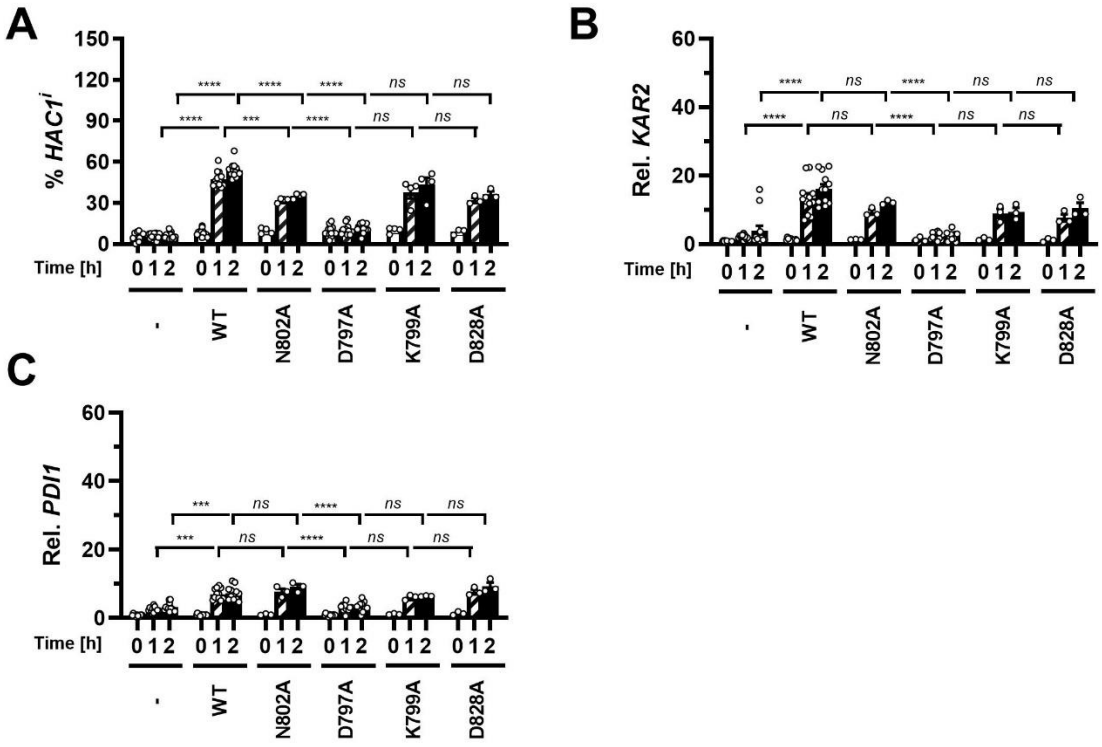

Figure 3.5. Comparison of percentage of *HAC1*^{i} mRNA, *KAR2* and *PDI1* mRNA levels in N802A and other single point mutations.

The graphs compare N802A Ire1 to WT Ire1, strains lacking Ire1 and to other single mutations. The percentage of *HAC1*^{i} mRNA (A), induction of *KAR2* mRNAs (B), and induction of *PDI1* mRNAs (C), are presented. The data presented in the graphs were obtained by calculating the average and standard error from three clones for each of the mutant strains (n=3). However, for the *IRE1* deletion strain, WT strain, and D797A strain, the data were obtained from four biological repeats of three clones, resulting in a total sample size of n=12. Significance determined by 2-way ANOVA and the stars indicate the ranges of p values that were calculated.

3.3 Characterisation and comparative analysis of K799A, D828A, and N802A mutations in Ire1

The primary objective of this analysis was to investigate the impact of the K799A, D828A, and N802A mutations in Ire1 on gene expression levels. Specifically, I aimed to determine whether different combinations of these mutations result in additive changes in gene expression compared to the Ire1 mutant alone.

3.3.1 Characterisation of K799A mutation in comparison to double or triple mutants

To explore *HAC1* splicing and gene expression levels in N802A, D828A, and N802A D828A in combination with the K799A mutation.

The results of these investigations were compared to those obtained with the K799A mutant to assess whether the observed differences in gene expression levels were specific to K799A or if they extended to other mutations. It is worth noting that although there was no statistically significant difference in percentage of $HAC1^{i}$ mRNA between WT and K799A Ire1 (Fig 3.6 A).

Additionally, in the case of the K799A N802A D828 Ire1 mutants, a significant decrease in percentage of $HAC1^{i}$ mRNA was observed after a 2 h treatment with 2 mM DTT (Fig 3.6 A), However, no significant differences were found in *KAR2* and *PDI1* mRNA levels (Figs. 3.6 B and 3.6 C). Moreover, there were no significant differences in percentage of $HAC1^{i}$ mRNA, *KAR2* and *PDI1* mRNA levels when comparing K799A to K799A N802A and K799A D828A mutants.

These finding suggest that the combination of the K799A mutation with the other mutations N802A and D828A (K799A N802A D828A) resulted in a significant decrease in $HAC1^{i}$ mRNA levels, indicating potential additive effects specifically on *HAC1* splicing. However, there was no significant impact on *KAR2* and *PDI1* mRNA levels observed.

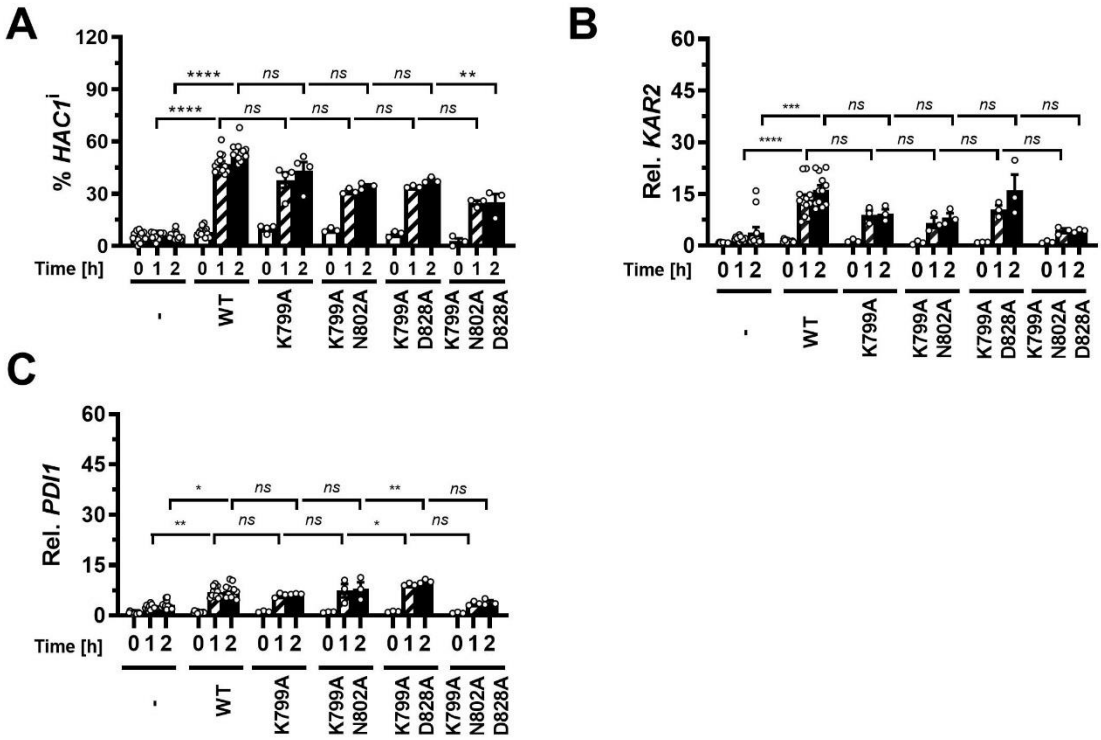

Figure 3.6. Comparison of spliced *HAC1* mRNA levels and induction of UPR target genes in K799A Ire1 and other mutants.

The graph displays a comparison between K799A Ire1 and WT Ire1, as well as K799A combined with other mutants including N802A, D828A, and N802A D828A, under ER stress. The graph presents the following data for different parameters: (A) the percentage of $HAC1^i$ mRNA, (B) induction of *KAR2* mRNAs, and (C) induction of *PDI1* mRNAs. The bars represent the standard errors. The data presented in the graphs were obtained by calculating the average and standard error from three clones for each of the mutant strains (n=3). However, for the *IRE1* deletion strain and WT strain, the data were obtained from four biological repeats of three clones, resulting in a total sample size of n=12. Statistical analyses were conducted using an ordinary two-way ANOVA with Tukey's correction for multiple comparisons. The stars indicate the ranges of p-values that were calculated.

3.3.2 Characterisation of D828A mutation in comparison to double or triple mutants

In the previous chapter, it was observed that the combination of the K799A mutation with the triple mutations (K799A N802A D828A) resulted in a significant decrease in *HAC1*^{i} mRNA levels, indicating additive effects on *HAC1* splicing. However, there were no significant changes observed in the mRNA levels of *KAR2* and *PDI1*.

Building upon these findings, I further explored whether combining additional mutations with the D828A mutation would have a similar effect on *HAC1* splicing as observed with the K799A mutation.

When comparing the D828A Ire1 mutant with other mutations (K799A D828A, N802A D828A, and K799A N802A D828A), no statistically significant differences were observed in the percentage of *HAC1*^{i} and *KAR2* mRNA (Figs. 3.7 A and 3.7 B). However, the levels of *PDI1* mRNA were significantly lower in K799A N802A D828A cells compared to D828A cells after 1 and 2 h of treatment with 2 mM DTT (Fig. 3.7 C).

These findings indicate that the additive effects of combining the D828A mutation with these specific mutations predominantly affect *PDI1* expression, leading to a notable decrease in mRNA levels.

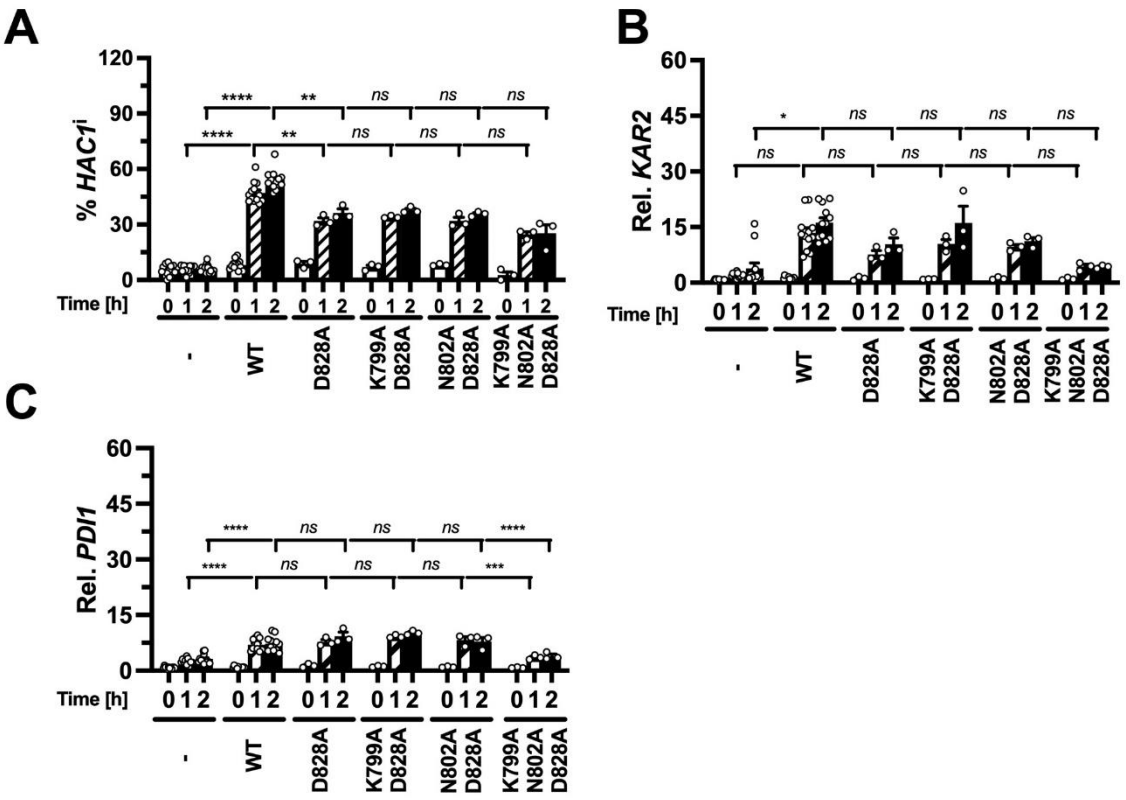

Figure 3.7. Comparison of ER stress-induced spliced *HAC1* mRNA levels and UPR target gene induction in D828A Ire1 mutant compared to WT, K799A D828A, N802A D828A and K799A N802A D828A Ire1 mutants.

The graph displays a comparison between D828A Ire1 and WT Ire1, as well as D828A combined with other mutants including K799A, N802A, and K799A N82A, under ER stress. The graph presents the following data for different parameters: (A) the percentage of $HAC1^i$ mRNA, (B) induction of *KAR2* mRNAs, and (C) induction of *PDI1* mRNAs. The bars represent the standard errors. The data presented in the graphs were obtained by calculating the average and standard error from three clones for each of the mutant strains (n=3). However, for the *IRE1* deletion strain and WT strain, the data were obtained from four biological repeats of three clones, resulting in a total sample size of n=12. Statistical analyses were conducted using an ordinary two-way ANOVA with Tukey's correction for multiple comparisons. The stars indicate the ranges of p-values that were calculated.

3.3.3 Characterisation of N802A mutation in comparison to double or triple mutants

Continuing from the investigations in the previous chapter, additional comparisons were conducted to examine the potential additive effects of combining additional mutations with the N802A mutation. The aim was to assess whether the presence of these additional mutations, in combination with N802A, would result in additive effects on gene expression levels.

When comparing the N802A Ire1 mutant with other mutations (K799A N802A, N802A D828A, and K799A N802A D828A), no statistically significant differences were observed in the percentage of *HAC1*^{i} and *KAR2* mRNAs (Figs. 3.8 A and 3.8 B). However, there was a significant decrease in *PDI1* mRNA levels in K799A N802A D828A cells compared to N802A cells after 1 and 2 h of treatment with 2 mM DTT (Fig. 3.8 C).

These findings suggest that combining the N802A mutation with additional mutations does not generally result in significant alterations in the percentage of *HAC1*^{i} and *KAR2* mRNA levels. However, the combination of the N802A mutation with the K799A and D828A mutations leads to a significant decrease in *PDI1* mRNA levels. These observations indicate gene-specific effects and highlight the potential additive impact of combining specific mutations on the regulation of *PDI1* expression.

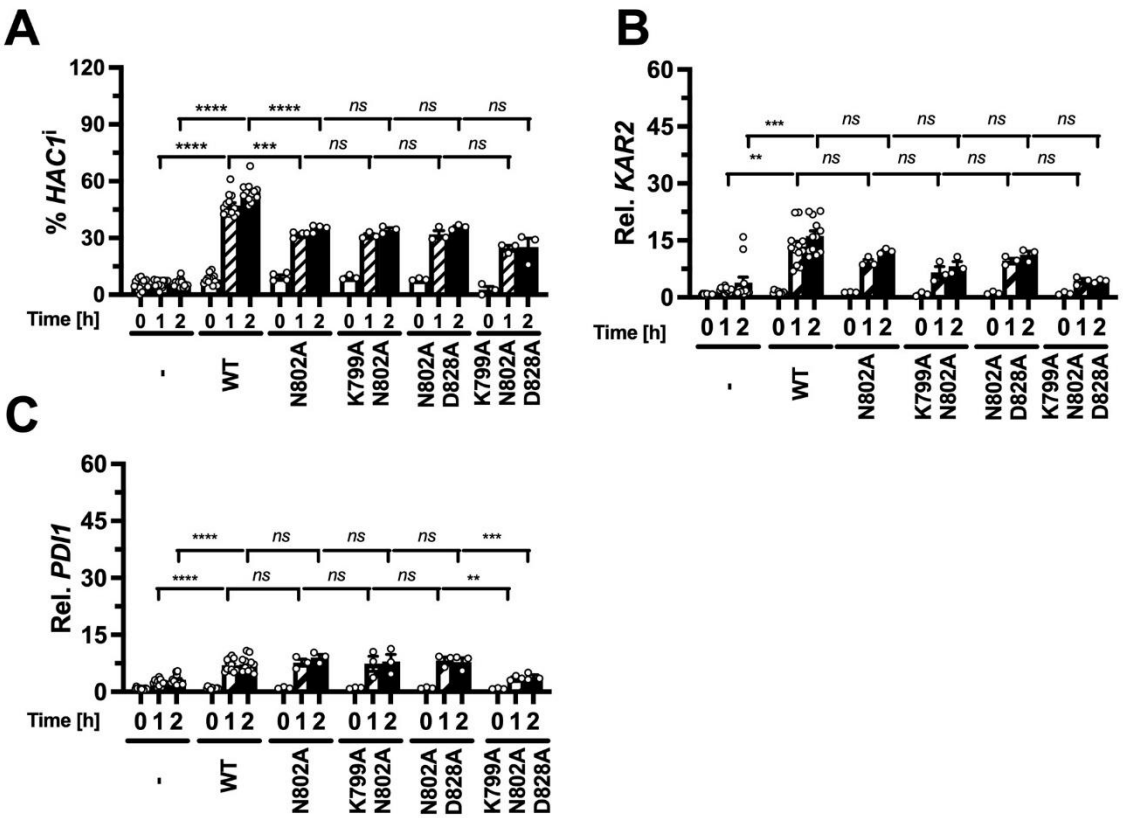

Figure 3.8. The effects of ER stress on spliced *HAC1* mRNA levels, *Kar2* and *PDI1* mRNAs induction in N802A Ire1 compared to other mutants.

The graph displays a comparison between N802A Ire1 and WT Ire1, as well as N802A combined with other mutants including K799A, D828A, and K799A D828A, under ER stress. The graph presents the following data for different parameters: (A) the percentage of $HAC1^i$ mRNA, (B) induction of *KAR2* mRNAs, and (C) induction of *PDI1* mRNAs. The bars represent the standard errors. The data presented in the graphs were obtained by calculating the average and standard error from three clones for each of the mutant strains (n=3). However, for the *IRE1* deletion strain and WT strain, the data were obtained from four biological repeats of three clones, resulting in a total sample size of n=12. Statistical analyses were conducted using an ordinary two-way ANOVA with Tukey's correction for multiple comparisons. The stars indicate the ranges of p-values that were calculated.

3.4 Intragenic suppression and restoration of RNase activity in Ire1 mutations

3.4.1 The catalytic role of K799 in the Ire1 protein kinase domain and its rescue of D797 through intragenic suppression

K799 is a key residue in the ATP-binding pocket of protein kinase domains and is essential for ATP binding and catalytic activity (Rubio et al., 2011; Valiev et al., 2007). Protein kinases catalyse the transfer of the γ-phosphate from ATP to substrates and K799, along with other amino acids, plays a role in this process by helping to stabilise and coordinate the γ-phosphate (Hanks & Hunter, 1995). Here, I investigated the functional role of residue K799 by characterising the K799A mutation and its potential role in rescuing defective mutants through intragenic suppression, as observed in a previous study where the K799N mutation rescued the D797N mutant (Rubio et al., 2011).

To further explore this phenomenon, I conducted Northern blot experiments to detect *HAC1* splicing in cells expressing both WT Ire1 and different Ire1 mutants, including the K799A mutant. To investigate the role of K799 in control of RNase activity and initiation of *HAC1* splicing by Ire1, alleles coding for WT and K799A Ire1 were introduced into a strain deleted for *IRE1*. After growth to mid-exponential growth phase, ER stress was induced by adding 2 mM DTT to cultures. RNA was extracted before addition of DTT and 1 and 2 h after addition of DTT and analysed by Northern blotting with probes against *HAC1*, *KAR2*, *PDI1* mRNAs and normalised to the loading control, pC4/2, which hybridises to 18 S rRNA (Schroeder, unpublished) (Fig 3.1).

The introduction of the K799A mutation into the D797A mutant resulted in the restoration of RNase activity, as evidenced by increased levels of *HAC1* mRNA and the induction of *PDI1* and *KAR2* mRNA (Figs. 3.9 A, 3.9 B, and 3.9 C), in the same way as reported before for the D797N K799N mutant (Rubio et al., 2011). 2 h after addition of DTT to cells expressing D797A K799A Ire1 the percentage reached $HAC1^i$ mRNA reached 30.7 % ± 3.1 %, while it is remaining at 11.3 % ± 0.8 % in cells expressing D797A Ire1. The percentage of $HAC1^i$ mRNA was higher in cells expressing WT Ire1 at 1 h and 2 h after exposure to 2 mM DTT than in cells expressing D797A K799A Ire1 (Fig 3.10 A). Two hours after induction of ER stress with 2 mM DTT, *KAR2* mRNA levels were significantly decreased in D797A K799A Ire1 mutants compared to cells expressing WT Ire1, however for *PDI1* the averages for D797A K799A Ire1 and WT-Ire1 were very similar (Figs. 3.10 B and 3.10 C).

These results indicate that the D797A Ire1 mutant has significantly impaired RNase activity, and this activity can be restored when the D797A and K799A mutations are combined. The K799A mutation acts as a suppressor or rescuer of the RNase activity phenotype in the D797A mutant.

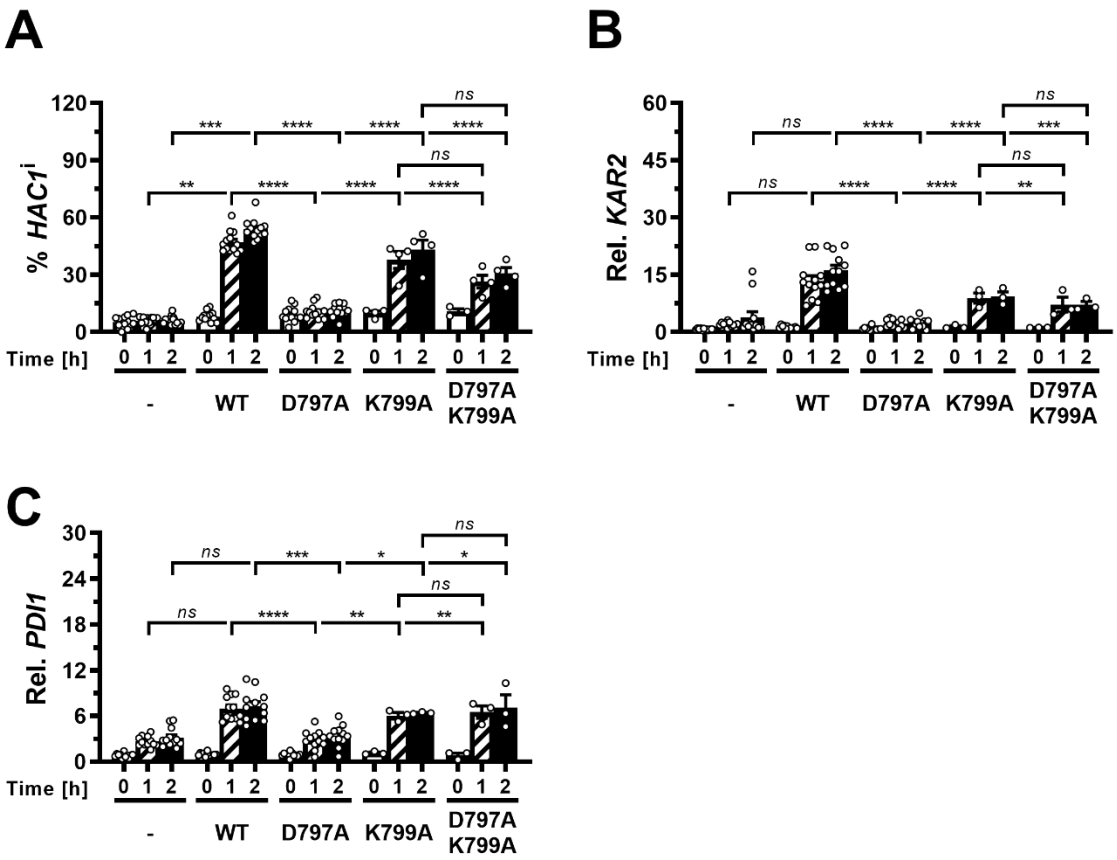

Figure 3.9. K799A Ire1 restores *HAC1* splicing to D797A Ire1.
The graph compares the results obtained from D797A Ire1 and WT Ire1, as well as K799A and D797A K799A, in response to ER stress. The graph presents data for various parameters, including (A) the percentage of $HAC1^{i}$ mRNA, (B) induction of *KAR2* mRNAs, and (C) induction of *PDI1* mRNAs. The bars represent the standard errors. The data presented in the graphs were obtained by calculating the average and standard error from three clones for each of the mutant strains (n=3). However, for the *IRE1* deletion strain, WT strain, and D797A strain, the data were obtained from four biological repeats of three clones, resulting in a total sample size of n=12.Statistical analyses were conducted using an ordinary two-way ANOVA with Tukey's correction for multiple comparisons. The stars indicate the ranges of p-values that were calculated. The p values are for the comparison of D797A Ire1 to WT, K799A, D797A K799A Ire1 and to strains lacking Ire1.

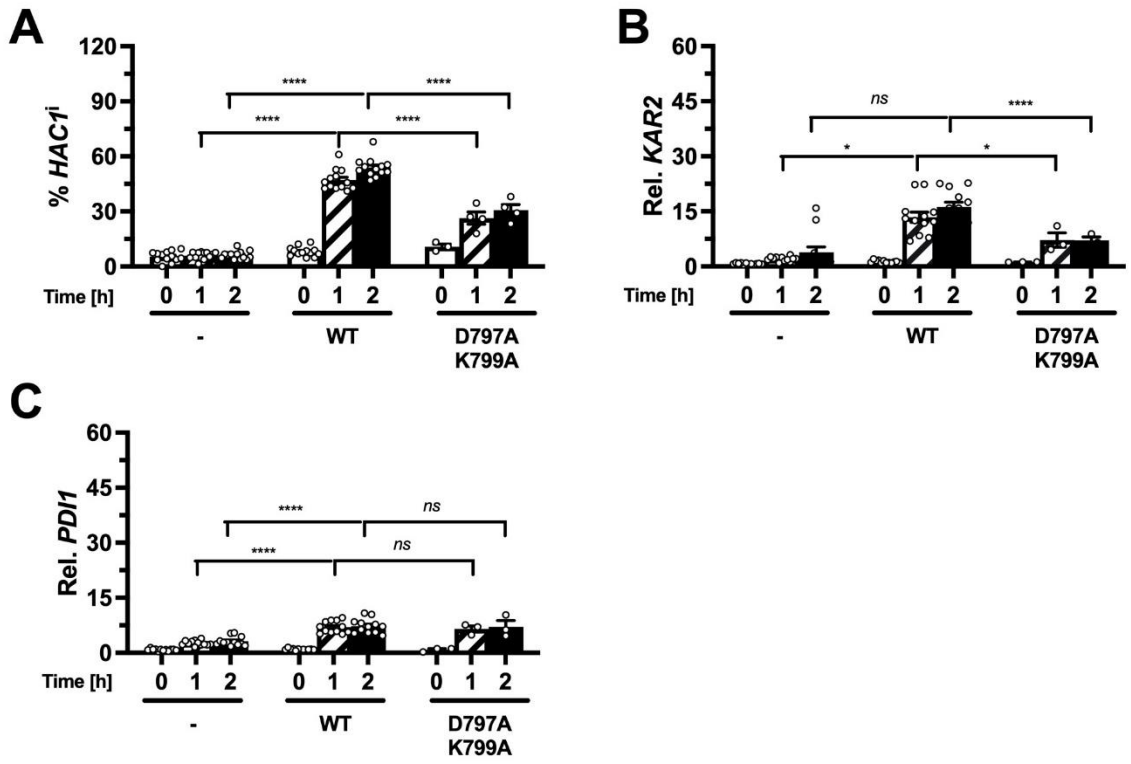

Figure 3.10. The D797A K799A Ire1 affect the *HAC1* and *KAR2* mRNAs differently compared to the WT under ER stress.

The percentage of *HAC1*^{i} mRNA (A), induction of *KAR2* mRNAs (B), and induction of *PDI1* mRNAs (C), are presented. The data presented in the graphs for D797A K799A were obtained by calculating the average and standard error from three clones (n=3). However, for the *IRE1* deletion strain and WT strain, the data were obtained from four biological repeats of three clones, resulting in a total sample size of n=12. Statistical analysis was performed using an ordinary two-way ANOVA with Tukey's correction for multiple comparisons. The stars on the graph indicate the calculated p-values. The p values are for the comparison of WT Ire1 to D797A K799A Ire1 and to strains lacking Ire1.

3.4.2 Rescue of defective D797A mutant by coupling magnesium coordinating loop mutants N802A and D828A in Ire1

In protein kinase domains, two Mg^{2+} ions are typically present and play critical roles in catalytic activity. The first Mg^{2+} ion ($Mg_1{}^{2+}$) coordinates with the carboxylate of D828 on the Mg^{2+} binding loop, neutralising the negative charges on the γ phosphate of ATP. This coordination helps stabilize the ATP molecule and facilitates the transfer of the γ phosphate to substrates. The second Mg^{2+} ion ($Mg_2{}^{2+}$) is coordinated by the amido group of N802 on the catalytic loop and the carboxylate of D828, further stabilising the negative charges formed during the breakage of the bond between the oxygen atom bridging the β and γ phosphates. Together, these Mg^{2+} ions contribute to the proper functioning of the protein kinase domain.

Building upon the findings in chapter 3.4.1, where the K799A mutation restored the activity of the defective D797A Ire1 mutant, I hypothesised that mutations affecting the residues involved in coordinating Mg^{2+} ions, such as D828A and N802A, may exhibit similar effects. This is due to their involvement in contacting the phosphates of ATP/ADP through Mg^{2+} ions. To test this hypothesis and evaluate the contribution of D828A and N802A Ire1 mutants in restoring RNase activity, I conducted Northern blot analysis.

To investigate the role of D828A and N802A in control of RNase activity and initiation of *HAC1* splicing by Ire1, alleles coding for WT and other mutants such as D828A Ire1 were introduced into a strain deleted for *IRE1*. After growth to mid-exponential growth phase, ER stress was induced by adding 2 mM DTT to cultures. RNA was extracted before addition of DTT and 1 and 2 h after addition of DTT and analysed by Northern blotting with probes against *HAC1*, *KAR2*, *PDI1* mRNAs and normalised to the loading control, pC4/2 (Figs 3.1 and 3.11).

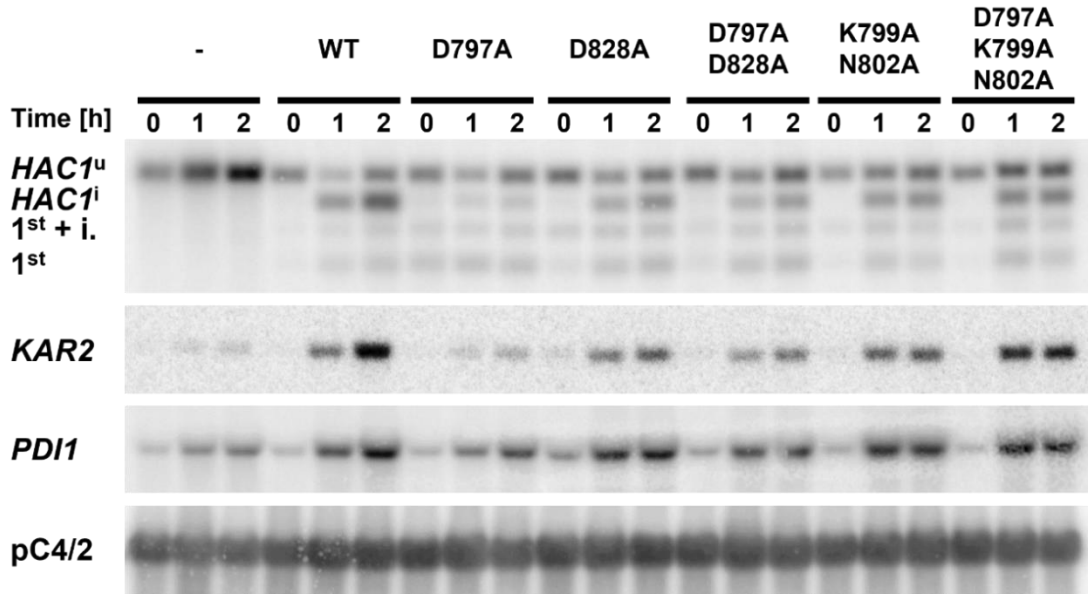

Figure 3.11. Northern Blots of IRE1 mutants: analysis of gene expression for *HAC1, KAR2, PDI1,* and loading control pC4/2.

Northern blots for *HAC1*, *KAR2*, *PDI1*, and the loading control pC4/2 on RNA extracted from *ire1*Δ strains carrying and expressing the indicated *IRE1* mutants from YCplac33 or empty vector (-). Cells in the mid-exponential-growth-phase were treated with 2 mM DTT for the indicated times. Abbreviations: *HAC1*^{u}, unspliced *HAC1* mRNA; *HAC1*^{i}, spliced *HAC1* mRNA; 1st + i., 1st exon of *HAC1*^{u} mRNA + the intron; 1st, 1st exon of *HAC1*^{u} mRNA.

3.4.2.1 Investigating intragenic suppression and restoration of RNase Activity: D828A Ire1 Rescues D797A Ire1

In Chapter 3.2, it was found that the D797A mutation significantly impaired RNase activity and resulted in decreased *HAC1* splicing efficiency. Building upon these previous findings, here I focus on examining the impact of introducing the D828A mutation into the D797A mutant on *HAC1* splicing efficiency.

Interestingly, the introduction of the D828A mutation into the D797A mutant resulted in the restoration of RNase activity. This restoration was evidenced by increased levels of *HAC1* mRNA and the induction of *PDI1* and *KAR2* mRNAs (Figs. 3.12 A, 3.12 B, and 3.12 C). Notably, the percentage of *HAC1*^{i} mRNA was higher in cells expressing the D797A D828A Ire1 mutant at 1 and 2 h after exposure to 2 mM DTT compared to cells expressing the D797A Ire1 mutant (Fig 3.12 A). Furthermore, following the induction of ER stress with 2 mM DTT at 1 and 2 h, the levels of *KAR2* and *PDI1* mRNAs were increased in D797A

D828A Ire1 mutants compared to cells expressing the D797A Ire1 mutant (Figs. 3.12 B and 3.12 C).

These findings clearly indicate that the introduction of the D828A mutation into the D797A mutant rescues the impaired RNase activity, resulting in restored *HAC1* splicing efficiency.

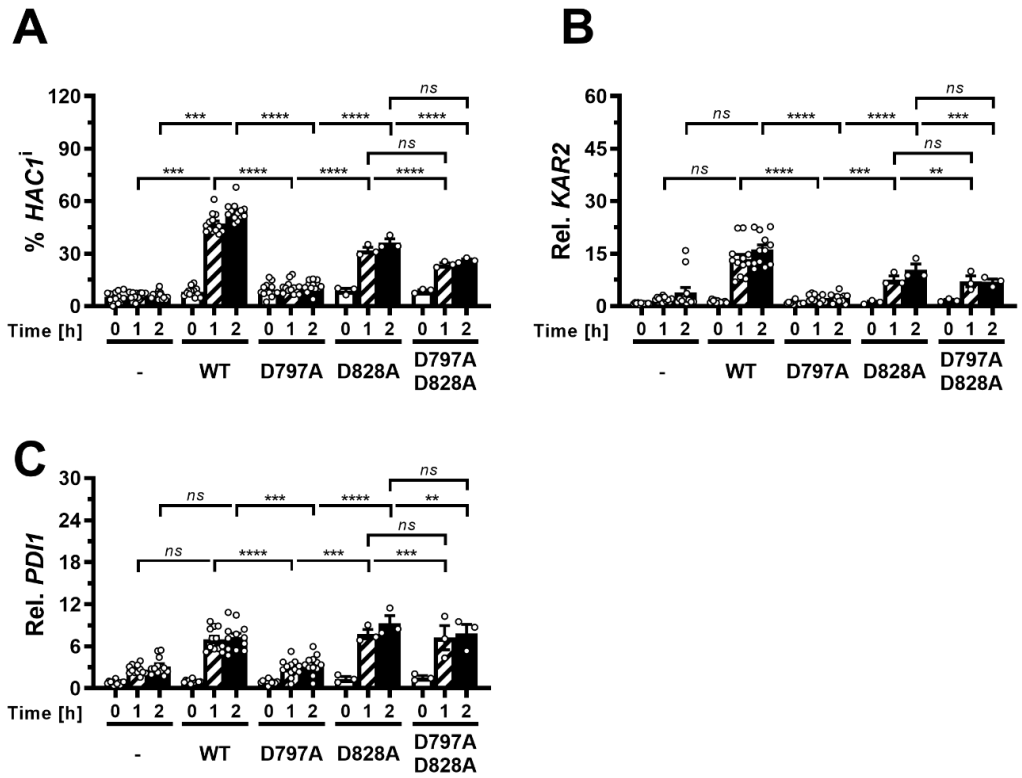

Figure 3.12. D828A Ire1 rescues D797A defective mutants and restores RNase Activity.

The graph presents data for various parameters, including (A) the percentage of *HAC1*^{i} mRNA, (B) induction of *KAR2* mRNAs, and (C) induction of *PDI1* mRNAs. The bars represent the standard errors. The data presented in the graphs were obtained by calculating the average and standard error from three clones for each of the mutant strains (n=3). However, for the *IRE1* deletion strain, WT strain, and D797A strain, the data were obtained from four biological repeats of three clones, resulting in a total sample size of n=12. Statistical analyses were conducted using an ordinary two-way ANOVA with Tukey's correction for multiple comparisons. The stars indicate the ranges of p-values that were calculated. The p values are for the comparison of D797A Ire1 to WT, D828A, D797A D828A Ire1 and to strains lacking Ire1.

3.4.2.2 Investigating intragenic suppression and restoration of RNase Activity: N802A Ire1 Rescues D797A Ire1

This investigation, building upon the findings of previous chapters (3.4.1 and 3.4.2.1), focuses on studying the effects of introducing the N802A mutation into the D797A mutant. The aim is to determine whether the N802A mutation can restore the impaired RNase activity observed in the D797A mutant. Previous chapters have demonstrated that introducing the K799A and D828A mutations into the D797A mutant can restore RNase activity and rescue the functional impairment.

By conducting this investigation, I aim to examine whether the introduction of the N802A mutation can also rescue the impaired RNase activity and restore the functionality of the D797A mutant. The focus will be on evaluating the levels of *HAC1* mRNA, *PDI1* mRNA, and *KAR2* mRNA to assess the efficiency of *HAC1* splicing.

The results indicate that introducing the N802A mutation into the D797A mutant leads to a restoration of RNase activity. Specifically, after a 2 h treatment with DTT, the percentage of $HAC1^{i}$ mRNA reached 31.7% ± 2.2% in cells expressing the D797A N802A Ire1 mutant, while it is remaining at 12.7 % ± 1.0 % in cells expressing D797A Ire1. These findings highlight the RNase activity is restored to the D797A mutant when combined with another mutation, such as D797A N802A Ire1.

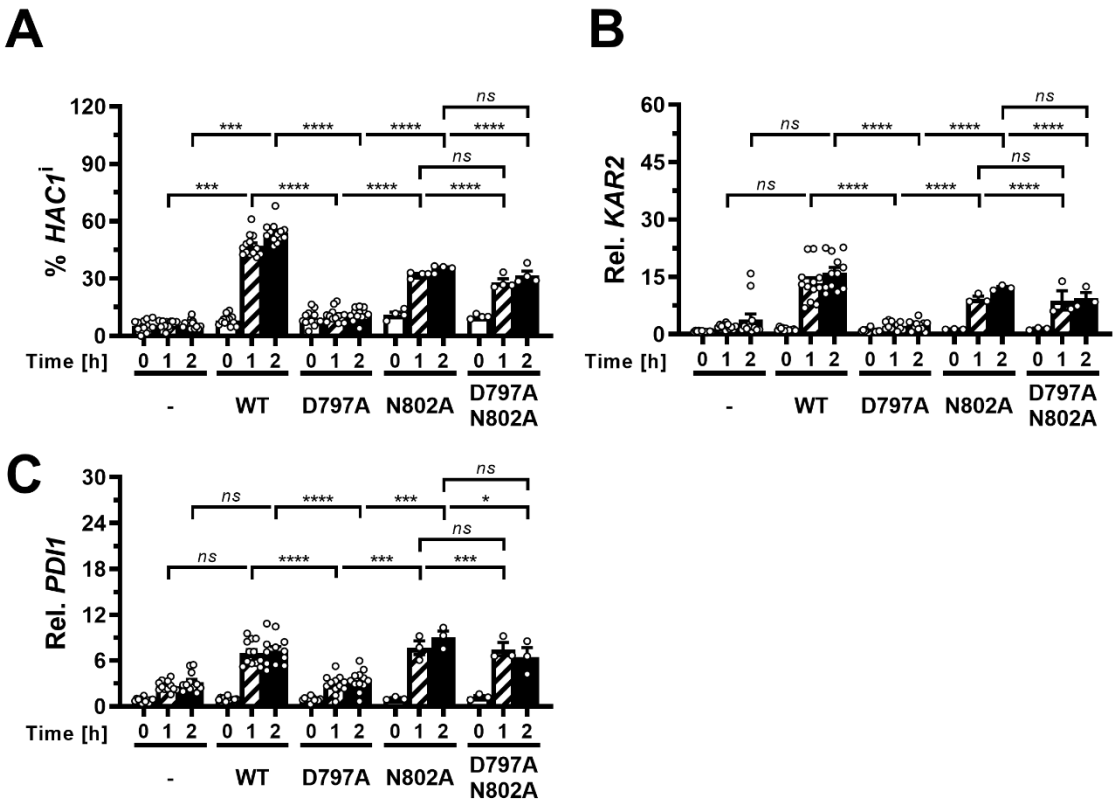

Figure 3.13. Rescue of D797A defective mutants and restoration of RNase Activity by N802A Ire1 mutant.

Various parameters were examined, including (A) the percentage of *HAC1*^{i} mRNA, (B) induction of *KAR2* mRNAs, and (C) induction of *PDI1* mRNAs. The bars on the graph represent the standard errors. The data presented in the graphs were obtained by calculating the average and standard error from three clones for each of the mutant strains (n=3). However, for the *IRE1* deletion strain, WT strain, and D797A strain, the data were obtained from four biological repeats of three clones, resulting in a total sample size of n=12. Statistical analysis was performed using an ordinary two-way ANOVA with Tukey's correction for multiple comparisons. The stars on the graph indicate the ranges of p-values that were calculated. The p values are for the comparison of D797A Ire1 to WT, N802A, D797A N802A Ire1 and to strains lacking Ire1.

3.5 Intragenic suppression by a double or triple mutation increases *HAC1* splicing after induction of ER stress

To investigate the potential enhancement of *HAC1* splicing and the induction of *KAR2* and *PDI1* mRNAs in the D797A mutant, a series of experiments was conducted using Northern blot analysis. As discussed in the previous chapter (3.4), specific single point mutations, including K799A, N802A, and D828A, were found to restore RNase activity in the D797A mutant, leading to increased levels of *HAC1*^{i} mRNA. Additionally, the findings from chapter 3.3 revealed that combining two of these mutations, such as K799A N802A and K799A D828A, did not show significant differences in the percentage of *HAC1*^{i} mRNA, *KAR2*, and *PDI1* levels compared to the single point mutants. Furthermore, when comparing N802A D828A to N802A or D828A alone, no significant differences were observed. These observations further support the hypothesis that double mutations, including K799A N802A, K799A D828A, and N802A D828A, might have the potential to restore *HAC1* splicing in the D797A mutant. To test this hypothesis, a set of comparisons was conducted, as outlined below:

a) D797A to D797A K799A N802A

b) D797A to D797A K799A D828A

c) D797A to D797A N802A D828A

d) D797A to D797A K799A N802A D828A

To achieve this, different alleles, including the WT and the double or triple mutants, were introduced into a strain deleted for *IRE1*. After growth to mid-exponential growth phase, ER stress was induced by adding 2 mM DTT to cultures. RNA was extracted before addition of DTT and 1 and 2 h after addition of DTT and analysed by Northern blotting with probes against *HAC1*, *KAR2*, *PDI1* mRNAs and normalised to the loading control, pC4/2 (Figs 3.14 and 3.15).

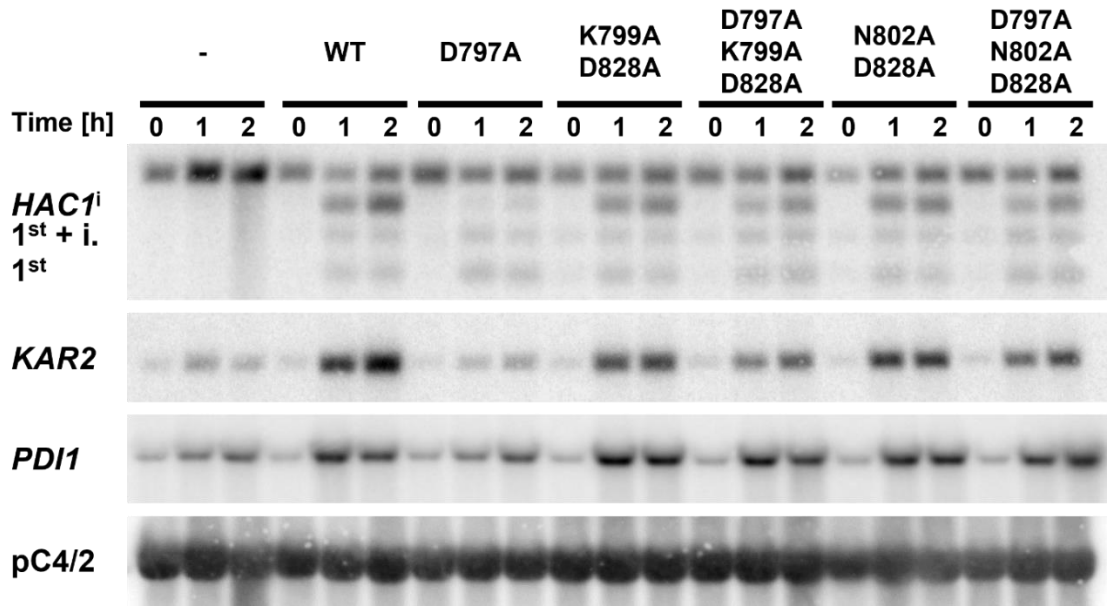

Figure 3.14. Northern Blots of IRE1 mutants: analysis of gene expression for *HAC1, KAR2, PDI1*, and loading control pC4/2.

Northern blots for *HAC1*, *KAR2*, *PDI1*, and the loading control pC4/2 on RNA extracted from *ire1*Δ strains carrying and expressing the indicated *IRE1* mutants from YCplac33 or empty vector (-). Cells in the mid-exponential-growth-phase were treated with 2 mM DTT for the indicated times. Abbreviations: H*AC1*^{u}, unspliced *HAC1* mRNA; *HAC1*^{i}, spliced *HAC1* mRNA; 1st + i., 1st exon of *HAC1*^{u} mRNA + the intron; 1st, 1st exon of *HAC1*^{u} mRNA.

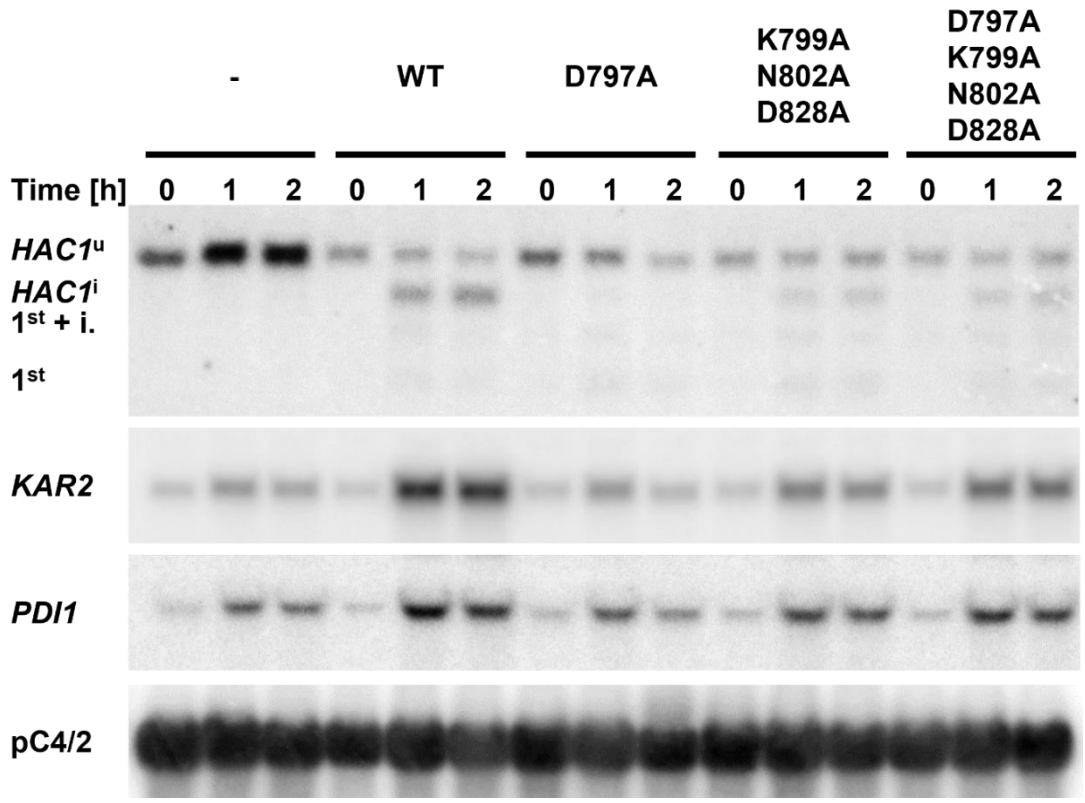

Figure 3.15. Northern Blots of IRE1 mutants: analysis of gene expression for *HAC1, KAR2, PDI1,* and loading control pC4/2.

Northern blots for *HAC1*, *KAR2*, *PDI1*, and the loading control pC4/2 on RNA extracted from *ire1*Δ strains carrying and expressing the indicated *IRE1* mutants from YCplac33 or empty vector (-). Cells in the mid-exponential-growth-phase were treated with 2 mM DTT for the indicated times. Abbreviations: H*AC1*^{u}, unspliced *HAC1* mRNA; *HAC1*^{i}, spliced *HAC1* mRNA; 1st + i., 1st exon of *HAC1*^{u} mRNA + the intron; 1st, 1st exon of *HAC1*^{u} mRNA.

The combination of the K799A N802A mutations had no effect on *HAC1* splicing, induction compared to the single mutants K799A or N802A Ire1 (Figs. 3.6 and 3.8). However, a significant increase was observed in the percentage of *HAC1*^{i} mRNA, *KAR2* and *PDI1* mRNAs levels when compared to D797A Ire1 (Fig 3.16 A, 3.16 B and 3.16 C). When the D797A mutant was combined with the K799A N802A mutation, the RNase activity was restored. These findings indicate that the introduction of the K799A N802A mutation restores RNase activity to D797A.

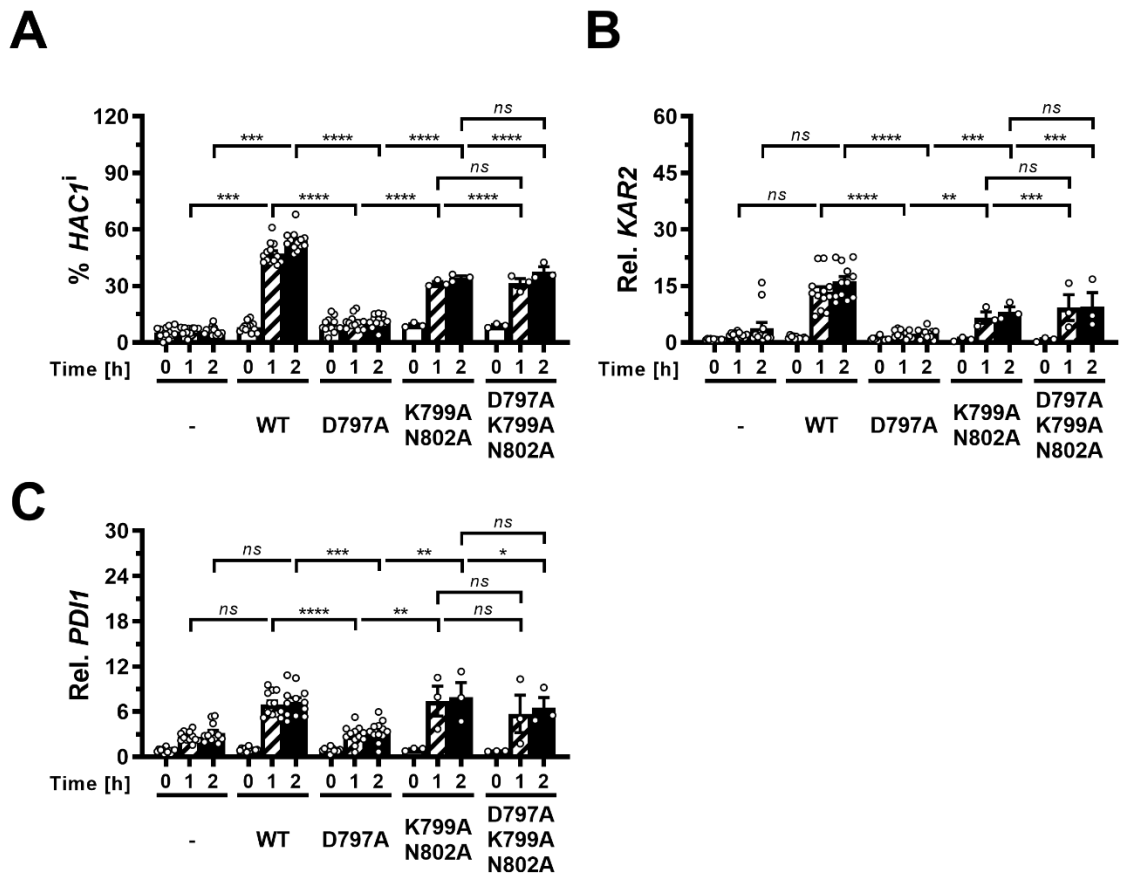

Figure 3.16. The K799A N802A Ire1 mutant rescues D797A defective mutants.
Various parameters, including (A) the percentage of *HAC1*^{i} mRNA, (B) induction of *KAR2* mRNAs, and (C) induction of *PDI1* mRNAs. The bars represent the standard errors. The data presented in the graphs were obtained by calculating the average and standard error from three clones for each of the mutant strains (n=3). However, for the *IRE1* deletion strain, WT strain, and D797A strain, the data were obtained from four biological repeats of three clones, resulting in a total sample size of n=12. Statistical analyses were conducted using an ordinary two-way ANOVA with Tukey's correction for multiple comparisons. The stars indicate the ranges of p-values that were calculated. The p values are for the comparison of D797A Ire1 to WT, K799A N802A, D797A K799A N802A Ire1 and to strains lacking Ire1.

Additionally, intragenic suppression was investigated in other multiple mutants, including K799A D828A, to examine any differences in RNase activity. The combination of the K799A D828A mutations had no effect on *HAC1* splicing compared to the single mutants K799A Ire1 or D828A (Figs. 3.6 and 3.7). However, a significant increase was observed in the percentage of *HAC1*^{i} mRNA, *KAR2* and *PDI1* mRNAs levels when compared to D797A Ire1 (Fig 3.17 A, 3.17 B and 3.17 C). When the K799A D828A mutation was introduced into the D797A mutant, it resulted in the restoration of RNase activity. These data suggest that even combining a double mutant such as K799A D828A with a single mutant D797A Ire1 restores RNase activity.

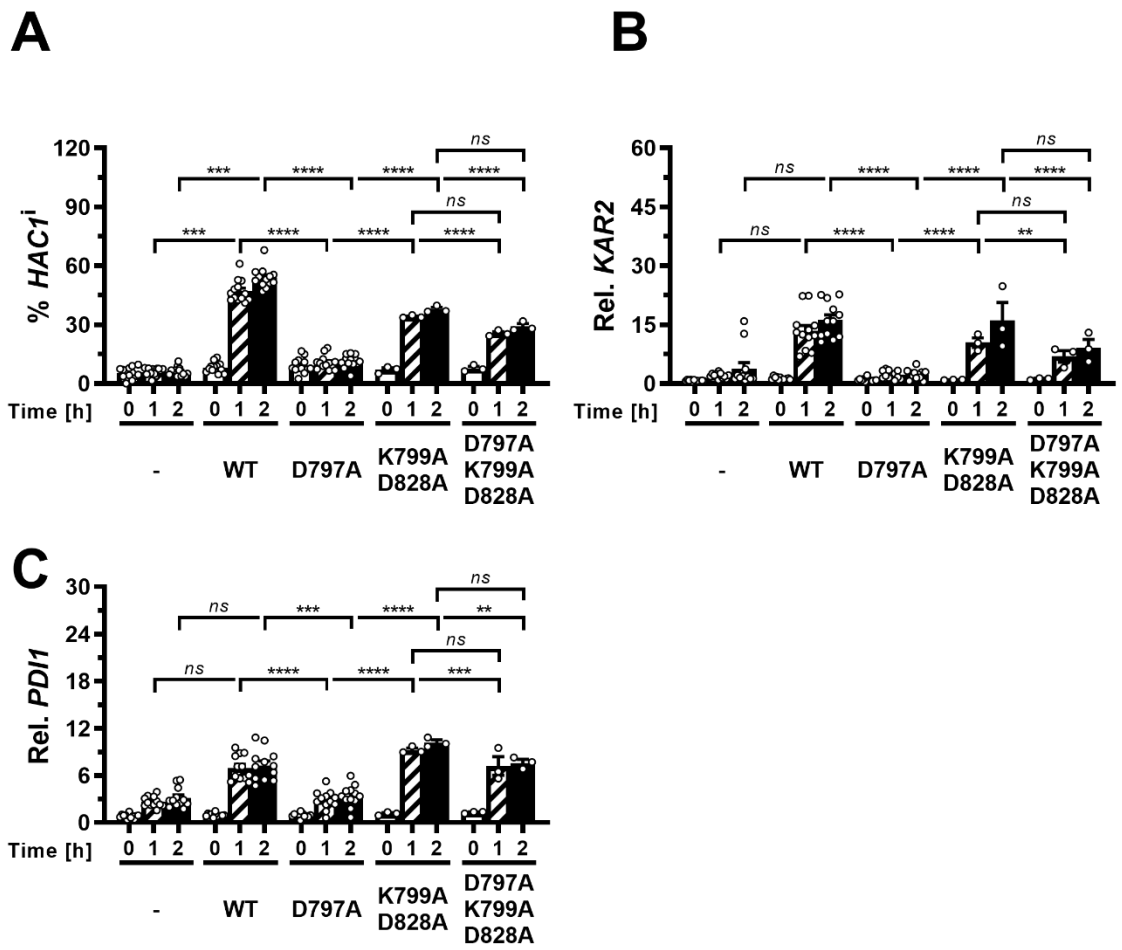

Figure 3.17. The K799A D828A Ire1 mutant rescues D797A defective mutants.
The graph compares the responses to ER stress between D797A Ire1, WT Ire1, K799A D828A, and D797A K799A D828A mutants. Various parameters were assessed, including (A) the percentage of *HAC1*^{i} mRNA, (B) induction of *KAR2* mRNAs, and (C) induction of *PDI1* mRNAs. The bars represent the standard errors. The data presented in the graphs were obtained by calculating the average and standard error from three clones for each of the mutant strains (n=3). However, for the *IRE1* deletion strain, WT strain, and D797A strain, the data were obtained from four biological repeats of three clones, resulting in a total sample size of n=12. Statistical analyses were conducted using an ordinary two-way ANOVA with Tukey's correction for multiple comparisons. The stars indicate the ranges of p-values that were calculated. The p values are for the comparison of D797A Ire1 to WT, K799A D828A, D797A K799A D828A Ire1 and to strains lacking Ire1.

The combination of the D828A and N802A mutations had no effect on *HAC1* splicing, induction of *KAR2* or *PDI1* mRNAs compared to the single mutants D828A or N802A Ire1 (Figs 3.7 and 3.8). However, a significant increase was observed when compared to D797A Ire1 (Fig 3.18 A, 3.18 B and 3.18 C). When the N802A D828A mutation was introduced into the D797A mutant, it resulted in the restoration of RNase activity. This was supported by higher levels of *HAC1* mRNA and the induction of *PDI1* and *KAR2* mRNAs (Figs 3.18 A, 3.18 B and 3.18 C). 2 h after addition of DTT to cells expressing D797A N802A D828A Ire1 the percentage of *HAC1*^{i} mRNA reached 32.8 % ± 2.3 %, while it is remaining at 11.3 % ±

0.8 % in cells expressing D797A Ire1. The results demonstrate that introduction N802A D828A Ire1 to D797A Ire1 restores RNA activity.

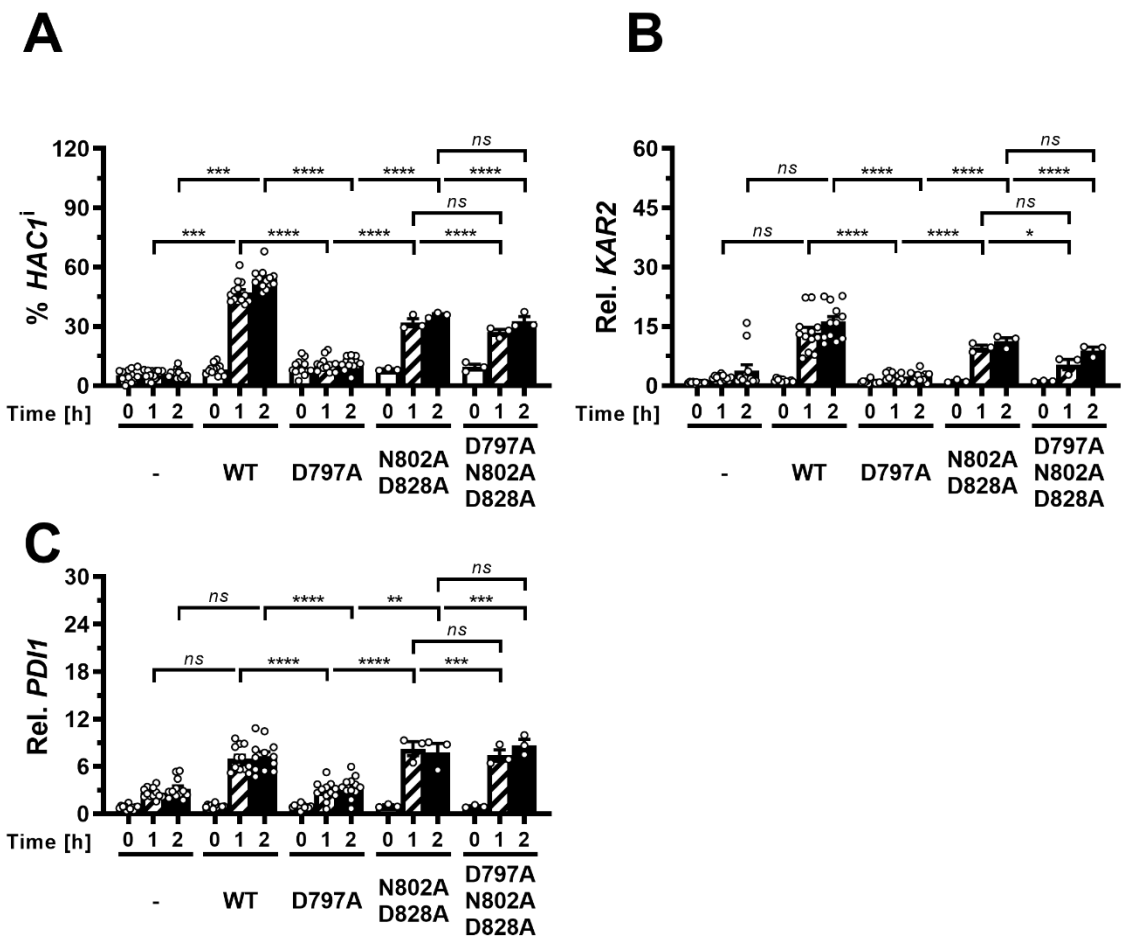

Figure 3.18. Catalytic residue mutations in the kinase domain affect RNase activity: N802A D828A Ire1 mutant rescues D797A defective mutants and restores RNase activity.
Several parameters were evaluated, including (A) the percentage of *HAC1*^{i} mRNA, (B) induction of *KAR2* mRNAs, and (C) induction of *PDI1* mRNAs. The bars represent the standard errors. The data presented in the graphs were obtained by calculating the average and standard error from three clones for each of the mutant strains (n=3). However, for the *IRE1* deletion strain, WT strain, and D797A strain, the data were obtained from four biological repeats of three clones, resulting in a total sample size of n=12. Statistical analyses were conducted using an ordinary two-way ANOVA with Tukey's correction for multiple comparisons. The stars indicate the ranges of p-values that were calculated. The p values are for the comparison of D797A Ire1 to WT, N802A D828A, D797A N802A D828A Ire1 and to strains lacking Ire1.

Here, I investigated intragenic suppression in the K799A N802A D828A mutant to determine if the triple mutant can restore RNase activity in the D797A Ire1. The introduction of the K799A N802A D828A mutation into the D797A mutant indeed resulted in the restoration of RNase activity, as evidenced by the increased levels of *HAC1*^{i} mRNA (Fig 3.19 A). After 2 h of DTT induction, the percentage of *HAC1*^{i} mRNA reached 31.8 % ± 2.4 % in cells expressing D797A K799A N802A D828A Ire1, while it remained at 7.7% ± 2.1% in cells expressing D797A Ire1. These findings suggest that the combination of multiple mutants, such as K799A N802A D828A, with the D797A mutant can effectively restore RNase activity.

To further assess the restoration of RNase activity in the K799A N802A D828A mutant, I compared the percentage of *HAC1*^{i}, *KAR2* and *PDI1* mRNA levels to that of WT Ire1. I observed a significant decrease in *KAR2* mRNA levels after 2 h of ER stress induction in cells expressing K799A N802A D828A Ire1 compared to WT Ire1 (Fig 3.20 B). Similarly, in the D797A K799A N802A D828A Ire1 mutant, *KAR2* mRNA levels were decreased compared to cells expressing WT Ire1 (Fig 3.20 B). However, at 2 h after ER stress induction, the decrease in *PDI1* mRNA levels was not as noticeable as that observed for *KAR2* mRNA in the K799A N802A D828A Ire1 mutant. In the D797A K799A N802A D828A Ire1 mutant, *PDI1* mRNA levels decreased after 1 h of ER stress induction but remained stable after 2 h (Fig 3.20 C). These findings suggest that while the restoration of RNase activity is evident in the D797A K799A N802A D828A mutant, the impact on gene expression may vary for different target mRNAs.

In summary, combining multiple mutants, such as K799A N802A D828A, with the D797A mutant restores RNase activity. The increased levels of *HAC1*^{i} mRNA indicate successful intragenic suppression. However, the extent of restoration compared to WT Ire1 varies for different target mRNAs, as demonstrated by the differential effects on *KAR2* and *PDI1* mRNA levels.

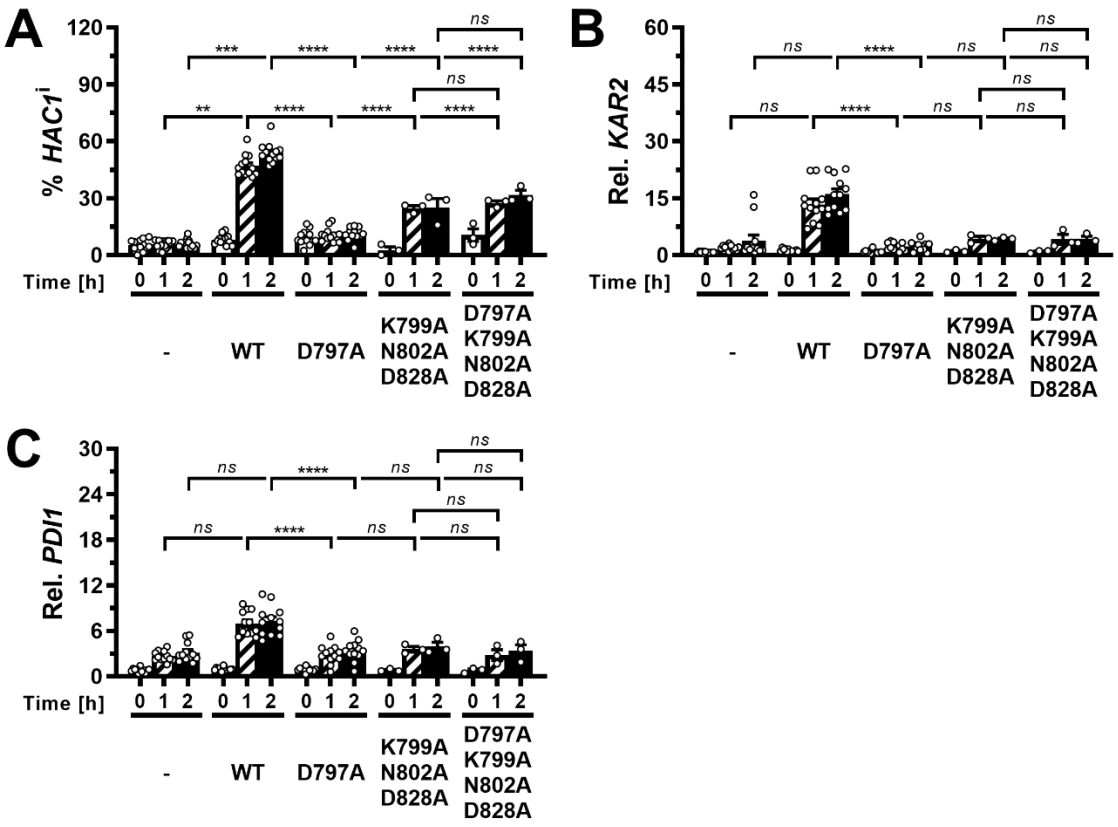

Figure 3.19. Triple mutations of K799, N802, and D828 enhance *HAC1* splicing and rescue D797A defective mutants by intragenic suppression.

Various parameters, including (A) the percentage of *HAC1*^{i} mRNA, (B) induction of *KAR2* mRNAs, and (C) induction of *PDI1* mRNAs. The bars represent the standard errors. The data presented in the graphs were obtained by calculating the average and standard error from three clones for each of the mutant strains (n=3). However, for the *IRE1* deletion strain, WT strain, and D797A strain, the data were obtained from four biological repeats of three clones, resulting in a total sample size of n=12. Statistical analyses were conducted using an ordinary two-way ANOVA with Tukey's correction for multiple comparisons. The stars indicate the ranges of p-values that were calculated. The p values are for the comparison of D797A Ire1 to WT, K799A N802A D828A, D797A K799A N802A D828A Ire1 and to strains lacking Ire1.

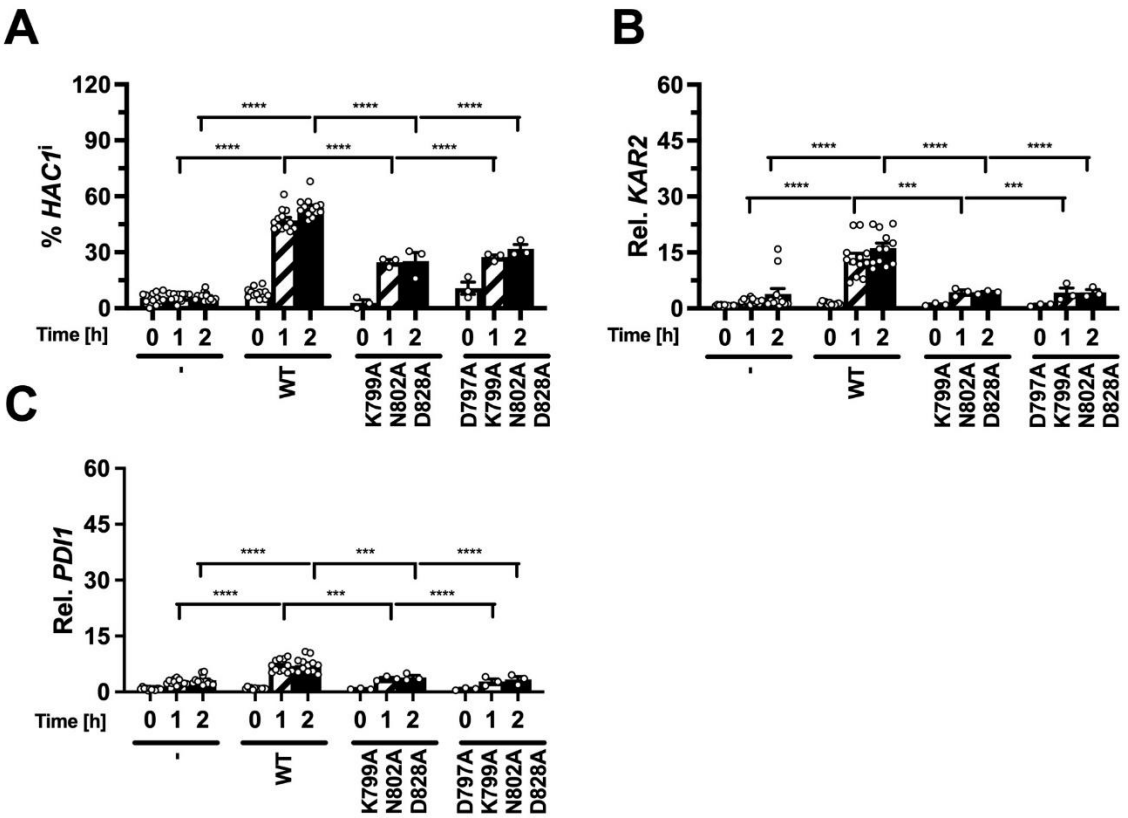

Figure 3.20. Triple mutations of K799, N802, and D828 in Ire1 compared to WT Ire1 in ER stress-induced responses.

Data for various parameters, including the percentage of *HAC1*^{i} mRNA (A), induction of *KAR2* mRNAs (B), and induction of *PDI1* mRNAs (C), are depicted. The data presented in the graphs were obtained by calculating the average and standard error from three clones for each of the mutant strains (n=3). However, for the *IRE1* deletion strain, WT strain, and D797A strain, the data were obtained from four biological repeats of three clones, resulting in a total sample size of n=12. Statistical analysis was performed using an ordinary two-way ANOVA with Tukey's correction for multiple comparisons. The stars on the graph indicate the calculated p-values. The p values are for the comparison of WT Ire1 to K799A N802A D828A, D797A K799A N802A D828A Ire1 and to strains lacking Ire1.

3.6 Discussion

3.6.1 Single protein kinase mutants K799A, D828A, and N802A, retain RNase activity and ability to splice *HAC1* mRNA

Previous studies have shown that mutations in conserved amino acids within the kinase catalytic core, including K702 in yeast Ire1 (Mori et al., 1993) and K599 in human IRE1α (Tirasophon et al., 1998), as well as D797 (Chawla et al., 2011; Lee et al., 2008; Mannan et al., 2013), D828 (Mannan et al., 2013; Mori et al., 1993), and autophosphorylation sites in the a-loop (Chawla et al., 2011; Lee et al., 2008; Mannan et al., 2013; Shamu & Walter, 1996), have been found to result in the loss of protein kinase and RNase activities. Mutations of conserved residues in the RNase domain have been found to eliminate RNase activity but leave the protein kinase activities of yeast and human Ire1 intact, indicating that RNase activity is dispensable for kinase activity (Mannan et al., 2013; Tirasophon et al., 2000). Moreover, the findings of previous studies (Shamu et al., 1996; Lee et al., 2008; Chawla et al., 2011; Mannan et al., 2013; Armstrong et al., 2017), which investigated phosphorylation site mutants, suggest that phosphorylation of the a-loop by the kinase activity of Ire1 necessary for nucleotide binding, oligomerisation, or RNase activity. This study aimed to investigate the role of specific mutations in the catalytic site K799A, N802A, and D828A of Ire1 in splicing *HAC1* mRNA. Northern blot analyses were performed to compare the splicing of *HAC1* mRNA between the mutants and the WT Ire1. Surprisingly, the mutations in the catalytic sites K799, N802, and D828 did not affect the RNase activity of Ire1. It is possible that these mutants may retain some level of protein kinase activity, which could contribute to their functionality despite the observed mutations in the catalytic sites K799, N802, and D828. Additionally, in *vivo*, Ire1 could potentially serve as a substrate for other protein kinases, which may compensate for any deficiency in its own protein kinase activity. These alternative mechanisms and potential interactions with other protein kinases could bypass the need for phosphorylation and contribute to the observed splicing of *HAC1* mRNA by Ire1. The results, as presented in Figures 3.3, 3.6 and 3.9 show no statistically significant differences in the levels of spliced *HAC1* mRNA between the K799A Ire1 mutant and WT Ire1, indicating similar behaviour. However, notable significant decrease was observed in the N802A and D828A Ire1 mutants compared to WT Ire1. The decrease in splicing capability may be attributed to the fact that the mutation of D828 or N802 interferes with Mg^{2+} binding, which subsequently affects adenine nucleotide binding (Schroeder unpublish). This suggests

that the altered mutants disrupt the normal coordination of Mg^{2+} ions within the protein, which can have functional consequences. Despite being located in the catalytic site of Ire1, the K799A, N802A, and D828A mutants do not disrupt RNase activity. The fact that mutations in these amino acids do not affect RNase activity indicates that their function is different from the previously characterised phosphorylation-dependent mechanisms. One possible interpretation is that these mutants in the catalytic site act as inhibitory elements, regulating RNase activity in the absence of mutations. By introducing the K799A, N802A, and D828A mutations, these inhibitory elements are removed, resulting in the retention of splicing capability. While the precise mechanisms underlying this phosphorylation-independent splicing activation remain unclear, several possibilities can be considered. It is conceivable that these mutants retain a minimal level of protein kinase activity or that other cellular protein kinases can phosphorylate Ire1, contributing to its RNase activity. These hypotheses could be investigated by introducing mutations in the phosphoacceptor sites within the activation loop, such as K799A D836A, N802A D836A, or D828A D836A, as suggested in previous study (Armstrong et al., 2017). The discovery of these K799A, N802A, and D828A mutants provides evidence for additional pathways or factors that can drive splicing activation independently of phosphorylation. The presence of the K799A, N802A, and D828A mutants in the catalytic site of Ire1 provides evidence for additional pathways or factors that can drive splicing activation independently of phosphorylation. These mutations are anticipated to decrease nucleotide binding, particularly to the triphosphate group of ATP, and result in reduced protein kinase activity. By removing inhibitory elements from the active site of Ire1, the altered conformation caused by these mutations may impact ATP binding and hydrolysis, potentially influencing the RNase activity of Ire1. This, in turn, facilitates the cleavage of RNA substrates necessary for *HAC1* mRNA splicing. The results suggest that specific mutations in the catalytic site K799A, N802A, and D828A of Ire1 do not affect RNase activity of Ire1. However, these mutations retain the ability to splice *HAC1* mRNA. It is possible that these mutants bypass phosphorylation and may retain some level of protein kinase activity, indicating the existence of alternative mechanisms for splicing activation.

3.6.2 Characterisation of the D797A Mutant

I focus on the characterisation of the D797A mutant and explore the factors influencing its defect in *HAC1* splicing. The data presented here showed that the D797A mutation had a significant decrease in *HAC1* splicing or induction of *KAR2* and *PDI1* mRNAs when

compared to other mutants. Previous work has concluded that D797A Ire1 does not possess RNase activity in *vivo* (Chawla et al., 2011; Lee et al., 2008). However, (Chawla et al., 2011) also show bands in their Northern blots which may represent splicing intermediates. Additionally, in my own observations within cells expressing D797A Ire1 (Figs. 3.1, 3.11, 3.14, and 3.15), I noticed the presence of weak bands that corresponded to RNA molecules showing characteristics of both splicing intermediates and cleavage intermediates of *HAC1* mRNA. Although these bands were not quantified in this study, they could provide important information into the functioning of Ire1. It is worth mentioning that these bands appear qualitatively increased in D797A, but are close to the background signal, making their quantification challenging. Their presence suggests that the defect in the D797A mutant may not arise solely from a deficiency in RNase activity, but rather from a potential impairment in the ligation process of the exons (Fig. 3.21). While these intermediates indicate incomplete splicing of *HAC1* mRNA, they may not have a significant impact on the activation of the UPR pathway. Therefore, measuring only these intermediates may not provide a complete understanding of the UPR response to ER stress. According to the data obtained in this study, inducing ER stress with 2 mM DTT resulted in a low level of *HAC1* splicing (about 10 %) in cells expressing D797A Ire1 after 2 h. These findings were consistent with previous reports (Chawla et al., 2011; Lee et al., 2008). Notably, the D797A mutant displayed an increase in cleavage intermediates, including 1^{st} exon + intron and 1^{st} exon (Figs. 3.1, 3.11, 3.14 and 3.15). This suggests that the D797A mutant may have significant RNase activity *in vivo*. This finding raises the intriguing possibility that the D797A mutant may still retain significant RNase activity *in vivo*, despite its apparent defect in *HAC1* splicing. To reconcile this finding, I can explore potential explanations for the observed discrepancy. One possible explanation could be that the defect in *HAC1* splicing seen in the D797A mutant is not solely attributed to the lack of RNase activity, but rather involves other factors or mechanisms that influence the splicing process. For instance, it is conceivable that the D797A mutation affects the interaction between Ire1 and other splicing factors or impairs the proper recognition and binding of *HAC1* mRNA substrates. Alternatively, there may be compensatory mechanisms or redundant pathways that partially rescue the splicing defect in the absence of full RNase activity. Furthermore, it is worth considering the possibility that the weak bands representing cleavage intermediates observed in the D797A mutant could be indicative of an alternative splicing pathway or non-canonical processing of *HAC1* mRNA. However, it seems unlikely because if this were the case, we would also expect to observe these intermediates in the *IRE1* deletion strain. As their presence is not observed in the deletion strain, it suggests that

the formation of these intermediates is dependent on the presence of Ire1.This could suggest the involvement of additional endoribonucleases or alternative RNA processing machinery that contribute to the overall splicing outcome in the presence of the D797A mutation. The findings suggest that the defect in *HAC1* splicing may not be solely attributed to the lack of RNase activity but could involve other factors or alternative splicing pathways that contribute to the overall splicing outcome in the presence of the D797A mutation.

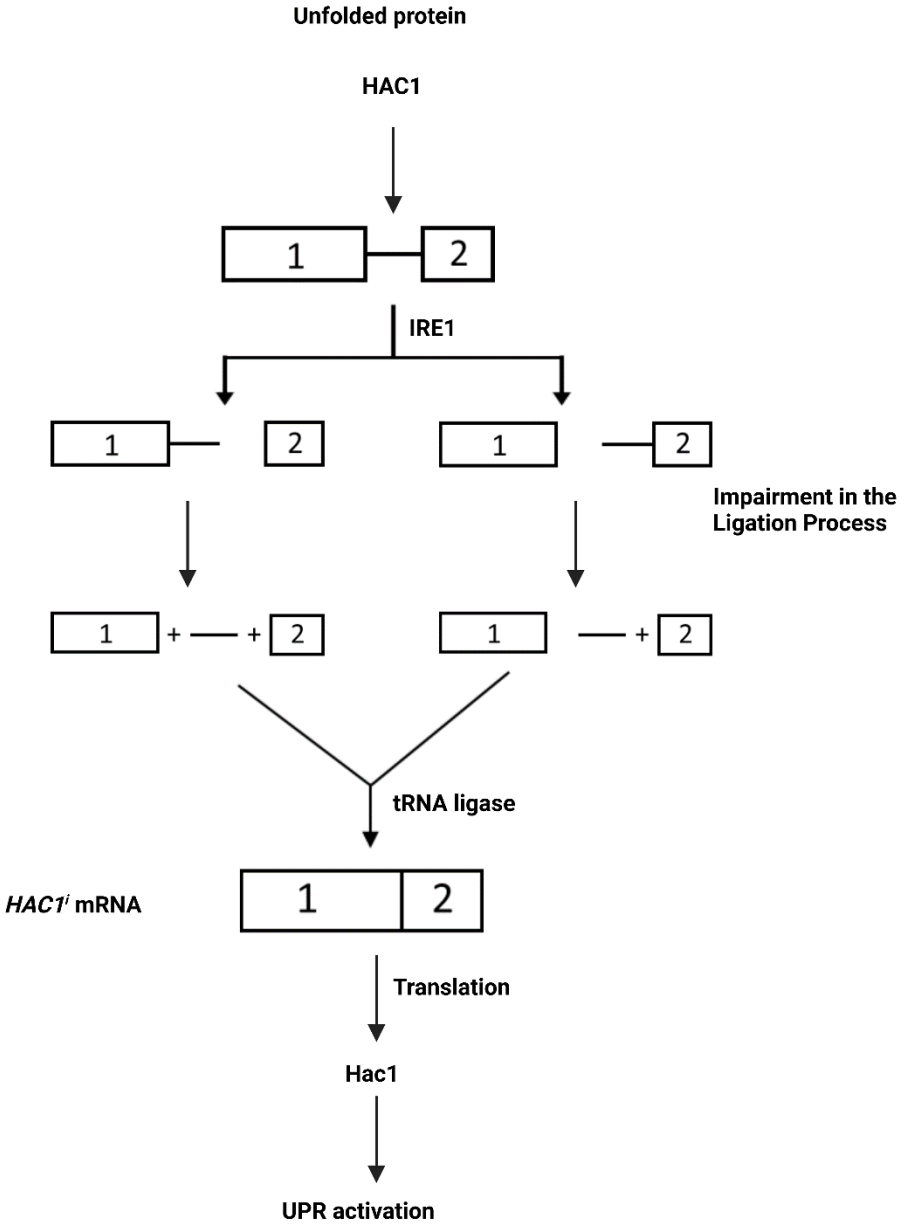

Figure 3.21. Diagram illustrating the presence of weak bands in the D797A variant of *HAC1* mRNA.
These weak bands suggest an impairment in the ligation process of exons. The two exons of *HAC1* mRNA are labeled 1 and 2 with an intron represented by a line between them.

3.6.3 Rescue of RNase activity defect in the D797A mutant by other protein kinase mutations

I investigate the phenomenon of intragenic suppression by combining the catalytic aspartate deficient D797A Ire1 mutant with other mutants and its impact on *HAC1* splicing and the induction of *KAR2* and *PDI1* mRNAs. Intragenic suppression refers to the phenomenon where the introduction of a second mutation compensates for the defective phenotype caused by the first mutation. Here, I assessed the RNase activity of these combination mutants using a Northern blot to elucidate the effects on *HAC1* splicing and gene induction. The results showed that all combinations of mutations that included to the catalytic aspartate-deficient D797A-Ire1 mutant restored *HAC1* splicing and some of the induction of *KAR2* and *PDI1* mRNAs. Furthermore, previous research has demonstrated that the combination of D797N K799N mutations inactivates Ire1 protein kinase activity while exhibiting significant RNase activity (Chawla et al., 2011; Rubio et al., 2011). Northern blots show increased levels of cleavage intermediates, and some spliced *HAC1* mRNA in cells expressing K799A Ire1 under non-stress conditions when compared to other mutants. Introduction of the K799A Ire1 mutation into D797A Ire1 resulted in an elevation of *HAC1*^{i} mRNA and induction of *PDI1* and *KAR2* mRNA (Fig 3.9), which is consistent with previous studies (Chawla et al., 2011; Rubio et al., 2011). Intragenic suppression by adding a second mutation to the defective mutant D797A Ire1 resulted in significant increases in spliced *HAC1* mRNA levels compared to strains lacking Ire1 and significant increased compared to WT, suggesting that the second mutation plays a role in RNase activation. These findings imply that the intragenic suppression observed in the presence of mutations K799, N802, and D828 signifies their involvement in regulating or exerting a negative influence on the RNase activity.

4 CHARACTERISING THE EFFECTS OF MUTATIONS ON THE INDUCTION OF AN UPRE-B-GALACTOSIDASE REPORTER

4.1 Rationale

The β-Galactosidase assay is crucial in this study as it serves to validate and confirm the RNA level data by assessing protein levels. Additionally, the assay enables the investigation of whether the observed changes in mRNA levels are mirrored at the protein level. By measuring the activation of the UPR using a UPRE-associated-β-galactosidase reporter assay, it becomes possible to assess the functional consequences of these mutants and their ability to initiate the UPR pathway. This assay will help determine if the retention of RNase activity in the absence of protein kinase activity is associated with UPR activation, thus shedding light on the potential compensatory mechanisms and the intricate relationship between phosphorylation and the activation of the RNase domain in Ire1.

β-galactosidase is an enzyme that catalyses the hydrolysis of β-galactosides. It is commonly used in molecular biology, particularly in gene expression studies, to identify cells in which a specific gene has been activated. The reporter is designed with the *lacZ* gene utilising the UPRE region from the *KAR2* gene. This UPRE region is inserted upstream of a crippled *CYC1* promoter that lacks an upstream activating sequence (UAS) *KAR2* is expressed as ER stress activates the UPR because of the UPRE in its promoter, which also causes *lacZ* to be expressed. The β-galactosidase generated cleaves ONPG to yield galactose (colourless) and *o*-nitrophenol (yellow), providing for a measure of colour change (measured at 419 nm) indicative of reporter activity. For additional details see the materials and methods (chapter 2.2.11). To activate expression, the UPR-associated gene *KAR2* needs mature *HAC1* mRNA to be translated (Kohno et al., 1993; Mori et al., 1992). Therefore, the activation of the RNase domain is necessary for splicing *HAC1* mRNA to produce the mature product. The strength of the colour change in the experiment is correlated with the strength of induction of UPRE-associated genes, indicating stronger RNase and UPR activation. Northern blots show both spliced and unspliced *HAC1* mRNA, indicating that the mRNA is present in the sample (Figs. 3.1, 3,7, 3.12 and 3.13). The presence of the mRNA is an indication of ER stress, as the UPR uses these proteins to cope with stress. The global investigation of protein expression has demonstrated that the concentration of many proteins within a cell cannot be accurately predicted based solely on mRNA levels (Ghaemmaghami et al., 2003). This suggests that the relationship between mRNA levels and protein expression is more complex and may be

influenced by additional factors such as post-transcriptional modifications, translation efficiency, and protein degradation. In this context, the β-galactosidase reporter provides a tool for directly measuring protein expression levels, allowing for the detection and characterisation of discrepancies between mRNA levels and protein abundance.

By measuring the activity of the reporter, I determine the extent of UPR protein expression that is induced by Ire1 ER stress signalling. To quantify this response, the amount of β-galactosidase produced was compared to the total amount of protein in the sample, which was determined using DC assay. This comparison allowed for the calculation of the β-galactosidase per unit of total protein, expressed in milliunits (mU) of β-galactosidase per milligram (mg) of total protein. The activity of the UPR in cells that have WT Ire1 or a strain lacking Ire1 (-) were used as reference points to compare the UPR activation in cells with different mutations. These reference cells were used to determine the level of activation of the UPR in each mutant. The data of the β-galactosidase assays were analysed by a non-parametric Scheirer-Ray-Hare test. The test was followed up by a Games-Howell post-hoc test. The Scheirer-Ray-Hare test was chosen instead of an ordinary two-way ANOVA, because the data retained unequal variances even after logarithmic transformation of the data. This chapter aims to employ the β-Galactosidase assay as a tool to examine the activity of the reporter and validate the findings derived from Northern blot analysis of Ire1 mutants. Specifically, I will focus on investigating single point mutations D797A, K799A, N802A, and D828A, along with the examination of double mutants. In addition, I carried out an in-depth examination of the protein kinase domain through a comprehensive mutational analysis. The primary objective was to explore the possibility of augmenting the β-galactosidase activity in the D797A mutant by introducing an extra point mutation within the protein kinase domain.

4.2 Characterisation of time course reporter activity for single point mutations

A time course analysis was conducted to examine the β-galactosidase activity of single point mutations (D797A, K799A, N802A, and D828A Ire1) in response to ER stress. This analysis provides insights into the kinetics, specific effects, and functional consequences of these mutations on the IRE1 pathway over time. To evaluate the activity of the reporter, 10 ml samples were collected at the start 0 h and compared with samples taken at 1 h and 2 h after the addition of 2 mM DTT. As anticipated, strains lacking Ire1 exhibited minimal UPR activation, resulting in a low β-galactosidase activity (Fig. 4.1 A). In contrast, WT cells

showed an increase in UPRE-*lacZ* activity over time, with the most significant difference observed between the 0 h sample and the 2 h sample (Fig. 4.1 B). There was no statistical difference, observed, for D797A cells, indicating that their behaviour closely resembles that of strains lacking Ire1 (Fig 4.1 C). The mutants K799A and N802A Ire1 exhibited an increase in β-galactosidase activity from 0 to 1 h, as well as from 0 to 2 h, and 1 to 2 h time points (Figs. 4.1 D and 4.1 E). In the case of D828A Ire1, there was no statistically significant difference between the 0 h and 1 h time points, but significant differences were observed between the 0 h and 2 h time points, as well as between the 1 h and 2 h time points (Fig 4.1 F). The findings suggest that different mutations in Ire1 have varying effects on the time course of β-galactosidase activity, ranging from loss of function to potential gain of function.

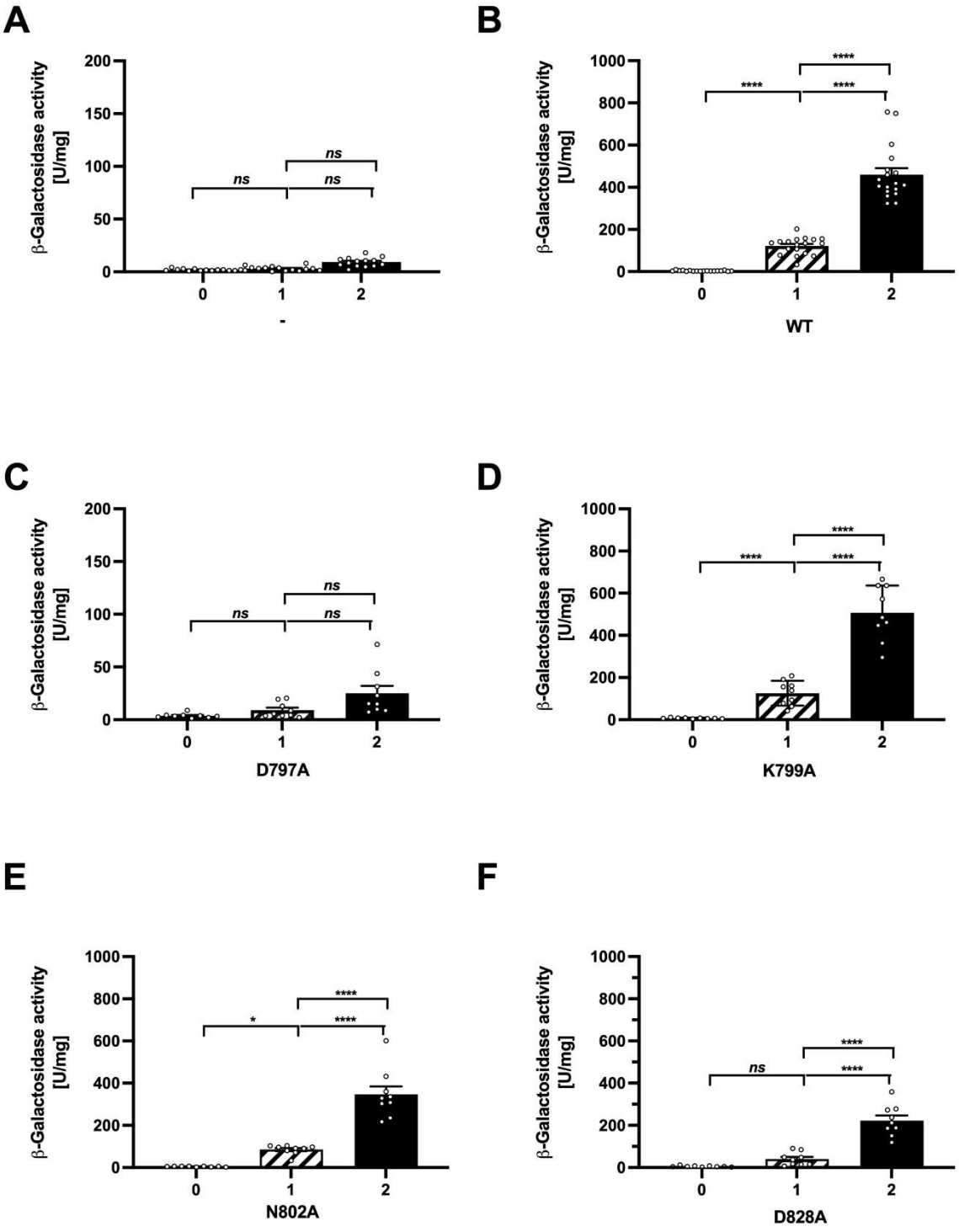

Figure 4.1. β-Galactosidase activity in single point mutations and WT Ire1 over time.

The graph presents quantified data from 2-6 biological replicates of three clones (n= 3-18) of the β-galactosidase reporter assays, demonstrating the activation ability of Ire1 mutants on the induction of the UPRE-*lacZ* reporter gene. β-Galactosidase activity is standardised to total cellular protein at 0, 1, and 2 h after inducing ER stress with 2 mM DTT in mid-exponential *Ire1* deletion cells expressing the indicated Ire1 mutants from YCplac33 or carrying the empty vector. (A) strain lacking Ire1 (-) (B) WT Ire1 (C) D797A Ire1 (D) K799A Ire1 (E) N802A Ire1 and (F) D828A Ire1. Bars represent standard errors. Games and Howell post-hoc tests on row factor (time) were used for the analysis. The stars indicate the ranges of p values that were calculated. *, $P \leq 0.05$; **, $P \leq 0.01$; ***, $P \leq 0.001$; ****, $P \leq 0.0001$.

Following that, the β-galactosidase activity of the single point mutations was investigated, comparing them to both WT Ire1 and the strain lacking Ire1, as well as assessing the differences in the reporter activity among the different mutations themselves.

At the time point 2 h after the addition of the inducer, statistically significant differences were observed when comparing the strain lacking Ire1 to both WT Ire1 and the single point mutations (Fig 4.2 A) (Table 4.1). However, no significant differences were observed at 2 h between the strain lacking Ire1and D797A Ire1 (Fig 4.2 A). Significant increases were observed at 2 h after the addition of 2 mM DTT when comparing the reporter activity of WT Ire1 to both the strain lacking Ire1 and D828A Ire1, however for K799A and N802A Ire1 showed no significant difference, indicating its similarity to WT (Fig 4.2 B). The D797A Ire1 mutant exhibited significantly lower β-galactosidase activity compared to the other mutants, resembling the low activity observed in the strain lacking Ire1 (Fig. 4.2 C). This finding suggests that the D797A mutation negatively affects the activation of the reporter, similar to the absence of Ire1. Comparing the K799A mutant to both the strain lacking Ire1 and the D797A mutant revealed a significant increase, while no significant differences were found when comparing it to WT and the N802A Ire1 mutant (Fig. 4.2 D). Furthermore, no significant difference was observed at the 2 h time point when comparing the N802A Ire1 mutant to the D828A mutant (Fig. 4.2 E). However, significant differences were identified between the D828A Ire1 mutant and WT Ire1, K799A, and D797A Ire1 mutants, suggesting distinct reporter activity profiles (Fig. 4.2 F).

The findings indicate that the D797A mutant exhibits reduced β-galactosidase activity similar to the strain lacking Ire1, while the K799A and N802A mutants show activity comparable to WT Ire1, and the D828A mutant displays distinct activity patterns, highlighting the specific effects of these mutations on reporter activation.

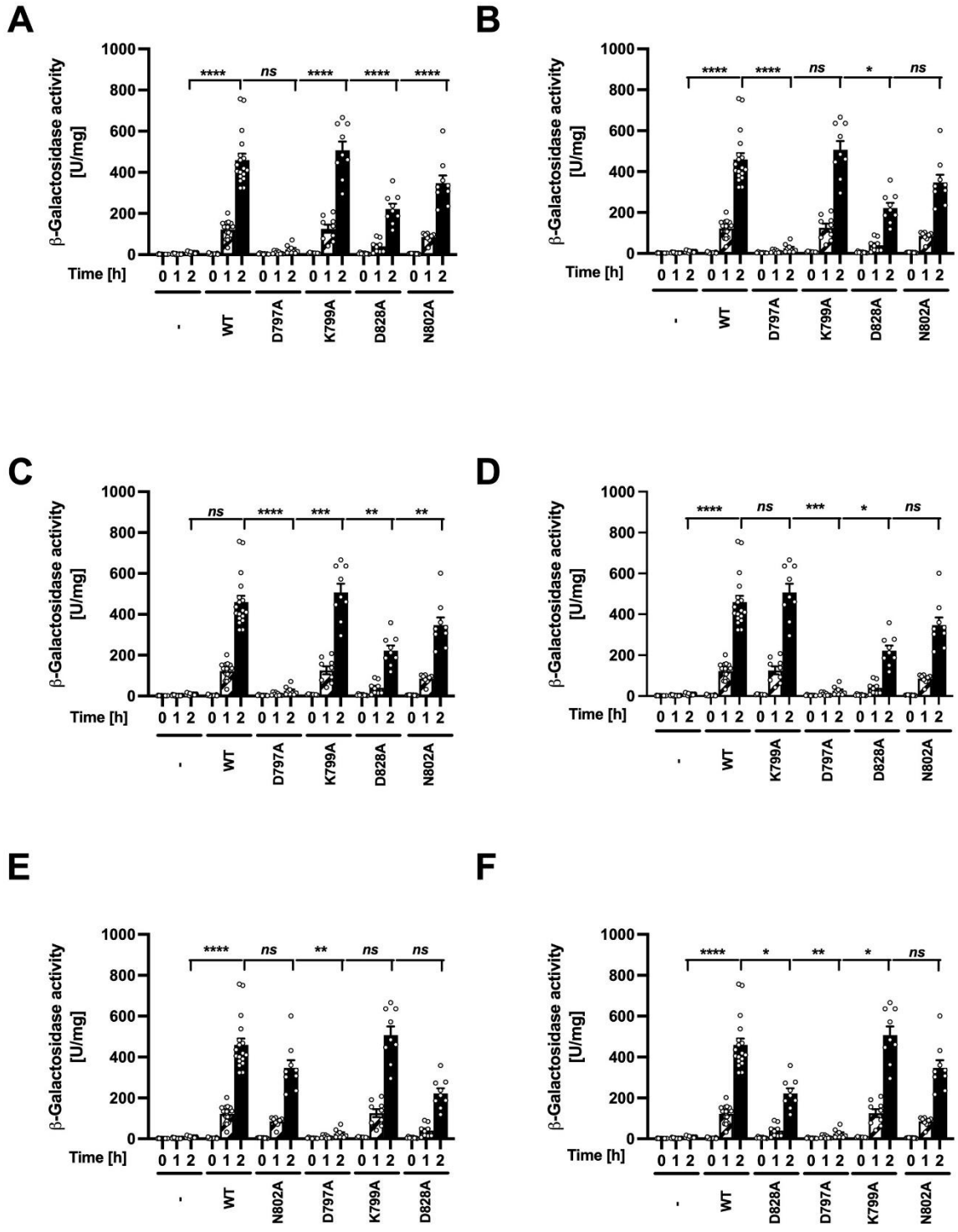

Figure 4.2. Comparison of β-galactosidase activity in single point mutations and WT Ire1 at 2 h time point.

The graph presents the β-galactosidase activity at 2 h time point for the following comparisons: (A) Strain lacking Ire1 (-) compared to WT Ire1 and single point mutations. (B) WT Ire1 compared to strain lacking Ire1 and single point mutations. (C) D797A Ire1 compared to WT Ire1, strain lacking Ire1 and single point mutations. (D) K799A Ire1 compared to WT Ire1, strain lacking Ire1 and single point mutations. (E) N802A Ire1 compared to WT Ire1, strain lacking Ire1 and single point mutations. (F) D828A Ire1 compared to WT Ire1, strain lacking Ire1 and single point mutations. Bars represent the standard errors. Quantified data from 2-6 biological replicates of three clones (n= 3-18). Games-Howell post-hoc tests were used for the analysis. The stars indicate the ranges of p values that were calculated. *, $P \leq 0.05$; **, $P \leq 0.01$; ***, $P \leq 0.001$; ****, $P \leq 0.0001$.

4.3 Characterisation of K799A, N802A, and D828A of reporter activity in comparison to double or triple mutants

4.3.1 Characterisation of K799A mutation and its interaction with other mutants in reporter activity

Here I focus on characterising the reporter activity of the K799A mutation in comparison to double or triple mutants, specifically K799A N802A, K799A D828A, and K799A N802A D828A. The aim is to provide additional information to complement the Northern blot results from the previous chapter, which indicated that combining two or three of these mutations does not further deteriorate *HAC1* splicing compared to the single point mutants. The goal is to validate and confirm the RNA analysis results presented in Chapter 3.3 by examining the corresponding protein expression levels through Northern blot analysis.

To analyse reporter activity, I grew cells to mid-log phase in uracil-deficient media (SD - Ura), then 10 ml samples were taken at the 0 h time point and compared with 10 ml samples after 1 or 2 h of exposure to 2 mM DTT. For more details see materials and methods (2.2.11). To ensure that endogenous Ire1 is not expressed the strain used was deleted for Ire1.

The objective of exploring the β-galactosidase activity in double or triple mutants combined with the K799A mutation was to determine if other mutants carrying the K799A mutation exhibit additive behaviour. This involved assessing whether the combined effect of the minor impact in the K799A mutant and the slight defect in the N802A mutant would result in a substantial defect in the double mutant K799A N802A. Furthermore, the results of these investigations were compared to those obtained with the K799A mutant to assess whether the observed differences in β-galactosidase activity were specific to K799A or if they extended to other mutations. Here I explore the β-galactosidase activity in double mutations combined with the K799A mutation such as K799A N802A, K799A D828A, and K799A N802A D828A.

The β-galactosidase activity of the K799A mutation showed no significant difference compared to the K799A N802A and K799A D828A mutations. However, the combination of K799A N802A D828A exhibited a significant decrease in activity (Fig. 4.3).

These findings indicate that combining the K799A mutation with other mutations does not significantly alter β-galactosidase activity compared to the K799A mutation alone, except for the triple mutant K799A N802A D828A, which showed a significant decrease in activity.

This suggests that the combination of K799A N802A D828A mutations results in a more substantial reduction in reporter activity compared to the individual or double mutations.

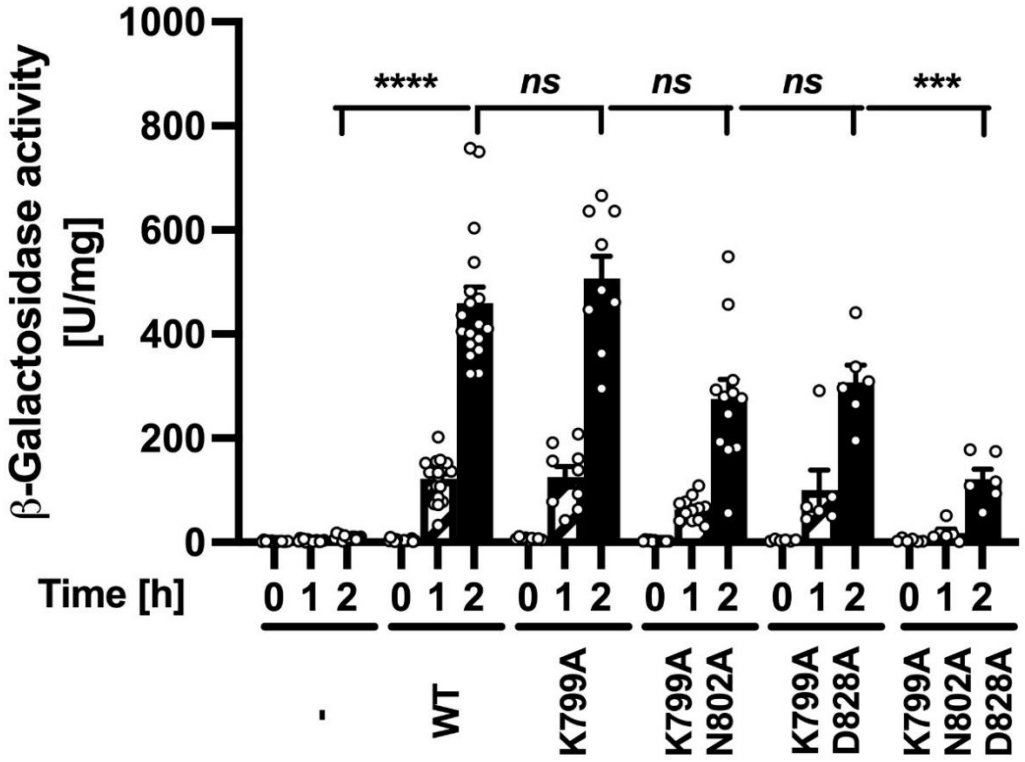

Figure 4.3. Comparative analysis of β-galactosidase activity in K799A Ire1 mutant and its combinations with other mutants.

The graph displays a comparison between K799A Ire1 and WT Ire1, as well as K799A combined with other mutants including N802A, D828A, and N802A D828A, under ER stress. Bars represent the standard errors. Quantified data from 2-6 biological replicates of three clones (n=3-18). Games-Howell post-hoc tests were used for the analysis. The stars indicate the ranges of p values that were calculated. *, $P \leq 0.05$; **, $P \leq 0.01$; ***, $P \leq 0.001$; ****, $P \leq 0.0001$. The p values are for the comparison of K799A Ire1 to WT, K799A, K799A D828A, K799A N802A D828A Ire1 and to strains lacking Ire1.

4.3.2 Characterisation of reporter activity by comparing the effects of N802A mutation in the magnesium coordinating loop with double or triple mutants

To inform the results from Chapter 3.3.3 obtained through Northern blot analysis, where the percentage of *HAC1*^{i} mRNA levels remained unaffected when comparing N802A to the double or triple mutants (K799A N802A, N802A D828A, and K799A N802A D828A), I further examined the β-galactosidase activity to assess the impact of the N802A mutation on Ire1 functionality in a reporter assay. This indicates that the N802A mutation may have subtle effects on reporter activity under ER stress.

Furthermore, to gain a better understanding of the combined effects of the N802A mutation with other mutations, I explored the β-galactosidase activity in the double and triple mutants. These mutants included K799A N802A, N802A D828A, and K799A N802A D828A.

The objective was to determine whether the presence of additional mutations would alter the β-galactosidase activity in a manner distinct from the N802A mutation alone. The investigation aimed to assess if these mutants exhibited additive behaviour, where the combined effects of multiple mutations are simply the sum of their individual effects.

Upon analysing the β-galactosidase activity, no significant differences were observed between the N802A mutation and the double mutations, indicating that the additional mutations did not substantially impact reporter activity beyond the effects of N802A alone. However, in the case of the triple mutation (K799A N802A D828A), a significant decrease in β-galactosidase activity was observed (Fig. 4.4).

This suggests that the combined effects of these three mutations resulted in a more reduction in reporter activity compared to the single or double mutants.

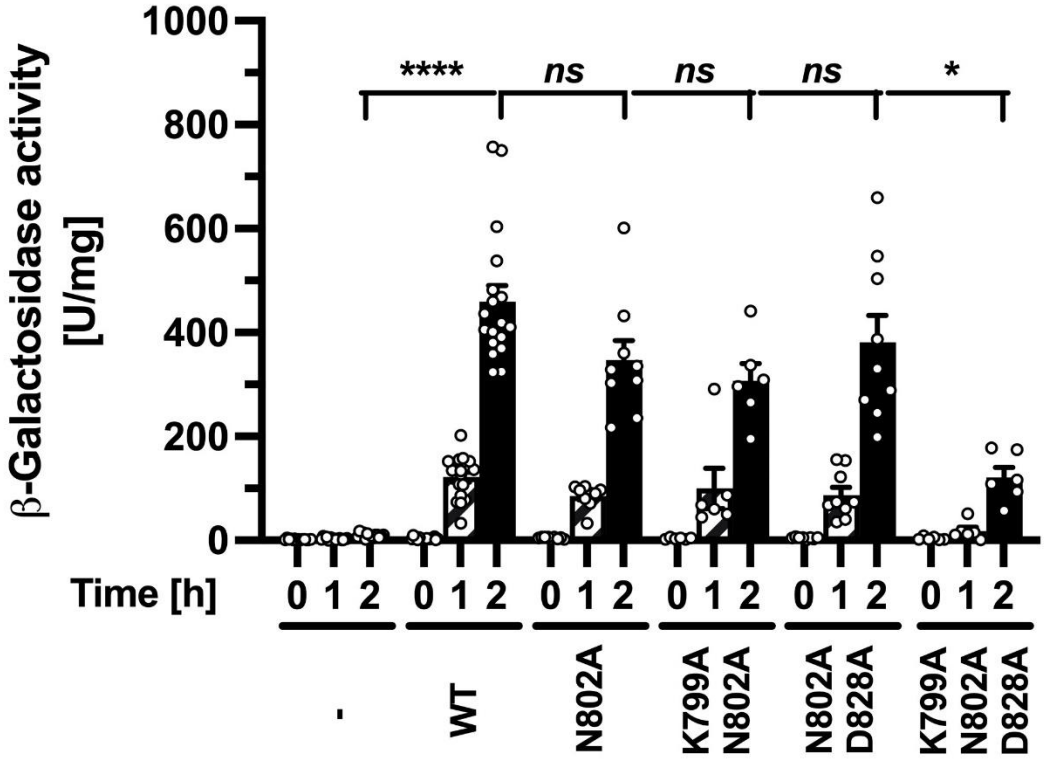

Figure 4.4. Comparative analysis of β-galactosidase activity in N802A Ire1 mutant and its combinations with other mutants.

The graph displays a comparison between N802A Ire1 and WT Ire1, as well as N802A combined with other mutants including, D828A, K799A and K799A D828A under ER stress. Bars represent the standard errors. Quantified data from 2-6 biological replicates of three clones (n= 3-18). Games-Howell post-hoc tests were used for the analysis. The stars indicate the ranges of p values that were calculated. *, $P \leq 0.05$; **, $P \leq 0.01$; ***, $P \leq 0.001$; ****, $P \leq 0.0001$. The p values are for the comparison of N802A Ire1 to WT, K799A N802A, N802A D828A, K799A N802A D828A Ire1 and to strains lacking Ire1.

4.3.3 Characterisation of reporter activity by comparing the effects of D828A mutation in the magnesium coordinating loop with double or triple mutants

To assess the impact of the D828A mutation on β-galactosidase activity, I conducted investigations based on the expectation of observing similar effects as seen with the K799A and N802A mutants. This expectation arises from the fact that all three mutations are involved in interactions with ATP/ADP phosphates facilitated by Mg^{2+} ions. The objective was to determine whether the D828A mutation exhibited similar characteristics to K799A and N802A mutants, and to assess whether other mutations displayed additive effects when combined with D828A Ire1.

The results revealed no significant differences in β-galactosidase activity between the D828A Ire1 mutant and the double mutations. Furthermore, the β-galactosidase activity among the triple mutations involving D828A did not show any significant differences (Fig 4.5).

These findings suggest that the D828A mutation does not exhibit the same impact on reporter activity as the K799A and N802A mutations. Unlike K799A and N802A, the presence of D828A does not significantly alter the reporter activity, indicating a distinct functional characteristic of D828A in comparison to K799A N802A D828A. Additionally, the data indicate that combining the D828A mutation in Ire1 with other mutations such as K799A, N802A and K799A N802A does not significantly alter β-galactosidase activity compared to D828A Ire.

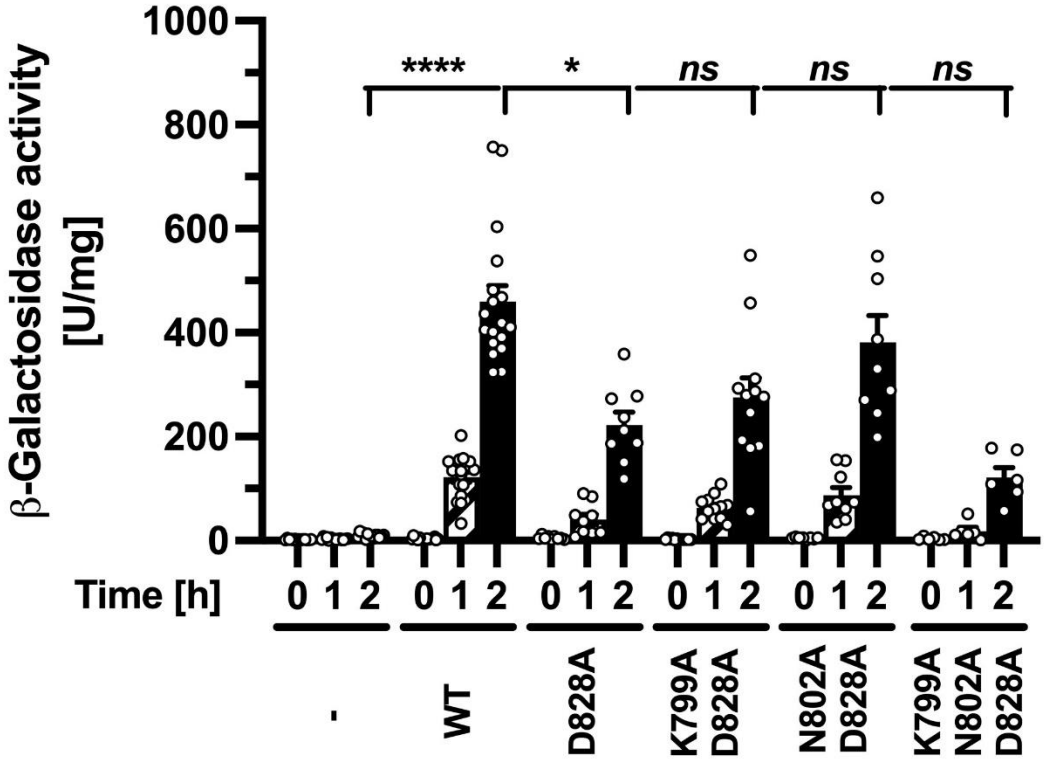

Figure 4.5. Comparison of β-galactosidase activity in D828A Ire1 and other mutants combined with D828A.

The graph illustrates the comparison of β-galactosidase activity in D828A Ire1 mutant and other mutants combined with D828A. The graph depicts the comparison between D828A Ire1 and WT Ire1, as well as D828A combined with other mutants including N802A, and K799A N802A, during ER stress. The error bars represent the standard errors, and the data is based on quantifications from 2-6 biological replicates of three clones (n= 3-18). Games-Howell post-hoc tests were used for the analysis. The stars indicate the significance levels with corresponding p values: *, $P \leq 0.05$; **, $P \leq 0.01$; ***, $P \leq 0.001$; ****, $P \leq 0.0001$. The p values are for the comparison of D828A Ire1 to WT, K799A D828A, N802A D828A, K799A N802A D828A Ire1 and to strains lacking Ire1.

4.4 Intragenic suppression and restoration of reporter activity in Ire1 mutations

4.4.1 The catalytic role of K799 in the Ire1 protein kinase domain and its rescue of D797 through intragenic suppression

Based on the data obtained from the observations made in Chapter 3.4 using Northern blots, it was found that the introduction of the K799A mutation rescues the defective D797A mutant and leads to a restoration of RNase activity, as evidenced by an increase in the percentage of *HAC1*^{i} mRNA, *KAR2* mRNA, and *PDI1* mRNA levels. In this context, the potential intragenic suppression of the D797A Ire1 mutation by introducing the K799A mutation and its effect on β-galactosidase activity were investigated to provide further insights based on the results from the Northern blot analysis.

Figure 4.6 illustrates that the introduction of the K799A mutation into the D797A mutant resulted in an increase in β-galactosidase activity. These findings suggest that the K799A mutation has a rescuing effect on the reduced β-galactosidase activity caused by the D797A mutation (Table 4.2).

These results support the notion that the K799A mutation can counteract the detrimental effects of the D797A mutation and restore reporter activity. The observed increase in β-galactosidase activity is indicative of a rescue phenomenon, where the introduction of the K799A mutation compensates for the functional defects caused by the D797A mutation. It is worth noting that the observed restoration of RNase activity, as demonstrated by the changes in mRNA levels in the Northern blot analysis, aligns with the rescue of reporter activity observed in the β-galactosidase assay.

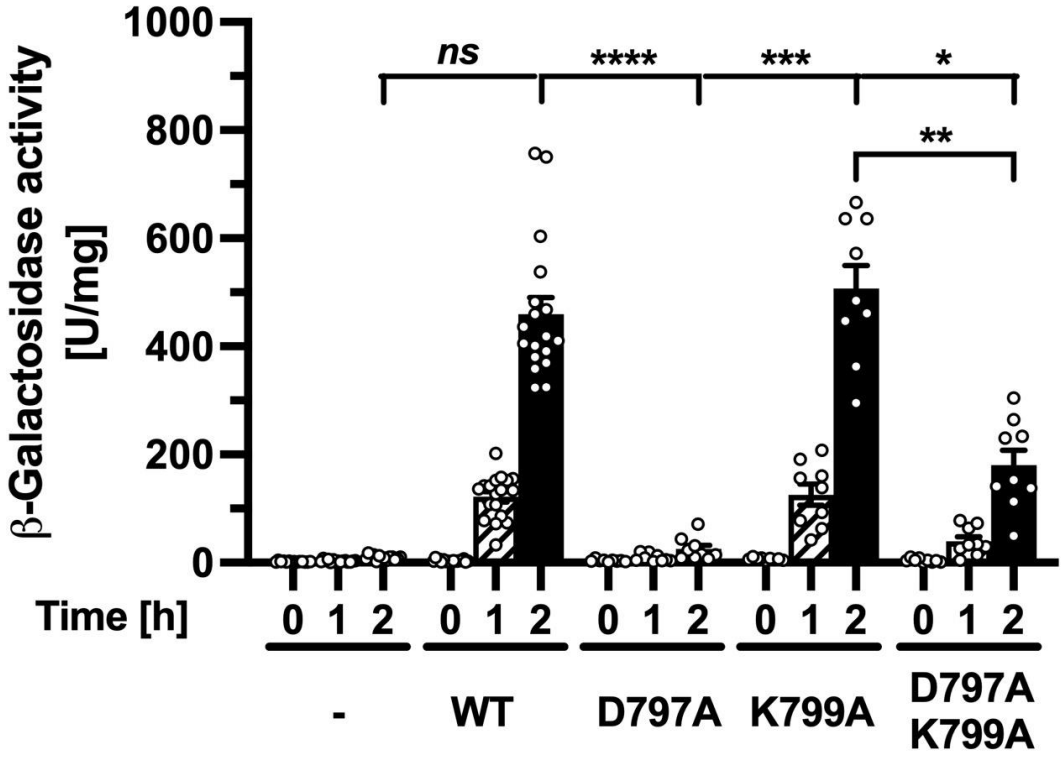

Figure 4.6. The introduction of the K799A mutation to the D797A mutation enhanced β-galactosidase activity under ER stress induction.

β-Galactosidase activity is standardised to total cellular protein at 0, 1, and 2 h after inducing ER stress with 2 mM DTT in mid-exponential Ire1 deletion cells expressing the indicated Ire1 mutants from YCplac33 or carrying the empty vector. The graph compares the results obtained from D797A Ire1 and WT Ire1, as well as K799A and D797A K799A, in response to ER stress. Bars represent the standard errors. Quantified data from 2-6 biological replicates of three clones (n= 3-18). Games-Howell post-hoc tests were used for the analysis. The stars indicate the ranges of p values that were calculated. *, $P \leq 0.05$; **, $P \leq 0.01$; ***, $P \leq 0.001$; ****, $P \leq 0.0001$. The p values are for the comparison of D797A Ire1 to WT, K799A, D797A K799A Ire1 and to strains lacking Ire1.

4.4.2 Rescue of the defective D797A mutant by the magnesium coordinating loop mutants N802A and D828A in Ire1

4.4.2.1 Rescue effects of N802A mutation on D797A mutant

The defective phenotype of the D797A mutant has been previously identified, and the rescue potential of the magnesium coordinating loop mutants N802A and D828A in Ire1 has been observed through Northern blot analysis. This chapter aims to investigate the rescue of the D797A mutant by these mutants using β-galactosidase activity as a measure. The goal is to validate and confirm the previous findings.

To assess the rescuing potential of the N802A mutation, the β-galactosidase activity was examined in the presence of the D797A mutant. Surprisingly, the introduction of the N802A mutation into the D797A mutant resulted in an increase in β-galactosidase activity (Fig. 4.7) (Table 4.2). These findings suggest that the N802A mutation acts as a rescuing factor, mitigating the negative impact of the D797A mutation and restoring β-galactosidase activity.

The observed increase in β-galactosidase activity in the N802A and D797A double mutant corresponds to the rescue of RNase activity previously demonstrated in the Northern blot analysis (Chapter 3.4). This alignment strengthens the evidence for the rescue effect of the N802A mutation on the D797A mutant, validating the findings from the previous chapter.

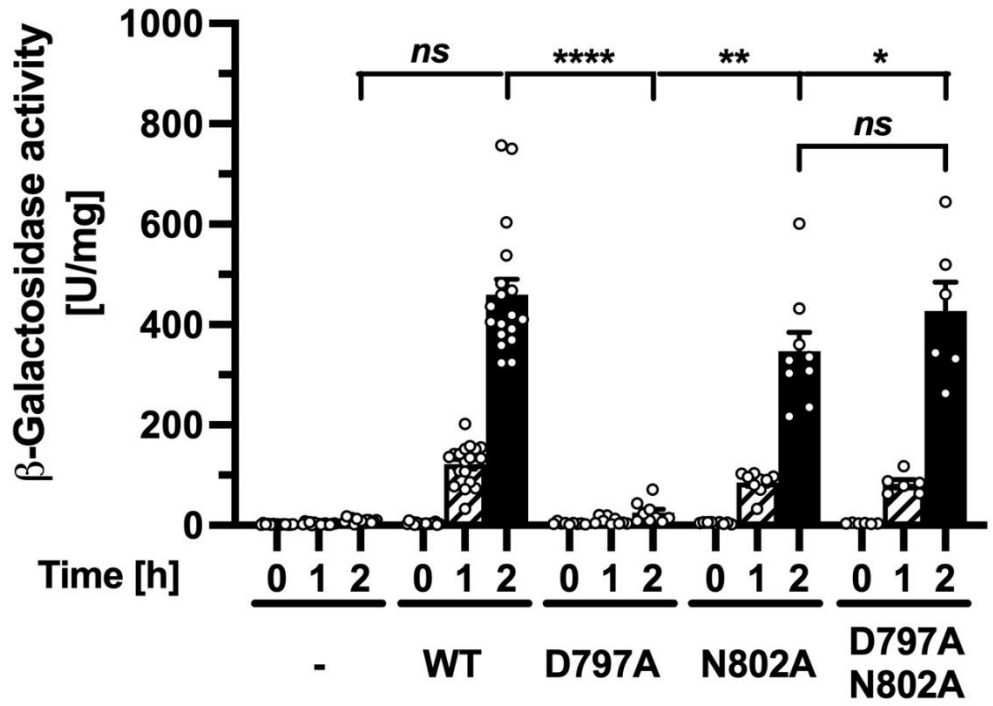

Figure 4.7. The introduction of the N802A mutation to the D797A mutation enhanced β-galactosidase activity under ER stress induction.

β-Galactosidase activity is standardised to total cellular protein at 0, 1, and 2 h after inducing ER stress with 2 mM DTT in mid-exponential Ire1 deletion cells expressing the indicated Ire1 mutants from YCplac33 or carrying the empty vector. The graph compares the results obtained from D797A Ire1 and WT Ire1, as well as N802A and D797A N802A, in response to ER stress. Bars represent the standard errors. Quantified data from 2-6 biological replicates of three clones (n= 3-18). Games-Howell post-hoc tests were used for the analysis. The stars indicate the ranges of p values that were calculated. *, $P \leq 0.05$; **, $P \leq 0.01$; ***, $P \leq 0.001$; ****, $P \leq 0.0001$. The p values are for the comparison of D797A Ire1 to WT, N802A, D797A N802A Ire1 and to strains lacking Ire1.

4.4.2.2 Rescue effects of D828A mutation on D797A mutant

Similar to the K799A and N802A mutations, the potential of the D828A mutation to reverse the negative effects caused by the D797A Ire1 mutation and restore β-galactosidase activity was also examined. Interestingly, introducing the D828A mutation into the D797A mutant resulted in an increase in β-galactosidase activity, indicating a rescue effect (Fig. 4.8) (Table 4.2). These findings demonstrate that the D828A mutation, like K799A and N802A, acts as a rescuing factor, effectively mitigating the detrimental effects of the D797A mutation and restoring the functional activity of Ire1.

The rescue effects observed in the D797A mutant by the N802A and D828A mutations further emphasise the significance of these mutants within the magnesium coordinating loop of Ire1. These findings support the notion that specific alterations in this region can alleviate the impaired functionality caused by the D797A mutation, leading to a restoration of β-galactosidase activity.

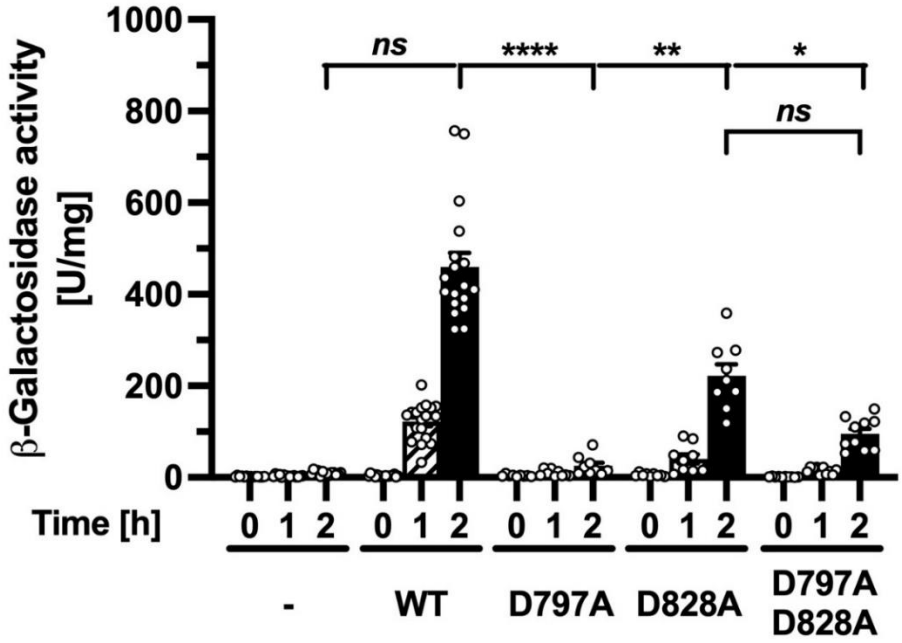

Figure 4.8. The introduction of the D828A mutation to the D797A mutation enhanced β-galactosidase activity under ER stress induction.
β-Galactosidase activity was measured and normalised to total cellular protein at different time points (0, 1, and 2 h) following the induction of ER stress with 2 mM DTT in Ire1 deletion cells expressing specific Ire1 mutants or in a strain lacking Ire1. The graph presents a comparison between D797A Ire1 and WT Ire1, as well as D828A and D797A D828A mutants, in response to ER stress. The error bars represent the standard errors, and the quantified data is based on measurements from 2-6 biological replicates of three clones (n= 3-18). Games-Howell post-hoc tests were used for the analysis. The stars indicate the significance levels with corresponding p values: *, $P \leq 0.05$; **, $P \leq 0.01$; ***, $P \leq 0.001$; ****, $P \leq 0.0001$. The p values are for the comparison of D797A Ire1 to WT, D828A, D797A D828A Ire1 and to strains lacking Ire1.

4.5 Intragenic suppression by a double or triple mutations in the protein kinase domain restore the ability to induce UPRE-*lacZ* reporters to the D797A Ire1 mutant

In the previous chapters, the impact of specific single point mutations, namely K799A, N802A, and D828A, on restoring RNase activity in the D797A Ire1 mutant was explored (Chapter 4.4). The analysis revealed that these mutations increased the activity of β-galactosidase, indicating a rescue of RNase functionality in the D797A mutant. Furthermore, investigations into the combination of two mutations, such as K799A N802A and K799A D828A, demonstrated no significant alteration in β-galactosidase activity compared to the single point mutants (Chapter 4.3). Building upon these findings, the potential of double or triple mutations to restore β-galactosidase activity in the D797A mutant is examined in this chapter. The focus is on exploring intragenic suppression by investigating the combination of these mutations such as D797A to D797A K799A N802A, D797A to D797A K799A D828A, D797A to D797A N802A D828A and D797A to D797A K799A N802A D828A within the protein kinase domain of Ire1, specifically in relation to the induction of UPRE-lacZ reporters.

Expression of the D797A Ire1 mutant significantly decreased β-galactosidase activity when compared to double or triple mutants (Fig. 4.9). In contrast, when the D797A mutant was combined with a double or triple mutation such as K799A N802A, K799A D828A, N802A D828A, and K799A N802A D828A, there was a notable increase in β-galactosidase activity (Fig. 4.9) (Table 4.2). These findings suggest that these additional mutations have a rescuing effect, counteracting the reduced β-galactosidase activity caused by the D797A mutation.

The results from the UPRE-*lacZ* reporter gene analysis support the findings obtained from Northern blot analysis, providing that mutations in the protein kinase domain can restore the ability to induce UPRE-controlled genes in the D797A Ire1 mutant. These findings highlight the presence of intragenic suppression mechanisms and the functional recovery of Ire1 in regulating UPRE-controlled genes.

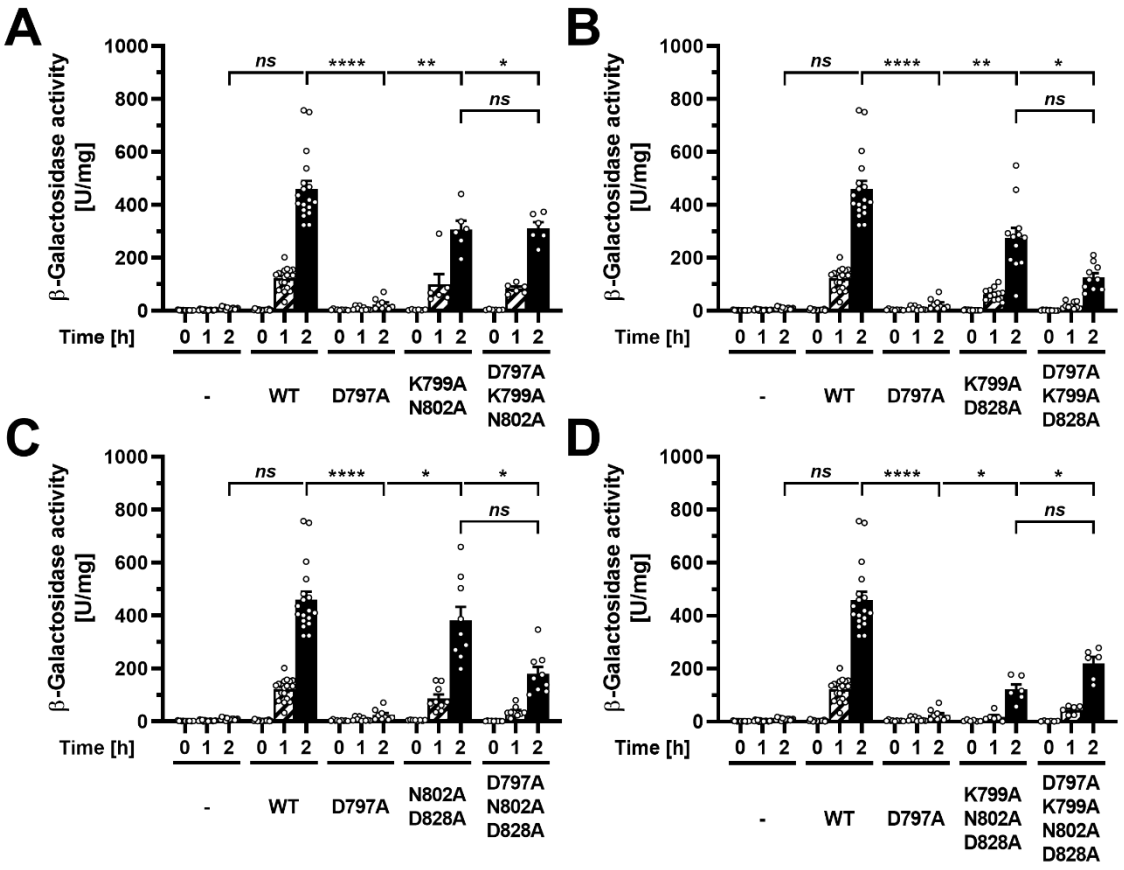

Figure 4.9. Restoration of β-galactosidase activity by introducing double or triple mutants to the defective D797A mutants.

The β-galactosidase activity was quantified using the UPRE-*lacZ* reporter gene in Ire1 deletion cells. Measurements were taken at 0, 1, and 2 h after inducing ER stress with 2 mM DTT. The graphs depict various comparisons: (A) D797A vs. K799A N802A and D797A K799A N802A, (B) D797A vs. K799A D828A and D797A K799A D828A, (C) D797A vs. N802A D828A and D797A N802A D828A, and (D) D797A vs. K799A N802A D828A and D797A K799A N802A D828A. The error bars in the graph represent the standard errors, and the quantified data is based on measurements obtained from 2-6 biological replicates of three clones. Games-Howell post-hoc tests were used for the analysis. The stars in the graph indicate the significance levels with their corresponding p-values: *, $P \leq 0.05$; **, $P \leq 0.01$; ***, $P \leq 0.001$; ****, $P \leq 0.0001$.

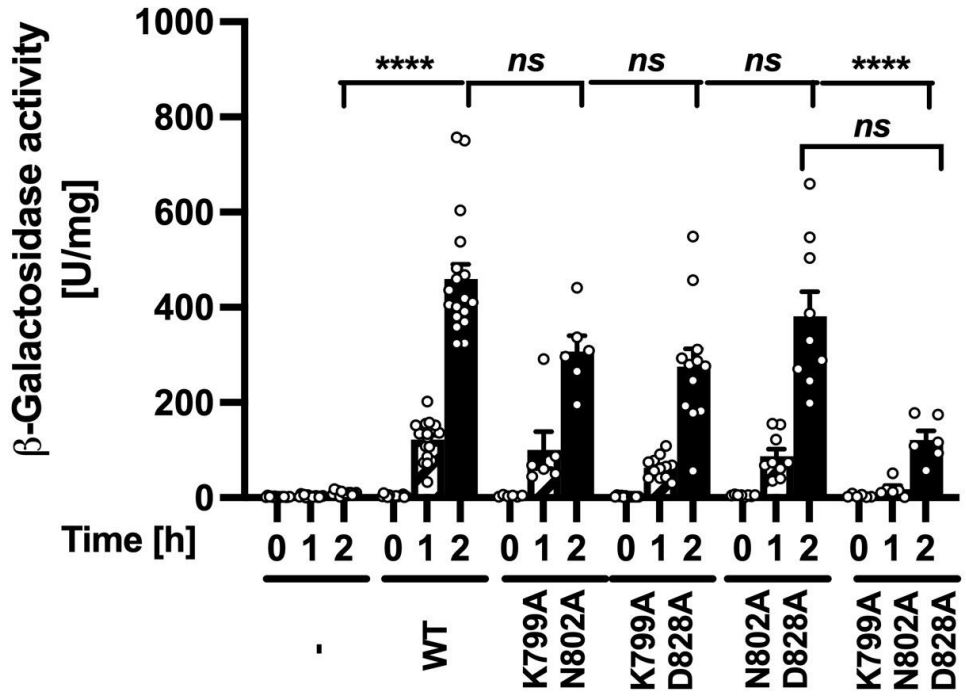

Figure 4.10. Comparative analysis of β-Galactosidase activity in double and triple Ire1 mutants and WT Ire1.

The graph depicts the comparison of β-galactosidase activity among different mutants, including K799A N802A, K799A D828A, N802A D828A, K799A N802A D828A, and WT Ire1, after a 2 h treatment with 2 mM DTT. The error bars represent the standard errors, and the data is based on quantifications from 2-6 biological replicates of three clones (n=3-18). Games-Howell post-hoc tests were used for the analysis. The stars indicate the significance levels with their corresponding p-values: *, $P \leq 0.05$; **, $P \leq 0.01$; ***, $P \leq 0.001$; ****, $P \leq 0.0001$. The p values are for the comparison of WT Ire1 to K799A N802A, K799A D828A, N802A D828A, K799A N802A D828A Ire1 and to strains lacking Ire1.

Table 4.1. Statistical data of mutants vs. WT and vs. the strain lacking Ire1 (-)

The p-values calculated from the non-parametric test showed statistically significant differences between WT and the mutants, as well as between the strain lacking Ire1 (-) and the mutants. It was found that, when compared to the strain lacking Ire1, all the differences among the Ire1 mutants were statistically significant, except for the D797A and K799A N802A D828A Ire1 mutant.

Comparison at 2 h of induction with 2 mM DTT	Significant	p value
WT vs. -	Yes	<0.0001
WT vs. D797A	Yes	<0.0001
WT vs. K799A	No	1.0000
WT vs. D797A K799A	Yes	0.0003
WT vs. N802A	No	0.9369
WT vs. D797A N802A	No	1.0000
WT vs. D828A	Yes	0.0015
WT vs. D797A D828A	Yes	<0.0001
WT vs. K799A N802A	No	0.427
WT vs. D797A K799A-N802A	No	0.1801
WT vs. K799A D828A	No	0.1960
WT vs. D797A K799A-D828A	Yes	<0.0001
WT vs. N802A D828A	No	1.0000
WT vs. D797A N802A-D828A	Yes	0.0002
WT vs. K799A N802A-D828A	Yes	<0.0001
WT vs. D797A K799A N802A-D828A	Yes	0.0023
- vs. D797A	No	>0.9280
- vs. K799A	Yes	0.0005
- vs. D797A K799A	Yes	0.0281
- vs. N802A	Yes	0.0031
- vs. D797A N802A	Yes	0.0395
- vs. D828A	Yes	0.0033
- vs. D797A D828A	Yes	0.0045

- vs. K799A N802A	Yes	0.0158
- vs. D797A K799A N802A	Yes	0.0023
- vs. K799A D828A	Yes	0.0045
- vs. D797A K799A D828A	Yes	0.0062
- vs. N802A D828A	Yes	0.0127
- vs. D797A N802A D828A	Yes	0.0219
- vs. K799A N802A D828A	No	0.0946
- vs. D797A K799A N802A D828A	Yes	0.0154

Table 4.2. Statistical comparison using non-parametric test between the defect mutant D797A Ire1 and other mutants.

Comparison at 2 h of induction with 2 mM DTT	Significant	p Value
D797A vs. K799A	Yes	0.0005
D797A vs. D797A K799A	Yes	0.0478
D797A vs. N802A	Yes	0.0038
D797A vs. D797A N802A	Yes	0.0451
D797A vs. D828A	Yes	0.0043
D797A vs. D797A D828A	No	0.0225
D797A vs. K799A N802A	Yes	0.0174
D797A vs. D797A K799A N802A	Yes	0.0016
D797A vs. K799A D828A	Yes	0.0070
D797A vs. D797A K799A D828A	Yes	0.0153
D797A vs. N802A D828A	Yes	0.0161
D797A vs. D797A N802A D828A	Yes	0.0371
D797A vs. K799A N802A D828A	Yes	0.1665
D797A vs. D797A K799A N802A D828A	Yes	0.0168

4.6 Discussion

The expression of UPRE-*lacZ* in yeast was used to further to confirm the results from the Northern blots. The single point mutations K799A, N802A, and D828A in the catalytic site of Ire1 did not significantly affect its RNase activity. Specifically, the K799A Ire1 mutant displayed similar levels of spliced *HAC1* mRNA compared to the WT Ire1, indicating comparable behaviour (Figs. 3.4 A). Moreover, the K799A Ire1 mutant exhibited increased *HAC1* splicing and β-galactosidase activity relative to other single point mutations (3.3 A and 4.2 D). Additionally, *KAR2* and *PDI1* mRNA levels were also elevated in the K799A Ire1 mutant (Figs. 3.3 B and 3.3 C), and its β-galactosidase activity closely resembled that of the WT Ire1 (Fig. 4.3). These findings indicate a close alignment between the data for β-galactosidase activity in the K799A mutant and the RNA data, providing evidence of a robust correlation.

Significant discrepancies were observed specifically in the D828A Ire1 mutants, while such differences were not observed in the N802A Ire1 mutants when compared to the WT Ire1. Both mutants, located in the Mg^{2+} coordinating domain, showed a significant reduction in *HAC1* splicing compared to the WT (Figs. 3.4 A and 3.5 A). Additionally, the D828A Ire1 mutant exhibited decreased β-galactosidase activity, whereas this decrease was not observed in the N802A Ire1 mutant (Figs. 4.4 and 4.5). Comparison of these mutants to a strain lacking Ire1 revealed a significant increase in activity (Table 4.1) (Fig. 4.2 A), indicating the critical role of the Mg^{2+} coordinating domain in regulating Ire1 activity and the expression of *HAC1* and β-galactosidase.

The D797A Ire1 mutant, exhibits a decrease in *HAC1* splicing, which correlates with a decrease in UPRE-*lacZ* activity, as well as *KAR2* or *PDI1* mRNA levels, compared to the WT Ire1(Figs. 3.9 and 4.6). However, the introduction of other mutants, such as K799A, N802A, and D828A, to the D797A Ire1 mutant through intragenic suppression restores RNase activity, as evidenced by the results from Northern blots (Figs. 3.9, 3.12, 3.13, 3.16, 3.17, 3.18 and 3.19). These findings suggest that the presence of these additional mutants partially compensates for the loss of function caused by the D797A mutation. The β-galactosidase reporter assay further supports these results by demonstrating consistent effects on RNase activity. The inclusion of mutants like K799A, N802A, and D828A in the D797A Ire1 mutant leads to improved expression of UPRE-*lacZ*, indicating that the restoration of RNase activity in the defective D797A mutant is indeed attributed to intragenic suppression.

During further investigation, the phenomenon of intragenic suppression was explored in the context of double and triple mutations. Notably, the N802A D828A Ire1 mutants exhibited significant increase in terms of *HAC1* splicing, β-galactosidase activity, and the levels of *KAR2* and *PDI1* mRNA when compared to the D797A Ire1 mutant (Figs. 3.14 and 4.10 C). As anticipated, the introduction of double mutations, specifically N802A and D828A, into Ire1 resulted in a substantial increase in *HAC1* splicing, β-galactosidase activity, and the levels of *KAR2* and *PDI1* mRNA, surpassing those observed in the single mutant D797A Ire1 (Figs. 3.18 A, 3.18 B, 3.18 C, and 4.9 C) (Table 4.2). In addition to that expression of Ire1 decreased β-galactosidase activity in K799A N802A D828A compared to N802A D828A (Fig. 4.10). Also, the β-galactosidase activity of K799A N802A D828A Ire1 was significantly decreased compared to the WT after induction with 2 mM DTT at 2 h (Fig 4.10). These data confirm the results obtained from Northern blot analysis, which also showed a significant decrease in the K799A N802A D828A mutant compared to WT (Fig. 3.20). These observations suggest that the combined mutations of K799A, N802A, and D828A in Ire1 lead to decreased RNase activity, resulting in decreased induction of the UPRE-*lacZ* reporter. The data presented in this chapter indeed confirm the alignment between the results obtained from the β-galactosidase assay and the findings from the Northern blots. This strong correlation supports the relationship between *HAC1* splicing, production of *HAC1* protein, and transcriptional induction by *HAC1*. These consistent results emphasise the significance of the specific mutations (K799A, N802A, and D828A) and highlight the potential of intragenic suppression to restore RNase activity in Ire1 mutants. The combination of mutants, including K799A, N802A, and D828A, with the defective D797A Ire1 mutant demonstrates partial compensation for the loss of function, resulting in restored RNase activity and improved UPRE-*lacZ* expression. These findings underscore the critical role of specific amino acids, such as K799, N802, and D828 in determining the functional capabilities of Ire1 within the UPR.

Importantly, among the studied mutations, the D828A mutation shows a more severe impact on Ire1 function. This suggests that the amino acid at position 828 (aspartic acid replaced with alanine) has distinct structural and functional consequences, further emphasising the significance of this particular alteration. Mutation of either D828 or N802 disrupts Mg^{2+} binding and subsequently affects adenine nucleotide binding. This disruption explains the defects observed in *HAC1* splicing in the Northern blots and the impaired β-galactosidase assay in the D828A mutant. The severity of the D828A mutation surpasses that of N802A

because the N802A mutation primarily interferes with Mg^{2+} binding while preserving the negative charge of D828. On the other hand, the D828A mutation not only interferes with Mg^{2+} binding but also eliminates the negative charge of D828. In the N802A mutant, the preservation of the negative charge increases the electrostatic charge repulsion, shifting the ratio of bound ADP to ATP in favour of ADP. In contrast, in the D828A mutant, where the negative charge is lost, the ratio is shifted towards ATP due to the intracellular abundance of ATP compared to ADP.

Considering the combined effect of the three mutants (K799A, N802A, and D828A), it is plausible to suggest that these mutations collectively contribute to the observed decrease in both β-galactosidase activity and RNA levels. The cumulative impact of multiple mutations can have a more significant effect on the measured parameters compared to each mutation individually. Although the N802A and D828A mutants exhibit relatively minor individual effects, when combined with the K799A mutation, they may interact additively, resulting in a more pronounced decrease in β-galactosidase activity and RNA levels.

5 EFFECTS OF ER STRESS ON IRE1 EXPRESSION IN YEAST

5.1 Rationale

Detecting Ire1 steady-state levels is critical for confirming earlier data and proving the expression of Ire1 mutants. Moreover, it was crucial to ensure that mutants behaved similarly to the WT in terms of Ire1 protein production levels. This was important to prevent any reduction in UPR activation in the mutants, which could potentially be due to reduced Ire1 protein levels during ER stress, when compared to the WT. To investigate the impact of ER stress on *IRE1* expression levels in mutants, a biochemical approach was implemented. Since Ire1 is a protein that responds to ER stress, the induction of ER stress in different mutants may have varying effects on *IRE1* expression. It is crucial to confirm that the mutants can express *IRE1* from the plasmid, as a lack of expression could impede the activation of UPR and the ability of the cell to tolerate ER stress (Cox et al., 1993; Mori et al., 1993). The centromeric plasmid used in this experiment contains an *IRE1-HA* allele under control of the *IRE1* promoter. HA-tagged Ire1 is produced by the cells, which can be specifically detected using anti-HA antibodies (see materials and methods, Table 2.8). Western blotting using SDS-PAGE was performed to detect Ire1, and a loading control was used to measure the relative levels of Ire1. β-actin was selected as the loading control because it remains stable during ER stress and should be uniformly expressed across mutants (Armstrong et al., 2017) (Table 2.8). Densitometric analysis was used to normalise the levels of Ire1 against the levels of β-actin. Any changes in β-actin expression would indicate uneven gel loading. In addition to the method described in the chapter, I used and optimised methods to detect steady levels of Ire1 and its mutants, such as the denaturation temperature to improve the detection of the target protein on Western blots.

5.2 Optimisation of denaturation temperature for western blotting

Western blotting is a method used to identify and quantify proteins in biological samples. Protein denaturation is a vital step in this approach, which is commonly accomplished by heating the sample in the presence of a detergent such as SDS. The denaturation temperature can significantly affect the quality and accuracy of the results, as it can impact the solubilisation of proteins and their subsequent binding to the membrane. Optimising the denaturation temperature is critical in Western blotting for several reasons. First, the denaturation step involves the complete unfolding of proteins, allowing them to be separated

effectively by size in SDS-PAGE gels. If the temperature is too high, it might lead to excessive protein aggregation or denaturation, resulting in weak bands or even a complete loss of protein signal. Conversely, a denaturation temperature that is too low may not fully denature the proteins, leading to incomplete separation and weak bands. Therefore, finding the optimal denaturation temperature is essential for obtaining clear and robust Western blot results. In my initial experiments, I used 70 °C as the denaturation temperature and obtained multiple weak bands (Fig. 5.1 A). To optimise the denaturation temperature for Western blotting, I tested a range of temperatures from 30 °C to 70 °C using a standard protocol for detecting a target protein in a cell lysate. After running the samples on an SDS-PAGE gel as described in the methods chapter (2.2.12.2), I found that decreasing the denaturation temperature to 40 °C resulted in stronger bands. The decrease in denaturation temperature from 70 °C to 40 °C appeared to result in a significant improvement in the Western blotting bands, but it is important to consider other factors that may have contributed to the observed differences. Alongside the change in denaturation temperature, variables such as exposure time, amount of protein loaded, incubation time conditions with antibodies, and the quality of antibodies used could have influenced the results. While the decrease in denaturation temperature likely played a role in the observed improvements, optimising these additional experimental parameters is crucial for accurately assessing their individual impacts on Western blotting outcomes. Considering these factors, the bands obtained at 40 °C showed enhanced intensity, improved clarity, increased specificity of target protein detection, and overall better representation and reproducibility of the protein expression pattern. These improvements suggest that the denaturation temperature, along with other experimental parameters, significantly influenced the quality and accuracy of the Western blotting results. Therefore, I chose 40 °C as the optimal denaturation temperature for Western blot experiments. To show the efficiency of this improvement, I compared the results obtained using the optimised technique with those obtained using the regular protocol. As shown in Figure 5.1 B, the optimised protocol resulted in a stronger and cleaner signal for the target protein. This optimisation step helped to ensure that the protein was fully denatured and separated properly on the SDS-PAGE gel, leading to better visualisation and detection on the Western blot. Also, this additional optimisation step may have contributed to the improved sensitivity and accuracy of the Western blot results.

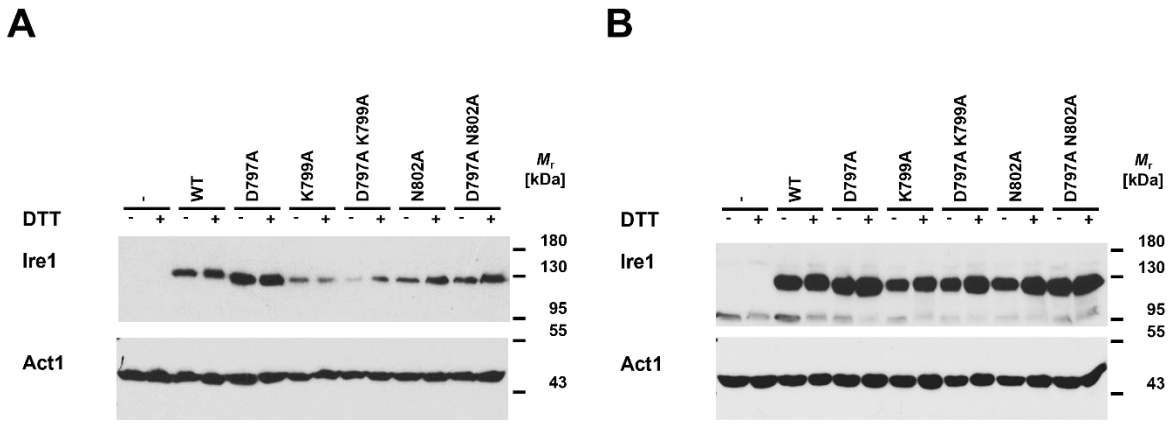

Figure 5.1. Optimisation of denaturation temperature for western blotting.
Western blot for HA-tagged Ire1 (MW ~ 130 kDa) and Act1 proteins (MW ~ 43 kDa) obtained from *ire1*Δ strains at mid-exponential growth phase. Two different denaturation temperatures were used in this experiment: A) 70 °C and B) 40 °C. At 70 °C, multiple weak bands were obtained for both proteins, indicating that the high denaturation temperature may have exacerbated the aggregation and precipitation of Ire1.

5.3 Expression levels of WT and mutant Ire1 proteins related to protein kinase activity

To ensure that the Ire1 protein encoded by the Ire1 allele present on the YCplac33 plasmid was being expressed, the mutants created through the transformation of PWY 260 cells with YCplac33 needed to undergo testing, which used the HA tag present on the plasmid encoding Ire1. I was interested in determining whether any of the protein kinase mutants expressed to the same level as the wild-type protein. Protein was extracted from mid-exponential growth phase cells. 50 µg of the extracted proteins were separated on a 10 % SDS-PAGE gel, and then transferred onto PVDF membranes. The membranes were then blotted for Ire1-HA and the actin loading control according to the procedures outlined in the materials and methods section (2.2.12). The bands on the images were then analysed using densitometry, which was performed using Cliqs software. The results presented in Fig. 5.2 suggest that all mutants have a similar ability to induce the expression of the Ire1 protein at levels comparable to those observed in the WT. Therefore, the variations in *HAC1* mRNA splicing and β-galactosidase activity seen in chapters 3 and 4 are unlikely to be caused by differences in Ire1 levels among the mutants. Therefore, these results imply that all the mutants express Ire1 protein effectively, and their expression is comparable to WT under stress conditions. These findings are crucial in ensuring the reliability of experiments designed to investigate the role of phosphorylation in relation to RNase activity of Ire1.

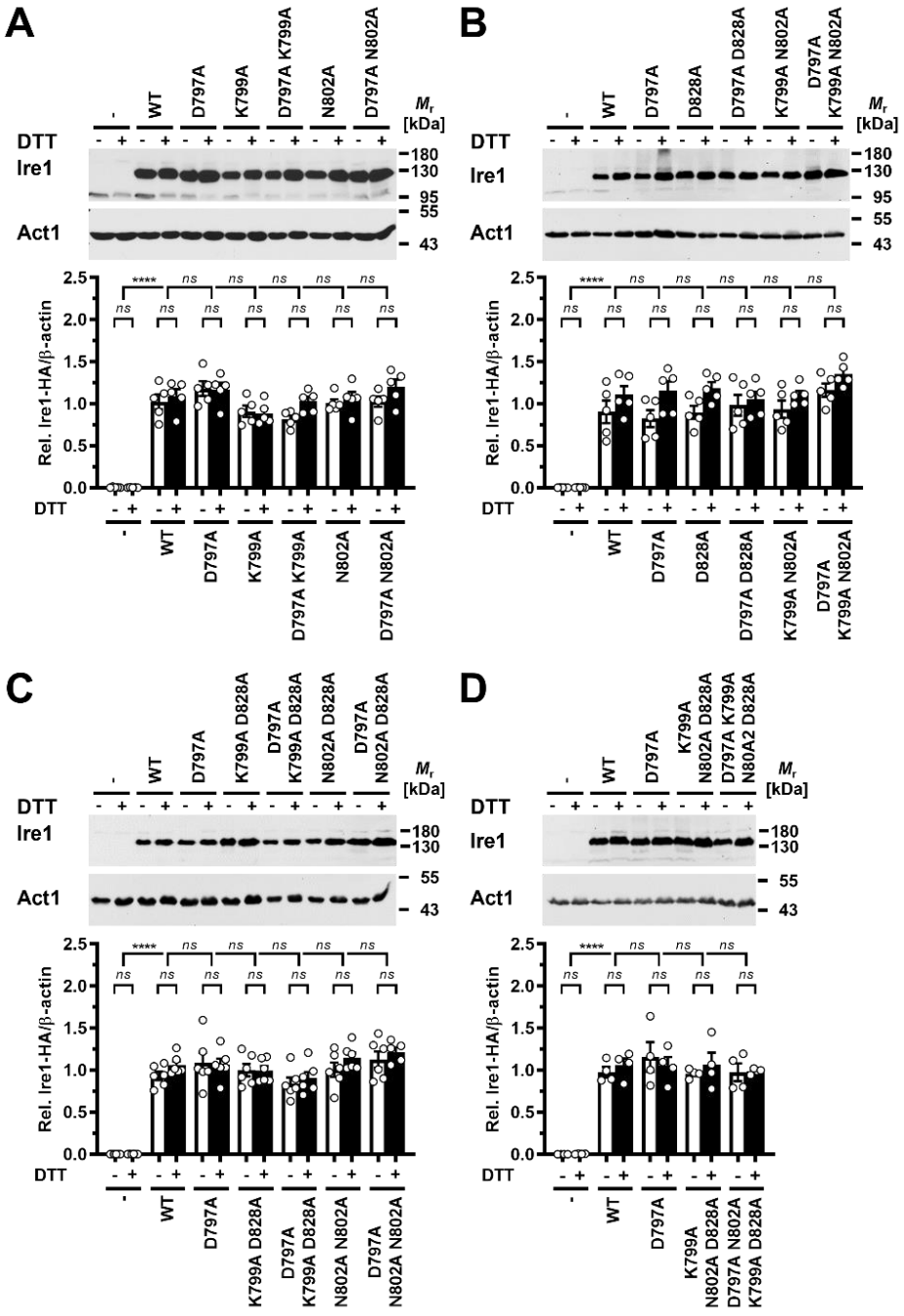

Figure 5.2. Expression of WT and mutant Ire1 proteins.
Western blot for HA-tagged Ire1 (MW ~ 130 kDa) and Act1 proteins (MW ~ 43 kDa) obtained from *ire1*Δ strains at mid-exponential growth phase. These proteins were expressed from different *IRE1* alleles carried on either a YCplac33 vector or an empty vector (-). Cells were treated with 2 mM DTT for 2 h, as indicated by a (+) sign. The proteins were separated using 10 % SDS-PAGE gels and transferred onto PVDF membranes. (A-D) Quantification of Ire1-HA levels relative to the Act1 loading control. The data were analysed using an ordinary two-way ANOVA with Tukey's correction for multiple comparisons. The comparisons were always made between the mutants and the WT. The results of the analysis indicated that no significant differences were detected in Ire1-HA expression levels, except for the negative control strain transformed with an empty vector. The data presented in the graphs were obtained by calculating the average and standard error of biological repeats with a sample size ranging from 3 to 6 (n = 3-6).

5.4 Discussion

This chapter presents a method used to confirm and measure the steady-state expression of HA-Ire1 and its mutants in the β-galactosidase assays and Northern blots. The method involved the expression and detection of the proteins using Western blots to observe the Ire1 target protein. The results obtained from these experiments (Chapter 3.3 and 4.2) indicated that the observed differences in levels of *HAC1* splicing, *KAR2* and *PDI1* mRNA, and β-galactosidase activity between the WT and mutant Ire1 proteins were not related to their protein kinase activity.

6 EVALUATING THE IMPACT OF IRE1 MUTATIONS ON ER STRESS TOLERANCE AND SURVIVAL

6.1 Rationale

The UPR plays a crucial role in the ability of cells to tolerate ER stress and survive under adverse conditions. Previous studies have suggested that a reduction in UPR activation could result in a decrease in ER stress tolerance (Kozutsumi et al., 1988; Travers et al., 2000) I used spotting assays to determine whether the reduction in the ER stress response, as indicated by the decrease in β-galactosidase activity and *HAC1* splicing observed in Northern blot analysis, impacts the ability of cells to survive ER stress. Spotting assays are a commonly used technique to assess the growth and survival of cells under different conditions. I used spotting assays to investigate the impact of mutations in protein kinase domain sites that have been shown to play a significant role in UPR activation based on data from previous studies on the ability of cells to survive ER stress induced by dithiothreitol (DTT), tunicamycin (Tm) and 2-deoxy-D-glucose (2 DDG). DTT, Tm and 2DDG are commonly used ER stressors that disrupt protein folding in the ER, leading to ER stress (Boyce & Yuan, 2006; Rutkowski & Kaufman, 2004; Zhang & Kaufman, 2008). Here I compared the survival ability of cells with different Ire1 mutations to those expressing the WT-Ire1 and cells lacking Ire1 (-).

6.2 D797A Ire1 mutants in the catalytic domain reveal no protection from ER stress and the intragenic rescue the D797A mutation by other mutations.

To confirm the results of the β-galactosidase reporter assay and Northern blots, and to demonstrate the physiological significance of the observed differences, further experiments were needed to fully understand the impact of various Ire1 mutations on the regulation of UPRE-*lacZ* and *HAC1* splicing. To address this, I conducted spotting assays with *ire1*Δ cells transformed with YCplac33 or carrying specific Ire1 mutations, exposed to different concentrations of drugs to evaluate their survival under stress. The cells were serially diluted tenfold and spotted onto plates containing different concentrations of Tm, DTT, and 2DDG and the results were analysed to determine whether the mutants were less able to survive under ER stress compared to WT cells. The leftmost spot in each row represents the undiluted cells that were initially spotted onto the plate. The number of cells in each subsequent spot to the right is reduced by 10-fold, resulting in a final dilution of 10^{-5} of the original cell number in the rightmost spot (Fig 6.1 A). All the spots were standardised to the lowest recorded

OD_{600} value as described in materials and methods, chapter 2.2.2. Each row in the assays represented a different mutant strain of cells that were exposed to different concentrations of ER stressors. The growth and survival of the cells across the different spots and concentrations were examined to assess the impact of the mutations on ER stress tolerance and survivability. I used different drugs in the assay to ensure that any effects on growth were caused by ER stress (Fig 6.1 B). Overall, the spotting assays revealed that the D797A Ire1 mutant in the catalytic domain was less able to survive under ER stress than WT cells and other mutants (Figs 6.2, 6.3 and 6.4). These results provide further evidence that the UPR plays a critical role in promoting ER stress tolerance and survival under adverse conditions. Figure 6.2 shows spotting assays performed with Ire1 cells expressing WT or mutant Ire1 alleles, including D797A, N802A, K799A, D828A, and double mutants D797A N802A, D797A D828A, and D797A K799A, from YCplac33. The mutations were compared with WT and an empty vector (-). The results indicated that D797A Ire1 cells were more sensitive to ER stress. All single mutants, including K799A, N802A, D828A, and D797A cells, grew similarly in the absence of DTT, Tm, and 2DDG. However, D797A cells showed reduced ability to survive when grown on plates containing different drugs, indicating a defect in the D797A mutant during ER stress. Interestingly, when two mutants were combined by generating double mutants D797A K799A, D797A N802A, and D797A D828A, growth was restored. This indicates that when certain mutations are combined, they can have a potentiating effect on cell that restores growth on the plate. Overall, these results demonstrate that specific mutations in Ire1 can affect cell survival under ER stress conditions, and that combining K799A, N802A, or D828A with D797A mutations can enhance cell survival.

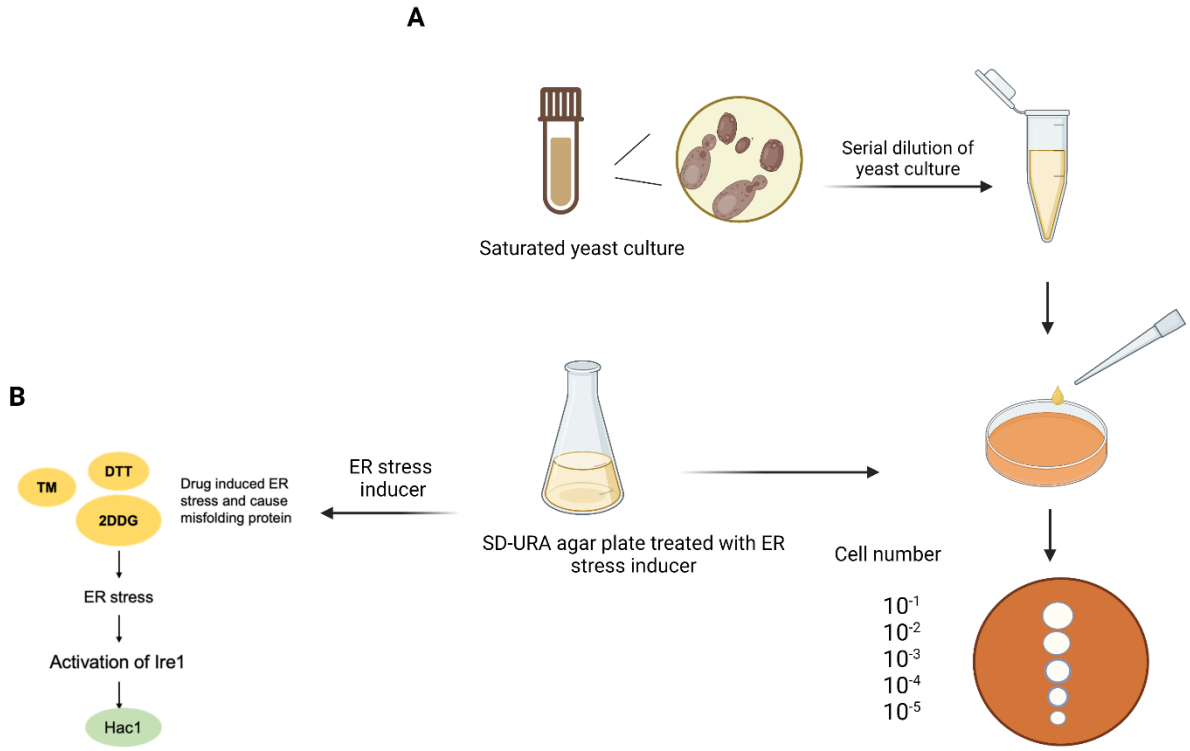

Figure 6.1. An illustration diagram of the Spotting Assay experiment.

A) spotting assay experiment. B) Scheme shows different drugs were used in experiment and their affect. Created with BioRender.com

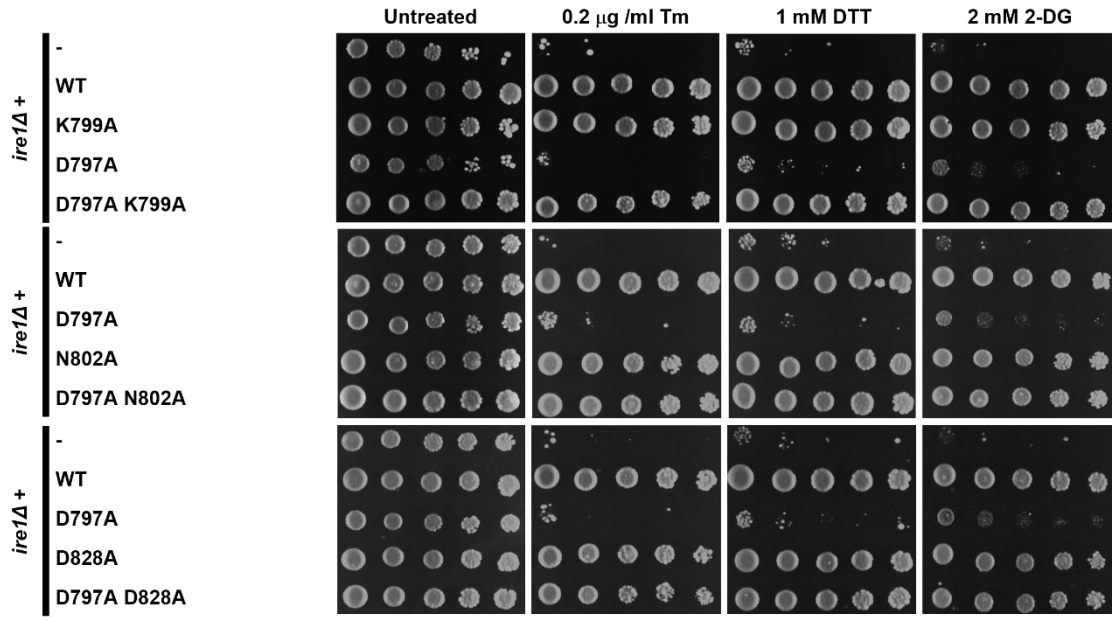

Figure 6.2. The introduction of a second mutant, such as K799A Ire1 or N802A Ire1, to the D797A Ire1 single mutant restored cell survivability.
Survival of ER stress by activation loop mutants. Serial 10-fold dilutions of fresh overnight cultures of *ire1*Δ cells expressing the indicated ire1 alleles from YCplac33 or carrying the empty vector (-) were spotted on SD agar plates lacking uracil and containing different concentrations of Tm (0.2 μg/ml), DTT (1 mM) and 2DDG (2 mM) and allow them to grow for 2 to 3 d before taking the images. The results show that D797A cells were reduced in their ability to survive when grown on plates with different induced of drugs. The experiment was repeated three times with the same results.

In Figure 6.3, spotting assays were conducted with Ire1 mutants and WT Ire1 using different inducers. The results showed that the single mutant D797A had reduced growth on plates containing growth medium with 1 mM DTT, 2 mM 2DDG, and 0.2 μg/ml Tm. In contrast, other mutants, such as K799A N802A D828A, K799A D828A, N802A D828A, and K799A N802A Ire1, showed increased survival when grown on the same plates. Interestingly, when these mutants were introduced into the D797A Ire1 single mutant, growth was restored. This suggests that the addition of an extra mutation to D797A Ire1 led to an increase in cell growth and survivability, indicating that multiple mutations can contribute to an overall improvement in cellular response to stress. The mutants showed similar behaviour and were able to protect cells from ER stress. This is consistent with the idea of intragenic suppression, which means that one mutation can compensate for the negative effects of another mutation within the same gene.

Most mutants had similar levels of *KAR2* and *PDI1* mRNA as the WT Ire1 in response to ER stress. However, the K799A N802A D828A mutant stood out as it exhibited lower levels of *HAC1* splicing, *KAR2* mRNA, and *PDI1* mRNA as described in previous chapter 3.5 in Fig.

3.18 (Fig 6.3), indicating a potential defect in its ability to regulate gene expression under ER stress. To further investigate this, additional spotting assays were performed on plates containing increasing concentrations of Tm (0.3, 0.4, and 0.5 µg/ml) for the K799A N802A D828A and D797A K799A N802A D828A mutants, as well as the WT and an Ire1 lacking strain (-), all on the same plate. Figure 6.4 shows that the growth of these mutants was significantly reduced compared to the WT, suggesting a defect in their ability to cope with ER stress. The observed growth differences between the WT and the K799A N802A D828A mutant strains at higher concentrations of Tm can be attributed to the varying potency of ER stress induction. Tm, known for its powerful ability to induce ER stress, triggers a robust UPR. In contrast, milder ER stressors like DTT and 2DDG, although they activate the UPR by promoting protein misfolding, do not exhibit the same level of strength as Tm. During the experiments, different concentrations of DTT and 2DDG were tested, and it was determined that the optimal concentrations for promoting growth were 1 mM for DTT and 2 mM for 2DDG. Moreover, increasing the concentrations beyond these optimal levels still resulted in similar growth effects. As a result, the higher concentrations of Tm used in the experiment lead to a more potent and significant activation of the UPR compared to the milder ER stressors. This discrepancy in the strength of ER stress induction likely explains the observed growth differences between the WT and the K799A N802A D828A mutant strains at higher concentrations of Tm. Overall, while some mutants showed significant differences in their steady-state levels of expression of the UPRE-*lacZ* reporter, these differences did not appear to reflect on the growth abilities of the different yeast strains.

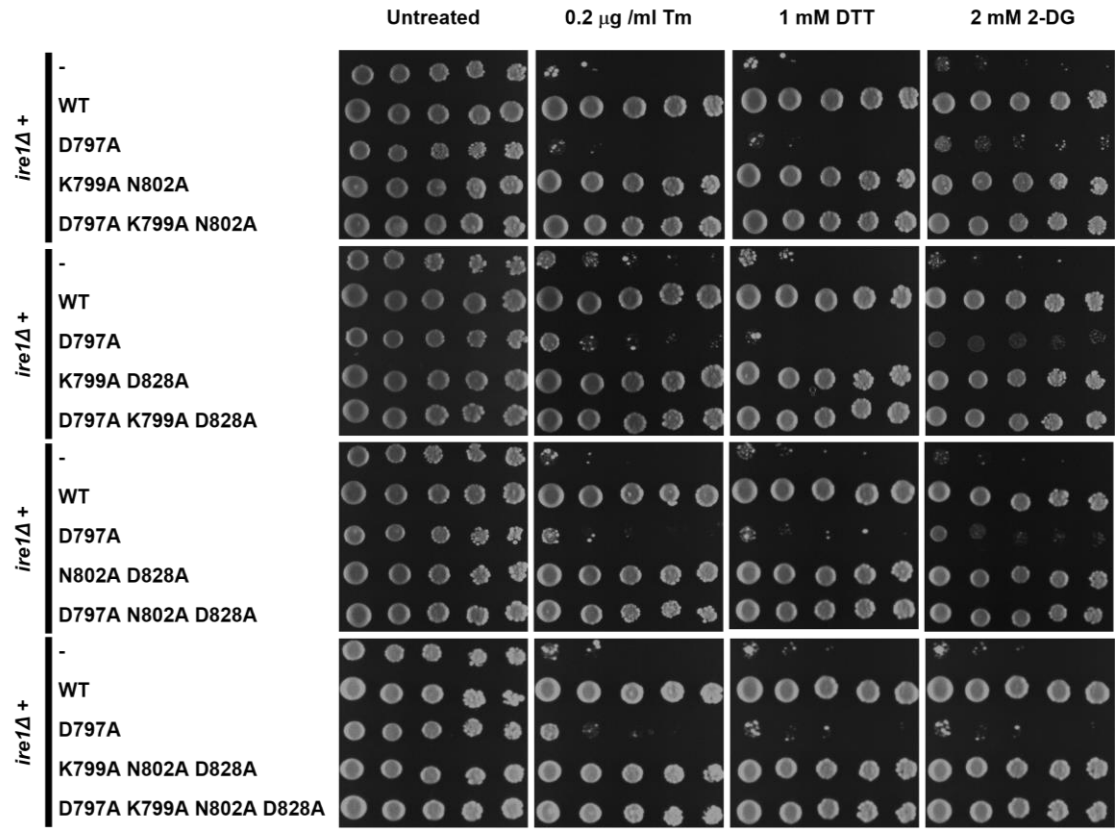

Figure 6.3. Cell survivability was restored when multiple mutations of K799A, N802A, and D828A were introduced to the D797A-Ire1.
Survival of ER stress by activation loop mutants. Serial 10-fold dilutions of fresh overnight cultures of *ire1*Δ cells expressing the indicated *ire1* alleles from YCplac33 or carrying the empty vector (-) were spotted on SD agar plates lacking uracil and containing different concentrations of Tm (0.2 μg/ml), DTT (1 mM) and 2DDG (2 mM) and allow them to grow for 2 to 3 d before taking the images. The results show that D797A cells were reduced in their ability to survive when grown on plates with different induced of drugs. The experiment was repeated three times with the same results.

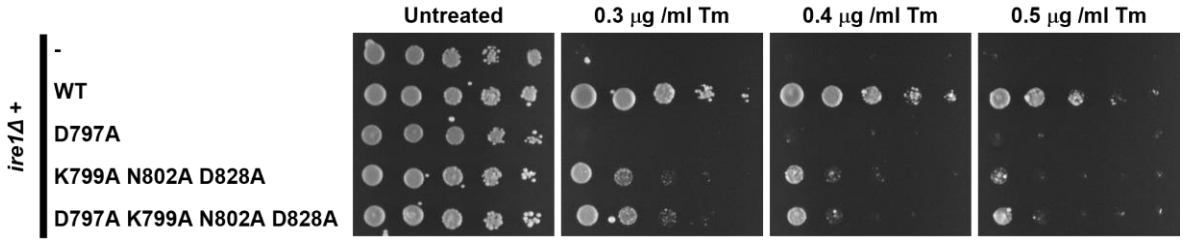

Figure 6.4. Spotting assays of K799A- N802A- D828A- and D797A- K799A- N802A- D828A- Ire1 on plates with increasing Tm concentrations.
The results show that the inclusion of these mutants decreases survivability of ER stress in cells at higher concentrations of Tm. These assays were repeated three times with reproducible results.

6.2 Discussion

The data suggest that combining D797A with other mutants, such as K799A, N802A, and D828A, enhances the ability of the cells to tolerate ER stress and improve growth. The D797A Ire1 mutant showed the most significant decrease in survival during ER stress, whereas other double mutants, such as D797A K799A, exhibited an increased ability to grow compared to the single mutant D797A Ire1 (Fig. 6.2). The D797A mutation caused a reduction in the survivability of ER stress to a degree comparable to the negative control where the empty vector was used. Although *HAC1* splicing was observed in the D797A mutant, there was no protection against ER stress, and no increase was observed in *KAR2* and *PDI1* mRNA, or the UPRE-*lacZ* reporter (Figs. 3.1, 3.5, 4.4, and 6.2). This suggests that the *HAC1* splicing observed in the D797A mutant is not sufficient to elicit a robust UPR and provide effective protection against ER stress. One interesting finding was the enhanced survival of the D797A mutant during ER stress when combined with other mutants, as shown in Figures 6.2, 6.3 and 6.4. Since the UPR pathway is known to promote ER stress tolerance (Jäger et al., 2012; Lin et al., 2007), the spotting assay experiments suggest that the activity of the mutant protein with D797A residue in the catalytic domain is rescued by the addition of other mutations. Based on the results, it was observed that the D797A mutants exhibited higher levels of *HAC1* splicing compared to the strain with *IRE1* deletion. However, despite the increase in *HAC1* splicing, it was found that this elevation did not have a significant physiological effect. Additionally, the levels of *KAR2* and *PDI1* mRNAs remained unchanged in the D797A mutants. Further analysis of the expression levels of *KAR2* and *PDI1* mRNA, showed significant differences between the D797A mutant and the WT Ire1. The UPR pathway in yeast plays an important role in promoting cell tolerance and survival during ER stress, as reported in previous studies (Cox et al., 1993). The D797A mutation has a significant impact on the UPR response, albeit not in the same manner as the WT Ire1 or other UPR pathway regulators. In conclusion, data provide evidence that the D797A mutation has a significant impact on the UPR response in yeast, as demonstrated by reduced survival during ER stress and impaired activation of UPR pathway markers. The data suggest that *HAC1* splicing may have a weaker correlation with cell growth compared to changes in *KAR2* and *PDI1* mRNA levels. Furthermore, our findings demonstrate that the addition of other mutations can rescue the reduced survival phenotype of the D797A mutant, highlighting the complexity of UPR regulation.

7 CHARACTERISATION OF IRE1 MUTATION CLUSTERING UNDER ER STRESS

7.1 Rationale

Upon detecting unfolded proteins in the ER lumen, Ire1 can form dimers and potentially promote oligomerisation. This mechanism is still not fully understood and remains a subject of debate. Some studies suggest that the formation of a disulphide bond between cysteine residues in the cytoplasmic domain of Ire1 is critical for dimerisation (Kimata et al., 2007; Zhou et al., 2006). Other studies propose that the interaction between the luminal domains of Ire1 plays a more important role in dimerisation and activation (Credle et al., 2005; Pincus et al., 2010). In addition to dimerisation, there is evidence that Ire1 can also form higher-order oligomers, although the functional significance of this phenomenon is not clear (Aragón et al., 2009; Kimata et al., 2007; Korennykh et al., 2009) Nevertheless, it is known that Ire1 molecules cluster in response to ER stress. Therefore, it is crucial to confirm that clustering of Ire1 is occurring in all the mutants being studied to ensure that the observed results are not due to a failure in Ire1 clustering, which could result in a reduced activation of the unfolded protein response. Ire1 clustering is an essential step in initiating the ER stress response and is a useful indicator of UPR activation response (Aragón et al., 2009; Kimata et al., 2007). This confirmation is particularly important when conducting β-galactosidase reporter assays, Northern blots, and spotting assays, as the observed results could be influenced by Ire1 clustering. By verifying that clustering is occurring in all mutants, the study can be certain that the observed results are due to the specific mutations being studied and not due to deficiencies in Ire1 clustering. I used a genetically modified strain of *S. cerevisiae* (MSY14-02) to investigate how Ire1 protein clusters in response to the accumulation of unfolded proteins. The strain was transformed with two plasmids: pJK59 and pEvA97.

The pJK59 plasmid carries a genetic sequence encoding a fusion protein consisting of green fluorescent protein (GFP) fused to Sec63, which is a mutant form of Sec63 with two mutations (S65T and V163A) that increase the fluorescence of the GFP protein (Crameri et al., 1996; Miesenböck et al., 1998). This allowed me to visualise ER membrane. The decision to use the MSY14-02 strain was based on prior work by the Schröder laboratory at Durham University, which had determined that this strain was optimal for observing an ER distribution of mCherry-tagged Ire1 expressed from plasmid pEvA97 which was used to visualise the localisation of Ire1.

During a 1 h time course, images were taken using a Zeiss LSM 880 microscope with Airyscan to observe how cells reacted to ER stress induced by 2 mM of DTT. According to previous studies (Aragón et al., 2009; Kimata et al., 2007), if the protein Ire1 is not activated by ER stress, then it will not form specific sites called foci. The expected behaviour of Ire1 in the WT is to form clusters of the mCherry signal after approximately 15 min. The microscope images were taken following the design and manufacturing of different Ire1 mutants. Sub-cloning was used to construct the final plasmid, which was then extracted from *E. coli* and digested using enzymes to validate the presence of the desired mutations. Next, I described the process of designing and manufacturing these plasmid constructs.

7.2 The process of cloning of the constructed plasmids

To create the final plasmid pEvA97-Ire1 mutant for testing different mutants using a microscope (Fig 7.1), sub-cloning techniques were used. First, the *Bss*HII-*Sac*I fragment (3493 bp) from pEvA97 was sub-cloned into YCplac33-IRE1-HA, using appropriate restriction enzymes and T4 DNA ligase for ligation. The resulting plasmid, YCplac33-mCherry-IRE1-HA, carried the genetic construct encoding the fluorescence protein Ire1 tagged with mCherry. Next, the *Hin*dIII-*Bam*HI fragment (2682 bp) from YCplac33-mCherry-IRE1-HA was sub-cloned into pEvA97 using the same techniques. To confirm the proper sub-cloning and ligation of the DNA fragments, restriction digest analysis was performed on the recombinant plasmids with suitable restriction enzymes. The resulting fragments were analysed using gel electrophoresis and compared to control plasmids as described in the methods chapter 2.2.7.

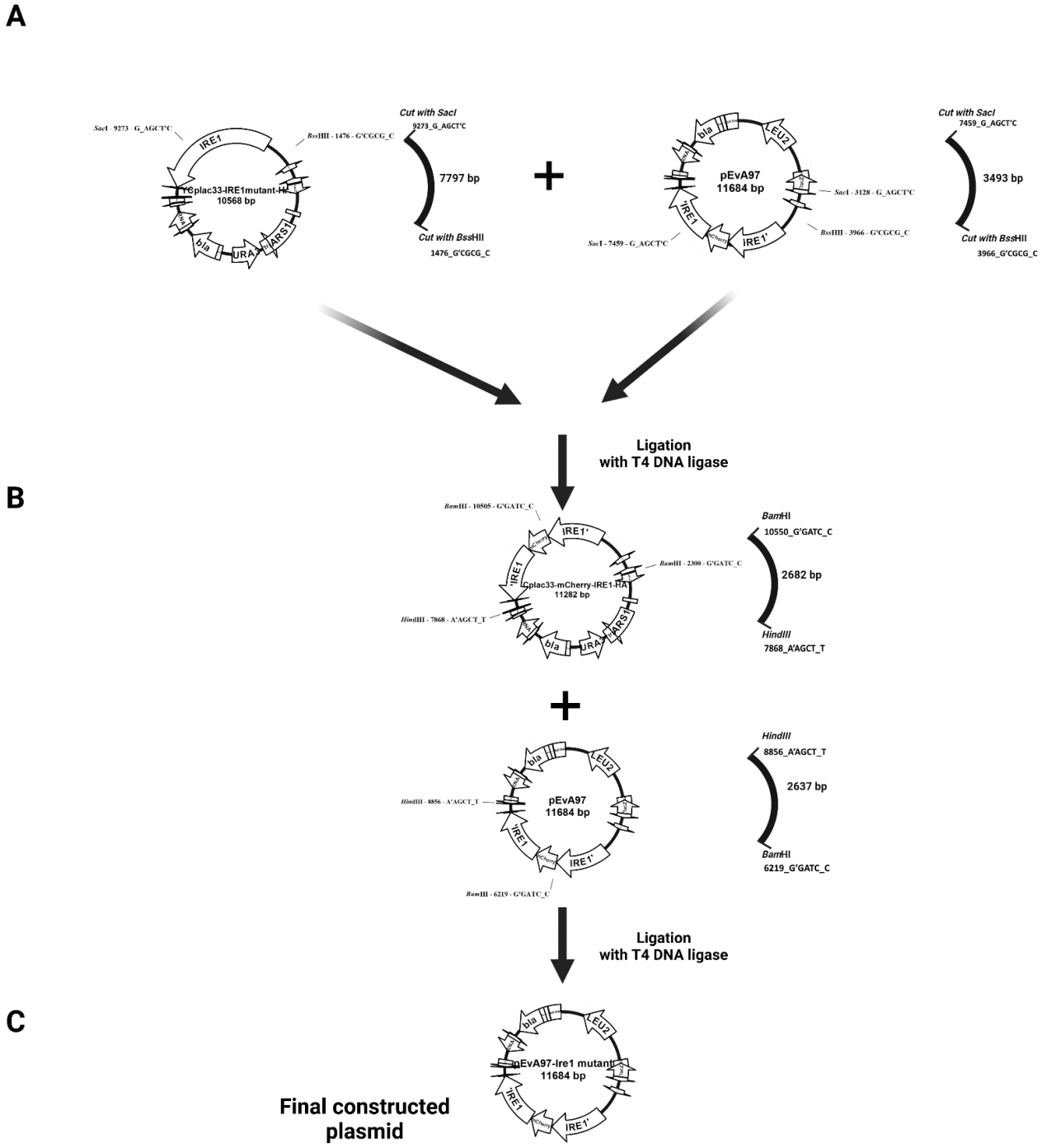

Figure 7.1. An illustration of a cloning strategy used to generate different mutants of Ire1 for microscopy analysis.

The strategy involves the following steps: A) The plasmid containing the different Ire1 mutants is digested with the *Bss*HII and *Sac*I restriction enzymes, which cut a 3493 bp fragment in green colour from pEvA97 and a 7797 bp fragment from YCplac33-IRE1-HA. The two fragments are then ligated together using T4 DNA ligase to form the plasmid YCplac33-mCherry-IRE1-HA. B) The 2682 bp fragment from YCplac33-mCherry-IRE1-HA is ligated with pEvA97 in place of the cut 2637 bp fragment, using T4 DNA ligase to form the final constructed plasmid, pEvA97-Ire1 mutant. C) The resulting plasmids are transformed into *S. cerevisiae* to generate different mutants of Ire1 suitable for microscopy analysis. Created with BioRender.com

7.3 No differences in clustering phenotypes of WT and mutant Ire1 under ER stress

To observe cells expressing both Ire1 and Sec63, a two-channel method was used. Moreover, only cells that showed signals from both Ire1-mCherry and Sec63-GFP were selected for imaging. The purpose of this approach was to investigate the localisation and behaviour of Ire1 during ER stress. Under normal conditions, the Ire1 signal should be evenly distributed along the cortical and perinuclear ER membrane without any specific foci sites (Fig.7.2), as the UPR is not activated (Kimata et al., 2007). The Sec63 protein, which is commonly used as an ER marker, is an ER membrane protein (Prinz et al., 2000; Voeltz et al., 2007) and should remain unaffected by the introduction of ER stress from DTT. This serves as a control to ensure that any observed phenotype is not due to the introduction of the Ire1 mutations and confirms the localisation of Ire1-mCherry to the ER membrane.

Under conditions of ER stress, the Ire1 protein starts to form clusters, which can be observed from the 15 min in figures 7.3, 7.4, 7.5, and 7.6 (provided below). This clustering occurs as the Ire1 proteins assemble along the ER, resulting in a stronger mCherry signal. To prove that there is no visible difference in appearance, all mutations must show the same features as WT protein at every time point. The images shown below are representative of the mutant proteins. To minimise the risk of photo-bleaching caused by prolonged laser exposure, the experiment involved taking 5 to 10 images of each mutant protein under the microscope, with each image containing an average of 2 to 5 cells. Although observing one cell at a time over the time course would have been ideal for the experiment, it was not feasible. Nevertheless, the approach used in this study should provide an accurate representation of Ire1 clustering in the mutants induced by ER stress using 2 mM of DTT.

Fluorescence microscopy images reveal that Ire1 protein clusters along the ER membrane in response to unfolded protein accumulation, but it does not indicate whether RNase activity is present. To confirm that the reduction in ER stress response observed in the D797A and other mutants is not due to a clustering phenotype, it would be expected that all mutants behave similarly to the WT. Figures 7.3, 7.4, 7.5, and 7.6 demonstrate that the mutations, including those with the D797A mutation or other combinations of mutations, cluster similarly to the WT. This suggests that the mutations do not prevent Ire1 clustering, indicating that specific individual mutations or their combinations within the gene may not be crucial for the formation of Ire1 clusters. After 15 min of exposure to DTT, it becomes apparent that the

molecules are clustering together. Then, after 60 min, the signal from the protein Ire1 can be seen in specific locations, called foci, along the membrane of the ER.

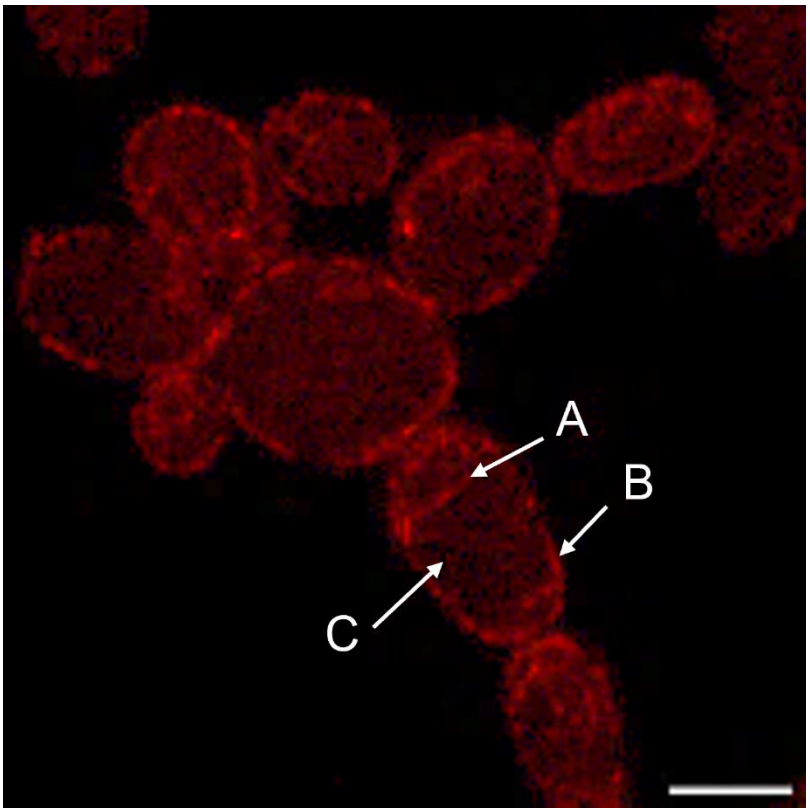

Figure 7.2. Localisation of mCherry-tagged Ire1 Protein in uninduced WT Cells
MSY 14-02 which contains Ire1 protein that has been tagged with a fluorescent molecule called mCherry. Ire1 protein is located in three places within the cell: (A) near the nucleus (perinuclear), (B) near the outer edge (cortical) of the ER and (C) the cell body (the fluorescence in the cell body arises from fluorescence in the vacuole (Schroeder, unpublished). The image provided has a scale bar that measures 5 µm.

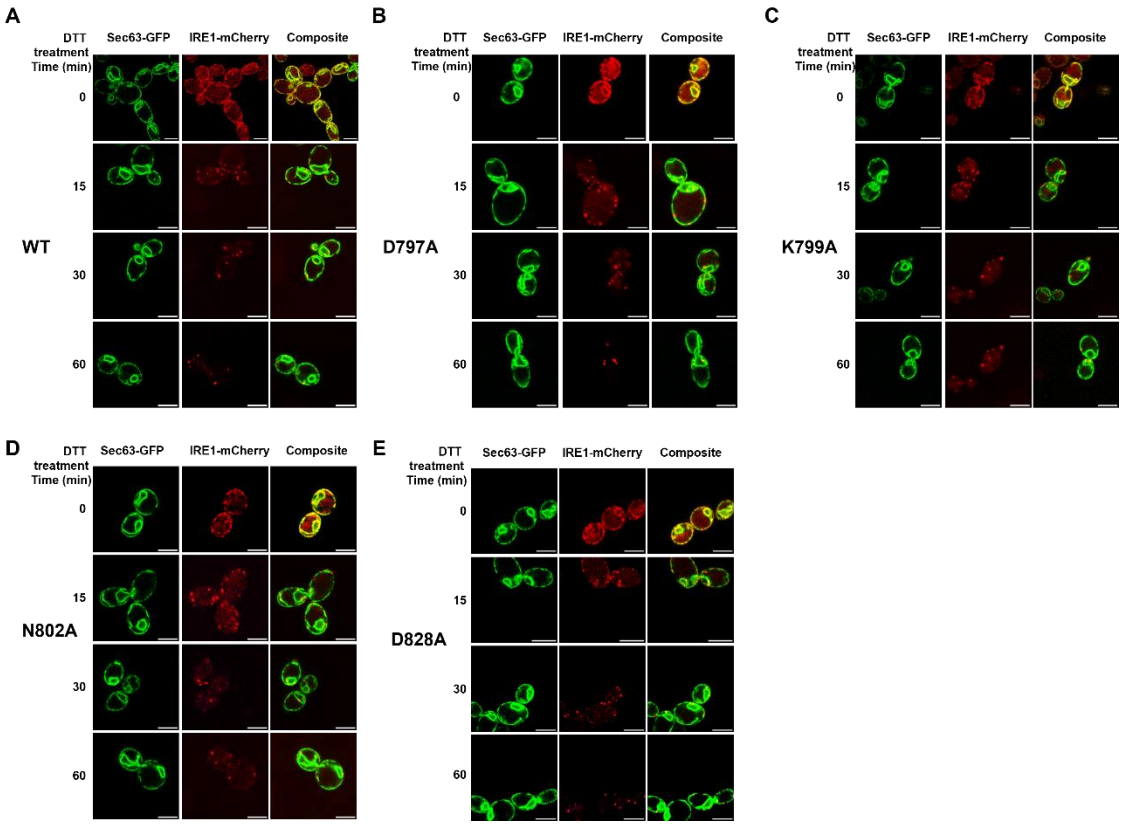

Figure 7.3. Time course analysis of Ire1 Protein mutants in response to DTT exposure.
Time course analysis of different mutants of the Ire1 protein, including (A) WT, (B) D797A, (C) K799A, (D) N802A, and (E) D828A, in response to increasing exposure to DTT over time. At the beginning (0 min), the Ire1 protein was localised along the membrane of the cortical and perinuclear ER. As the exposure to DTT increased, the Ire1 signal started to cluster into specific foci sites, which became more pronounced by the 60 min time point. The signal remained somewhat evenly spread along the cortical ER but decreased as the treatment time progressed. The Ire1 protein signal appeared to be solely confined to the foci sites after 60 min of DTT exposure. Scale bar 5 µm.

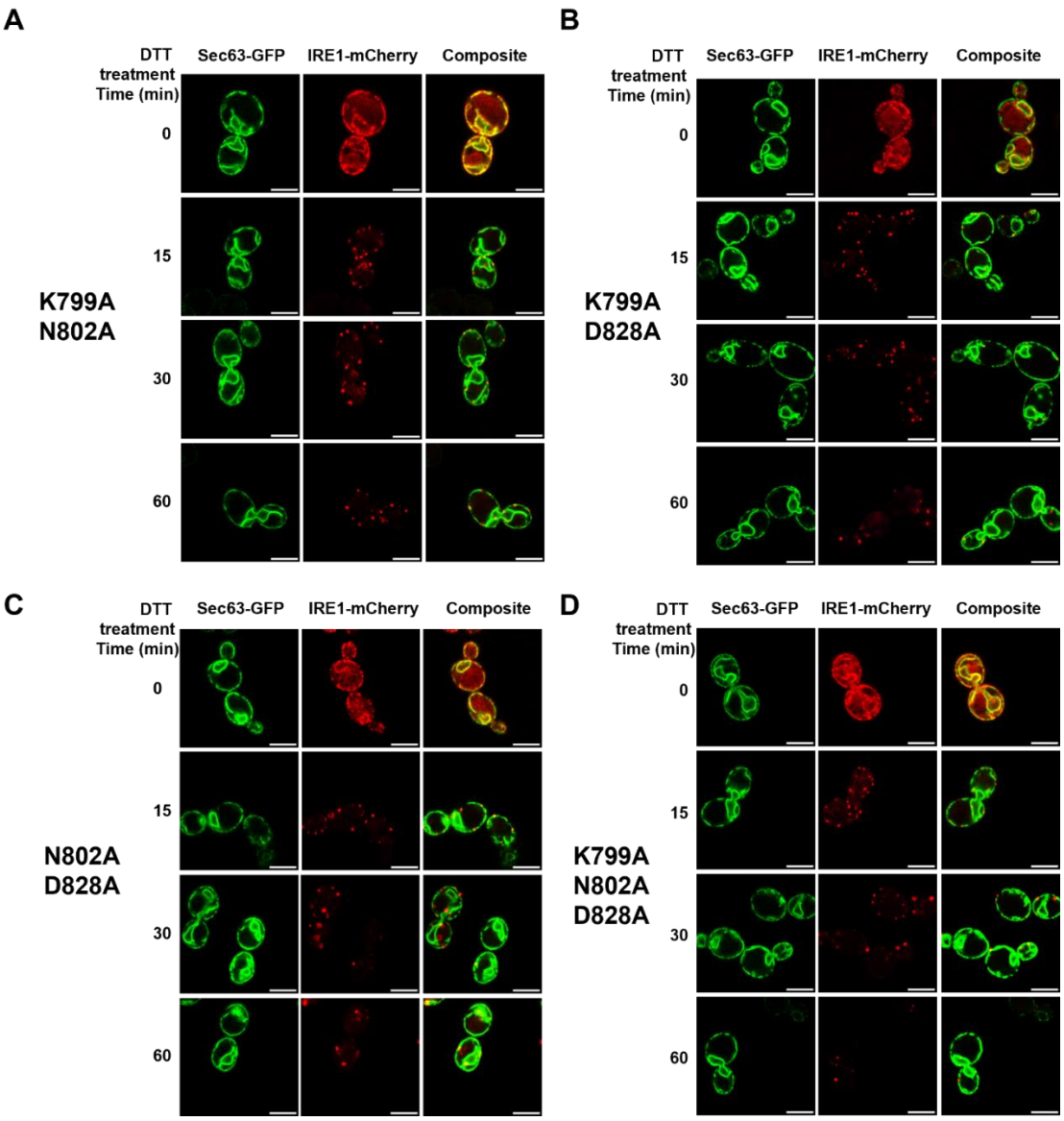

Figure 7.4. Time course analysis of double and multiple mutants of the Ire1 protein.
Time course analysis of double and multiple mutants of the Ire1 protein, including (A K799A N802A, (B) K799A D828A, (C) N802A D828A, and (D) K799A N802A D828A, in response to increasing exposure to DTT over time. At the beginning (0 min), the Ire1 protein was localised along the membrane of the cortical and perinuclear ER. As the exposure to DTT increased, the Ire1 signal started to cluster into specific foci sites, which became more pronounced by the 60 min time point. The signal remained somewhat evenly spread along the cortical ER but decreased as the treatment time progressed. The Ire1 protein signal appeared to be solely confined to the foci sites after 60 min of DTT exposure. Scale bar 5 µm.

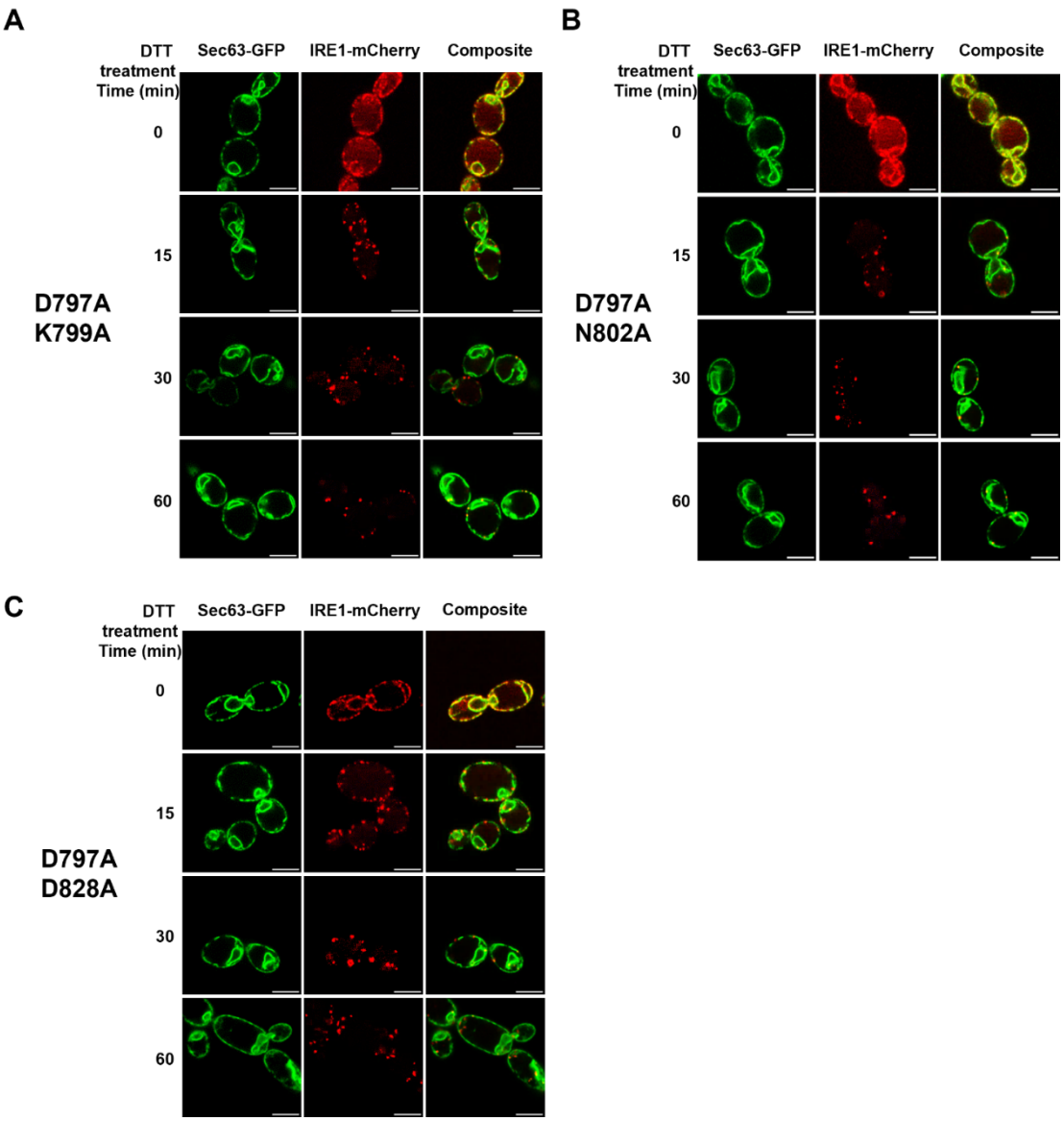

Figure 7.5. Microscope Images: Effect of Adding D797A Mutation to single Ire1 Protein Mutants.
Microscope images demonstrating the effect of adding the D797A mutation to the single mutants of the Ire1 protein, including (A) K799A, (B) N802A, and (C) D828A, during DTT treatment over time. Similar to the other mutants, the formation of Ire1 foci sites occurred after 15 min of DTT treatment, and after 60 min, the signal of Ire1 appeared to be confined solely to the foci sites. The inclusion of the D797A mutation to other mutants resulted in the same arrangement of DTT stress foci sites as observed in the other mutants. Scale bar 5 µm.

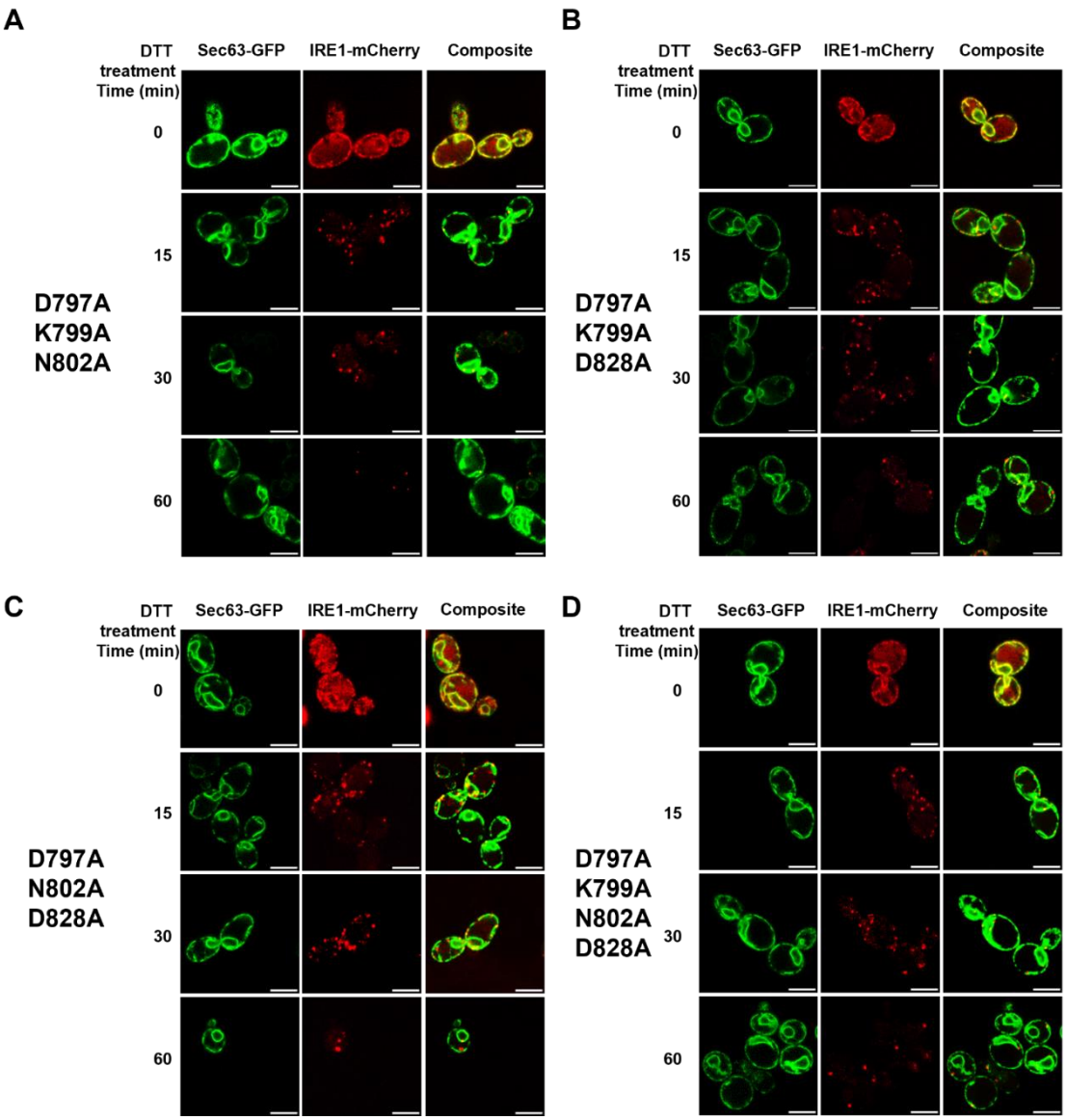

Figure 7.6. Microscope Images: Effect of Adding D797A Mutation to Double and Triple Ire1 Protein Mutants

Microscope images showed the effect of adding the D797A mutation to various double or multiple mutants of the Ire1 protein, including (A) K799A N802A, (B) K799A D828A, (C) N802A D828A, and (D) K799A N802A D828A, during DTT treatment over time. Similar to the other mutants, the formation of Ire1 foci sites occurred after 15 min of DTT treatment, and after 60 min, the signal of Ire1 appeared to be confined solely to the foci sites. The inclusion of the D797A mutation to other mutants resulted in the same arrangement of DTT stress foci sites as observed in the other mutants. Scale bar 5 µm**.**

7.4 Discussion

Previous studies have shown that Ire1 can form oligomers and that oligomerisation is required for RNase activity (Korennykh et al., 2009; Lee et al., 2008). However, the data presented here suggest that the reduction in ER stress signalling observed in the D797A and D828A mutations is not due to a clustering phenotype. The fact that all mutations behaved similarly to the WT regarding clustering indicates that the mutations tested do not result in a lack of Ire1 clustering. This suggests that protein kinase activity is not necessary for the formation or clustering of foci. It is important to note that the observation of foci sites only indicates clustering and does not confirm the formation of dimers or oligomers. The formation of foci sites in the Ire1 protein during ER stress signalling is not affected by phosphorylation, as indicated in previous research (Armstrong et al., 2017). Mutants of phosphoacceptor sites in the activation loop of Ire1 did not exhibit any qualitative defects in the formation of foci sites. Previous studies have shown that the D797A mutation affects both kinase and RNase activity of Ire1(Lee et al., 2008). The observed decrease in ER stress signalling in the mutant strains is not caused by an Ire1 clustering phenotype. Other functions of the Ire1 protein, in addition to clustering, could also be altered in these mutants. Additionally, it is important to mention that the current analysis is qualitative, and more subtle defects in foci formation may not have been detected. Therefore, it is concluded that the observed reduction in ER stress signalling in *HAC1* splicing and β-galactosidase activity cannot be solely attributed to a lack of clustering in the mutants. To further investigate the formation and structure of Ire1 oligomers, the crystal structure of Ire1 under ER stress conditions would need to be determined. Therefore, understanding the structure of Ire1 oligomers could provide insight into the regulation of Ire1 RNase activity and its role in UPR activation.

8 FINAL DISCUSSION

8.1 Ire1 RNase activity does not require kinase activity

Ire1 is a bifunctional protein kinase-endoribonuclease (RNase), and it becomes active when there is an accumulation of unfolded proteins in the ER lumen. Under ER stress conditions, Ire1 forms complexes and activates its RNase domain. The smallest functional unit showing RNase activity is the Ire1 dimer (Ishiwata-Kimata et al., 2013; Lee et al., 2008). Adenine nucleotides play a critical role in promoting the dimerisation of the RNase domain, which is necessary for its RNase activity (Lee et al., 2008; Papa et al., 2003). Additionally, the formation of larger structures by Ire1 dimers may further enhance its RNase activity (Korennykh et al., 2009).

The kinase domain of Ire1 is believed to be involved in regulating the accessibility of adenine nucleotides to the nucleotide binding pocket (NBP) within the kinase domain, thereby influencing the activation of the RNase activity (Lee et al., 2008; Mannan et al., 2013a; Shamu & Walter, 1996).

The residues K799, N802, and D828 are deemed crucial for regulating the RNase activity of Ire1. Notably, K799 plays a significant role in catalysing the transfer of the γ phosphate of ATP, while D828 coordinates the β and γ phosphates with Mg^{2+}. Additionally, N802 likely participates in Mg^{2+} coordination. Previous studies have demonstrated that ADP exerts a more potent stimulatory effect on the RNase activity of Ire1 than ATP (Sidrauski & Walter, 1997) This finding highlights the critical role of ADP in activating the RNase domain and regulating the overall function of Ire1. The strategic positioning of residues K799, N802, and D828 within or near key catalytic sites involved in ATP transfer and phosphate coordination with Mg^{2+} suggests that when ADP binds to Ire1 carrying these mutations, it may form more stable interactions compared to ATP. This enhanced binding affinity between ADP and the mutant residues could induce conformational changes within the active site region of Ire1, facilitating optimal substrate alignment for efficient cleavage by its RNase domain. The activation of the RNase domain by ADP is crucial for effectively regulating the function of Ire1 in response to cellular stress.

In the current study, intriguing results were obtained for these same mutants. The K799A mutant showed RNase activity similar to that of the WT Ire1. However, the N802A and D828A Ire1 mutants exhibited partial retention of RNase activity, displaying reduced levels

compared to WT Ire1 (Figs. 3.4, 3.5, 4.2 E and 4.2 F). Interestingly, these mutants displayed RNase activity, supporting the hypothesis that phosphorylation might not be essential for *HAC1* splicing (Chawla et al., 2011; Rubio et al., 2011).

This finding suggests that the absence of kinase activity may not be the sole factor governing the activation of the RNase domain. However, it is crucial to consider the possibility of residual protein kinase activity in the K799A mutant, even at significantly reduced levels. Previous studies have demonstrated that certain mutants with substantially diminished protein kinase activity can still retain a fraction of the WT activity, approximately 0.3 % (Gibbs & Zoller, 1991). This raises the question of whether even a minor amount of kinase activity could suffice to support the observed RNase activity in the K799A, N802A, or D828A mutants. Moreover, exploring the potential involvement of other cellular protein kinases that might compensate for Ire1 in phosphorylating its activation loop and facilitating ATP/ADP binding is essential.

The findings from L. Sutcliffe, PhD thesis, Durham University, where the D711A- IRE1α mutant was found to support XBP1 splicing, provide additional information into the complexity of IRE1 regulation. The D711A mutation in human IRE1α disrupts the DFG motif. The observation that the D711A mutant retains XBP1 splicing activity despite DFG motif disruption in human IRE1α suggests the presence of alternative residues or regulatory factors that can contribute to the activation of the RNase domain in mammalian cells. In this study, the D828A mutant, which also disrupts the DFG motif, similar to the D711A IRE1α mutant known to stabilise the active conformation of many protein kinases. Surprisingly, despite this disruption, the D828A mutant was found to retain *HAC1* splicing activity, bypassing the need for phosphorylation by Ire1.

This intriguing finding indicates that the DFG motif may not be the sole determinant of the RNase activity of IRE1α and its ability to carry out XBP1 splicing. Considering the differences in ADP/ATP regulation between yeast and mammalian Ire1/IRE1α, it becomes essential to closely examine the activation mechanisms of IRE1α in mammals. Understanding the unique regulatory features of mammalian IRE1 proteins, such as the unexpected splicing activity observed in the D711A mutant and the *HAC1* splicing activity in the D828A mutant in yeast, will be crucial for developing effective therapeutic strategies for ER stress-related diseases in humans.

8.2 Impaired RNase activity in the D797A mutation

The D797A mutation in Ire1 leads to impaired *HAC1* splicing, as supported by previous research showing that this mutation lacks detectable protein kinase or RNase activity (Lee et al., 2008). In my investigation, I confirmed a significant reduction in RNase activity in the D797A mutant compared to the WT Ire1.

The consequences of the D797A mutation extend beyond the impairment in RNase activity. It also reduces UPR target gene induction and disrupts the connection between Ire1 and its downstream effector, *HAC1* mRNA (Fig. 4.2 C). This disturbance in the connection impairs *HAC1* mRNA splicing and translation, eventually leading to diminished UPR activation (Fig. 3.2 C). Furthermore, the D797A mutant of Ire1 has a much worse cell survival during ER stress than the WT Ire1 (Fig. 6.2-6.4). The critical role of the D797 residue in kinase activity and autophosphorylation highlights its importance in activating the RNase domain and facilitating efficient *HAC1* splicing. The disruption caused by the D797A mutation leads to compromised RNA cleavage and processing, resulting in reduced *HAC1* splicing and impaired activation of downstream targets involved in the UPR.

In my observations of cells expressing D797A Ire1 (Figs. 3.1, 3.11, 3.14, and 3.15), I noticed the presence of weak bands corresponding to RNA molecules displaying characteristics of both splicing intermediates and cleavage intermediates of *HAC1* mRNA. The qualitative increase in these bands in D797A suggests that the defect in this mutant may not solely arise from a deficiency in RNase activity but might also be related to a potential impairment in the ligation process of the exons (Fig. 3.21). One possible explanation for this finding could be related to a defect in tRNA ligase within the cells. tRNA ligase is an enzyme responsible for catalysing the ligation or joining of RNA molecules, specifically tRNA molecules, during various cellular processes, including RNA splicing.

If there is a defect or impairment in the tRNA ligase activity within the cells carrying the D797A mutation, it could affect the proper ligation of *HAC1* exons during the splicing process. As a result, the ligation process might not be as efficient or accurate, leading to the observed increase in bands on the Northern blots.

In summary, the D797A mutation in Ire1 leads to impaired RNase activity, resulting in reduced *HAC1* splicing and compromised downstream UPR activation. The presence of weak bands on the Northern blots indicates potential impairment in the ligation process of *HAC1*

exons, highlighting the importance of RNase activity in efficient *HAC1* splicing and UPR activation.

8.3 Rescue D797A by other mutants K799A, N802A and D828A

The findings of this study demonstrated that the D797A mutant exhibits significantly impaired *HAC1* splicing, indicating a deficiency in its ability to cleave and process RNA efficiently. Interestingly, the introduction of the K799A, N802A, and D828A mutations effectively rescues the RNase activity of the D797A mutant, leading to restored *HAC1* splicing and improved expression of UPR target genes (Figs. 3.9, 3.12 and 3.13). While the D797A mutant shows compromised RNA cleavage and processing, resulting in reduced *HAC1* splicing, the K799A, N802A, and D828A mutants may exhibit different effects on the activation of the RNase domain. These residues (K799, N802, and D828) have been identified as crucial for regulating the RNase activity of Ire1, with K799 being involved in catalysing the transfer of the γ phosphate of ATP, D828 coordinating the β and γ phosphates with Mg^{2+}, and N802 likely participating in Mg^{2+} coordination.

The differences in phenotypes between the D797A mutant and the K799A, N802A, and D828A mutants could be attributed to the specific functions of these residues in the RNase activation process. For example, the D797A mutation may directly impair the activation of the RNase domain, leading to reduced *HAC1* splicing and UPR activation. On the other hand, the K799A, N802A, and D828A mutants may still retain some level of RNase activity, allowing for partial *HAC1* splicing and UPR activation.

Regarding the D797A K799A double mutant showing more *HAC1* splicing than the D797A mutant (Fig. 3.9), this result could be explained by the compensatory effects of the K799A mutation. The K799A mutation partially rescues the impaired RNase activity caused by the D797A mutation, resulting in increased *HAC1* splicing compared to the D797A mutant alone. The K799A mutation, located in or near the active site of the Protein kinase domain, may interact with critical residues or domains, leading to alterations in the domains structure or activity. These changes induced by the K799A mutation can potentially enhance the functionality of the RNase domain, allowing it to cleave and process RNA more efficiently, despite the presence of the D797A mutation.

In the previous studies (Han et al., 2009; Upton et al., 2012), inhibiting IRE1α kinase activity increased survival during ER stress. This suggests that IRE1α kinase activity may negatively

influence the UPR response under specific ER stress conditions or that the protein kinase activity activates apoptosis. The current work, on the other hand, shows that the D797A mutant, which lacks detectable kinase activity, retains some RNase activity, and that this activity may be boosted further by adding mutations in the kinase domain (K799A, N802A, and D828A). This indicates that the kinase domain may have a modulatory or compensatory function in controlling the RNase activity of Ire1, which modulates the UPR response.

Furthermore, my results raise intriguing issues concerning the potential interaction between the kinase and RNase activities of Ire1 and their contributions to cell survival during ER stress.

This study sheds light on the complexities of the role of Ire1 in UPR control and cell survival. The rescue of the D797A mutant by the K799A, N802A, and D828A mutations highlights the significance of these residues in modulating RNase activity and suggests potential therapeutic targets for ER stress-related diseases.

9 CONCLUSION AND FUTURE STUDIES

9.1 Conclusion

The study has demonstrated the critical role of intragenic suppression in compensating for the RNase-defective D797A mutation within the Ire1 protein kinase domain. Combining the D797A mutant with K799A, N802A, and D828A mutations provides additional understanding and specific mechanisms to enhance cellular responses to ER stress and UPR activation. Maximizing the beneficial effects of the loss of RNase activity due to the D797A mutation, intragenic suppression is essential. This can be achieved by combining D797A with other mutants such as K799A, N802A, and D82A residues to retain maximum UPR activation. These combined mutations may potentially bypass the need for phosphorylation, or they might still allow for sufficient phosphorylation to enable RNase activity.

While phosphorylation events are known to be critical for Ire1 activation and regulation, the observed results with the K799A, N802A, and D828A mutants suggest the existence of additional pathways or factors that can enhance the function of D797A through intragenic suppression.

The residue K799 plays a critical role in the ATP-binding pocket of this domain (Adams, 2001), being essential for ATP binding and catalysis. Furthermore, the residues N802A and D828A are involved in coordinating magnesium ions and neutralising charges on the phosphate groups of ATP/ADP. These residues, particularly K799A, are significant in their interaction with the phosphates of ATP/ADP through Mg^{2+} ions, thereby contributing to their functional importance.

Characterisation of specific single point mutations, including K799A, N802A, and D828A, revealed their ability to restore RNase activity in the D797A mutant, resulting in an increased percentage of *HAC1* splicing, improved survival ability, and enhanced expression of UPRE-*lacZ*. However, combining two of these mutations, such as K799A N802A and K799A D828A, did not show significant differences in the percentage of *HAC1* mRNA, *KAR2*, and *PDI1* levels, survival ability, or the expression of UPRE-*lacZ* compared to the single point mutants. Similarly, when comparing N802A D828A to N802A or D828A alone, no significant differences were observed, casting doubt on the hypothesis that double mutations, including K799A N802A, K799A D828A, and N802A D828A, can fully restore RNase activity in the D797A mutant.

Overall, the work presented here suggests that the kinase domain may be the driving factor in the regulation of RNase activity in Ire1.

9.2 Future Studies

Given more time and resources, this project could be expanded to explore various approaches that can deepen our understanding of UPR regulation and its underlying mechanisms. Building upon the findings of this study, several potential research directions can be pursued.

9.2.1 Characterisation of splicing intermediates in D797A

To further understand the role of these splicing intermediates and their implications for Ire1 function, future studies could focus on quantifying and characterising the weak bands in the defective mutant D797A Ire1 more precisely. An effective approach would be to compare the decay rates of $HAC1^{u}$ in yeast strains expressing different *IRE1* alleles, including the D797A mutant with the rlg1-148 mutation. This comparison would help determine whether the D797A mutant exhibits decreased RNase activity in *vivo*. Additionally, conducting in *vitro* RNA cleavage assays would directly assess the RNase activity of the D797A mutant and provide more information into the functional consequences of altered splicing intermediates. These investigations would shed light on the specific mechanisms underlying the impairment in ligation caused by the D797A mutation, offering more comprehensive information about its impact on Ire1 activity. These methods would help elucidate the specific mechanisms underlying the impairment in ligation and the functional consequences of altered splicing intermediates. These investigations would give more information into the molecular basis of the D797A mutation that impact on Ire1 activity and its significance in the context of the ER stress response and cell survival during ER stress.

9.2.2 Investigating Compensatory Mechanisms

Exploring compensatory mechanisms that enhance the function of the D797A mutant in the absence of phosphorylation is an intriguing area for future research. To investigate compensatory mechanisms that enhance the function of the D797A mutant in the absence of phosphorylation, introducing site-directed mutations in the phosphoacceptor sites within the activation loop can help determine their influence on the D797A mutant. Additionally, investigating the impact of the presence of D836 in the activation loop (Armstrong et al., 2017) on RNase activity can be achieved by creating mutants like K799A D836A, D828A

D836A, and N802A D836A. Identifying alternative phosphorylation sites within Ire1 or associated proteins that can compensate for the loss of phosphorylation at residue 797 could reveal regulatory pathways in UPR activation.

9.2.3 Exploring Post-Translational Modifications

Investigating post-translational modifications such as acetylation, methylation, or ubiquitination might reveal how these modifications specifically modulate the function of the D797A mutant.

9.2.4 Comparative Studies Across Organisms

Conducting comparative studies across different organisms, including humans, will not only validate the relevance of findings from *S. cerevisiae* but also uncover potential species-specific differences in UPR regulation. Understanding the regulatory processes underlying UPR activation holds significant therapeutic implications for diseases associated with ER stress and protein misfolding, providing potential targets for intervention and treatment.

10 BIBLIOGRAPHY

Bibliography

Adams, J. A. (2001). Kinetic and Catalytic Mechanisms of Protein Kinases. *Chemical Reviews, 101*(8), 2271-2290. https://doi.org/10.1021/cr000230w

Adolph, T. E., Tomczak, M. F., Niederreiter, L., Ko, H. J., Böck, J., Martinez-Naves, E., Glickman, J. N., Tschurtschenthaler, M., Hartwig, J., Hosomi, S., Flak, M. B., Cusick, J. L., Kohno, K., Iwawaki, T., Billmann-Born, S., Raine, T., Bharti, R., Lucius, R., Kweon, M. N., . . . Blumberg, R. S. (2013). Paneth cells as a site of origin for intestinal inflammation. *Nature, 503*(7475), 272-276. https://doi.org/10.1038/nature12599

Aebi, M., Bernasconi, R., Clerc, S., & Molinari, M. (2010). N-glycan structures: recognition and processing in the ER. *Trends Biochem Sci, 35*(2), 74-82. https://doi.org/10.1016/j.tibs.2009.10.001

Ali, M. M., Bagratuni, T., Davenport, E. L., Nowak, P. R., Silva-Santisteban, M. C., Hardcastle, A., McAndrews, C., Rowlands, M. G., Morgan, G. J., Aherne, W., Collins, I., Davies, F. E., & Pearl, L. H. (2011). Structure of the Ire1 autophosphorylation complex and implications for the unfolded protein response. *Embo j, 30*(5), 894-905. https://doi.org/10.1038/emboj.2011.18

Angel, P., Szabowski, A., & Schorpp-Kistner, M. (2001). Function and regulation of AP-1 subunits in skin physiology and pathology. *Oncogene, 20*(19), 2413-2423. https://doi.org/10.1038/sj.onc.1204380

Aragón, T., van Anken, E., Pincus, D., Serafimova, I. M., Korennykh, A. V., Rubio, C. A., & Walter, P. (2009). Messenger RNA targeting to endoplasmic reticulum stress signalling sites. *Nature, 457*(7230), 736-740. https://doi.org/10.1038/nature07641

Armstrong, M., Šesták, S., Ali, A. A., Sagini, H. A. M., Brown, M., Baty, K., Treumann, A., & Schröder, M. (2017). Bypass of Activation Loop Phosphorylation by Aspartate 836 in Activation of the Endoribonuclease Activity of Ire1. *Molecular and Cellular Biology, 37*.

Back SH, S. M., Lee K, Zhang K, Kaufman RJ. (2005). ER stress signaling by regulated splicing: IRE1/HAC1/XBP1. *Methods, 35*(4), 395-416.

Bertolotti, A., Zhang, Y., Hendershot, L. M., Harding, H. P., & Ron, D. (2000). Dynamic interaction of BiP and ER stress transducers in the unfolded-protein response. *Nat Cell Biol*, *2*(6), 326-332. https://doi.org/10.1038/35014014

Birnboim, H. C., & Doly, J. (1979). A rapid alkaline extraction procedure for screening recombinant plasmid DNA. *Nucleic Acids Research*, *7*(6), 1513-1523. https://doi.org/10.1093/nar/7.6.1513

Bonifacino, J. S., & Glick, B. S. (2004). The mechanisms of vesicle budding and fusion. *Cell*, *116*(2), 153-166. https://doi.org/10.1016/s0092-8674(03)01079-1

Boyce, M., & Yuan, J. (2006). Cellular response to endoplasmic reticulum stress: a matter of life or death. *Cell Death Differ*, *13*(3), 363-373. https://doi.org/10.1038/sj.cdd.4401817

Brodsky, J. L., & Skach, W. R. (2011). Protein folding and quality control in the endoplasmic reticulum: Recent lessons from yeast and mammalian cell systems. *Curr Opin Cell Biol*, *23*(4), 464-475. https://doi.org/10.1016/j.ceb.2011.05.004

Brown, M. S., & Goldstein, J. L. (1999). A proteolytic pathway that controls the cholesterol content of membranes, cells, and blood. *Proc Natl Acad Sci U S A*, *96*(20), 11041-11048. https://doi.org/10.1073/pnas.96.20.11041

Brown, T., & Mackey, K. (1997). Analysis of RNA by Northern and Slot Blot Hybridization. *Current Protocols in Molecular Biology*, *37*(1), 4.9.1-4.9.16. https://doi.org/https://doi.org/10.1002/0471142727.mb0409s37

Brownell, J. E., Zhou, J., Ranalli, T., Kobayashi, R., Edmondson, D. G., Roth, S. Y., & Allis, C. D. (1996). Tetrahymena histone acetyltransferase A: a homolog to yeast Gcn5p linking histone acetylation to gene activation. *Cell*, *84*(6), 843-851. https://doi.org/10.1016/s0092-8674(00)81063-6

Bulleid, N. J., & Ellgaard, L. (2011). Multiple ways to make disulfides. *Trends Biochem Sci*, *36*(9), 485-492. https://doi.org/10.1016/j.tibs.2011.05.004

Chapman, R. E., & Walter, P. (1997). Translational attenuation mediated by an mRNA intron. *Curr Biol*, *7*(11), 850-859. https://doi.org/10.1016/s0960-9822(06)00373-3

Chawla, A., Chakrabarti, S., Ghosh, G., & Niwa, M. (2011). Attenuation of yeast UPR is essential for survival and is mediated by IRE1 kinase. *J Cell Biol*, *193*(1), 41-50. https://doi.org/10.1083/jcb.201008071

Chen, D. C., Yang, B. C., & Kuo, T. T. (1992). One-step transformation of yeast in stationary phase. *Curr Genet*, *21*(1), 83-84. https://doi.org/10.1007/bf00318659

Chen, Y., & Brandizzi, F. (2013). IRE1: ER stress sensor and cell fate executor. *Trends Cell Biol*, *23*(11), 547-555. https://doi.org/10.1016/j.tcb.2013.06.005

Chomczynski, P. (1992). Solubilzation in formamide protects RNA from degradation. *Nucleic Acids Research*, *20*(14), 3791-3792. https://doi.org/10.1093/nar/20.14.3791

Christianson, J. C., & Ye, Y. (2014). Cleaning up in the endoplasmic reticulum: ubiquitin in charge. *Nature Structural & Molecular Biology*, *21*(4), 325-335. https://doi.org/10.1038/nsmb.2793

Collart, M. A., & Oliviero, S. (1993). Preparation of Yeast RNA. *Current Protocols in Molecular Biology*, *23*(1), 13.12.11-13.12.15. https://doi.org/https://doi.org/10.1002/0471142727.mb1312s23

Cox, J. S., Chapman, R. E., & Walter, P. (1997). The unfolded protein response coordinates the production of endoplasmic reticulum protein and endoplasmic reticulum membrane. *Mol Biol Cell*, *8*(9), 1805-1814. https://doi.org/10.1091/mbc.8.9.1805

Cox, J. S., Shamu, C. E., & Walter, P. (1993). Transcriptional induction of genes encoding endoplasmic reticulum resident proteins requires a transmembrane protein kinase. *Cell*, *73*(6), 1197-1206. https://doi.org/https://doi.org/10.1016/0092-8674(93)90648-A

Cox, J. S., & Walter, P. (1996). A novel mechanism for regulating activity of a transcription factor that controls the unfolded protein response. *Cell*, *87*(3), 391-404. https://doi.org/10.1016/s0092-8674(00)81360-4

Crameri, A., Whitehorn, E. A., Tate, E., & Stemmer, W. P. C. (1996). Improved Green Fluorescent Protein by Molecular Evolution Using DNA Shuffling. *Nature Biotechnology*, *14*(3), 315-319. https://doi.org/10.1038/nbt0396-315

Credle, J. J., Finer-Moore, J. S., Papa, F. R., Stroud, R. M., & Walter, P. (2005). On the mechanism of sensing unfolded protein in the endoplasmic reticulum. *Proc Natl Acad Sci U S A*, *102*(52), 18773-18784. https://doi.org/10.1073/pnas.0509487102

Das, I., Krzyzosiak, A., Schneider, K., Wrabetz, L., D'Antonio, M., Barry, N., Sigurdardottir, A., & Bertolotti, A. (2015). Preventing proteostasis diseases by selective inhibition of a phosphatase regulatory subunit. *Science*, *348*(6231), 239-242. https://doi.org/10.1126/science.aaa4484

Di Santo, R., Aboulhouda, S., & Weinberg, D. E. (2016). The fail-safe mechanism of post-transcriptional silencing of unspliced HAC1 mRNA. *Elife*, *5*. https://doi.org/10.7554/eLife.20069

Ellgaard, L., & Helenius, A. (2003). Quality control in the endoplasmic reticulum. *Nat Rev Mol Cell Biol*, *4*(3), 181-191. https://doi.org/10.1038/nrm1052

Esposito, M. S., & Esposito, R. E. (1969). THE GENETIC CONTROL OF SPORULATION IN SACCHAROMYCES I. THE ISOLATION OF TEMPERATURE-SENSITIVE SPORULATION-DEFICIENT MUTANTS. *Genetics*, *61*(1), 79-89. https://doi.org/10.1093/genetics/61.1.79

Fischer, G., Bang, H., & Mech, C. (1984). [Determination of enzymatic catalysis for the cis-trans-isomerization of peptide binding in proline-containing peptides]. *Biomed Biochim Acta*, *43*(10), 1101-1111. (Nachweis einer Enzymkatalyse für die cis-trans-Isomerisierung der Peptidbindung in prolinhaltigen Peptiden.)

Gardner, B., Pincus, D., Gotthardt, K., Gallagher, C., & Walter, P. (2013). Endoplasmic Reticulum Stress Sensing in the Unfolded Protein Response. *Cold Spring Harbor perspectives in biology*, *5*. https://doi.org/10.1101/cshperspect.a013169

Gardner, B. M., & Walter, P. (2011). Unfolded proteins are Ire1-activating ligands that directly induce the unfolded protein response. *Science*, *333*(6051), 1891-1894. https://doi.org/10.1126/science.1209126

Gething, M. J., & Sambrook, J. (1992). Protein folding in the cell. *Nature*, *355*(6355), 33-45. https://doi.org/10.1038/355033a0

Ghaemmaghami, S., Huh, W.-K., Bower, K., Howson, R. W., Belle, A., Dephoure, N., O'Shea, E. K., & Weissman, J. S. (2003). Global analysis of protein expression in yeast. *Nature*, *425*(6959), 737-741. https://doi.org/10.1038/nature02046

Gibbs, C. S., & Zoller, M. J. (1991). Rational scanning mutagenesis of a protein kinase identifies functional regions involved in catalysis and substrate interactions. *J Biol Chem*, *266*(14), 8923-8931.

Gietz, R. D., & Sugino, A. (1988). New yeast-Escherichia coli shuttle vectors constructed with in vitro mutagenized yeast genes lacking six-base pair restriction sites. *Gene*, *74*(2), 527-534. https://doi.org/10.1016/0378-1119(88)90185-0

Glembotski, C. C. (2014). Roles for ATF6 and the sarco/endoplasmic reticulum protein quality control system in the heart. *J Mol Cell Cardiol*, *71*, 11-15. https://doi.org/10.1016/j.yjmcc.2013.09.018

Goldberg, J., Nairn, A. C., & Kuriyan, J. (1996). Structural Basis for the Autoinhibition of Calcium/Calmodulin-Dependent Protein Kinase I. *Cell*, *84*(6), 875-887. https://doi.org/https://doi.org/10.1016/S0092-8674(00)81066-1

Han, D., Lerner, A. G., Vande Walle, L., Upton, J. P., Xu, W., Hagen, A., Backes, B. J., Oakes, S. A., & Papa, F. R. (2009). IRE1alpha kinase activation modes control

alternate endoribonuclease outputs to determine divergent cell fates. *Cell, 138*(3), 562-575. https://doi.org/10.1016/j.cell.2009.07.017

Hanks, S. K., & Hunter, T. (1995). The eukaryotic protein kinase superfamily: kinase (catalytic) domain structure and classification1. *The FASEB Journal*, *9*(8), 576-596. https://doi.org/https://doi.org/10.1096/fasebj.9.8.7768349

Harding, H. P., Zhang, Y., & Ron, D. (1999). Protein translation and folding are coupled by an endoplasmic-reticulum-resident kinase. *Nature*, *397*(6716), 271-274. https://doi.org/10.1038/16729

Hartl, F. U. (1996). Molecular chaperones in cellular protein folding. *Nature*, *381*(6583), 571-579. https://doi.org/10.1038/381571a0

Haze, K., Yoshida, H., Yanagi, H., Yura, T., & Mori, K. (1999). Mammalian transcription factor ATF6 is synthesized as a transmembrane protein and activated by proteolysis in response to endoplasmic reticulum stress. *Mol Biol Cell*, *10*(11), 3787-3799. https://doi.org/10.1091/mbc.10.11.3787

He, Y., Sun, S., Sha, H., Liu, Z., Yang, L., Xue, Z., Chen, H., & Qi, L. (2010). Emerging roles for XBP1, a sUPeR transcription factor. *Gene Expr*, *15*(1), 13-25. https://doi.org/10.3727/105221610x12819686555051

Hebert, D. N., & Molinari, M. (2007). In and Out of the ER: Protein Folding, Quality Control, Degradation, and Related Human Diseases. *87*(4), 1377-1408. https://doi.org/10.1152/physrev.00050.2006

Hetz, C. (2012). The unfolded protein response: controlling cell fate decisions under ER stress and beyond. *Nature Reviews Molecular Cell Biology*, *13*(2), 89-102. https://doi.org/10.1038/nrm3270

Hetz, C., & Glimcher, L. H. (2009). Fine-tuning of the unfolded protein response: Assembling the IRE1alpha interactome. *Mol Cell*, *35*(5), 551-561. https://doi.org/10.1016/j.molcel.2009.08.021

Hetz, C., Zhang, K., & Kaufman, R. J. (2020). Mechanisms, regulation and functions of the unfolded protein response. *Nat Rev Mol Cell Biol*, *21*(8), 421-438. https://doi.org/10.1038/s41580-020-0250-z

Hodgson, D. R., & Schröder, M. (2011). Chemical approaches towards unravelling kinase-mediated signalling pathways. *Chemical Society Reviews*, *40*(3), 1211-1223.

Hollien, J., Lin, J. H., Li, H., Stevens, N., Walter, P., & Weissman, J. S. (2009). Regulated Ire1-dependent decay of messenger RNAs in mammalian cells. *J Cell Biol*, *186*(3), 323-331. https://doi.org/10.1083/jcb.200903014

Hollien, J., & Weissman, J. S. (2006). Decay of endoplasmic reticulum-localized mRNAs during the unfolded protein response. *Science*, *313*(5783), 104-107. https://doi.org/10.1126/science.1129631

Hoozemans, J. J., van Haastert, E. S., Nijholt, D. A., Rozemuller, A. J., Eikelenboom, P., & Scheper, W. (2009). The unfolded protein response is activated in pretangle neurons in Alzheimer's disease hippocampus. *Am J Pathol*, *174*(4), 1241-1251. https://doi.org/10.2353/ajpath.2009.080814

Hubbard, S. R., Wei, L., Ellis, L., & Hendrickson, W. A. (1994). Crystal structure of the tyrosine kinase domain of the human insulin receptor. *Nature*, *372*(6508), 746-754. https://doi.org/10.1038/372746a0

Isaka, T., Yoshida, M., Owada, M., & Toyoshima, K. (1975). Alterations in membrane polypeptides of chick embryo fibroblasts induced by transformation with avian sarcoma viruses. *Virology*, *65*(1), 226-237. https://doi.org/10.1016/0042-6822(75)90023-9

Ishiwata-Kimata, Y., Yamamoto, Y. H., Takizawa, K., Kohno, K., & Kimata, Y. (2013). F-actin and a type-II myosin are required for efficient clustering of the ER stress sensor Ire1. *Cell Struct Funct*, *38*(2), 135-143. https://doi.org/10.1247/csf.12033

Jäger, R., Bertrand, M. J. M., Gorman, A. M., Vandenabeele, P., & Samali, A. (2012). The unfolded protein response at the crossroads of cellular life and death during endoplasmic reticulum stress. *Biology of the Cell*, *104*(5), 259-270. https://doi.org/https://doi.org/10.1111/boc.201100055

Joshi, A., Newbatt, Y. M., McAndrew, P. C., Stubbs, M., Burke, R., Richards, M. W., Bhatia, C., Caldwell, J., McHardy, T., Collins, I., & Bayliss, R. (2015). Molecular mechanisms of human IRE1 activation through dimerization and ligand binding. *Oncotarget*, *6*, 13019 - 13035.

Kaser, A., Lee, A. H., Franke, A., Glickman, J. N., Zeissig, S., Tilg, H., Nieuwenhuis, E. E., Higgins, D. E., Schreiber, S., Glimcher, L. H., & Blumberg, R. S. (2008). XBP1 links ER stress to intestinal inflammation and confers genetic risk for human inflammatory bowel disease. *Cell*, *134*(5), 743-756. https://doi.org/10.1016/j.cell.2008.07.021

Kaufman, R. J. (2002). Orchestrating the unfolded protein response in health and disease. *J Clin Invest*, *110*(10), 1389-1398. https://doi.org/10.1172/jci16886

Khuri, A. I. (2013). Introduction to Linear Regression Analysis, Fifth Edition by Douglas C. Montgomery, Elizabeth A. Peck, G. Geoffrey Vining. *International Statistical Review*, *81*(2), 318-319. https://doi.org/https://doi.org/10.1111/insr.12020_10

Kimata, Y., Ishiwata-Kimata, Y., Ito, T., Hirata, A., Suzuki, T., Oikawa, D., Takeuchi, M., & Kohno, K. (2007). Two regulatory steps of ER-stress sensor Ire1 involving its cluster formation and interaction with unfolded proteins. *The Journal of Cell Biology*, *179*, 75 - 86.

Kimata, Y., Kimata, Y. I., Shimizu, Y., Abe, H., Farcasanu, I. C., Takeuchi, M., Rose, M. D., & Kohno, K. (2003). Genetic evidence for a role of BiP/Kar2 that regulates Ire1 in response to accumulation of unfolded proteins. *Mol Biol Cell*, *14*(6), 2559-2569. https://doi.org/10.1091/mbc.e02-11-0708

Kimata, Y., Oikawa, D., Shimizu, Y., Ishiwata-Kimata, Y., & Kohno, K. (2004). A role for BiP as an adjustor for the endoplasmic reticulum stress-sensing protein Ire1. *J Cell Biol*, *167*(3), 445-456. https://doi.org/10.1083/jcb.200405153

Kimmig, P., Diaz, M., Zheng, J., Williams, C. C., Lang, A., Aragón, T., Li, H., & Walter, P. (2012). The unfolded protein response in fission yeast modulates stability of select mRNAs to maintain protein homeostasis. *Elife*, *1*, e00048. https://doi.org/10.7554/eLife.00048

Knighton, D. R., Zheng, J. H., Ten Eyck, L. F., Ashford, V. A., Xuong, N. H., Taylor, S. S., & Sowadski, J. M. (1991). Crystal structure of the catalytic subunit of cyclic adenosine monophosphate-dependent protein kinase. *Science*, *253*(5018), 407-414. https://doi.org/10.1126/science.1862342

Kohno, K., Normington, K., Sambrook, J., Gething, M. J., & Mori, K. (1993). The promoter region of the yeast KAR2 (BiP) gene contains a regulatory domain that responds to the presence of unfolded proteins in the endoplasmic reticulum. *Mol Cell Biol*, *13*(2), 877-890. https://doi.org/10.1128/mcb.13.2.877-890.1993

Korennykh, A. V., Egea, P. F., Korostelev, A. A., Finer-Moore, J., Zhang, C., Shokat, K. M., Stroud, R. M., & Walter, P. (2009). The unfolded protein response signals through high-order assembly of Ire1. *Nature*, *457*(7230), 687-693. https://doi.org/10.1038/nature07661

Kozutsumi, Y., Segal, M., Normington, K., Gething, M. J., & Sambrook, J. (1988). The presence of malfolded proteins in the endoplasmic reticulum signals the induction of glucose-regulated proteins. *Nature*, *332*(6163), 462-464. https://doi.org/10.1038/332462a0

Kukuruzinska, M. A., & Lennon, K. (1998). Protein N-glycosylation: molecular genetics and functional significance. *Crit Rev Oral Biol Med*, *9*(4), 415-448. https://doi.org/10.1177/10454411980090040301

Kyriakis, J. M., Banerjee, P., Nikolakaki, E., Dai, T., Rubie, E. A., Ahmad, M. F., Avruch, J., & Woodgett, J. R. (1994). The stress-activated protein kinase subfamily of c-Jun kinases. *Nature*, *369*(6476), 156-160. https://doi.org/10.1038/369156a0

Laemmli, U. K. (1970). Cleavage of structural proteins during the assembly of the head of bacteriophage T4. *Nature*, *227*(5259), 680-685. https://doi.org/10.1038/227680a0

Lee, K. P., Dey, M., Neculai, D., Cao, C., Dever, T. E., & Sicheri, F. (2008). Structure of the dual enzyme Ire1 reveals the basis for catalysis and regulation in nonconventional RNA splicing. *Cell*, *132*(1), 89-100. https://doi.org/10.1016/j.cell.2007.10.057

Li, H., Korennykh, A. V., Behrman, S. L., & Walter, P. (2010). Mammalian endoplasmic reticulum stress sensor IRE1 signals by dynamic clustering. *Proc Natl Acad Sci U S A*, *107*(37), 16113-16118. https://doi.org/10.1073/pnas.1010580107

Lin, J. H., Li, H., Yasumura, D., Cohen, H. R., Zhang, C., Panning, B., Shokat, K. M., Lavail, M. M., & Walter, P. (2007). IRE1 signaling affects cell fate during the unfolded protein response. *Science*, *318*(5852), 944-949. https://doi.org/10.1126/science.1146361

Lipson, K. L., Fonseca, S. G., Ishigaki, S., Nguyen, L. X., Foss, E., Bortell, R., Rossini, A. A., & Urano, F. (2006). Regulation of insulin biosynthesis in pancreatic beta cells by an endoplasmic reticulum-resident protein kinase IRE1. *Cell Metab*, *4*(3), 245-254. https://doi.org/10.1016/j.cmet.2006.07.007

Liu, C.-Y., Schröder, M., & Kaufman, R. J. (2000). Ligand-independent Dimerization Activates the Stress Response Kinases IRE1 and PERK in the Lumen of the Endoplasmic Reticulum*. *The Journal of Biological Chemistry*, *275*, 24881 - 24885.

Malhotra, J. D., & Kaufman, R. J. (2007). The endoplasmic reticulum and the unfolded protein response. *Semin Cell Dev Biol*, *18*(6), 716-731. https://doi.org/10.1016/j.semcdb.2007.09.003

Mannan, M. A.-u., Shadrick, W. R., Biener, G., Shin, B.-S., Anshu, A., Raicu, V., Frick, D. N., & Dey, M. (2013a). An ire1-phk1 chimera reveals a dispensable role of autokinase activity in endoplasmic reticulum stress response. *Journal of molecular biology*, *425*(12), 2083-2099. https://doi.org/10.1016/j.jmb.2013.02.036

Mannan, M. A.-u., Shadrick, W. R., Biener, G., Shin, B.-S., Anshu, A., Raicu, V., Frick, D. N., & Dey, M. (2013b). An Ire1–Phk1 Chimera Reveals a Dispensable Role of Autokinase Activity in Endoplasmic Reticulum Stress Response. *Journal of Molecular Biology*, *425*(12), 2083-2099. https://doi.org/https://doi.org/10.1016/j.jmb.2013.02.036

Marciniak, S. J., Yun, C. Y., Oyadomari, S., Novoa, I., Zhang, Y., Jungreis, R., Nagata, K., Harding, H. P., & Ron, D. (2004). CHOP induces death by promoting protein synthesis and oxidation in the stressed endoplasmic reticulum. *Genes Dev*, *18*(24), 3066-3077. https://doi.org/10.1101/gad.1250704

Martinon, F., & Glimcher, L. H. (2011). Regulation of innate immunity by signaling pathways emerging from the endoplasmic reticulum. *Current Opinion in Immunology*, *23*(1), 35-40. https://doi.org/https://doi.org/10.1016/j.coi.2010.10.016

Maurel, M., Chevet, E., Tavernier, J., & Gerlo, S. (2014). Getting RIDD of RNA: IRE1 in cell fate regulation. *Trends Biochem Sci*, *39*(5), 245-254. https://doi.org/10.1016/j.tibs.2014.02.008

Miesenböck, G., De Angelis, D. A., & Rothman, J. E. (1998). Visualizing secretion and synaptic transmission with pH-sensitive green fluorescent proteins. *Nature*, *394*(6689), 192-195. https://doi.org/10.1038/28190

Miller, J. H. (1972). Experiments in molecular genetics.

Molinari, M., LEGGIO, M. G., DE MARTIN, M., CERASA, A., & THAUT, M. (2003). Neurobiology of Rhythmic Motor Entrainment. *Annals of the New York Academy of Sciences*, *999*(1), 313-321. https://doi.org/https://doi.org/10.1196/annals.1284.042

Moore, K. A., & Hollien, J. (2012). The Unfolded Protein Response in Secretory Cell Function. *Annual Review of Genetics*, *46*(1), 165-183. https://doi.org/10.1146/annurev-genet-110711-155644

Mori, K. (2009). Signalling pathways in the unfolded protein response: development from yeast to mammals. *J Biochem*, *146*(6), 743-750. https://doi.org/10.1093/jb/mvp166

Mori, K., Kawahara, T., Yoshida, H., Yanagi, H., & Yura, T. (1996). Signalling from endoplasmic reticulum to nucleus: transcription factor with a basic-leucine zipper motif is required for the unfolded protein-response pathway. *Genes to Cells*, *1*(9), 803-817. https://doi.org/https://doi.org/10.1046/j.1365-2443.1996.d01-274.x

Mori, K., Ma, W., Gething, M. J., & Sambrook, J. (1993). A transmembrane protein with a cdc2+/CDC28-related kinase activity is required for signaling from the ER to the nucleus. *Cell*, *74*(4), 743-756. https://doi.org/10.1016/0092-8674(93)90521-q

Mori, K., Ogawa, N., Kawahara, T., Yanagi, H., & Yura, T. (1998). Palindrome with spacer of one nucleotide is characteristic of the cis-acting unfolded protein response element in Saccharomyces cerevisiae. *J Biol Chem*, *273*(16), 9912-9920. https://doi.org/10.1074/jbc.273.16.9912

Mori, K., Sant, A., Kohno, K., Normington, K., Gething, M. J., & Sambrook, J. F. (1992). A 22 bp cis-acting element is necessary and sufficient for the induction of the yeast KAR2 (BiP) gene by unfolded proteins. *Embo j*, *11*(7), 2583-2593. https://doi.org/10.1002/j.1460-2075.1992.tb05323.x

Nagashima, Y., Mishiba, K., Suzuki, E., Shimada, Y., Iwata, Y., & Koizumi, N. (2011). Arabidopsis IRE1 catalyses unconventional splicing of bZIP60 mRNA to produce the active transcription factor. *Sci Rep*, *1*, 29. https://doi.org/10.1038/srep00029

Nikawa, J. i., & Yamashita, S. (1992). IRE1 encodes a putative protein kinase containing a membrane-spanning domain and is required for inositol phototrophy in Saccharomyces cerevisiae. *Molecular Microbiology*, *6*.

Nishitoh, H., Matsuzawa, A., Tobiume, K., Saegusa, K., Takeda, K., Inoue, K., Hori, S., Kakizuka, A., & Ichijo, H. (2002). ASK1 is essential for endoplasmic reticulum stress-induced neuronal cell death triggered by expanded polyglutamine repeats. *Genes Dev*, *16*(11), 1345-1355. https://doi.org/10.1101/gad.992302

Nolen, B., Taylor, S., & Ghosh, G. (2004). Regulation of protein kinases; controlling activity through activation segment conformation. *Mol Cell*, *15*(5), 661-675. https://doi.org/10.1016/j.molcel.2004.08.024

Normington, K., Kohno, K., Kozutsumi, Y., Gething, M. J., & Sambrook, J. (1989). S. cerevisiae encodes an essential protein homologous in sequence and function to mammalian BiP. *Cell*, *57*(7), 1223-1236. https://doi.org/10.1016/0092-8674(89)90059-7

Ogawa, N., & Mori, K. (2004). Autoregulation of the HAC1 gene is required for sustained activation of the yeast unfolded protein response. *Genes Cells*, *9*(2), 95-104. https://doi.org/10.1111/j.1365-2443.2004.00704.x

Özcan, U., Cao, Q., Yilmaz, E., Lee, A.-H., Iwakoshi, N. N., Özdelen, E., Tuncman, G., Görgün, C., Glimcher, L. H., & Hotamisligil, G. S. (2004). Endoplasmic Reticulum Stress Links Obesity, Insulin Action, and Type 2 Diabetes. *306*(5695), 457-461. https://doi.org/10.1126/science.1103160 %J Science

Palade, G. (1975). Intracellular aspects of the process of protein synthesis. *189*(4200), 347-358. https://doi.org/10.1126/science.1096303 %J Science

Papa, F. R., Zhang, C., Shokat, K., & Walter, P. (2003). Bypassing a kinase activity with an ATP-competitive drug. *Science*, *302*(5650), 1533-1537. https://doi.org/10.1126/science.1090031

Patil, C. K., Li, H., & Walter, P. (2004). Gcn4p and novel upstream activating sequences regulate targets of the unfolded protein response. *PLoS Biol*, *2*(8), E246. https://doi.org/10.1371/journal.pbio.0020246

Pincus, D., Chevalier, M. W., Aragón, T., van Anken, E., Vidal, S. E., El-Samad, H., & Walter, P. (2010). BiP binding to the ER-stress sensor Ire1 tunes the homeostatic behavior of the unfolded protein response. *PLoS Biol*, *8*(7), e1000415. https://doi.org/10.1371/journal.pbio.1000415

Preissler, S., & Ron, D. (2019). Early Events in the Endoplasmic Reticulum Unfolded Protein Response. *Cold Spring Harb Perspect Biol*, *11*(4). https://doi.org/10.1101/cshperspect.a033894

Prinz, W. A., Grzyb, L., Veenhuis, M., Kahana, J. A., Silver, P. A., & Rapoport, T. A. (2000). Mutants Affecting the Structure of the Cortical Endoplasmic Reticulum in Saccharomyces cerevisiae. *Journal of Cell Biology*, *150*(3), 461-474. https://doi.org/10.1083/jcb.150.3.461

Reimold, A. M., Iwakoshi, N. N., Manis, J., Vallabhajosyula, P., Szomolanyi-Tsuda, E., Gravallese, E. M., Friend, D., Grusby, M. J., Alt, F., & Glimcher, L. H. (2001). Plasma cell differentiation requires the transcription factor XBP-1. *Nature*, *412*(6844), 300-307. https://doi.org/10.1038/35085509

Riemer, J., Bulleid, N., & Herrmann, J. M. (2009). Disulfide formation in the ER and mitochondria: two solutions to a common process. *Science*, *324*(5932), 1284-1287. https://doi.org/10.1126/science.1170653

Ron, D., & Walter, P. (2007). Signal integration in the endoplasmic reticulum unfolded protein response. *Nature Reviews Molecular Cell Biology*, *8*(7), 519-529. https://doi.org/10.1038/nrm2199

Roth, R., Halvorson, H. O. (1969). The culture of the blue-green alga, Anacystis nidulans, on defined media: the kinetics of growth and phosphate uptake. *Journal of Bacteriology*, *98*(2), 831-843.

Rubio, C., Pincus, D., Korennykh, A., Schuck, S., El-Samad, H., & Walter, P. (2011). Homeostatic adaptation to endoplasmic reticulum stress depends on Ire1 kinase activity. *J Cell Biol*, *193*(1), 171-184. https://doi.org/10.1083/jcb.201007077

Rüegsegger, U., Leber, J. H., & Walter, P. (2001). Block of HAC1 mRNA translation by long-range base pairing is released by cytoplasmic splicing upon induction of the unfolded protein response. *Cell*, *107*(1), 103-114. https://doi.org/10.1016/s0092-8674(01)00505-0

Rutkowski, D. T., & Kaufman, R. J. (2004). A trip to the ER: coping with stress. *Trends Cell Biol*, *14*(1), 20-28. https://doi.org/10.1016/j.tcb.2003.11.001

Schenborn, E. a. G., V. . (1993). *Promega Notes*, *41*, 11-13.

Schindler, A. J., & Schekman, R. (2009). In vitro reconstitution of ER-stress induced ATF6 transport in COPII vesicles. *Proc Natl Acad Sci U S A*, *106*(42), 17775-17780. https://doi.org/10.1073/pnas.0910342106

Schneppenheim, R., Budde, U., Dahlmann, N., & Rautenberg, P. (1991). Luminography – a new, highly sensitive visualization method for electrophoresis. *ELECTROPHORESIS*, *12*(5), 367-372. https://doi.org/https://doi.org/10.1002/elps.1150120508

Schröder, M., Chang, J. S., & Kaufman, R. J. (2000). The unfolded protein response represses nitrogen-starvation induced developmental differentiation in yeast. *Genes Dev*, *14*(23), 2962-2975. https://doi.org/10.1101/gad.852300

Schröder, M., Clark, R., Liu, C. Y., & Kaufman, R. J. (2004). The unfolded protein response represses differentiation through the RPD3-SIN3 histone deacetylase. *The EMBO Journal*, *23*(11), 2281-2292.

Schröder, M., & Kaufman, R. J. (2005a). ER stress and the unfolded protein response. *Mutat Res*, *569*(1-2), 29-63. https://doi.org/10.1016/j.mrfmmm.2004.06.056

Schröder, M., & Kaufman, R. J. (2005b). The mammalian unfolded protein response. *Annu Rev Biochem*, *74*, 739-789. https://doi.org/10.1146/annurev.biochem.73.011303.074134

Shamu, C. E., & Walter, P. (1996). Oligomerization and phosphorylation of the Ire1p kinase during intracellular signaling from the endoplasmic reticulum to the nucleus. *Embo j*, *15*(12), 3028-3039.

Sherman, F. (1991). Getting started with yeast. *Methods Enzymol*, *194*, 3-21.

Shiu, R. P., Pouyssegur, J., & Pastan, I. (1977). Glucose depletion accounts for the induction of two transformation-sensitive membrane proteinsin Rous sarcoma virus-transformed chick embryo fibroblasts. *Proc Natl Acad Sci U S A*, *74*(9), 3840-3844. https://doi.org/10.1073/pnas.74.9.3840

Shoulders, M. D., Ryno, L. M., Genereux, J. C., Moresco, J. J., Tu, P. G., Wu, C., Yates, J. R., 3rd, Su, A. I., Kelly, J. W., & Wiseman, R. L. (2013). Stress-independent activation of XBP1s and/or ATF6 reveals three functionally diverse ER proteostasis environments. *Cell Rep*, *3*(4), 1279-1292. https://doi.org/10.1016/j.celrep.2013.03.024

Sidrauski, C., Cox, J. S., & Walter, P. (1996). tRNA ligase is required for regulated mRNA splicing in the unfolded protein response. *Cell*, *87*(3), 405-413. https://doi.org/10.1016/s0092-8674(00)81361-6

Sidrauski, C., & Walter, P. (1997). The transmembrane kinase Ire1p is a site-specific endonuclease that initiates mRNA splicing in the unfolded protein response. *Cell*, *90*(6), 1031-1039. https://doi.org/10.1016/s0092-8674(00)80369-4

Smith, P. K., Krohn, R. I., Hermanson, G. T., Mallia, A. K., Gartner, F. H., Provenzano, M. D., Fujimoto, E. K., Goeke, N. M., Olson, B. J., & Klenk, D. C. (1985). Measurement of protein using bicinchoninic acid. *Analytical Biochemistry*, *150*(1), 76-85. https://doi.org/https://doi.org/10.1016/0003-2697(85)90442-7

Stevens, F. J., & Argon, Y. (1999). Protein folding in the ER. *Semin Cell Dev Biol*, *10*(5), 443-454. https://doi.org/10.1006/scdb.1999.0315

Stone, K. R., Smith, R. E., & Joklik, W. K. (1974). Changes in membrane polypeptides that occur when chick embryo fibroblasts and NRK cells are transformed with avian sarcoma viruses. *Virology*, *58*(1), 86-100. https://doi.org/10.1016/0042-6822(74)90143-3

Su, S. S., & Mitchell, A. P. (1993). Identification of functionally related genes that stimulate early meiotic gene expression in yeast. *Genetics*, *133*(1), 67-77. https://doi.org/10.1093/genetics/133.1.67

Tan, J. H., Cao, R. C., Zhou, L., Zhou, Z. T., Chen, H. J., Xu, J., Chen, X. M., Jin, Y. C., Lin, J. Y., Zeng, J. L., Li, S. J., Luo, M., Hu, G. D., Yang, X. B., Jin, J., & Zhang, G. W. (2020). ATF6 aggravates acinar cell apoptosis and injury by regulating p53/AIFM2 transcription in Severe Acute Pancreatitis. *Theranostics*, *10*(18), 8298-8314. https://doi.org/10.7150/thno.46934

Tirasophon, W., Lee, K., Callaghan, B., Welihinda, A., & Kaufman, R. (2000). The endoribonuclease activity of mammalian IRE1 autoregulates its mRNA and is required for the unfolded protein response. *Genes & development*, *14*, 2725-2736.

Tirasophon, W., Welihinda, A. A., & Kaufman, R. J. (1998). A stress response pathway from the endoplasmic reticulum to the nucleus requires a novel bifunctional protein kinase/endoribonuclease (Ire1p) in mammalian cells. *Genes Dev*, *12*(12), 1812-1824. https://doi.org/10.1101/gad.12.12.1812

Travers, K. J., Patil, C. K., Wodicka, L., Lockhart, D. J., Weissman, J. S., & Walter, P. (2000). Functional and genomic analyses reveal an essential coordination between the

unfolded protein response and ER-associated degradation. *Cell*, *101*(3), 249-258. https://doi.org/10.1016/s0092-8674(00)80835-1

Tsaytler, P., Harding, H. P., Ron, D., & Bertolotti, A. (2011). Selective inhibition of a regulatory subunit of protein phosphatase 1 restores proteostasis. *Science*, *332*(6025), 91-94. https://doi.org/10.1126/science.1201396

Tukey, J. W. (1949). Comparing individual means in the analysis of variance. *Biometrics*, *5*(2), 99-114.

Upton, J. P., Wang, L., Han, D., Wang, E. S., Huskey, N. E., Lim, L., Truitt, M., McManus, M. T., Ruggero, D., Goga, A., Papa, F. R., & Oakes, S. A. (2012). IRE1α cleaves select microRNAs during ER stress to derepress translation of proapoptotic Caspase-2. *Science*, *338*(6108), 818-822. https://doi.org/10.1126/science.1226191

Urano, F., Wang, X., Bertolotti, A., Zhang, Y., Chung, P., Harding, H. P., & Ron, D. (2000). Coupling of stress in the ER to activation of JNK protein kinases by transmembrane protein kinase IRE1. *Science*, *287*(5453), 664-666. https://doi.org/10.1126/science.287.5453.664

Valiev, M., Yang, J., Adams, J. A., Taylor, S. S., & Weare, J. H. (2007). Phosphorylation reaction in cAPK protein kinase-free energy quantum mechanical/molecular mechanics simulations. *J Phys Chem B*, *111*(47), 13455-13464. https://doi.org/10.1021/jp074853q

Vattem, K. M., & Wek, R. C. (2004). Reinitiation involving upstream ORFs regulates ATF4 mRNA translation in mammalian cells. *Proc Natl Acad Sci U S A*, *101*(31), 11269-11274. https://doi.org/10.1073/pnas.0400541101

Voeltz, G. K., Prinz, W. A., Shibata, Y., Rist, J. M., & Rapoport, T. A. (2007). A Class of Membrane Proteins Shaping the Tubular Endoplasmic Reticulum. *Cell*, *130*.

Volmer, R., van der Ploeg, K., & Ron, D. (2013). Membrane lipid saturation activates endoplasmic reticulum unfolded protein response transducers through their transmembrane domains. *Proceedings of the National Academy of Sciences*, *110*, 4628 - 4633.

Walsh, G. (2010). Post-translational modifications of protein biopharmaceuticals. *Drug Discov Today*, *15*(17-18), 773-780. https://doi.org/10.1016/j.drudis.2010.06.009

Walter, F., Schmid, J., Düssmann, H., Concannon, C. G., & Prehn, J. H. M. (2015). Imaging of single cell responses to ER stress indicates that the relative dynamics of IRE1/XBP1 and PERK/ATF4 signalling rather than a switch between signalling

branches determine cell survival. *Cell Death & Differentiation*, *22*(9), 1502-1516. https://doi.org/10.1038/cdd.2014.241

Walter, P., & Ron, D. (2011). The unfolded protein response: from stress pathway to homeostatic regulation. *Science*, *334*(6059), 1081-1086. https://doi.org/10.1126/science.1209038

Wang, Y., Shen, J., Arenzana, N., Tirasophon, W., Kaufman, R. J., & Prywes, R. (2000). Activation of ATF6 and an ATF6 DNA binding site by the endoplasmic reticulum stress response. *J Biol Chem*, *275*(35), 27013-27020. https://doi.org/10.1074/jbc.M003322200

Welihinda, A. A., Tirasophon, W., Green, S. R., & Kaufman, R. J. (1998). Protein serine/threonine phosphatase Ptc2p negatively regulates the unfolded-protein response by dephosphorylating Ire1p kinase. *Mol Cell Biol*, *18*(4), 1967-1977. https://doi.org/10.1128/mcb.18.4.1967

Welihinda, A. A., Tirasophon, W., & Kaufman, R. J. (1999). The cellular response to protein misfolding in the endoplasmic reticulum. *Gene Expr*, *7*(4-6), 293-300.

Welihinda, A. A., Tirasophon, W., & Kaufman, R. J. (2000). The transcriptional co-activator ADA5 is required for HAC1 mRNA processing in vivo. *J Biol Chem*, *275*(5), 3377-3381. https://doi.org/10.1074/jbc.275.5.3377

Wickersham, L. J. (1951). Taxonomy of Yeasts. *1029*. https://ideas.repec.org/p/ags/uerstb/156394.html

Xu, C., Bailly-Maitre, B., & Reed, J. C. (2005). Endoplasmic reticulum stress: cell life and death decisions. *J Clin Invest*, *115*(10), 2656-2664. https://doi.org/10.1172/jci26373

Ye, J., Rawson, R. B., Komuro, R., Chen, X., Davé, U. P., Prywes, R., Brown, M. S., & Goldstein, J. L. (2000). ER stress induces cleavage of membrane-bound ATF6 by the same proteases that process SREBPs. *Mol Cell*, *6*(6), 1355-1364. https://doi.org/10.1016/s1097-2765(00)00133-7

Zhang, F., Strand, A., Robbins, D., Cobb, M. H., & Goldsmith, E. J. (1994). Atomic structure of the MAP kinase ERK2 at 2.3 Å resolution. *Nature*, *367*, 704-711. https://doi.org/10.1038/367704a0

Zhang, K., & Kaufman, R. J. (2004). Signaling the Unfolded Protein Response from the Endoplasmic Reticulum*. *Journal of Biological Chemistry*, *279*, 25935 - 25938.

Zhang, K., & Kaufman, R. J. (2008). From endoplasmic-reticulum stress to the inflammatory response. *Nature*, *454*(7203), 455-462. https://doi.org/10.1038/nature07203

Zhou, J., Liu, C. Y., Back, S. H., Clark, R. L., Peisach, D., Xu, Z., & Kaufman, R. J. (2006). The crystal structure of human IRE1 luminal domain reveals a conserved dimerization interface required for activation of the unfolded protein response. *Proc Natl Acad Sci U S A*, *103*(39), 14343-14348. https://doi.org/10.1073/pnas.0606480103

Zhou, L., Tan, J. H., Cao, R. C., Xu, J., Chen, X. M., Qi, Z. C., Zhou, S. Y., Li, S. B., Mo, Q. X., Li, Z. W., & Zhang, G. W. (2019). ATF6 regulates the development of chronic pancreatitis by inducing p53-mediated apoptosis. *Cell Death Dis*, *10*(9), 662. https://doi.org/10.1038/s41419-019-1919-0